

STRUCTURAL STUDIES OF INHIBITION OF THE HUMAN
INDUCIBLE PROSTAGLANDIN E SYNTHASE MPGES1

By

Edward B. Prage

Dissertation

Submitted to the Faculty of the
Graduate School of Vanderbilt University
in partial fulfillment of the requirements

for the degree of

DOCTOR OF PHILOSOPHY

in

Chemistry

May, 2012

Nashville, Tennessee

Approved:

Professor Richard N. Armstrong

Professor Brian O. Bachmann

Professor Lawrence J. Marnett

Professor John A. McLean

For my wife

ACKNOWLEDGEMENTS

I primarily acknowledge and thank my wife, Janelle, for providing her unconditional belief in me and for giving me an inordinate amount of emotional support over the past several years. She has also been a fantastic mother to our two amazing sons, all of whom have proven to be the best support system a scientist could want or need. I also thank my mother, Marilyn, to whom I attribute everything good about myself.

I give my thanks to Sven Pawelzik, Ralf Morgenstern, and Per-Johan Jakobsson of the Karolinska Institutet in Stockholm, Sweden, for the opportunity to learn new analytical techniques and to explore a remarkable city on the other side of the world. I thank Donald Stec and Markus Voehler of the NMR facilities as well as David Hachey, Wade Calcutt, Melissa Carter, Dawn Overstreet, and Julie Coleman of the mass spectrometry research center for their indispensable expertise and assistance.

I thank current and former members of the Armstrong lab including Megan Branch, Daniel Brown, Laura Busenlehner, Mary Keithly, Matthew Schaab, Nina Stourman, and Matthew Thompson for their friendship and helpful discussions. I would also like to thank Brian Bachmann, Lawrence Marnett, and John McLean for serving on my Ph.D. committee and for offering their valuable advice throughout the course of my research. Finally, I would like to thank Richard Armstrong for serving as my advisor and for giving me the opportunity, patience, and freedom to pursue a research project in which I have been genuinely interested.

These studies were supported by the National Institutes of Health (R01 GM030910, T32 GM008320, T32 GM ES007028, F32 ES013105, and P30 ES000267), the Swedish Research Council, the Ulla och Gustaf af Ugglas foundation, and the Center in Molecular Toxicology at Vanderbilt University.

TABLE OF CONTENTS

	Page
DEDICATION	ii
ACKNOWLEDGEMENTS	iii
LIST OF TABLES	v
LIST OF FIGURES	vi
LIST OF ABBREVIATIONS	xii
Chapter	
I. INTRODUCTION	
Inflammation	1
Eicosanoids	6
Prostanoids	7
Leukotrienes	17
Lipoxins and Eoxins	20
Cytochrome P450-derived Eicosanoids	24
The MAPEG Superfamily	26
Glutathione Transferases	26
MAPEG Discoveries	28
MAPEG Structures	33
MAPEG Functions	39
Microsomal Prostaglandin E Synthase 1	41
MPGES1 Catalytic Function	42
MPGES1 Chemical Mechanism	44
MPGES1 Structure	46
MPGES1 as a Drug Target	49
Hydrogen/Deuterium Exchange Mass Spectrometry of Membrane Proteins	56
H/D Exchange Theory	57
H/D Exchange MS Methodology	58
H/D Exchange MS of Membrane Proteins	61
Challenges of Membrane Protein H/D Exchange MS	66
Prospects for H/D Exchange MS	69
Purpose of These Studies	70
II. MATERIALS AND METHODS	
Materials	76
Methods	76

III. TOPOLOGY OF MICROSOMAL PROSTAGLANDIN E SYNTHASE 1	
Results.....	91
Discussion.....	95
IV. LOCATION OF INHIBITOR BINDING SITES IN THE HUMAN INDUCIBLE PROSTAGLANDIN E SYNTHASE MPGES1	
Results.....	102
Discussion.....	110
V. OBSERVATION OF TWO MODES OF INHIBITION OF HUMAN MICROSOMAL PROSTAGLANDIN E SYNTHASE 1 BY THE CYCLOPENTENONE 15-DEOXY- $\Delta^{12,14}$ -PROSTAGLANDIN J ₂	
Results.....	116
Discussion.....	127
VI. CONCLUSION	
Discussion.....	130
Future Studies	132
APPENDIX.....	134
REFERENCES	167

LIST OF TABLES

Table	Page
1. Drug Leads of MPGES1	53
2. Inhibitors of MPGES1 Used in H/D Exchange Kinetic Analysis.....	103
3. Amplitudes and Rate Constants for Amide H/D Exchange in the Analysis of Inhibitor Binding.....	108
4. NMR Data of the Glutathione Conjugate of 15d-PGJ ₂ in CD ₃ OD and D ₂ O	155

LIST OF FIGURES

Figure	Page
1. Compounds for the Therapeutic Treatment of Inflammation	4
2. Arachidonic Acid	6
3. Chemical Mechanism of the Cyclooxygenase Reaction.....	9
4. The Prostanoid Cascade	10
5. Synthesis of PGF ₂	13
6. Cyclopentenone Prostaglandins	16
7. The Leukotriene Cascade.....	18
8. Synthesis of Lipoxins.....	21
9. Aspirin-triggered Lipoxins.....	22
10. Synthesis of Eoxins	23
11. Cytochrome P450-derived Eicosanoids	24
12. Glutathione.....	26
13. Glutathione Transferase Activities of Microsomal Glutathione Transferase 1 and Leukotriene C ₄ Synthase.....	29
14. Glutathione-dependent Activity of MGST2 and MGST3	31
15. PGE Synthase Activity of MPGES1.....	32
16. The MAPEG Superfamily.....	33
17. The Conserved Structure of the MAPEG Superfamily.....	34
18. Crystal Structure of MGST1	35
19. Crystal Structure of FLAP	36
20. Crystal Structure of LTC ₄ S	37
21. Crystal Structure of MPGES1.....	38

22. Decomposition of PGH ₂	42
23. Substrates of MGPES1	43
24. Chemical Mechanism of MPGES1	45
25. Structural Analysis of MPGES1	47
26. GSH Binding of MPGES1	49
27. The Linderström-Lang Model of H/D Exchange.....	58
28. H/D Exchange MS Experimental Method	59
29. H/D Exchange Kinetic Analysis	60
30. H/D Exchange MS of MGST1.....	62
31. H/D Exchange MS of CcO	63
32. H/D Exchange MS of Bacteriorhodopsin	64
33. H/D Exchange MS of β_2 AR.....	65
34. Prediction of Topology of MPGES1 by Computational Methods.....	92
35. Prediction of Topology of MPGES1 by Sequence Alignment	93
36. H/D Exchange Kinetic Profiles for MPGES1 as a Function of Detergent	94
37. Determination of Topology of MPGES1 by H/D Exchange MS	95
38. Comparison of Prediction Methods	97
39. Transmembrane Helices of MPGES1	98
40. Detergents	99
41. H/D Exchange Kinetic Profiles for MPGES1 at the Micelle Boundary.....	100
42. H/D Exchange Kinetic Behavior at the Micelle Boundary.....	100
43. H/D Exchange Kinetic Profiles for MPGES1 at the Cofactor Site.....	105
44. Stereoviews of the Residues in Close Proximity to the Sulfhydryl Group of GSH ..	105

45. Qualitative map of the effect of inhibitor binding to the MPGES1•GSH complex...	106
46. Effects of Inhibitor Binding on the H/D Exchange Kinetic Profiles of MPGES1.....	107
47. The Impact of Inhibitor Binding on the H/D Exchange Behavior of the MPGES1•GSH Complex	110
48. Comparison of the Differential Impact of GSH/I Binding on MPGES1	111
49. Definition of the Hydrophobic Cleft.....	113
50. Reaction of 15d-PGJ ₂ with GSH.....	117
51. Stereoselectivity of GSH Addition	118
52. Inhibition of the Isomerase Activity of MPGES1.....	122
53. Recovery of the Isomerase Activity of MPGES1	123
54. H/D Exchange Kinetic Profiles of MPGES1•GSH as a Function of 15d-PGJ ₂	124
55. Structural Impact of 15d-PGJ ₂ Binding on MPGES1•GSH	125
56. H/D Exchange Kinetic Profiles of MPGES1•GSO ₃ ⁻ as a Function of 15d-PGJ ₂	126
57. Structural Impact of 15d-PGJ ₂ Binding on MPGES1•GSO ₃ ⁻	127
58. MPGES1 Peptic Peptide Map.....	135
59. H/D Exchange Kinetic Profiles for MPGES1 as a Function of Micelle, Residues 2 – 39.....	136
60. H/D Exchange Kinetic Profiles for MPGES1 as a Function of Micelle, Residues 37 – 92.....	137
61. H/D Exchange Kinetic Profiles for MPGES1 as a Function of Micelle, Residues 92 – 140.....	138
62. H/D Exchange Kinetic Profiles for MPGES1 as a Function of Micelle, Residues 141 – 152.....	139
63. Determination of GSO ₃ ⁻ IC ₅₀	139
64. H/D Exchange Kinetic Profiles for MPGES1 as a Function of GSH/I Binding, Residues 2 – 39	140

65. H/D Exchange Kinetic Profiles for MPGES1 as a Function of GSH/1 Binding, Residues 37 – 92	141
66. H/D Exchange Kinetic Profiles for MPGES1 as a Function of GSH/1 Binding, Residues 92 – 140.....	142
67. H/D Exchange Kinetic Profiles for MPGES1 as a Function of GSH/1 Binding, Residues 141 – 152.....	143
68. Synthesis of MF63, Step 1: 1-(3-Phenanthryl)ethanone Oxime.....	143
69. Synthesis of MF63, Step 2: 3-Phenanthrylamine	144
70. Synthesis of MF63, Step 3: 3-Chlorophenanthrene.....	144
71. Synthesis of MF63, Step 4: 3-Chlorophenanthrene-9,10-dione	145
72. Synthesis of MF63, step 5: 6-Chloro-2-(2,6-dibromophenyl)-3a,11b-dihydro-1H-phenanthro[9,10-d]imidazole.....	145
73. Synthesis of MF63, Final Step.....	146
74. H/D Exchange Kinetic Profiles for MPGES1•GSH as a Function of Inhibitor Binding, Residues 2-27	147
75. H/D Exchange Kinetic Profiles for MPGES1•GSH as a Function of Inhibitor Binding, Residues 28-58.....	148
76. H/D Exchange Kinetic Profiles for MPGES1•GSH as a Function of Inhibitor Binding, Residues 60-92.....	149
77. H/D Exchange Kinetic Profiles for MPGES1•GSH as a Function of Inhibitor Binding, Residues 92-129.....	150
78. H/D Exchange Kinetic Profiles for MPGES1•GSH as a Function of Inhibitor Binding, Residues 130-152.....	151
79. Fragmentation Spectrum of Cys-15d-PGJ ₂	152
80. ¹ H-NMR Spectra of 9-GS-15d-PGJ ₂ at 900 MHz	152
81. Two-dimensional NMR Spectroscopy of 9-GS-15d-PGJ ₂ at 600 MHz.....	153
82. Two-dimensional NMR Spectroscopy of 9-GS-15d-PGJ ₂ at 900 MHz.....	154
83. Fragmentation Spectrum of MPGES1 C59-15d-PGJ ₂	156

84. H/D Exchange Kinetic Profiles for MPGES1 as a Function of 15d-PGJ ₂ Binding, Residues 2-17.....	157
85. H/D Exchange Kinetic Profiles for MPGES1 as a Function of 15d-PGJ ₂ Binding, Residues 18-27.....	158
86. H/D Exchange Kinetic Profiles for MPGES1 as a Function of 15d-PGJ ₂ Binding, Residues 28-39.....	159
87. H/D Exchange Kinetic Profiles for MPGES1 as a Function of 15d-PGJ ₂ Binding, Residues 37-59.....	160
88. H/D Exchange Kinetic Profiles for MPGES1 as a Function of 15d-PGJ ₂ Binding, Residues 60-78.....	161
89. H/D Exchange Kinetic Profiles for MPGES1 as a Function of 15d-PGJ ₂ Binding, Residues 78-92.....	162
90. H/D Exchange Kinetic Profiles for MPGES1 as a Function of 15d-PGJ ₂ Binding, Residues 92-107.....	163
91. H/D Exchange Kinetic Profiles for MPGES1 as a Function of 15d-PGJ ₂ Binding, Residues 108-129.....	164
92. H/D Exchange Kinetic Profiles for MPGES1 as a Function of 15d-PGJ ₂ Binding, Residues 130-140.....	165
93. H/D Exchange Kinetic Profiles for MPGES1 as a Function of 15d-PGJ ₂ Binding, Residues 141-152.....	166

LIST OF ABBREVIATIONS

9-GS-15d-PGJ ₂	9-(S-Glutathionyl)-15-deoxy- $\Delta^{12,14}$ -prostaglandin J ₂
9-GS-11-OH-15d-PGJ ₂	9-(S-Glutathionyl)-11-hydroxy-15-deoxy- $\Delta^{12,14}$ - prostaglandin J ₂
11-OH-15d-PGJ ₂	11-Hydroxy-15-deoxy- $\Delta^{12,14}$ -prostaglandin J ₂
12-HHT	12-(S)-Hydroxy-8,10- <i>trans</i> -5- <i>cis</i> -heptadecatrienoic acid
15d-PGJ ₂	15-Deoxy- $\Delta^{12,14}$ -prostaglandin J ₂
15-epi-LX	15-Epimeric-lipoxin
AIDS	Acquired immunodeficiency syndrome
AKR	Aldo-keto reductase
ALS	Acid-labile surfactant
ALX	Aspirin-triggered lipoxin receptor
APC	Adenomatous polyposis coli
ATL	Aspirin-triggered lipoxin
BLT	B leukotriene receptor
β ME	2-Mercaptoethanol
CcO	Cytochrome <i>c</i> oxidase
CDNB	1-Chloro-2,4-dinitrobenzene
CHAPS	3-[(3-Cholamidopropyl)dimethylammonio]-1-propane Sulfonate
CHAPSO	2[(3-Cholamidopropyl)dimethylammonio]-2-hydroxy-1- Propanesulfonate
CIA	Collagen-induced arthritis
CID	Collision-induced dissociation

CMC	Critical micelle concentration
COSY	Correlation spectroscopy
COX	Cyclooxygenase
Coxib	Cyclooxygenase-2-selective drug
CPGES	Cytosolic prostaglandin E synthase
cPLA ₂	Cytosolic phospholipase A ₂
CV	Cardiovascular
CYP	Cytochrome P450
Cys-LT	Cysteinyl leukotriene
CysLT1/2	Cysteinyl leukotriene receptor 1/2
cyPG	Cyclopentenone prostaglandin
DDM	<i>n</i> -Dodecyl- β -D-maltoside
DEAE	Diethylaminoethyl weak anion exchange
DHET	Dihydroxyeicosatrienoic acid
DMPC	1,2-Dimyristoyl- <i>sn</i> -glycero-3-phosphocholine
DMSO	Dimethyl sulfoxide
DP	D prostanoid receptor
DQF-COSY	Double-quantum filtered correlation spectroscopy
DTT	Dithiothreitol
ECD	Electron capture dissociation
EDTA	Ethylenediaminetetraacetic acid
EET	Epoxyeicosatrienoic acid
EGF	Epidermal growth factor

EP	E prostanoid receptor
ER	Endoplasmic reticulum
ESI	Electrospray ionization
ETD	Electron transfer dissociation
EX	Eoxin
FAB	Fast atom bombardment
FLAP	5-Lipoxygenase-activating protein
Fos	Fosfomycin-resistance proteins
FP	F prostanoid receptor
FPRL-1	Formyl peptide receptor-like 1
GGCX	γ -Glutamyl carboxylase
GGT	γ -Glutamyl transpeptidase
GPCR	G-protein-coupled receptor
GSH	Glutathione
GSO ₃ ⁻	Glutathione sulfonate
GST	Glutathione transferase
H/D exchange	Hydrogen/deuterium exchange
HETE	Hydroxyeicosatetraenoic acid
HIV	Human immunodeficiency virus
HLB	Hydrophilic-lipophilic balance
HPETE	Hydroperoxyeicosatetraenoic acid
H-PGDS	Hematopoietic prostaglandin D synthase
Hsp90	Heat shock protein 90

HSQC	Heteronuclear single-quantum correlation spectroscopy
HTS	High throughput screening
IgE	Immunoglobulin E
IgM	Immunoglobulin M
IKK	I κ B kinase
IL-1 β	Interleukin-1 β
IP	I prostanoid receptor
IPTG	Isopropyl- β -D-thiogalactopyranoside
KI	Knock-in
KO	Knockout
LC	Liquid chromatography
LLC	Lewis lung carcinoma
LOX	Lipoxygenase
L-PGDS	Lipocalin type prostaglandin D synthase
LPS	Lipopolysaccharide
LT	Leukotriene
LTA4H	Leukotriene A ₄ hydrolase
LTC4S	Leukotriene C ₄ synthase
LX	Lipoxin
MALDI	Matrix-assisted laser desorption/ionization
MAPEG	Membrane-associated proteins in eicosanoid and glutathione metabolism
MDA	Malondialdehyde
MGST	Microsomal glutathione transferase

MPGES	Microsomal prostaglandin E synthase
MRP	Multidrug resistance protein
MS	Mass spectrometry
MWCO	Molecular weight cut-off
NADH	Nicotinamide adenine dinucleotide
NADPH	Nicotinamide adenine dinucleotide phosphate
NEM	<i>N</i> -ethylmaleimide
NF- κ B	Nuclear factor- κ B
NMR	Nuclear magnetic resonance
NOESY	Nuclear Overhauser effect spectroscopy
NSAID	Non-steroidal anti-inflammatory drug
OA	Osteoarthritis
PAGE	Polyacrylamide gel electrophoresis
PDB	Protein Data Bank
PG	Prostaglandin
PGDS	Prostaglandin D synthase
PGES	Prostaglandin E synthase
PGIS	Prostacyclin synthase
PGI ₂	Prostacyclin
PGP	Pro-Gly-Pro chemotactic tripeptide
PLA ₂	Phospholipase A ₂
PMN	Polymorphonuclear cells
PPAR γ	Proliferator-activated receptor γ

RA	Rheumatoid arthritis
RBL	Rat basophilic leukemia
SDS	Sodium dodecyl sulfate
SRM	Single reaction monitoring
TBA	Thiobarbituric acid
TGF- β 1	Transforming growth factor- β 1
THF	Tetrahydrofuran
TM	Transmembrane helix
TNF- α	Tumor necrosis factor- α
TP	T prostanoid receptor
Tris	Tris(hydroxymethyl)aminomethane
Triton X-100	α -[4-(1,1,3,3-Tetramethylbutyl)phenyl]- ω -hydroxy-poly(oxy-1,2-ethanediyl)
TX	Thromboxane
TXS	Thromboxane synthase
VEGF	Vascular endothelial growth factor
WT	Wild-type

CHAPTER I

INTRODUCTION

Inflammation

Inflammation is an immune response involving a series of complex events on a microscopic scale that includes responses such as vasodilation and increases in vascular permeability and blood flow.¹ The release of pro-inflammatory mediators following exposure to toxic chemicals, microbial infection, or tissue injury launches a series of signaling cascades that destroy the invasive pathogen and repair tissue damage.² Acute inflammation, characterized by pain, heat, redness, swelling, and loss of function, is a protective response that is an important aspect of the healing process.³

The inflammatory response, however, is also implicated in a variety of disease states. Because inflammation can occur as a result of exposure to toxins and tumor growth, deficiencies in the inflammatory response can compromise the host.¹ In addition, when acute inflammation is unresolved and escalates to a state of chronic inflammation, it can lead to organ failure or one of many diseases including atherosclerosis, Alzheimer's disease, rheumatoid arthritis (RA), and cancer, amongst others.⁴

Inflammatory Diseases

There are several types of immunopathologic inflammatory processes. For example, allergic inflammation involves the stimulation of immunoglobulin E (IgE) production in response to certain antigens.⁵ Subsequent binding of IgE to receptors on

basophils and mast cells results in the secretion of cytoplasmic granules including histamine, as well as the production of pro-inflammatory mediators such as leukotrienes (LTs). This signaling results in altered blood flow, increased vascular permeability and bronchoconstriction, reactions that are commonly associated with allergic responses including seasonal allergies and asthma.

Inflammation is also mediated by cytotoxic antibodies including complement-fixing antibodies, a component of the complement system that clears pathogens from the host as part of the innate immune system.⁶ Binding of IgG or IgM to an antigen, however, can lead to complement activation and deposition of complement fragments on the cellular surfaces of erythrocytes, platelets, or leukocytes, which activate the complement cascade leading to the generation of pro-inflammatory mediators. Many rheumatic diseases, such as lupus erythematosus, are associated with the development of antibodies to cells.

Similarly to cytotoxic antibody-induced inflammation, inflammatory signaling can be mediated by immune complexes.⁷ Following complement activation by IgG- or IgM-antigen complexes, several complement-derived peptides with pro-inflammatory activity are generated and deposited in various tissues. This can lead to the release of toxic metabolites and pro-inflammatory cytokines from phagocytes that cause damage to blood vessels, hemorrhagic necrosis and local tissue destruction, resulting in rheumatic diseases including RA.

Another type of immunopathologic inflammatory process is known as delayed-type hypersensitivity. After exposure of an antigen to skin, allergic reactions occur within minutes and complement activation-mediated reactions occur within 24 hours, while

delayed-type hypersensitivity reactions peak at 48 to 72 hours.² When antigens are recognized by receptors on T lymphocytes, the production of cytokines is stimulated, attracting and activating neutrophils, macrophages, and other lymphocytes, leading to inflammatory responses. While delayed-type hypersensitivity reactions appear to be important for the destruction of intracellular parasites, tumor cells, and viruses, they are also associated with diseases such as tuberculosis and polymyositis.

Therapeutic Treatment of Inflammation

The therapeutic treatment of inflammation predates modern medicine. Ancient Egyptians, circa 1500 B.C., utilized the bark of willow trees to treat stiff and painful joints as noted in the Ebers papyrus, a medical text containing various therapeutic treatments for physical and mental diseases.⁸ One thousand years later, ancient Greek physicians continued to recommend various willow tree preparations to alleviate pain, fever, and inflammation.⁹ The first clinical trial of willow bark for the treatment of inflammation was performed by the reverend Edward Stone in 1763, in which he successfully treated fever in 50 patients using powdered willow bark suspended in water, tea, or beer.⁸

It was not until 1828 that the active anti-inflammatory component of willow bark, salicin (Figure 1), was isolated by Johann Andreas Buchner.¹⁰ Named after the Latin for its source, *Salix alba*, salicin can be hydrolyzed then oxidized to yield salicylic acid, a process first discovered by Raffaele Piria in 1838.¹⁰ Salicylic acid possesses potent anti-inflammatory properties, and thanks to the design of its *de novo* synthesis by Hammond Kolbe, salicylic acid was produced on an industrial scale beginning in 1874.¹⁰

Motivated by his father's intolerance of salicylic acid due to its relatively severe gastrointestinal side-effects and bitter taste, Felix Hoffmann, a chemist working for Bayer in Germany, developed the derivative acetylsalicylic acid in 1897.⁸ The drug was introduced to the market in 1899 under the trade name Aspirin, derived from *A* for acetyl, *spir* for the meadowsweet tree *Spiraea ulmaria* in which salicylic acid is naturally produced, and *in* for the then-common suffix of medicines.¹⁰ Though aspirin possesses some gastrointestinal side-effects similar to, though less severe than, that of salicylic acid, it has several effective therapeutic properties including the resolution of inflammation, reduction of fever, curing of headaches, and inhibition of platelet aggregation.^{8,11}

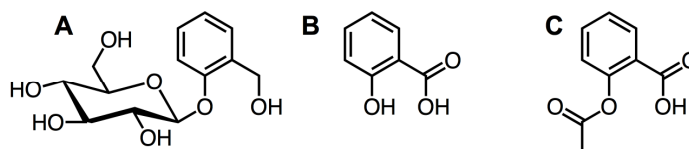


Figure 1. Compounds for the therapeutic treatment of inflammation. (A) Salicin is a β -glucoside alcohol naturally produced in the bark of willow trees. (B) The hydrolysis and subsequent oxidation of salicin produces salicylic acid, a monohydroxybenzoic acid that possesses potent anti-inflammatory properties. (C) Acetylsalicylic acid, introduced to the market as “aspirin,” is a derivative of salicylic acid that has similar therapeutic properties with fewer adverse side effects.

For nearly fifty years, aspirin remained the only commercially available non-steroidal anti-inflammatory drug (NSAID), until phenylbutazone, phenacetin, and phenazone were developed in 1940s as therapeutic treatments for arthritis and other painful inflammatory diseases.¹² As a result of the development of animal models, the 1950s and 1960s saw the syntheses of indomethacin and ibuprofen, both of which are still commonly used today.¹³ These two drug discoveries were followed by a large-scale

effort by many pharmaceutical companies to develop a range of new NSAIDs including numerous derivatives of ibuprofen, piroxicam, mefenamic acid, and diclofenac amongst others.^{12,14,15} Though great efforts were made in the development of these drugs during this time period, little was known with respect to how they worked.

Immense strides were subsequently made with respect to research involving the biology of inflammation and the bioactivities of NSAIDs. In 1971, Vane, Smith, and Willis defined the mechanism of action of these drugs as the inhibition of the enzymatic production of prostaglandins (PGs).^{16, 17} PGs were discovered in the 1930s as a depressor substance in seminal fluid, and since then their biological significance has become well characterized.¹⁸ These lipid-derived compounds are mediators of a wide range of normal physiological functions as well as several pathological processes.¹⁹ The biosynthesis and biological activities of these signaling molecules are the focus of the following section of this introduction.

The defensive response of inflammation is crucial to the healing process from damage caused by toxins, physical trauma, or infection. Inflammation, though, can lead to immunopathologic inflammatory processes, resulting in various types of inflammatory diseases. The critical role that inflammation plays in pathologic events makes its regulation crucial to the prevention and treatment of various diseases, hence the importance and prominence of drugs such as NSAIDs.

The therapeutic treatment of inflammation dates back thousands of years. The success of NSAIDs as a treatment for inflammatory conditions such as RA and osteoarthritis (OA) highlight their pharmacological importance. Still, there is room for progress. The fact that aspirin was used for nearly one hundred years before its

mechanism of action was determined is telling of this. Ongoing research into the mechanisms that generate and regulate the inflammatory response are clearly needed for the benefit of those who suffer from inflammatory diseases.

Eicosanoids

Metabolites of polyunsaturated fatty acids serve as potent signaling molecules that regulate various cellular responses through receptor-mediated pathways.^{19,20} One such class of mediators are metabolized from arachidonic acid (Figure 2), which is derived from the essential fatty acid linoleic acid supplied in the diet.²⁰ The twenty-carbon molecule arachidonic acid contains four non-conjugated carbon-carbon double bonds at positions C-5, C-8, C-11, and C-14. As the Greek word for twenty is *eikosi*, arachidonic acid-derived mediators are referred to as *eicosanoids*. Eicosanoids are hormone-like molecules with potent signaling effects at low concentrations.¹⁹ However, unlike hormones, they are not transported by the circulatory system due to their biochemically unstable nature and thus act locally as autocrine or paracrine mediators of physiological and pathological functions.²¹

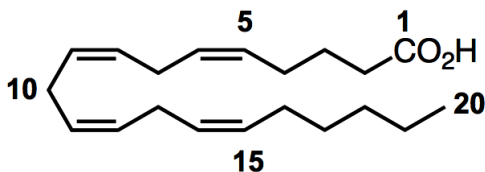


Figure 2. Arachidonic acid. Metabolized from the essential fatty acid linoleic acid, arachidonic acid is a 20-carbon carboxylic acid with four *cis* double bonds. Signaling molecules that are derived from arachidonic acid are known as *eicosanoids*.

Arachidonic acid metabolism is a critical process that is mediated by a multitude of enzymes. Stored in cells as a component of the membrane bilayer, arachidonic acid is esterified at the *sn*-2 position of the glycerol moiety of phospholipids.²² Phospholipase A₂ (PLA₂) hydrolyzes the acyl group at this *sn*-2 position, yielding free arachidonic acid.²³ Once released from the membrane, arachidonic acid is metabolized along one of several routes, forming distinct classes of eicosanoids. Cytochrome P450 (CYP) enzymes utilize arachidonic acid as a substrate to form epoxyeicosatrienoic acids (EETs), hydroxyeicosatetraenoic acids (HETEs), and dihydroxyeicosatrienoic acids (DHETs).²⁴ The LTs, lipoxins (LXs), and eoxins (EXs) arise from lipoxygenase (LOX) metabolism,²⁵ and prostanoids including PGs and thromboxane (TX) are arachidonic acid derivatives formed via the cyclooxygenase (COX) pathway.^{26,27} These classes of eicosanoids are discussed here, with particular emphasis placed on the prostanoids.

Prostanoids

Prostanoids are structurally unique among the eicosanoids, in that they possess a five- or six-membered ring within their carbon chain, whereas the other classes consist of linear carbon chain molecules. Synthesis of the prostanoids is initiated by the release of arachidonic acid from the lipid bilayer, an activity of cytosolic PLA₂ (cPLA₂), which is translocated to the membrane as a result of the mobilization of intracellular calcium.^{28,29} In this way, cPLA₂ plays a substrate-limiting role in the regulation of prostanoid synthesis. The membrane-anchored enzyme COX then catalyzes the committed step in prostanoid synthesis. This heme-dependent *bis*-oxygenation and cyclization of arachidonic acid forms the lipid endoperoxide-hydroperoxide intermediate PGG₂.²⁶ A

separate peroxidase site within the same enzyme then catalyzes the reduction of the hydroperoxide, giving PGH₂.³⁰ PGH₂ does not accumulate but is quickly converted into biologically relevant mediators by specific terminal synthases.

Cyclooxygenase

The mechanism by which COX oxygenates arachidonic acid to PGG₂ has been well-characterized (Figure 3).³¹⁻³³ COX-bound arachidonic acid is positioned by hydrogen-bonding interactions between the carboxyl group of the substrate and Arg-120 of the enzyme. The first chemical step of the mechanism is performed by a heme-generated tyrosyl radical at position 385, which oxidizes arachidonic acid by abstracting the pro-*S* hydrogen at position C-13, developing a carbon radical at C-11. Oxygen insertion then occurs at C-11 on the opposite side of hydrogen abstraction, generating an 11(*R*)-hydroperoxyl radical. This then adds to C-9, forming a cyclic peroxide and a carbon radical at C-8. A second cyclization reaction occurs as the radical at C-8 adds to C-12, generating a radical that is delocalized over C-13 to C-15. Finally, a second molecule of oxygen is added to C-15, producing a 15-hydroperoxyl radical that abstracts a hydrogen atom from Tyr-385, giving rise to PGG₂. From here, PGG₂ is transferred to the peroxidase site within the same enzyme where the C-15 hydroperoxide is reduced to the corresponding hydroxyl group, forming PGH₂.

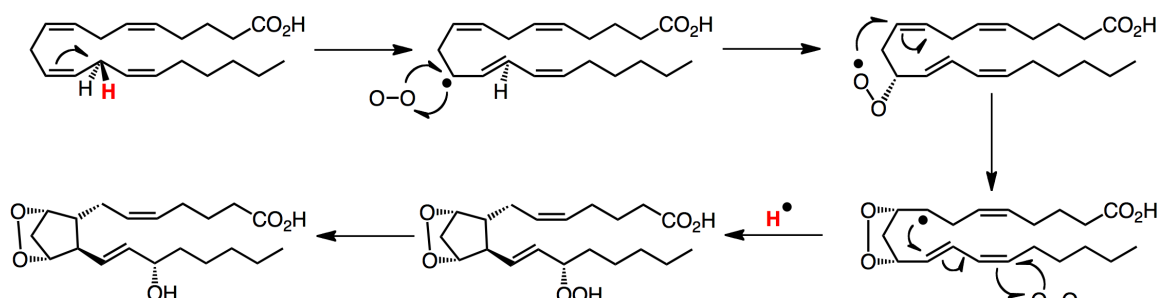


Figure 3. Chemical mechanism of the cyclooxygenase reaction. The reaction is initiated at the cyclooxygenase site of COX. Abstraction of the pro-*S* hydrogen at position C-13 by a Tyr-385 radical is followed by O₂ addition to C-11, forming an 11(*R*)-hydroperoxyl radical. An endoperoxide is then formed by reaction of the oxygen radical with C-9, centering the radical at position C-8. The cyclization reaction is completed by bond formation of C-8 to C-12, centering the radical at position C-15. The addition of a second molecule of oxygen to C-15 is followed by addition of a hydrogen atom from Tyr-385, forming PGG₂. Finally, the reduction of the hydroperoxide at C-15, catalyzed at the peroxidase site of COX, results in the formation of PGH₂.

The membrane-anchored enzyme, COX, is located on the luminal surface of the endoplasmic reticulum (ER) and the inner membrane of the nuclear envelope.³⁴ There are two isoforms of COX, denoted COX-1 and COX-2. Although the two enzymes catalyze the same reactions and their amino acid sequences are about 65% identical, they differ in their expression pattern and biological function.³⁵ COX-1 is typically a constitutive enzyme, expressed in a wide range of tissues and is assumed to maintain homeostatic levels of the primary prostanoids, which regulate biological processes such as gastric mucosal maintenance, renal blood flow, and platelet function.³⁶ COX-2, on the other hand, is an inducible enzyme whose expression is up-regulated by a series of inflammatory stimuli, including pro-inflammatory cytokines, lipopolysaccharide (LPS), epidermal growth factors (EGF), and hormones.³⁷ The induction of COX-2 expression is associated with pain, fever, inflammation, neurological disorders, and several types of cancer.³⁶ The product of COX, PGH₂, serves as a substrate for several terminal synthases

that catalyze the formation of PGD₂, PGE₂, PGF₂, PGI₂ (prostacyclin), and TXA₂ (Figure 4).³⁸⁻⁴² The activities of these enzymes are summarized below.

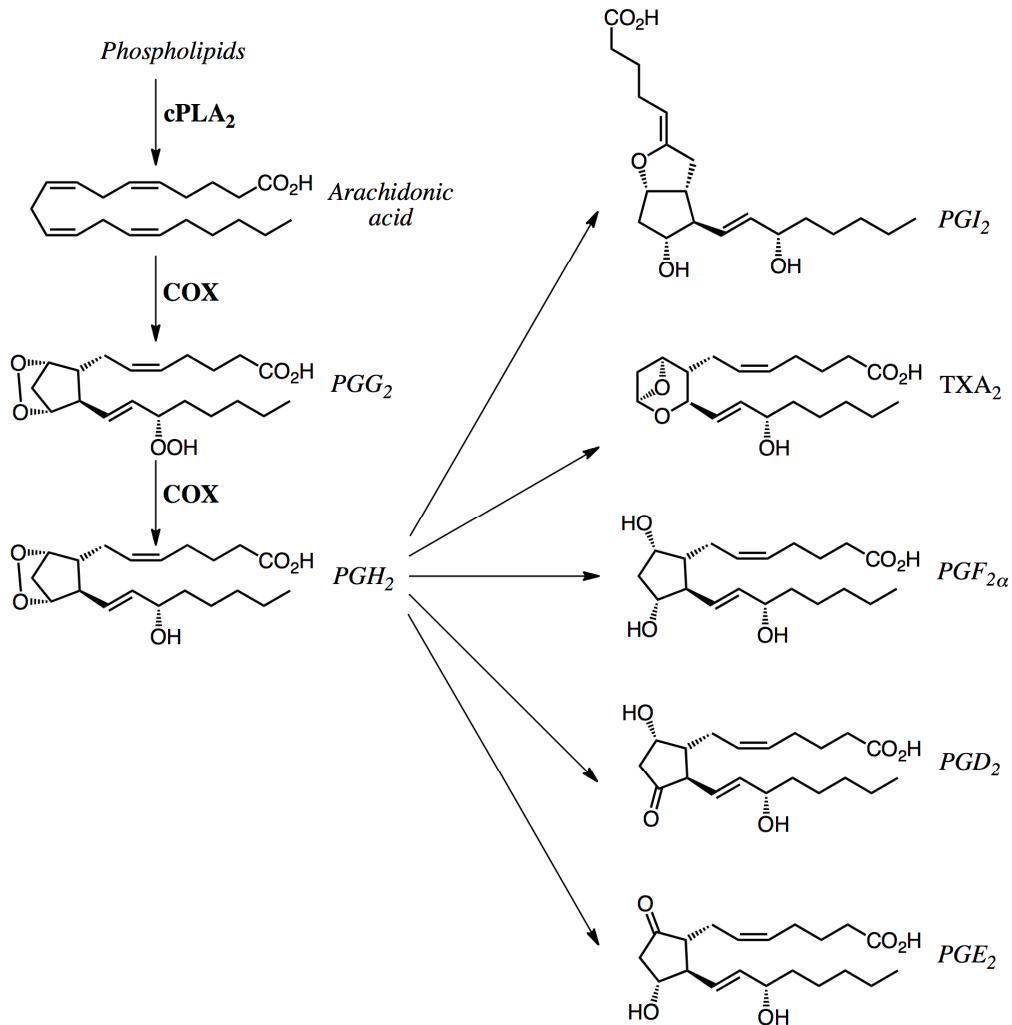


Figure 4. The prostanoid cascade. The prostanoids are lipid mediators that include the prostaglandins PGD₂, PGE₂, and PGF_{2α}, prostacyclin (PGI₂) and thromboxane (TXA₂). The formation of prostanoids is catalyzed by one of several terminal synthases that utilize PGH₂ as a substrate.

PGD Synthase

PGD synthase (PGDS) catalyzes the isomerization of the 9,11-endoperoxide group of PGH₂, resulting in 9-hydroxy and 11-keto groups on the prostane ring. There are

two types of PGDS enzymes including the lipocalin type (L-PGDS) and the hematopoietic enzymes (H-PGDS).^{43,44} L-PGDS activity requires a sulfhydryl-containing compound such as glutathione (GSH), dithiothreitol (DTT), 2-mercaptoethanol (β ME), or cysteine and is predominately expressed in the central nervous system, by epithelial cells, and by Leydig cells in the testis.^{43,44} H-PGDS is a cytosolic GSH transferase (GST) enzyme that specifically requires GSH as a cofactor for its activity and is expressed in immune and inflammatory cells.^{43,45}

PGE Synthase

Similarly to PGDS, PGE synthase (PGES) isomerizes the endoperoxide of PGH_2 , but the catalysis results in the keto and hydroxyl groups in positions that are opposite to that of PGD_2 . There are three PGES enzymes, including a cytosolic protein (CPGES) and two membrane-bound proteins (MPGES1 and MPGES2).⁴⁶⁻⁴⁸ CPGES, similarly to H-PGDS, is a member of the cytosolic GST family of proteins, and it is identical to the heat shock protein 90 (Hsp90)-binding protein, p23.⁴⁸ CPGES is a constitutive enzyme that is expressed in most cells and displays a marked preference for COX-1-derived PGH_2 over that of COX-2, suggesting that CPGES produces homeostatic levels of PGE_2 .⁴⁸

The integral membrane protein MPGES1 is a GSH-dependent enzyme whose expression is induced by pro-inflammatory stimuli, such as LPS, interleukin- 1β (IL- 1β), and tumor necrosis factor- α (TNF- α).⁴⁹ It is co-localized with COX in the same subcellular compartments, the perinuclear membrane, and the ER.³⁴ Since its localization and regulation are both coupled with that of the inducible COX-2, MPGES1 is associated with the induced production of PGE_2 .⁵⁰

The third PGES enzyme, MPGES2, is a membrane-anchored protein that, unlike CPGES and MPGES1, is not dependent on GSH.⁴⁷ While the enzyme can utilize GSH as a cofactor, it can also use other thiols such as β ME, DTT, or a native cysteine residue within the active site to catalyze the isomerization of PGH₂.⁵¹ While MPGES2 is a constitutive enzyme, it displays no preferential functional coupling to either COX-1 or COX-2.⁵²

PGF Synthase

PGF₂ prostanoids are widely distributed in tissues throughout the body and can be formed through metabolism of PGH₂, PGD₂, or PGE₂ (Figures 4 and 5). The PGH₂ isomerase 9,11-endoperoxide reductase, whose activity results in the formation of hydroxyl groups at both the C-9 and C-11 positions of the cyclopentane ring, produces PGF_{2 α} in the presence of nicotinamide adenine dinucleotide (NADH) or NADH phosphate (NADPH).⁴³ This membrane-associated protein is GSH-dependent and is a member of the GST family of proteins.⁵³

Another method by which PGF_{2 α} is formed is via reduction of the keto group of PGE₂ by PGE 9-ketoreductase, which is a cytosolic enzyme dependent on NADH or NADPH, and possesses a high sequence similarity to aldo-keto reductase (AKR) superfamily members.⁴³ Similarly, the keto group of PGD₂ may be reduced by PGD 11-ketoreductase, a NADH- or NADPH-dependent enzyme with high homology to the AKR superfamily.⁵³ Unlike PGE 9-ketoreductase, however, reduction of PGD₂ by PGD 11-ketoreductase results in the formation of 9 α ,11 β -PGF₂.

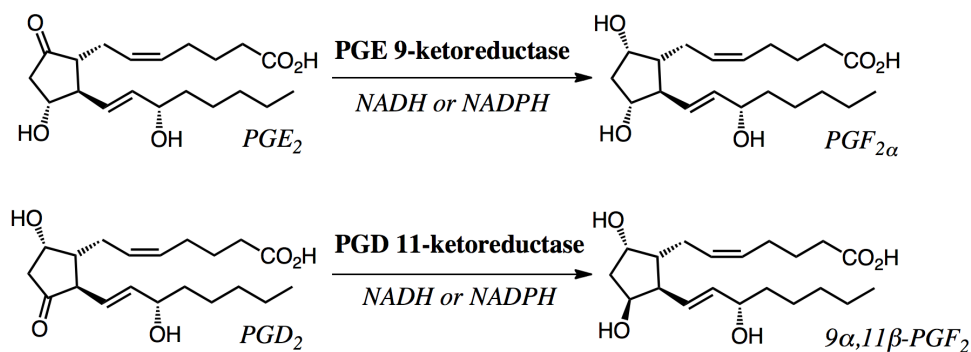


Figure 5. Synthesis of PGF₂. The formation of PGF_{2α} is catalyzed by the isomerization of PGH₂ by 9,11-endoperoxide reductase or by the reduction of PGE₂ by PGE 9-ketoreductase. The formation of 9α,11β-PGF₂ is catalyzed by the reduction of PGD₂ by PGD 11-ketoreductase.

PGI and TX Synthases

The unstable prostanoid PGI₂ is metabolized from PGH₂ by PGI synthase (PGIS), a membrane-bound hemoprotein belonging to the CYP superfamily and located in endothelial and smooth muscle cells.⁴¹ The catalytic activity of PGIS is different from the previously discussed prostanoid synthases, in that it catalyzes the rearrangement of the endoperoxide of PGH₂, forming an oxygen-containing heterocycle, as opposed to the traditional five-membered prostane ring structure.⁵⁴

Another unstable prostanoid, TXA₂, is synthesized from PGH₂ by the heme-dependent, membrane-bound, CYP family member TX synthase (TXS), which is expressed in platelets and macrophages.⁵⁵ Like PGIS, the TXS isomerization of PGH₂ results in the generation of an unstable oxygen-containing heterocycle.⁵⁴

Prostanoid Signaling

The biological signaling effects of prostanoids are carried out by specific binding to cell-surface G protein-coupled receptors (GPCRs). These include the D prostanoid

(DP) receptors DP1 and DP2 for PGD₂, EP1, EP2, EP3, and EP4 for PGE₂, FP for PGF₂, IP for PGI₂, and TP for TXA₂.⁵⁶ All of the prostanoid receptors are class A rhodopsin-like receptors with the exception of DP2, which belongs to the leukocyte chemoattractant receptor family.⁵⁷ The cellular responses that prostanoids elicit are dependent upon the type and condition of cell in which they are produced. As such, they are mediators of a wide range of biological responses including vascular permeability, platelet aggregation, smooth muscle tone, pain, and fever.⁵⁸⁻⁶²

Prostanoids are molecules with an array of normal physiological signaling effects. For instance, a major mediator of sleep-wake processes is PGD₂, in that it promotes physiological sleep and is a regulator of body temperature during sleep.⁶³ Prostanoids also have important signaling effects related to reproduction, in that PGE₂ softens the cervix and causes uterine contraction during labor, and PGF_{2α} induces labor.⁵⁶ Bone health is also a regulatory signaling function of prostanoids, given that PGE₂ stimulates bone resorption by osteoclasts.⁵⁶

Also, the maintenance of cardiovascular (CV) homeostasis is a central role of prostanoid signaling. The mediators PGD₂, PGE₂, and PGI₂ are all vasodilators, while TXA₂ is a vasoconstrictor.⁶⁴ The importance of prostanoid signaling in CV health is highlighted by the important balance of PGI₂ and TXA₂, which are anti-thrombotic and pro-thrombotic mediators, respectively.^{65,66} As is the case with PGI₂, 9α,11β-PGF₂ also inhibits TXA₂-induced platelet aggregation.⁵³

Prostanoids not only regulate normal biological processes but are also mediators involved in pathology. By activating their corresponding receptors, these lipid mediators have a direct effect on the production of chemokines, cytokines, and growth factors, as

well as expression levels of several pro-inflammatory enzymes.⁵⁶ PGs in general, and PGE₂ and PGI₂ in particular, are detected in nearly all experimental models of inflammation, as well as in the synovial fluid of arthritic patients.⁶⁷ In addition to PGE₂ and PGI₂ being predominant pro-inflammatory signaling molecules, PGE₂ is a potent pyretic agent; both PGF_{2α} and 9α,11β-PGF₂ cause contraction of bronchial, vascular, and arterial smooth muscle, and many of the prostanoids exert immuno-suppressive effects.⁶⁸⁻⁷¹ PGE₂ in particular has been implicated in increased susceptibility to infection, including several forms of cancer.⁷²

Playing yet another role in pathology, prostanoids not only propagate pathological processes – they can stimulate their resolution. A subset of prostanoids called cyclopentenone PGs (cyPGs) are non-enzymatic dehydration products of PGD₂ and PGE₂ (Figure 6), resulting in the PGJ₂ and PGA₂ series, respectively, of which some possess anti-inflammatory, anti-neoplastic, and anti-viral properties.⁷³ Electrophilic centers on the cyclopentenone rings of these cyPGs can form Michael adducts with sulfhydryl groups of intracellular regulatory proteins, modulating their function.⁷⁴ For instance, 15-deoxy-Δ^{12,14}-PGJ₂ (15d-PGJ₂) can bind to peroxisome proliferator-activated receptor γ (PPARγ), IκB kinase (IKK), or nuclear factor-κB (NF-κB) *in vitro*, each event resulting in the inhibition of the DNA binding activity of NF-κB, and having the effect of down-regulating several pro-inflammatory genes.⁷⁵⁻⁷⁷ It should be noted, however, that a great amount of uncertainty remains regarding the significance, or even the existence, of cyPGs *in vivo*.^{78,79}

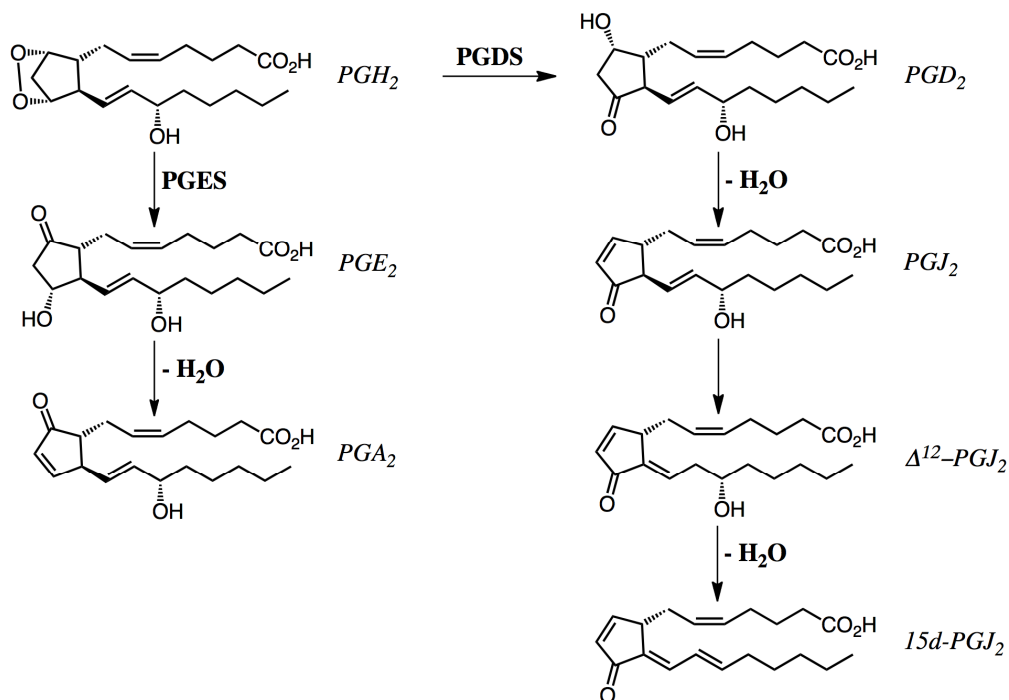


Figure 6. Cyclopentenone prostaglandins. Spontaneous dehydration of PGE_2 leads to the formation of the cyPG PGA_2 . Multiple steps of dehydration and isomerization of PGD_2 lead to the formation of the PGJ_2 series of cyPGs. These lipid mediators have been implicated as signaling molecules that promote the resolution of inflammation.

Prostanoids play a delicate and complex role in the regulation of normal biological processes, the propagation of pathological events, and the resolution of such events. They are clearly important lipid mediators involved in a multitude of signaling pathways. Their importance is highlighted by the common therapeutic inhibition of COX enzymes. As summarized in the previous section of this introduction, NSAIDs are widely used as therapeutics for the treatment of pain, inflammation, and fever. The pharmaceutical mechanism of action of these small molecules involves the inhibition of COX, which subsequently inhibits primary prostanoid synthesis.¹⁶

Since the isoform COX-2 has been associated with inflammation and several forms of cancer, COX-2-selective drugs (coxibs) such as celecoxib and rofecoxib were developed to better target the synthesis of specific prostanoids, particularly PGE_2 .^{80,81}

Since drugs that target the COX enzymes are relatively non-specific for the inhibition of prostanoid production, treatment can lead to adverse gastrointestinal and cardiovascular side effects, which is described in more detail later in this introduction.^{82,83} In order to minimize such side effects, the specific targeting of the terminal prostanoid synthases immediately downstream of the COX enzymes holds promise as an alternative to treatment with NSAIDs and coxibs, but such drugs are not currently available. Though prostanoid research has progressed substantially for over half a century, much more progress is yet to be made.

Leukotrienes

Another pathway by which arachidonic acid may be metabolized is by way of LOX enzymes, which are non-heme, iron-containing dioxygenases. Of particular interest is the enzyme 5-LOX, which catalyzes the formation of LTs (Figure 7), potent mediators of inflammation that are associated with acute and chronic inflammatory diseases such as asthma, rhinitis, and atherosclerosis.^{84,85} There are several isoforms of LOX including 5-, 12-, and 15-LOX, named for the carbon position of arachidonic acid to which they add molecular oxygen, and they are present in leukocytes, platelets, and endothelial cells, respectively.⁸⁶⁻⁸⁸ Since 5-LOX synthesizes LTs and generates potent mediators of the allergic response, it has become the most widely studied of the isoforms with respect to inflammation research.

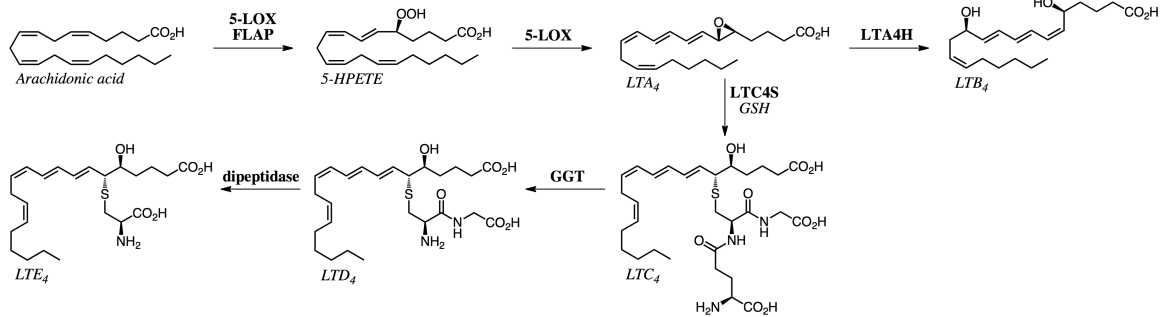


Figure 7. The leukotriene cascade. Arachidonic acid is metabolized by the non-heme, iron-containing dioxygenase 5-LOX, resulting in the formation of LTA₄. This fatty acid serves as a substrate for LTA₄ hydrolase and LTC₄ synthase in the ultimate synthesis of LTB₄, LTC₄, LTD₄, and LTE₄, which are potent mediators of the allergic response.

The 5-LOX cascade of arachidonic acid metabolism requires the formation of a multi-protein complex at the nuclear membrane that is induced by several immune and inflammatory signals.⁸⁹ Similarly to the initiation of the COX pathway, cPLA₂ is phosphorylated and translocated to the membrane along with 5-LOX as a result of the mobilization of intracellular calcium, at which point arachidonic acid is released from the lipid bilayer by cPLA₂.^{28,90} Upon 5-LOX translocation to the membrane, the membrane-bound 5-LOX-activating protein (FLAP) acts as a scaffold, theoretically playing the role of delivering arachidonic acid to 5-LOX.^{89,91}

5-LOX converts arachidonic acid to the unstable lipid epoxide LTA₄ in a two-step process with 5-hydroperoxyeicosatetraenoic acid (5-HPETE) as an intermediate.⁹² LTA₄ is subsequently metabolized along one of two routes, being utilized as a substrate by either LTA₄ hydrolase (LTA₄H) or LTC₄ synthase (LTC₄S). LTA₄H is a widely distributed protein in almost all mammalian cells that converts LTA₄ to the chemotactic agent LTB₄ via epoxide hydrolysis.⁹³ Though LTB₄ is generally considered to be a proinflammatory compound, LTA₄H may also play a role in the resolution of inflammation, in that it degrades the chemotactic tripeptide Pro-Gly-Pro (PGP).⁹⁴

LTC₄S, which catalyzes the addition of the tripeptide GSH to the epoxide of LTA₄ to form LTC₄, has been observed in eosinophils, mast cells, and monocytes.⁹⁵ The tripeptide moiety of LTC₄ may subsequently undergo successive hydrolysis steps to generate LTD₄ and LTE₄. This class of LTs, called cysteinyl-leukotrienes (Cys-LTs) and previously known as the *slow-reacting substance of anaphylaxis*, is highly implicated in inflammatory diseases including asthma.⁹⁶ While there continues to be uncertainty as to which enzymes catalyze the formation of LTD₄ and LTE₄ *in vivo*, the γ -glutamyl residue of LTC₄ can be cleaved by γ -glutamyl transpeptidase (GGT) forming LTD₄, and the remaining glycyl moiety of LTD₄ can then be hydrolyzed by several dipeptidases, forming LTE₄.⁹⁷⁻¹⁰²

Prior to hydrolysis, LTC₄ is exported from the cell by multidrug resistance protein (MRP) 1 and MRP2.¹⁰³ LTB₄ is also typically exported from the leukocyte, but the mechanism of its secretion is not fully understood.¹⁰⁴ The signaling effects of LTs are carried out by binding to rhodopsin-class receptors located at the plasma membrane of structural and inflammatory cells, including B LT receptor 1 (BLT1) and BLT2 for LTB₄ and Cys-LT receptor 1 (CysLT1) and CysLT2 for the Cys-LTs.^{105,106}

LTs are lipid mediators that contribute to a variety of inflammatory and allergic diseases. LTB₄ is a chemoattractant and activator of neutrophils, monocytes, and lymphocytes,^{105,107,108} LTD₄ attracts eosinophils,¹⁰⁹ and all Cys-LTs increase vascular permeability.¹⁰⁹ Recent evidence suggests, however, that LT signaling also facilitates the host response against various types of infection,¹¹⁰ and they may even play a role in anti-inflammation signaling.¹¹¹

LTs represent an important class of arachidonic acid metabolites. They have a clear role in the initiation and propagation of inflammatory diseases and the allergic response, particularly with respect to asthma. This is underlined by the fact that asthma is therapeutically treated with 5-LOX inhibitors, such as zileuton, which is sold under the trade name Zyflo.⁹⁶ Similarly, asthma and seasonal allergies are controlled using CysLT1 antagonist drugs like montelukast and zafirlukast, whose trade names are Singulair and Accolate, respectively.⁶⁴ Since the protein FLAP is essential to the initiation of LT synthesis, several FLAP inhibitors are currently in clinical development for the treatment of inflammation.^{50,112} Research regarding LT synthesis and signaling represents fertile ground for scientists with respect to developing treatments for allergic and inflammatory diseases.

Lipoxins and Eoxins

A third pathway of arachidonic acid metabolism involves LOX enzymes in trans-cellular biosynthesis. LXA₄ and LXB₄ may be produced via two different pathways involving such cell-cell interactions (Figure 8). In the first, 5-LOX catalyzes the conversion of arachidonic acid to LTA₄ similarly to the first step of LT synthesis, at which point LTA₄ is transferred to adherent permeabilized platelets and is converted to either LXA₄ or LXB₄ by the oxygenation activity of 12-LOX.¹¹³ In the second pathway, arachidonic acid is first oxygenated by 15-LOX in endothelial cells, producing 15(*S*)-HPETE.¹¹⁴ This is subsequently taken up by polymorphonuclear cells (PMNs) or monocytes, converted to a 5,6-epoxytetraene intermediate by 5-LOX, and hydrolyzed by LXA₄ hydrolase or LXB₄ hydrolase, generating LXA₄ or LXB₄, respectively.¹¹⁵

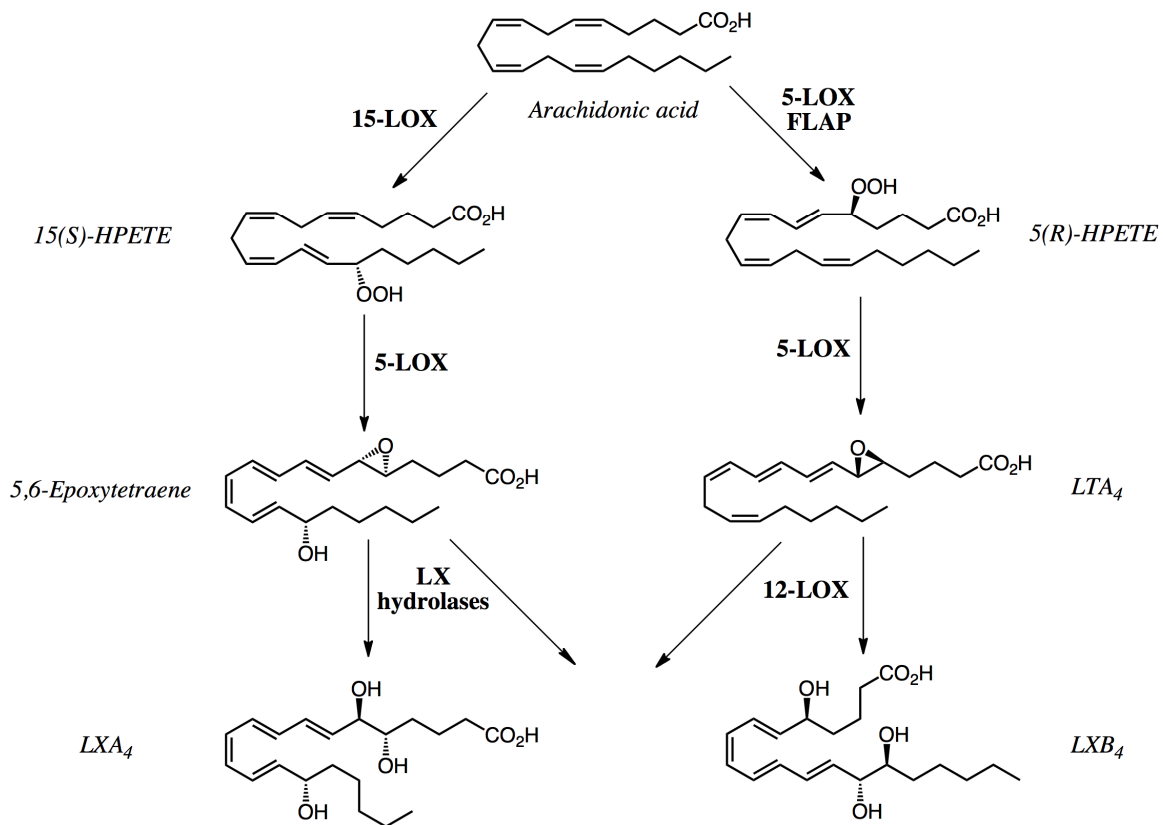


Figure 8. Synthesis of lipoxins. Products of LOX metabolism, lipoxins are arachidonic acid derivatives produced by trans-cellular biosynthesis. They have been implicated as anti-inflammatory lipid mediators.

Another class of LX called aspirin-triggered LX (ATL) is formed in endothelial cells following the acetylation of COX-2 (Figure 9). Therapeutic treatment with aspirin irreversibly acetylates Ser-516 of COX-2, resulting in arachidonic acid conversion to 15(R)-HETE, as opposed to PGG₂.¹¹⁶ This is then taken up by adherent leukocytes and oxygenated by 5-LOX, forming the 15-epimeric-LXs (15-epi-LXs) 15-epi-LXA₄ and 15-epi-LXB₄.¹¹⁷

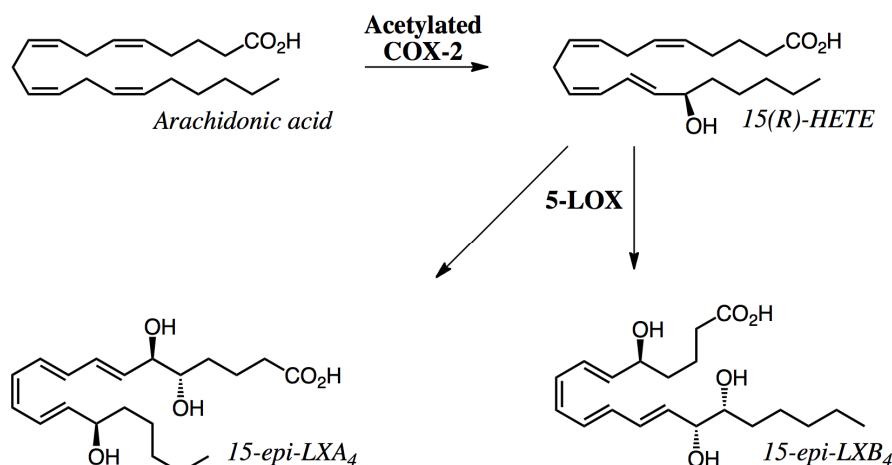


Figure 9. Aspirin-triggered lipoxins. Acetylation of COX-2 results in the trans-cellular formation of aspirin-triggered lipoxins, which may serve biologically as anti-inflammatory and pro-resolution signaling molecules.

Less is known of LX-receptor interactions, as compared to prostanoid- and LT-receptor interactions. However, it is known that LXA₄ and the ATLs bind to the GPCR formyl peptide receptor-like 1 (FPRL-1 or ALX) and that LXs act as partial agonists of the receptor CysLT1.^{118,119} LXs are known as anti-inflammatory and pro-resolution mediators. At nanomolar concentrations, they stimulate macrophages to ingest and clear neutrophils,¹²⁰ and their signaling can elevate the levels of the anti-inflammatory cytokine transforming growth factor-β1 (TGF-β1), which down-regulates several pro-inflammatory genes.¹²¹ LXs reduce the proliferation of fibroblasts, thereby counteracting the fibrotic response and improving tissue remodeling, and they have been observed to provide beneficial effects in various experimental models of infection, inflammation, and inflammatory diseases.¹²²⁻¹²⁸

A relatively recently recognized class of eicosanoids is the EXs (Figure 10). Similar to the metabolism of arachidonic acid by 15-LOX described above, the synthesis of EXs is initiated in eosinophils, mast cells, or nasal polyps by the oxygenation activity

of 15-LOX, giving rise to 15(*S*)-HPETE.¹²⁹ The resulting hydroperoxide is then dehydrated either spontaneously or by the 12-LOX activity of 15-LOX, giving rise to the lipid epoxide 14,15-LTA₄, or so-called EXA₄.¹³⁰ EXA₄ may then be utilized as a substrate by LTC4S, which catalytically adds GSH to the epoxide, forming EXC₄.¹³¹ Similarly to LTC₄, EXC₄ can be further metabolized to EXD₄ and EXE₄, lipid mediators that have similar signaling effects as the Cys-LTs, though less potent.¹³¹

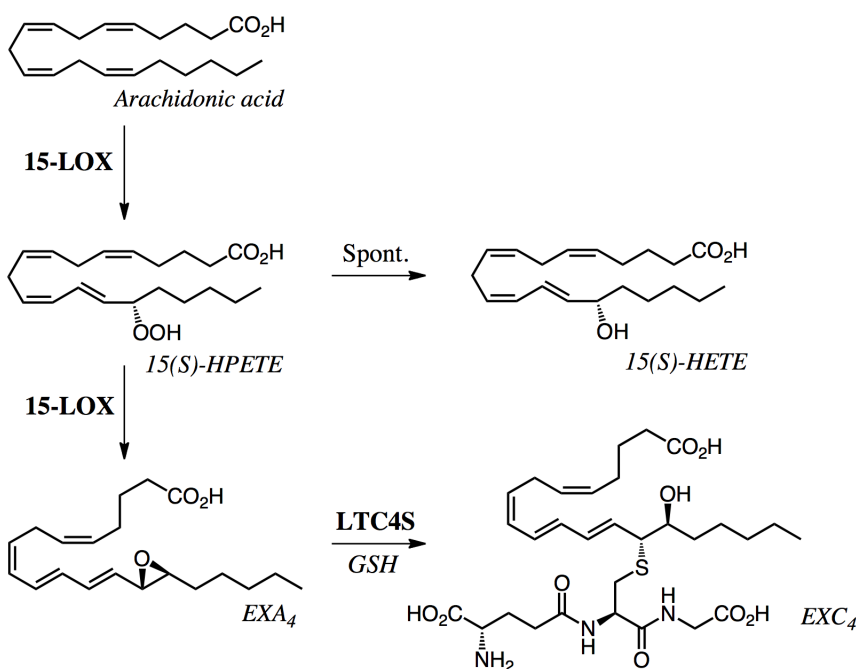


Figure 10. Synthesis of eoxins. Arachidonic acid is metabolized by 15-LOX to the epoxide EXA₄, with 15(*S*)-HPETE as an intermediate. Similar to LTA₄, EXA₄ serves as a substrate for LTC4S for the synthesis of EXC₄, which has similar pro-inflammatory signaling properties as LTC₄.

LXs and EXs represent less well-characterized classes of eicosanoids. They clearly contribute to inflammatory, as well as anti-inflammatory, responses *in vitro*. Being relatively unrecognized yet important classes, they highlight the need for continued eicosanoid research.

Cytochrome P450-derived Eicosanoids

The primary chemistry of the membrane-bound, heme-containing CYP enzymes involves the oxidation of exogenous compounds, including toxins and drugs, as well as carcinogens.¹³² Though less well-characterized than the previously discussed eicosanoids, CYP metabolites of arachidonic acid represent yet another class of these lipid mediators (Figure 11). Oxygenation and hydroxylation of arachidonic acid by CYP enzymes give rise to EETs, HETEs, and DHETs, which have anti-inflammatory and anti-thrombotic signaling properties.¹³³⁻¹³⁵

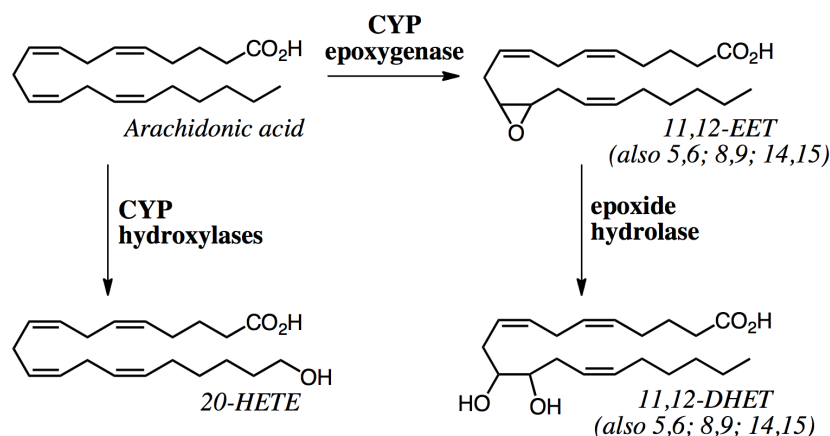


Figure 11. Cytochrome P450-derived eicosanoids. A variety of cytochrome P450 enzymes may utilize arachidonic acid as a substrate for the production of various lipid mediators that may serve as anti-inflammatory and anti-thrombotic signaling molecules.

EETs derive their anti-inflammatory role by inhibiting IKK or by binding to PPAR γ , having the effect of down-regulating several pro-inflammatory signaling pathways downstream of NF- κ B, similar to the bioactivity of 15d-PGJ₂ described above.^{135,136} In addition, EETs inhibit platelet aggregation resulting from vascular injury.¹³⁷ HETEs are anti-inflammatory mediators with respect to the fact that they inhibit

LT biosynthesis, and they are anti-thrombotic in that they have been demonstrated to inhibit TX-induced platelet aggregation.^{138,139}

As with LXs and EXs, the EETs, HETEs, and DHETs represent classes of eicosanoids that are clearly in need of further research. They highlight the important and complex nature of lipid mediators, particularly with respect to those derived from arachidonic acid.

The eicosanoids constitute a widespread and complex family of lipid mediator molecules derived from arachidonic acid. The potent signaling activities of these mediators include a multitude of normal biological processes, as well as the initiation and propagation of pathological events. As eicosanoid research has progressed, the importance of these molecules has been established.

Pathways of polyunsaturated fatty acid oxygenation analogous to that of arachidonic acid metabolism have relatively recently given light to new classes of lipid mediators that possess anti-inflammatory and pro-resolving properties.¹⁴⁰ These so-called *protectins* and *resolvins* include metabolites of the omega-3 fatty acids eicosapentaenoic acid (EPA) and docosahexaenoic acid (DHA).¹⁴¹ While these mediators are not technically eicosanoids, in that they are not derived from arachidonic acid, they do highlight the expanding frontier of research regarding lipid mediator signaling pathways of the inflammatory response. It proves that continued efforts in this field are obviously important to further the understanding of the biology of inflammation.

The MAPEG Superfamily

Glutathione Transferases

GSTs are enzymes with a wide array of activities principally functioning in the metabolic detoxification of xenobiotic and endogenous compounds.¹⁴² GST activity mainly involves the nucleophilic addition of the reduced tripeptide GSH (Figure 12) to compounds containing an electrophilic carbon, nitrogen, or sulfur atom.¹⁴³⁻¹⁴⁵ In addition to GSH conjugation, however, GSTs catalyze reactions as thiol transferases, peroxidases, and isomerases, and they also possess non-catalytic activity including ligand binding.¹⁴⁵⁻¹⁴⁷ GST activity has arisen independently at least four separate times in evolutionary history, resulting in four distinct GST families classified as cytosolic, mitochondrial, bacterial, and microsomal, that are divergent in sequence and structure.^{148,149}

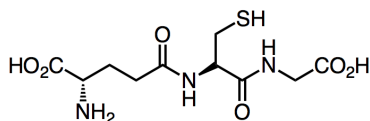


Figure 12. Glutathione. γ -L-Glutamyl-L-cysteinylglycine is the major low-molecular weight thiol in cells of eukaryotes and gram-negative bacteria and is the primary substrate of the glutathione transferases.

The Cytosolic Family

The ancient family of cytosolic GSTs is ubiquitous in all aerobic organisms and is the most abundant of the GST families.¹⁴⁵ It is divided into seven classes, including Alpha, Mu, Pi, Sigma, Theta, Omega, and Zeta, based on sequence similarity and immunological reactivity.¹⁴⁵ Recently, a novel class of cytosolic GSTs termed *Nu* has been described, consisting of unique structural and functional properties.¹⁵⁰ Even though

each monomer of the cytosolic GSTs is catalytically independent, nearly all are active only as dimers, with heterodimerization restricted to subunits belonging to the same class.^{151,152} All cytosolic GSTs, with the exception of the aforementioned Nu class, display a high level of structural conservation with a common three-dimensional fold in addition to the dimeric structural formation. Each subunit is composed of two domains, with the N-terminal GSH-binding thioredoxin domain consisting of β strands and α helices. The C-terminal domain is all-helical and contains a binding site for hydrophobic substrates.^{144,145,153}

The Mitochondrial Family

The mitochondrial family of GSTs, also referred to as the Kappa class, has homologues in eukaryotes and bacteria and is located in mitochondria and peroxisomes.¹⁴⁹ As with the cytosolic family of GSTs, the mitochondrial GSTs possess a thioredoxin GSH-binding domain.^{154,155} Unlike the C-terminal alpha-helical domain of the cytosolic GSTs, though, the equivalent alpha-helical domain is inserted into the thioredoxin domain of mitochondrial GSTs, underlining the divergent evolution of these two families from a common ancestor.^{144,149,154}

The Bacterial Family

The family of bacterial fosfomycin-resistance proteins (Fos) are found in plants, animals, and bacteria.¹⁴⁹ The divalent metal-binding Fos proteins, related to glyoxylases and extradiol dioxygenases, are divided into three classes including FosA, FosB, and FosX, depending on their utilization of GSH, other sulfhydryl-containing compounds, or

H₂O as the primary substrate, respectively.¹⁵⁶⁻¹⁵⁸ The conserved structure of these enzymes is unique from those of the cytosolic and mitochondrial families, underlining another independent evolutionary route of GST activity.¹⁴⁹

The Microsomal Family

What was once termed *the microsomal family* is now known as a widespread superfamily of proteins called the “membrane-associated proteins in eicosanoid and glutathione metabolism” (MAPEG).^{159,160} This is something of a misnomer, however, since hydrophobicity plots and several determined crystal structures suggest that all members possess multiple membrane-spanning regions, making them integral membrane proteins.¹⁶¹⁻¹⁶⁶ They exist in eukaryotes as well as prokaryotes, and six mammalian members of the superfamily have been identified including microsomal GST 1 (MGST1), MGST2, MGST3, LTC4S, FLAP, and MPGES1.^{46,161,167-171} The MAPEG superfamily is discussed in further detail below.

MAPEG Discoveries

MGST1 and LTC4S

The mammalian MAPEG members were discovered in the 1980s and 1990s, with MGST1 the first to be identified. The membrane-bound GST was first isolated in 1982 from rat liver, constituting 2.5 – 3% of the overall microsomal protein.¹⁶⁷ Differences from cytosolic GSTs in molecular weight and substrate specificity, in addition to the fact

that antibodies that react with cytosolic GSTs did not react with MGST1, demonstrated the identification of the first microsomal GST.

Three years later LTC4S was identified when it was observed that the microsomal fraction of rat basophilic leukemia (RBL) cells produced LTC₄ when in the presence of LTA₄ and GSH.¹⁶⁸ Because MGST1 is also capable of catalyzing the addition of GSH to LTA₄ (Figure 13), it was initially uncertain as to whether or not LTC4S and MGST1 were the same protein. However, LTC4S could be chromatographically separated from MGST1. Also, LTC4S was unable to catalyze the addition of GSH to the common laboratory GST substrate 1-chloro-2,4-dinitrobenzene (CDNB), a catalytic function of MGST1. Further, the LTC4S catalytic addition of GSH to LTA₄ proved to be kinetically different than that of MGST1. Finally, the inhibition kinetics by S-hexylglutathione of the LTC₄ synthesis reaction differed between the two enzymes, indicating that LTC4S was not MGST1 but a unique microsomal protein.

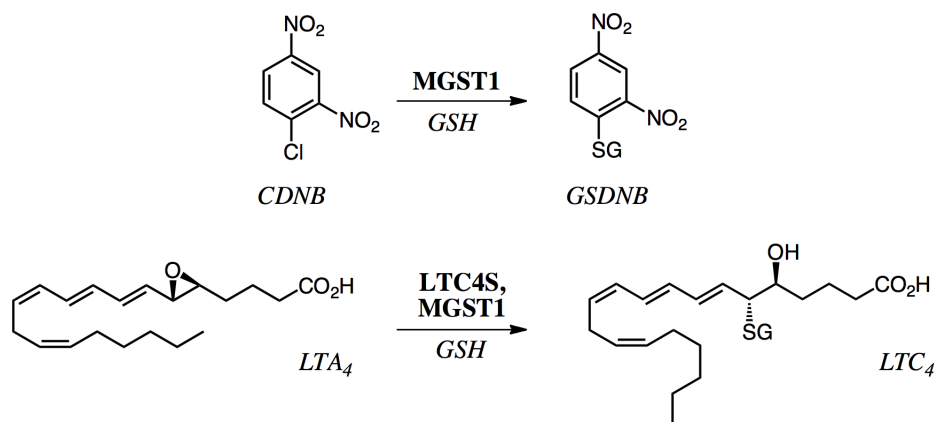


Figure 13. Glutathione transferase activities of microsomal glutathione transferase 1 and leukotriene C₄ synthase. Both MGST1 and LTC4S are capable of catalytically adding GSH to LTA₄, while only MGST1 is capable of utilizing CDNB as a secondary substrate.

FLAP

The identification of FLAP is an interesting story. The enzyme 5-LOX converts arachidonic acid to LTA₄ in a two-step process with 5-HPETE as an intermediate, as described in the previous section of this introduction.^{92,172,173} It was observed in 1989 that the orally active compound MK-886 inhibited LTA₄ synthesis, and it was initially assumed that this molecule bound to 5-LOX. However, it was subsequently realized that, while LT synthesis is inhibited by MK-886 in whole human PMN leukocytes, it has no inhibitory effect on broken cell preparations or purified 5-LOX.¹⁷⁴ The following year, the cellular target of MK-886 was identified using an ¹²⁵I radio-labeled photo-affinity MK-886 analogue. Subsequently, MK-886-linked agarose gels were utilized as affinity matrices to isolate FLAP, the true target of MK-886.¹⁶⁹

MGST2 and MGST3

The remaining three mammalian members of the MAPEG superfamily, MGST2, MGST3, and MPGES1, were identified in the 1990s. A TBLASTN search of GenBank utilizing the amino acid sequence of FLAP revealed a gene product with 33% and 44% sequence identity to FLAP and LTC₄S, respectively. Northern blot analysis showed that the mRNA of this protein, MGST2, is expressed in tissues throughout the body but that it differs from FLAP and LTC₄S in distribution and expression level. MGST2 displays GST activity toward CDNB and LTA₄, and it is also capable of reducing the hydroperoxide of 5-HPETE to 5-HETE in the presence of GSH (Figure 14).^{170,171}

The amino acid sequence of MGST2 was then utilized in a TBLASTN search of GenBank to reveal MGST3, a clone 20, 22, 27, and 36% identical to FLAP, MGST1,

LTC4S, and MGST2, respectively. Similarly to MGST2, Northern blot analysis revealed that the mRNA expression for MGST3 has a wide tissue distribution. The enzyme does not display GST activity toward CDNB, but it does catalytically add GSH to LTA₄ and is capable of reducing 5-HPETE in the presence of GSH.¹⁷¹



Figure 14. Glutathione-dependent peroxidase activity of MGST2 and MGST3. Both of the enzymes MGST2 and MGST3 catalyze the reduction of 5-HPETE to 5-HETE in the presence of GSH.

MPGES1

Similarly to the identification of MGST2 and MGST3, the amino acid sequence of MGST1 was utilized in a TBLASTN search of GenBank to reveal a gene product with 38% sequence identity with MGST1.^{46,175} Northern blot analysis showed that the mRNA of this protein, MPGES1, is expressed in placenta, prostate, testis, mammary gland, and bladder. In addition, the mRNA is highly expressed in A549 and HeLa cancer cell lines. When A549 cells are grown in the presence of IL-1 β , a significant induction of MPGES1 is observed.¹⁷¹ Because COX-2 is also induced in A549 cells in the presence of IL-1 β and converts arachidonic acid to PGH₂, it was hypothesized that MPGES1 might utilize PGH₂ as a substrate.^{171,176-178} As such, the membrane fraction of recombinant MPGES1 was shown to catalyze the GSH-dependent oxido-reduction of PGH₂ to PGE₂ (Figure 15).¹⁷¹

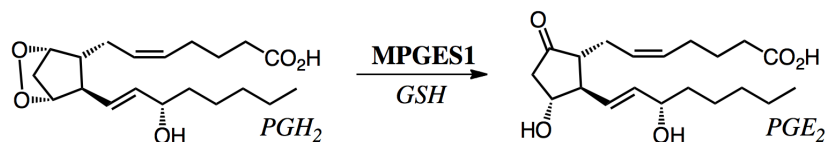


Figure 15. PGE synthase activity of MPGES1. MPGES1 catalyzes the oxido-reduction of the endoperoxide of PGH₂ in the presence of GSH, giving rise to PGE₂.

MAPEG Families

Through the use of multiple sequence alignments and phylogenetic calculations, the MAPEG superfamily can be divided into six families (Figure 16) named for the mammalian members that each contains.¹⁶¹ In addition, there are ancient prokaryotic subfamilies belonging to the MGST2, FLAP, and LTC4S families, as well as two distinct subfamilies belonging to *Escherichia coli* and *Synechocystis sp.* Insect members are similar to the MGST1 and MPGES1 families, while MAPEG members from fish are found in all six mammalian families. Though the evolutionary tree clearly divides the MAPEG superfamily, some families can be grouped together according to sequence similarity. Group I consists of MGST2, FLAP, and LTC4S, group II is occupied only by MGST3, group III is comprised of the unique bacterial enzymes, and group IV consists of MGST1 and MPGES1.¹⁶⁰

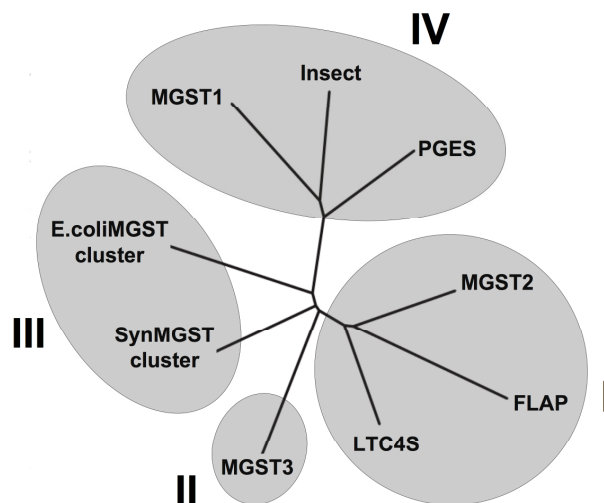


Figure 16. The MAPEG superfamily. The superfamily of membrane-associated proteins in eicosanoid and glutathione metabolism can be broken up into several families belonging to one of four groups, based on phylogenetic analysis. The figure is adapted from one of reference 160.

MAPEG Structures

Initial structural analyses of the MAPEG superfamily utilizing sequence alignments along with hydropathy plots suggested that the proteins contained multiple membrane-spanning regions.^{159,161,179-181} Subsequently, the three-dimensional crystal structures of MGST1 and MPGES1 were determined by electron microscopy of two-dimensional crystals, and those of FLAP and LTC4S were determined by X-ray diffraction.¹⁶²⁻¹⁶⁶ The first of these to be determined was MGST1, and the structure revealed a homotrimer with four transmembrane (TM) helices per monomer. The N- and C-termini protrude from the luminal boundary of the membrane, and each subunit contains one large cytosolic loop. MGST1 was crystallized in the presence of GSH, and the structure reveals three molecules of GSH bound at the interface of neighboring subunits.¹⁶² These characteristics have proven to be conserved among the other members

of the MAPEG superfamily (Figure 17), with the exception of FLAP, which has not been shown to bind GSH.¹⁶³⁻¹⁶⁶ The structure of each of these proteins is discussed in more detail below.

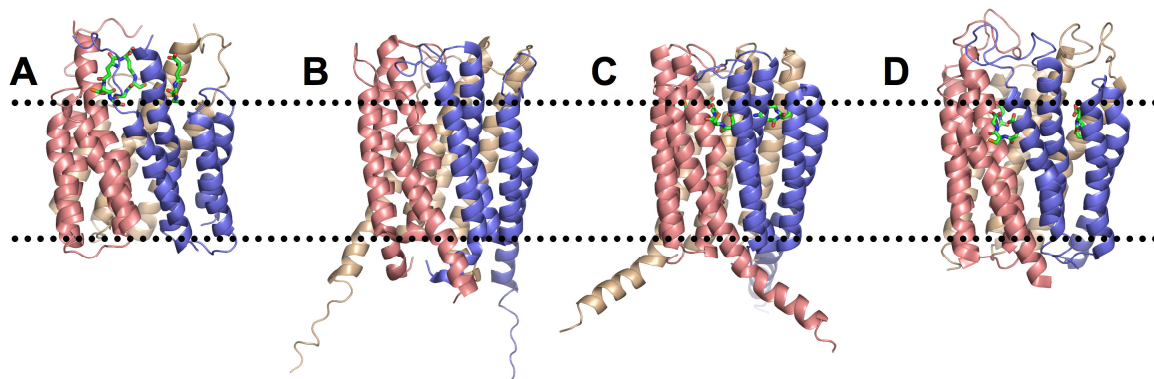


Figure 17. The conserved structure of the MAPEG superfamily. The homotrimeric structures of (A) MGST1, (B) FLAP, (C) LTC4S, and (D) MPGES1 are shown in salmon, slate, and wheat highlighting individual subunits. Dotted lines represent approximate boundaries of the lipid bilayer. All of the crystal structures reveal four TM helices per monomer, the carboxy and amino termini protruding into the luminal space of the perinuclear membrane (bottom), and extended loops exposed to the cytosolic space (top). All of the proteins were crystallized in the presence of GSH (green sticks) with the exception of FLAP, which has not been shown to bind GSH.

MGST1 Structure

The crystal structure of rat MGST1 in complex with GSH (Figure 18) was determined to 3.2 Å resolution by electron diffraction of two-dimensional crystals.¹⁶² As noted above, MGST1 adopts a homotrimeric conformation with a total of twelve TM helices, with TM II forming the core region of the enzyme. TM II is connected to TM I by a large, flexible cytosolic loop and to TM III by a short luminal loop. TM III, then, is connected to TM IV by a short proline-rich loop on the cytoplasmic side of the membrane. The binding site for the primary substrate of MGST1, GSH, is located at the interface of neighboring subunits.^{162,182} This location is in agreement with

hydrogen/deuterium (H/D) exchange mass spectrometry (MS) data, which also suggest conformation dynamics among TM I, TM II, and TM III upon GSH binding.¹⁸³ The crystal structure reveals three occupied GSH binding sites, however only one site is catalytically active at a time.^{162,184-187} In addition to the GSH site, H/D exchange kinetic data suggest two distinct secondary substrate binding sites: one for hydrophilic compounds and the other for hydrophobic compounds.¹⁸³

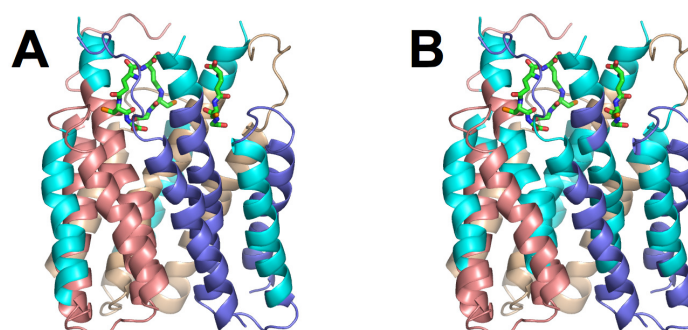


Figure 18. Crystal structure of MGST1. MGST1 is a homotrimeric integral membrane protein consisting of a total of twelve TM helices. Individual subunits are colored in salmon, slate, and wheat. Three molecules of GSH are bound at the interface of neighboring subunits and are represented by green sticks. H/D exchange kinetic analysis reveals conformational dynamics induced by ligand binding and two overlapping secondary substrate-binding sites, highlighted in cyan: one for electrophilic substrates (A) and another for hydrophobic substrates (B).

FLAP Structure

The crystal structure of human FLAP in complex with the LT synthesis inhibitor MK-591 (Figure 19) was determined to 4.0 Å by X-ray diffraction.¹⁶⁵ As with MGST1, FLAP is a homotrimeric integral membrane protein with four TM helices per monomer, in which the N- and C- termini protrude into the lumen, TM I and TM II as well as TM III and TM IV are connected by cytosolic loops, and TM II and TM III are connected by a short luminal loop. A structural comparison with MGST1, however, reveals that the

GSH binding site is not conserved within FLAP. In fact, co-crystallization of FLAP with GSH fails to produce electron density for GSH in the corresponding putative GSH binding site. Inhibitor MK-591 is bound within the plane of the nuclear membrane, making contacts with residues on TM I and TM II of one subunit and TM IV of the neighboring subunit.

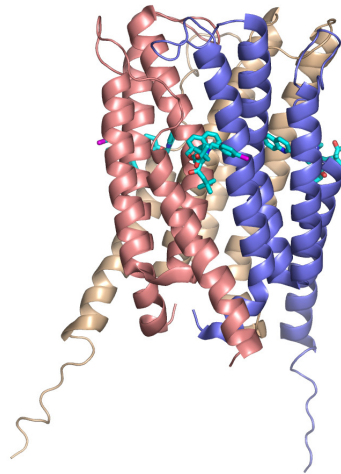


Figure 19. Crystal structure of FLAP. Like MGST1, FLAP is a homotrimeric protein with four TM helices per monomer. Unlike MGST1, FLAP has no known catalytic function and has not been shown to bind GSH. The protein was crystallized in the presence of the LT synthesis inhibitor MK-591, shown in cyan sticks bound at the interface of neighboring subunits.

LTC4S Structure

The X-ray crystal structure of human LTC4S in complex with GSH (Figure 20) was determined to 3.3 Å, and at the same time, the apo and GSH-bound forms were determined to 2.00 and 2.15 Å, respectively, by two separate research groups.^{163,164} As with MGST1 and FLAP, LTC4S is a homotrimeric integral membrane protein with four TM helices, two cytosolic loops, and one luminal loop per monomer. Unlike the former proteins, however, LTC4S contains a fifth, C-terminal helix that, along with the N-

terminus, protrudes beyond the luminal membrane boundary. Three molecules of GSH bind in a U-shaped conformation, making contacts with residues on TM I and TM II of one subunit and TM II, TM III, and TM IV of the neighboring subunit. The sulfhydryl group of each GSH is exposed to the lipid bilayer, coming within 3.2 Å of Arg-104, which possibly plays the role of shifting its pK_a to activate thiolate formation. In each of the published studies, an *n*-dodecyl- β -D-maltoside (DDM) detergent molecule was observed bound within the bilayer space, making contacts with residues of TM I and TM II of one subunit and TM IV of its neighbor. This DDM-binding pocket has been proposed as the putative LTA₄ substrate-binding site.

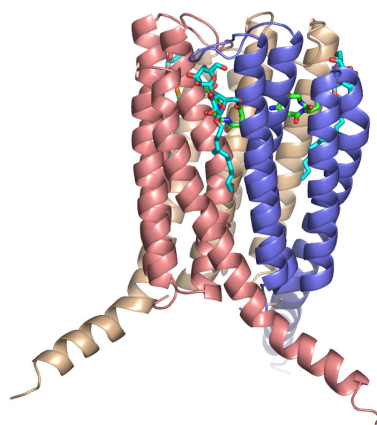


Figure 20. Crystal structure of LTC4S. The overall structure of LTC4S is conserved amongst the other determined structures of the MAPEG superfamily. However, in addition to the four TM helices of each subunit of the homotrimeric LTC4S, a fifth α -helix extends into the luminal space of the endoplasmic reticulum. Three molecules of GSH, shown in green sticks, are bound at the interface of neighboring subunits in a U-shaped conformation. Three molecules of the detergent DDM, shown in cyan sticks, are bound within a hydrophobic cleft overlapping the GSH-binding site and have been proposed as occupying the LTA₄ substrate-binding sites.

MPGES1 Structure

The crystal structure of human MPGES1 complexed with GSH (Figure 21) was determined by electron diffraction of two-dimensional crystals to 3.5 Å.¹⁶⁶ Similarly to the other MAPEG members, MPGES1 is a homotrimer with four TM helices per subunit, with the N- and C- termini extending into the luminal space of the ER. Each monomer also contains one elongated cytosolic loop, one short cytosolic loop, and one short luminal loop. As with LTC4S, GSH is bound in a U-shaped conformation within the plane of the membrane, making contacts with TM I and TM II from one monomer and TM II, TM III, and TM IV of its neighbor. Another similarity with LTC4S is that the GSH sulfhydryl comes within 3.8 Å of Arg-126 and is oriented toward the lipid bilayer, but unlike LTC4S the thiol moiety of GSH is not exposed to the lipid bilayer. Three key residues within the membrane region along TM IV have been proposed as the entrance for the PGH₂ substrate binding site.¹⁸⁸ The structure of MPGES1 is described in greater detail in the following section.

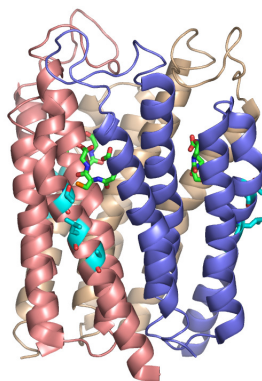


Figure 21. Crystal structure of MPGES1. Consistent with the other MAPEG members, MPGES1 is a homotrimeric integral membrane protein composed of twelve TM helices. Like LTC4S, three GSH molecules (green sticks) are bound at the interface of neighboring subunits in a U-shaped conformation. Mutagenesis and inhibition kinetics analyses reveal the putative entrance to the active site along TM IV, highlighted in cyan.

MAPEG Functions

Cytoprotection

MGST1 is a widely expressed enzyme, and it is present at especially high levels in the liver, where it constitutes up to 3% of the total microsomal protein.¹⁶⁷ It efficiently catalyzes the conjugation of GSH to xenobiotic and endogenous electrophiles, such as the common laboratory substrate CDNB as well as polyhalogenated unsaturated hydrocarbons. It is a rather inefficient GST, however, when utilizing epoxides such as LTA₄ as substrates.¹⁸⁹⁻¹⁹¹ The reaction rate of GST and GSH-dependent peroxidase activity of MGST1 is enhanced by electrophilic reagents such as *N*-ethylmaleimide (NEM), which covalently modify a cytosolic cysteine residue on the enzyme.¹⁹²⁻¹⁹⁴ MGST1 is also activated by, and provides cellular protection from, oxidative stress as it catalyzes the reduction of hydrophobic peroxides derived from lipids and fatty acids.¹⁹⁵⁻¹⁹⁸ Taken together, these facts suggest a cellular protective role for MGST1, particularly with respect to oxidative damage to membranes.

Less is known of the cellular functions of MGST2 and MGST3. However, it is known that both enzymes catalyze the GSH-dependent reduction of 5-HPETE to 5-HETE, and that MGST2 adds GSH to electrophiles such as CDNB, suggesting that both enzymes may play a role in cellular detoxification.^{170,171}

Eicosanoid Biosynthesis

Several members of the MAPEG superfamily are involved in the synthesis of eicosanoids. Since this topic is detailed in the previous section, it is only briefly

mentioned here, with respect to the MAPEG members implicated. Involved in the synthesis of the pro-inflammatory LTs are FLAP and LTC4S. The LT pathway of arachidonic acid metabolism is dependent on the presence of FLAP, acting as a scaffold for 5-LOX, which catalyzes the conversion of arachidonic acid to LTA₄.^{89,91} The determined crystal structure of FLAP suggests that its binding site within the bilayer is ideal for capturing laterally-diffusing arachidonic acid, and it is assumed that arachidonic acid is presented to 5-LOX by FLAP, however the structural basis for this process is unknown.^{165,199-201} The 5-LOX product LTA₄ is subsequently metabolized along one of two routes. LTA4H catalyzes the hydrolysis of LTA₄ to LTB₄, while LTC4S catalytically adds GSH to LTA₄, giving rise to LTC₄, the first member of the potent Cys-LTs.^{93,95,168,202}

Two other members of the MAPEG superfamily may potentially play roles in the 5-LOX pathway of arachidonic acid metabolism. MGST2 catalyzes the addition of GSH to LTA₄ *in vitro*, but the role of MGST2 as an LTC₄ synthase *in vivo* has not been established.^{170,171} While MGST1 does not catalyze the synthesis of LTC₄ as rapidly as does LTC4S, it is capable of tightly binding the LT within the plane of the membrane.^{183,203} The physiological function for this, however, remains uncertain.

In addition to LT synthesis, the MAPEG superfamily plays a role in the production of PGE₂. The COX-2-derived PGH₂ serves as a substrate for MPGES1 in the formation of inducible PGE₂, which is a predominant mediator of pain, fever, and inflammation.⁵⁰ The role of MPGES1 in the production of PGE₂ and its implication in pathologic events is detailed in the following section of this introduction.

The MAPEG superfamily represents a unique set of GST proteins. The GSH conjugating and GSH-dependent peroxidase activities of MGST1, MGST2, and MGST3 impart important detoxification properties to these family members. In addition, their integral membrane structures make them particularly effective in providing cytoprotection to membranes from oxidative damage.

In addition to detoxification, the MAPEG superfamily plays an important role in arachidonic acid metabolism. FLAP, LTC4S, and MPGES1 are crucial to the syntheses of LTs, Cys-LTs, and PGE₂, respectively, and their structures make them ideal for binding unstable hydrophobic ligands and substrates within the bilayer. Since these lipid mediators are important pro-inflammatory signaling molecules, FLAP, LTC4S, and MPGES1 represent promising therapeutic targets for the treatment of inflammatory disease.

Microsomal Prostaglandin E Synthase 1

At physiological conditions, the chemically unstable endoperoxide of PGH₂ rapidly decomposes into a mixture of the prostanoids PGD₂ and PGE₂ (Figure 22) with a half-life on the order of several minutes.²⁰⁴ Being potent biologically active signaling molecules, the synthesis of prostanoids must be tightly controlled. As such, several prostanoid synthases exist that utilize PGH₂ as a substrate, as summarized in the Eicosanoid section of this introduction.

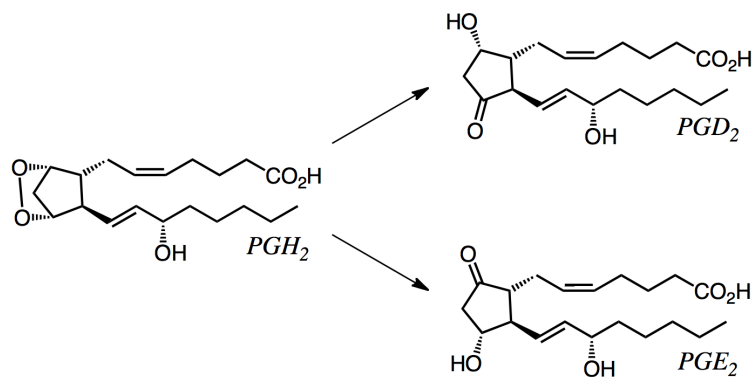


Figure 22. Decomposition of PGH_2 . Under physiological conditions, the endoperoxide of PGH_2 undergoes spontaneous oxido-reduction, resulting in the formation of PGD_2 and PGE_2 .

With regard to PGE_2 synthesis, there are three PGES enzymes that catalyze the isomerization of PGH_2 resulting in a keto group at position C-9 and a hydroxyl group at C-11. These enzymes include the cytosolic CPGES and the membrane-bound proteins MPGES1 and MPGES2. It is generally accepted that CPGES and MPGES2 produce homeostatic levels of PGE_2 , while MPGES1 synthesizes the inducible form of the prostanoid.⁴⁶⁻⁴⁸ In this section, particular emphasis is placed on the structural and functional properties of MPGES1, as well as its physiological and pathological roles in biology.

MPGES1 Catalytic Function

MPGES1 is a GSH-dependent PGH_2 isomerase, having a K_M value for GSH of 0.71 mM and K_M and k_{cat}/K_M values for PGH_2 of 0.16 mM and $310 \text{ mM}^{-1} \text{ s}^{-1}$, respectively.²⁰⁵ Given that the reaction is an oxido-reduction, GSH is not consumed. MPGES1 is also capable of utilizing PGG_2 as an alternate substrate (Figure 23) with similar kinetics, producing 15-hydroperoxy- PGE_2 , which can then be reduced by the

peroxidase activity of COX giving PGE₂, though this route of PGE₂ production is not likely to occur *in vivo*.^{205,206}

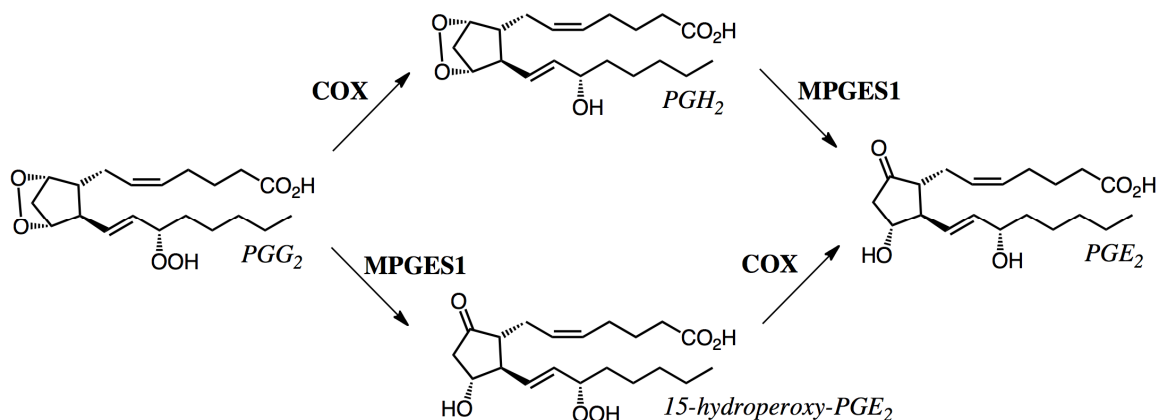


Figure 23. Substrates of MPGES1. MPGES1 catalyzes the oxido-reduction of the endoperoxide bridge of both PGG₂ and PGH₂ *in vitro*. However, the utilization of PGG₂ as a substrate is unlikely to occur *in vivo*.

In addition to catalyzing the isomerization of PGG₂ and PGH₂, MPGES1 catalyzes the conjugation of GSH to CDNB with a specific activity of 0.8 $\mu\text{mol min}^{-1} \text{mg}^{-1}$.²⁰⁵ This common GST activity, while relatively low compared to a typical GST, highlights the close evolutionary relationship of MPGES1 to the MGSTs of the MAPEG superfamily. Another common GST activity that MPGES1 possesses is the GSH-dependent reduction of hydroperoxides, in that it reduces cumene hydroperoxide and 5-HPETE with specific activities of 0.17 $\mu\text{mol min}^{-1} \text{mg}^{-1}$ and 0.043 $\mu\text{mol min}^{-1} \text{mg}^{-1}$, respectively.²⁰⁵ Since the catalytic rates are relatively low for MPGES1 when utilizing CDNB, cumene hydroperoxide, or 5-HPETE as substrates, these GST and GSH-dependent peroxidase activities are unlikely to be functions of the enzyme *in vivo*, but they do highlight the evolutionary relationship of MPGES1 to the GSTs.

MPGES1 Chemical Mechanism

The chemical mechanism for the catalytic formation of PGE₂ by MPGES1 (Figure 24) has been proposed based on the crystal structure of the enzyme.¹⁶⁶ Because MPGES1 also catalyzes the GSH-dependent peroxidase of lipid hydroperoxides, a GSH-dependent peroxidase-like mechanism is favored, as opposed to a concerted acid-base mechanism, and involves GSH thiolate attack on an oxygen atom of PGH₂. Thiolate formation is stabilized by Arg-126, which is within 3.8 Å of the GSH sulfhydryl. The chemical reaction begins with thiolate attack on oxygen at position C-9 of the PGH₂ endoperoxide. This is followed by proton donation by Arg-126 to the oxygen at C-11, forming the hydroxyl group. Finally, Arg-126 abstracts a proton from carbon C-9, forming the carbonyl as the oxygen-sulfur bond is broken, and the GSH thiolate is regenerated.

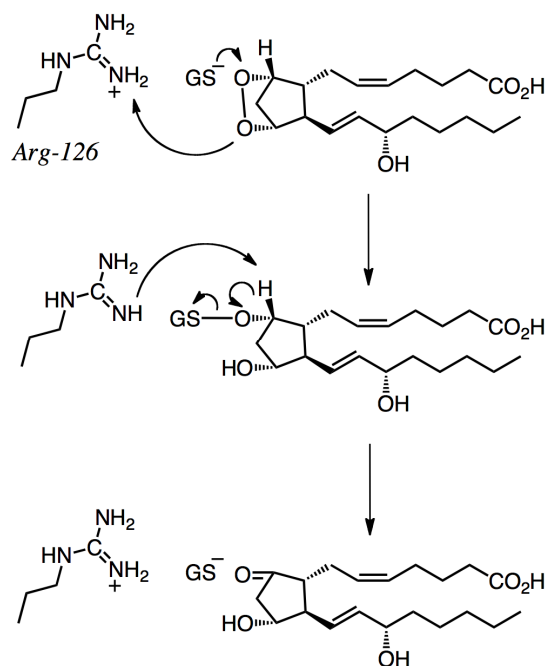


Figure 24. Chemical mechanism of MPGES1. The formation of the thiolate form of GSH, denoted GS⁻, is stabilized by residue Arg-126. The reaction is initiated by GS⁻ attack on the oxygen at position C-9 of PGH₂, followed by protonation of the oxygen at position C-11 by Arg-126. A proton from C-9 is then abstracted by Arg-126, forming a carbonyl and breaking the oxygen-sulfur bond, which regenerates GS⁻.

The corresponding arginine residue in LTC₄S, Arg-104, is critical for thiolate formation, suggesting that arginine may play a conserved role in MAPEG catalysis.²⁰⁷ However, mutation of Arg-126 to either alanine or glutamine converts MPGES1 from a GSH-dependent isomerase into a GSH-dependent reductase that produces PGF_{2α} from PGH₂, suggesting that Arg-126 is important for catalysis but not necessary for thiolate formation.²⁰⁸ Though the crystal structure favors Arg-126 as both the proton donor and acceptor in the reaction, other residues may play these roles in the mechanism. Since Tyr-28 and Tyr-130 are within 3.6 and 7.1 Å of the GSH thiol, respectively, they are reasonable candidates for proton donation to oxygen at C-11 and proton abstraction from carbon C-9 of PGH₂.¹⁶⁶ This suggests that there could be alternatives to the proposed mechanism that may involve a single tyrosine, a combination of tyrosine residues, or a

combination of tyrosine and arginine. Clearly, additional structure-function studies combining crystallography with mutagenesis are needed to improve the understanding of the mechanism.

MPGES1 Structure

Membrane proteins encompass 20-30% of the proteome of most organisms.²⁰⁹ Pharmacologically, membrane proteins represent about 40% of all human drug targets, which are often GPCRs, being that they are therapeutically attractive due to their fundamental role in signal transduction.²¹⁰ Even so, structural information of membrane proteins is relatively lacking. This is highlighted by the fact that membrane proteins account for only about 1% of all entries in the Protein Data Bank (PDB).²¹¹ In fact, even though crystal structures of soluble proteins were first determined in the 1950s, it was nearly thirty years before the same could be said of a membrane protein.^{212,213} While crystallography of membrane proteins is challenging due to the hydrophobicity of the protein surface and the fact that they tend to be flexible and unstable, significant progress has been made in determining the structures of the MAPEG proteins.¹⁶²⁻¹⁶⁶

The three-dimensional structure of MPGES1 (Figure 25) was determined by electron diffraction of two-dimensional crystals induced in the presence of phospholipids.¹⁶⁶ The 3.5 Å resolution structure of the human enzyme, complexed with the essential cofactor GSH, gives insight into the dynamic behavior of this integral membrane protein. As summarized in the previous section, MPGES1 possesses the conserved structure of the MAPEG proteins, in that it is a homotrimeric integral membrane protein with each subunit contributing four TM helices.

Of the twelve-helical bundle, TM II forms the core of the protein, which is surrounded by the remaining helices. A proline residue at position 81 gives TM II a slight kink, resulting in a cone-shaped cavity opening toward the cytoplasmic portion of the enzyme. Extended cytosolic loops, connecting TM I to TM II partially cover this opening. A short luminal loop connects TM II to TM III, and TM III and TM IV are connected by a short cytosolic loop. The amino termini protruding from the luminal side of the membrane are flexible, and so the first ten residues are disordered in the structure. The N-terminus of TM I is in close proximity to the C-terminus at the end of TM IV of the neighboring subunit.

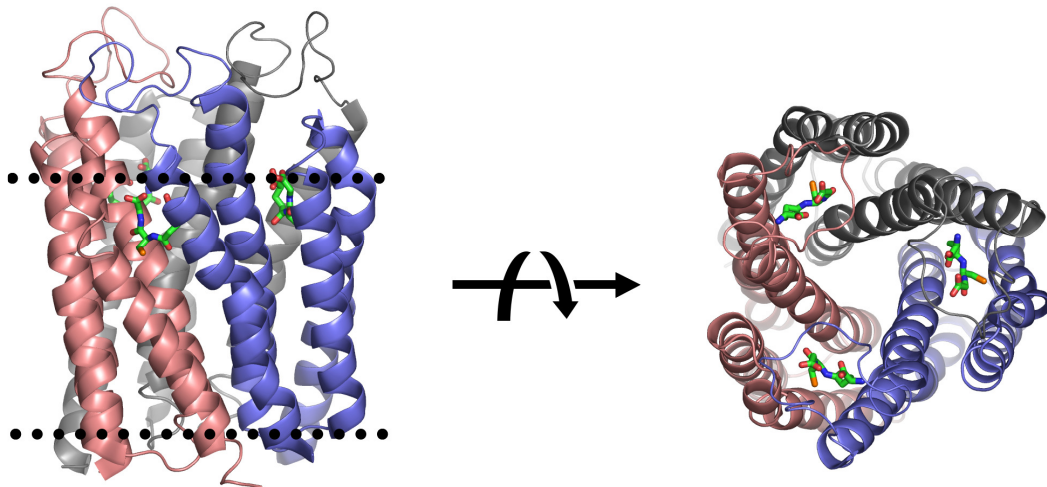


Figure 25. Structural analysis of MPGES1. MPGES1 is a homotrimeric integral membrane protein, with each subunit colored here in salmon, slate, and grey. The dotted lines denote the approximate boundaries of the lipid bilayer. The enzyme consists of a total of twelve TM helices, with the amino and carboxy termini protruding into the luminal (bottom) space of the endoplasmic reticulum. Three molecules of GSH (green sticks) are bound in a polar pocket at the interface of neighboring subunits, and the binding site is partially covered by extended cytosolic (top) loops.

The effects of site-directed mutagenesis, coupled with analysis of the crystal structure, highlight important molecular contacts.^{50,166,214} Side chain interactions between

polar and acidic residues of TM II and basic residues of TM III, toward the bottom of the cavity mentioned above, provide stabilization to the core of the structure. Several polar residues along the cytoplasmic face of TM II, toward the center of the cavity, provide contacts to GSH that are crucial to its binding. Also in this region is a salt bridge between His-72 and Glu-77 of neighboring TMs II. There is an additional salt bridge in this vicinity, connecting TM I and TM II of the same monomer, between Lys-26 and Asp-75.

The cofactor GSH binds at the interface of neighboring subunits in a U-shaped conformation (Figure 26), similar to that observed for LTC4S,^{163,164} making contacts with TM I and TM II of one subunit and TM II, TM III, and TM IV of its neighbor.¹⁶⁶ In addition to the polar interactions with TM II mentioned above, the carboxylate groups at either end of the GSH molecule make salt bridge contacts with Arg-38 of TM I and Arg-70 of TM II. The sulfhydryl group of GSH is oriented toward the lipid bilayer, stabilized by Arg-126, but makes no contact with the membrane as it is blocked by TM I and TM IV of neighboring subunits. This is in correlation with the apo-structure of LTC4S, which also displays this “closed” conformation.¹⁶⁴ This is, however, in contrast to the GSH-complexed structure of LTC4S in which a V-shaped opening between TM I and TM IV is occupied by a DDM molecule, exposing the GSH thiol.^{163,164} This suggests that there is a dynamic opening of these helices that allows substrate access to GSH, which may also be true for the structurally homologous MPGES1.

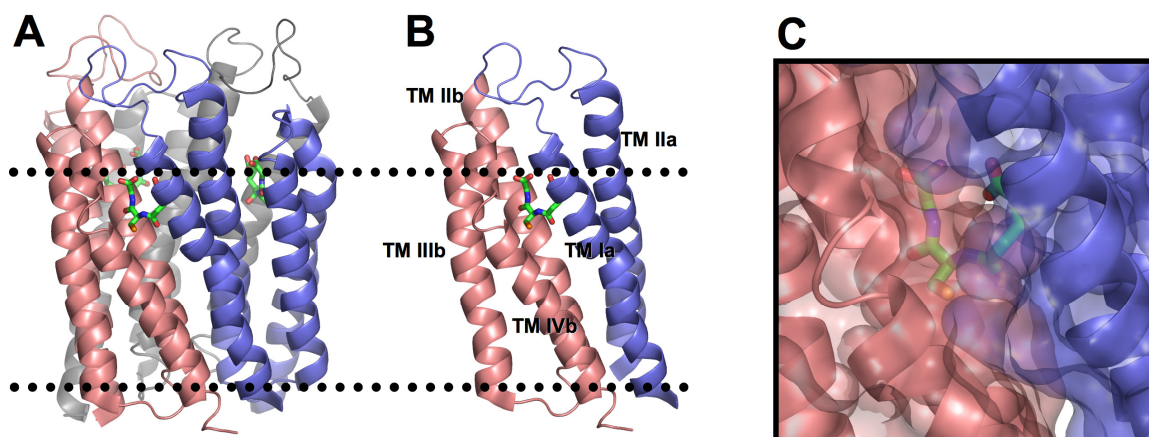


Figure 26. GSH binding of MPGES1. The subunits of MPGES1 are colored salmon, slate, and grey. Dotted lines represent the boundaries of the lipid bilayer. (A) MPGES1 binds three molecules of GSH (green sticks) in a U-shaped conformation within the plane of the membrane. (B) The bound GSH molecule makes contacts with TM I and TM II of one subunit and TM II, TM III, and TM IV of its neighbor. (C) The sulfhydryl of the GSH molecule is oriented toward the lipid bilayer, but it makes no contact with the bilayer, as it is obscured by TM I of one subunit and TM IV of the adjacent subunit.

MPGES1 as a Drug Target

Under normal physiological conditions, MPGES1 expression is relatively low and has been observed in placenta, prostate, testis, mammary gland, and bladder.⁴⁶ However, the enzyme is dramatically induced in response to several pro-inflammatory stimuli including LPS, IL-1 β , and TNF- α , similarly to COX-2 induction.⁵⁰ The down-regulation of MPGES1, much like that of COX-2, can be brought about with the administration of glucocorticoids, which suggests a functional coupling between these two inducible enzymes.⁴⁹

As discussed previously, there are two COX isozymes. The isoform COX-1 is a constitutive enzyme that produces homeostatic levels of the primary prostanoids, while COX-2 is an inducible enzyme whose up-regulation results in the production of prostanoids causative of inflammation.^{36,37} Basal levels of production of PGE₂ are

thought to contribute to the maintenance of the gastric mucosa by maintaining the mucus bicarbonate barrier and inducing growth factors including the vascular endothelial growth factor (VEGF).²¹⁵ Therapeutic treatment with NSAIDs such as aspirin and ibuprofen inhibits both COX isozymes, prevents production of all primary prostanoids including PGE₂, and subsequently leads to adverse gastrointestinal side effects.^{82,215}

Since COX-2 contributes to the induced formation of PGE₂ leading to inflammation, NSAID development in the 1990s focused on the selective inhibition of this enzyme. The hypothesis entailed maintaining basal levels of PGE₂ while reducing induced levels of PGE₂ in an effort to avoid such side effects observed with traditional NSAIDs. Two such coxibs developed include celecoxib and rofecoxib whose trade names are Celebrex and Vioxx, respectively.^{80,216} Unfortunately, the long-term selective inhibition of COX-2 leads to adverse cardiovascular side effects due to a decreased production of PGI₂ relative to TXA₂, which are inhibitors and inducers of platelet aggregation, respectively.²¹⁷ Subsequently, it has been suggested from meta-analysis studies of randomized trials that long-term use of traditional, non-selective NSAIDs is also associated with an increased risk of adverse cardiovascular events.²¹⁸ Because the principal function of MPGES1 is the production of induced PGE₂, and since the enzyme is immediately downstream of COX-2 in the inducible PGE₂ pathway, it represents a promising therapeutic target for the treatment of inflammatory diseases.

MPGES1 Mouse Knockout Studies

Most knowledge of the physiological and pathological roles of MPGES1 has been obtained through gene knockout (KO) experiments with mice. Mice lacking MPGES1

were generated by targeted homologous recombination on an inbred background.²¹⁹ The lack of any observable phenotype as compared to wild-type (WT) mice indicates that MPGES1 does not produce PGE₂ as a mediator involved in development or essential biological processes. However, when tested in inflammation models including collagen-induced arthritis (CIA) and delayed-type hypersensitivity, the mice show marked reduction in inflammatory responses.^{219,220} Under a model experiment for pain known as the writhing test, in which dilute acetic acid is injected intraperitoneally, the KO mice display a decrease in pain perception similar to that of a control of WT mice treated with NSAIDs.²¹⁹

In two separate studies, MPGES1-deficient mice showed a decrease in fever response from LPS injection as compared to WT controls.^{220,221} Yet another study demonstrated that MPGES1 KO mice exhibit a decreased incidence in neuropathic pain.²²² Finally, unlike COX-2 KO mice, MPGES1 KO mice display no decrease in anti-thrombotic PGI₂ production.²²³ These experiments highlight the promise of targeting MPGES1 to treat inflammatory disease.

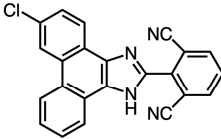
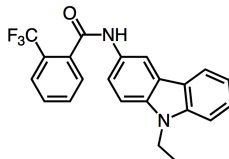
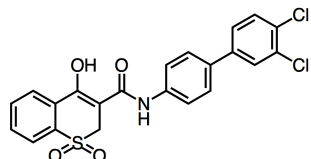
In light of these promising results, however, there may be complications that arise by targeting MPGES1 therapeutically. For instance, one study has demonstrated that mice deficient in MPGES1 exhibit an increase in blood pressure when administered synthetic mineralocorticoid while given a high-salt diet, a well-established model of hypertension.²²⁴ Other studies have revealed that PGE₂ may play a role in the resolution phase of inflammation. For example, PGE₂ down-regulates several pro-inflammatory genes by dissociating nuclear trafficking subunits of NF-κB in RA synovial fibroblasts.²²⁵ Also, MPGES1-derived PGE₂ displays a resolution role in mouse models of

neuroinflammation.²²⁶ On the other hand, the expression of MPGES1 rapidly drops to basal levels during the resolution phase in mouse CIA models, while COX-2 expression is maintained.²²⁷ Inhibiting COX-2 during this phase has the effect of perpetuating inflammation, suggesting that maintaining COX-2 expression while inhibiting MPGES1 activity should hasten the resolution of inflammation brought about by arthritis.²²⁷ Despite the uncertainty of the role of PGE₂ as a mediator of resolving inflammation, MPGES1 has been the focus of drug development for the treatment of inflammatory disease, and several MPGES1-specific inhibitors have been developed.

MPGES1 Drug Development

Several drug leads (Table 1) have emerged from both academia and the pharmaceutical industry. One example developed by Pfizer Inc. in St. Louis, MO, is the oxicam compound PF-9184, a selective MPGES1 inhibitor with an IC₅₀ value of 16.5 nM.²²⁸ In RA synovial fibroblasts induced with IL-1 β , PF-9184 decreases PGE₂ production without inhibiting COX-2. Unfortunately, MPGES1 inhibition by this compound results in the shunting of PGH₂ to the PGFS pathway, which could possibly result in unwanted side effects when used in animal models or as a drug. Another example of a drug lead is the carbazole benzamide AF3442 synthesized by the Angelini Research Center in Rome, Italy, which specifically inhibits MPGES1 with an IC₅₀ value of 60 nM.²²⁹ In this case, the compound significantly reduces PGE₂ formation in human monocytes induced with LPS with no evidence of shunting PGH₂ to alternate synthase pathways.

Table 1. Drug leads targeting MPGES1. Several compounds that selectively inhibit MPGES1 have emerged as drug leads in recent years. These compounds, developed by both the pharmaceutical industry and academia, inhibit the isomerization activity of MPGES1 with IC₅₀ values in the nanomolar range.

Inhibitor	Structure	IC ₅₀
Merck MF63		1.3 nM
G.d'Annunzio University AF3442		60 nM
Pfizer PF-9184		17 nM

Merck Frosst, formerly in Quebec, Canada, developed several compounds targeting MPGES1. For instance, the phenanthrene imidazole MF63 is a potent, orally available MPGES1 inhibitor with an IC₅₀ value of 1.3 nM.²³⁰ Utilizing animals including mice with a knock-in (KI) of the human enzyme as well as guinea pigs, oral administration of MF63 selectively decreases PGE₂ production without effecting the production of other prostanoids, as compared to controls, in an LPS-induced air pouch model. In addition, MF63 substantially decreases hyperalgesia, pyresis, and chronic osteoarthritic pain induced by LPS without causing gastrointestinal toxic effects. Subsequently, the Merck Frosst group has made progress in developing mono- and disubstituted phenanthrene imidazoles as well as trisubstituted ureas as potent and selective MPGES1 inhibitors to be utilized in pre-clinical studies.^{231,232}

As a result of these inhibitor studies, it has come to light that inter-species differences of MPGES1 have a profound effect on inhibitor potencies. For instance, the compounds PF-9184 and MF63 display IC₅₀ values in the nanomolar range against the human enzyme but are relatively ineffective against the mouse orthologue.^{228,230} A similar effect has been observed for the rat enzyme.¹⁸⁸ It was subsequently demonstrated that the differences in potencies could be attributed to three key amino acid residues along TM IV of the enzyme that act as gate keepers for the entrance of the active site.¹⁸⁸ This obstacle to pre-clinical trials was overcome in the aforementioned Merck Frosst studies by generating mice that express human MPGES1 instead of the mouse enzyme, as well as by using guinea pigs whose MPGES1 orthologue more closely represents the human enzyme.²³⁰⁻²³² This solution to inter-species differences in pre-clinical studies still presents difficulties in drug development, however, in that it complicates the evaluation of relevant off-target effects in the animal models.

MPGES1 and Cancer

The induced production of PGE₂ is highly correlated with cancer cell growth and survival, involving several signaling mechanisms that increase proliferation and invasiveness and inhibit apoptosis.²³³ COX-2 is highly expressed in various cancer cell lines, is generally assumed to be the major source of PGH₂ production in cancer cells, and is therefore likely to play a major role in the production of PGE₂ in cancer.³⁶ Because MPGES1 is co-regulated with COX-2 and is the terminal enzyme in inducible PGE₂ synthesis, it represents a potential target for the treatment of cancer.²³⁴

Initial studies of mouse cancer models with genetic deletions of MPGES1 have shown promise. In a colorectal cancer model, mice with mutations in the adenomatous polyposis coli (APC) gene were compared to MPGES1 KO mice containing the same APC mutations.^{235,236} MPGES1 KO mice display a significant suppression in intestinal cancer growth, even when induced by azoxymethane injections. In a separate study, shRNA was utilized to knock-down the MPGES1 gene of two cancer cells lines.²³⁷ The prostate cancer cell line DU145, which constitutively expresses MPGES1, and the non-small lung cancer cell line A549, in which MPGES1 is inducible, both show slower colony growth in clonogenic assays. In addition, when the cells are injected into nude mice, the MPGES1 knock-down cells exhibit delayed tumor growth as compared to injection with WT cells.

In addition to the knock-down study mentioned above, MPGES1 knock-down and overexpression in Lewis lung carcinoma (LLC) cells have also revealed the role of MPGES1 in the progression of cancer.²³⁸ The MPGES1 knock-down cells display a reduction in proliferation and invasiveness, while the overexpression of MPGES1 confers an increase in proliferation and invasiveness. Also, tumor growth is attenuated in WT mice subcutaneously injected with the LLC MPGES1 knock-down cells, as compared to LLC cells over-expressing the enzyme. In addition, when WT LLC cells are grafted onto MPGES1 KO mice, tumor growth is decreased as compared to grafting onto WT mice. Though in the relatively early stages of research, these studies suggest that PGE₂ production by MPGES1 plays a role in the progression of colon, prostate, and lung cancers.

MPGES1 is a GSH-dependent PGH₂ isomerase whose oxido-reduction activity gives rise to PGE₂. The other catalytic activities of this enzyme highlight its evolutionary relationship to other MAPEG members, as well as to the other GST families. The catalytic mechanism of MPGES1 has been proposed based on its crystal structure, however uncertainties remain. The structure does, however, underline the homology of MPGES1 with other MAPEG members including MGST1, FLAP, and LTC₄S. PGE₂ production is important for a wide range of normal biological functions, but it has also been associated with pathological processes including inflammation. The co-regulation of MPGES1 with COX-2 highlights its role in the production of induced PGE₂ synthesis and gives it promise as a target to treat inflammation and perhaps several forms of cancer. Initial animal model studies, including KO and knock-down experiments, as well as administration of orally available MPGES1-specific inhibitors, are only just beginning to deliver on the potential of that promise.

Hydrogen/Deuterium Exchange Mass Spectrometry of Membrane Proteins

The understanding of a protein's function on a molecular level is often aided by the determination of its three-dimensional structure. Two common techniques often employed in structural biology include nuclear magnetic resonance (NMR) and X-ray crystallography. Both methods are well-recognized techniques that provide high-resolution structural information of proteins, protein-ligand interactions, and protein-protein interactions.^{212,239} Both of these methods, however, suffer from obstacles that hinder their utility. A major challenge of X-ray crystallography is the difficulty in crystallizing certain proteins including many membrane proteins, as well as those that are

intrinsically disordered.²⁴⁰ In addition, analyses can only be made in the non-native solid-state. NMR suffers from the fact that many proteins are simply too large for analysis, and the technique requires relatively high concentrations of protein to be successful.²⁴¹

Backbone amide H/D exchange MS has emerged as a useful tool for the study of protein structure and dynamics, as a complementary or alternative technique to NMR and crystallography. A clear advantage of this method is the ability to perform structural analyses in nearly any solution condition or protein concentration. The phenomenon of protein H/D exchange was first described by Kaj Ulrik Linderstrøm-Lang in the 1950s when he measured the extent of deuteration of D₂O-solubilized proteins utilizing density gradient tubes.²⁴² The first MS analysis of H/D exchange came in 1993 when horse cytochrome *c* was incubated in D₂O as a function of time, proteolyzed by pepsin, and subsequently analyzed using fast atom bombardment (FAB) MS.²⁴³ The advent of electrospray ionization (ESI) and matrix-assisted laser desorption/ionization (MALDI) in the late 1980s made MS an analytical tool amenable to intact proteins.^{244,245} As such, the first structural dynamics study of a whole protein in solution utilizing H/D exchange coupled to LC and ESI-MS appeared in 1994 when the technique was used to observe deuterium incorporation for apo- and holo-myoglobin.²⁴⁶

H/D Exchange Theory

Hydrogen exchange is both acid- and base-catalyzed.²⁴⁷ At physiological pH, the reaction is predominantly base-catalyzed, in that an amide nitrogen proton is first abstracted by hydroxide ion and subsequently protonated by a solvent proton. The kinetics of H/D exchange are modulated by factors including pH, polypeptide

conformation, solvent exposure, and structural dynamics that alter the chemical environment of reactive sites on the protein.²⁴⁸ Rapid H/D exchange kinetics, having an intrinsic exchange rate of about 10 s^{-1} ,²⁴⁹ is indicative of solvent exposure (Figure 27), while slow kinetics indicate either solvent protection or involvement in hydrogen bonding. The exchange of hydrogen for deuterium of hydrogen-bonding backbone amides is mediated by structural fluctuations that disrupt the hydrogen bonds, resulting in temporary solvent access. Taken together, measuring the rate of deuterium incorporation as a function of time reveals aspects of conformation, as well as conformational changes due to structural perturbations.

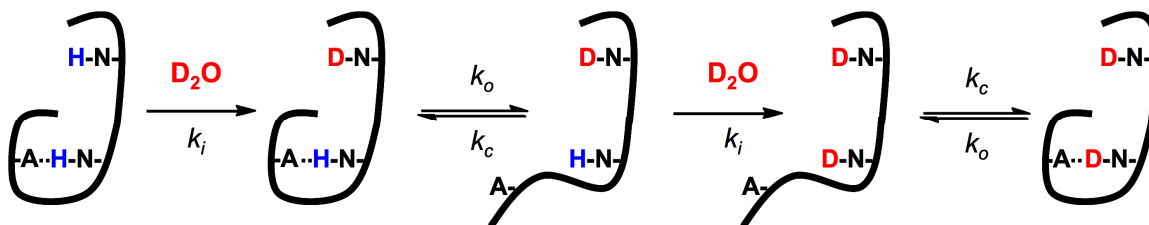


Figure 27. The Linderstrøm-Lang model of H/D exchange. Amide protons that are exposed exchange with deuterons in the solvent with a half-life on the order of milliseconds. Those amide protons that are buried or are involved in hydrogen bonding exchange with a half-life on the order of seconds to years. Structural perturbations in folded regions allow solvent access and incorporation of deuterium. In this way, kinetic analysis of H/D exchange reveals aspects of structural conformation, as well as conformational dynamics.

H/D Exchange MS Methodology

The most common method of H/D exchange MS involves continuous labeling (Figure 28).²⁵⁰ In this procedure, purified native protein in a buffered solution made with H_2O is diluted in deuterated solvent and incubated at room temperature and neutral pH for time periods ranging from a few seconds to several hours. This “in-exchange” process is quenched by acidification to pH 2.5 by dilution with ice-cold buffer made with H_2O ,

reducing the rate of exchange by several orders of magnitude for backbone amide nitrogens.²⁵¹ The exchange kinetics of other sites on the protein are significantly less reduced, and those sites therefore “back-exchange” with hydrogen in the solvent, resulting in labeling that is exclusive to backbone amide nitrogens. The remainder of the procedure is performed at 0 °C, which reduces the rate of exchange by an additional order of magnitude. After proteolysis by an acidic protease such as pepsin, the resulting peptides are analyzed by reversed-phase LC-MS utilizing an ESI source in positive mode, observing deuterium incorporation as an increase in average mass for each peptide. Due to the relative lack of cleavage specificity of pepsin, all analyzed peptides are sequenced by MS/MS prior to H/D exchange kinetic analysis.

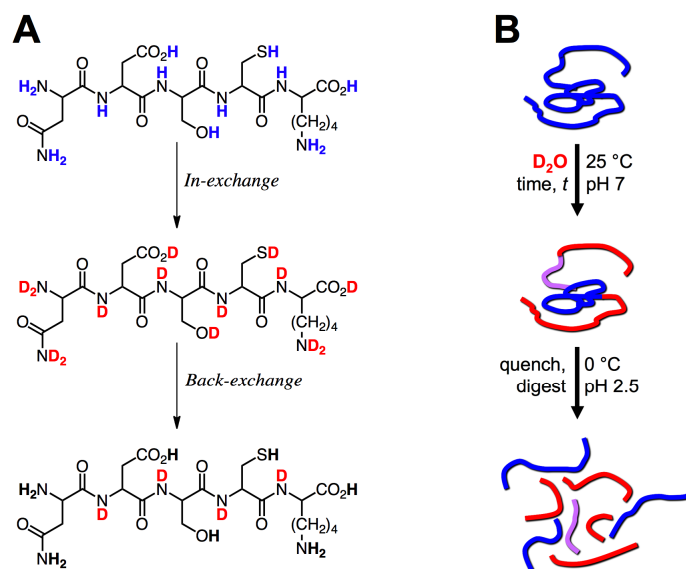


Figure 28. H/D exchange MS experimental method. (A) Incubation of a protein in deuterated solvent results in the incorporation, or “in-exchange,” of deuterium at multiple sites. Quenching the incorporation and diluting the protein in solvent lacking deuterium results in the loss, or “back-exchange,” of deuterium at all sites except for those of backbone amide nitrogens. This leads to deuterium labeling that is exclusive to the backbone of the protein and can be exploited for making structural analyses. (B) The H/D exchange assay involves a range of D₂O incubation times followed by quenching and proteolysis. Each resulting peptide is subsequently analyzed for deuterium incorporation as a function of time by LC-MS.

For each experimental time point, the number of deuterons incorporated onto the backbone amide nitrogens of each peptide is calculated from its mass spectrum (Figure 29), using the centroid of the resulting isotopic envelope. The number of incorporated deuterons is then plotted as a function of time and fit to a sum of first-order exponential rate terms. H/D exchange kinetic rates are generally divided into three phases including fast ($\sim 10 \text{ s}^{-1}$), intermediate, and slow, with slow exchange defined as no deuterium incorporation throughout the time course of the experiment (typically several hours). As mentioned above, fast exchange kinetics is indicative of protein conformation. In fact, all three phases of exchange can be utilized to analyze structural perturbations of a protein as a result of experimental conditions that cause some conformational change.

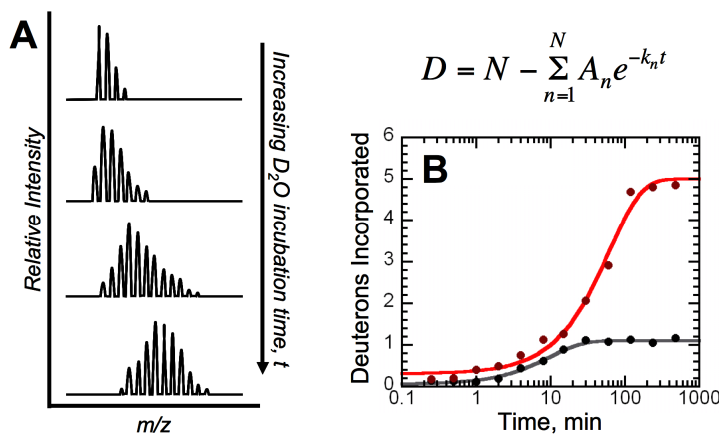


Figure 29. H/D exchange kinetic analysis. (A) The incorporation of deuterium for each peptide is observed in a series of mass spectra as an increase in average mass. (B) The number of deuterons incorporated onto each peptide is plotted as a function of time and fit to a sum of first-order exponential rate terms. Perturbing the structure of the protein results in significant changes in H/D exchange kinetics, illustrated by the red and black traces, which represent two different experimental conditions. These changes in kinetics as a result of structural perturbations are used to make conformational determinations.

H/D Exchange MS of Membrane Proteins

Structural studies of membrane proteins are inherently difficult due to their typically low overexpression in heterologous expression systems.²⁵² In addition, micelle or surfactant solubilization as a substitute for the native lipid bilayer commonly results in degradation and precipitation of membrane proteins.²⁵³ With respect to LC-MS, many hydrophobic peptides do not readily elute from reversed-phase columns, and detergents tend to suppress ionization from the electrospray source,²⁵⁴ as detailed below. With respect to H/D exchange, deuterium incorporation kinetics for membrane proteins are somewhat different than those for soluble proteins due to limited solvent access of the membrane- or micelle-embedded regions.

Despite these challenges, progress has been made in the field of membrane protein H/D exchange MS. For instance, the H/D exchange kinetics of short transmembrane peptides within the lipid bilayer have been analyzed with respect to structural topology and conformational flexibility.^{255,256} The method has also been successfully utilized to analyze the interaction between membrane-associated proteins and their ligands,²⁵⁷ as well as their interactions with the bilayer itself.²⁵⁸ There are even a few examples of H/D exchange MS studies of intact integral membrane proteins that clearly reveal the extent of conformational dynamics within the bilayer, which are summarized here.

H/D Exchange MS of MGST1

The detoxification enzyme MGST1, a homotrimeric protein with a total of twelve TM helices, responds to chemical and oxidative stress.¹⁶² It is involved in multiple roles

of cellular protection by functioning as a GSH-dependent peroxidase with lipid hydroperoxides and as a GST with various electrophilic species including epoxides. H/D exchange MS of MGST1 solubilized in the detergent Triton X-100 reveals the location of the cytoplasmic GSH binding site (Figure 30), as well as the structurally-overlapping binding site for hydrophobic substrates.^{183,194} The method was also used to determine that GSH binding induces a significant conformational change amongst several TM helices.¹⁹⁴ In addition, it was observed that a cytoplasmic cysteine residue acts a stress sensor that responds to chemical modification by pre-organizing the aforementioned TM helices, resulting in enzyme activation.¹⁹⁴

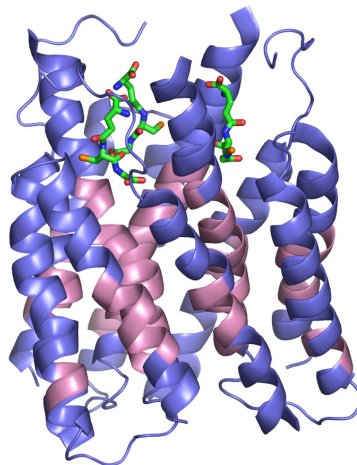


Figure 30. H/D exchange MS of MGST1. The detoxification enzyme MGST1 is a homotrimeric integral membrane protein with a total of twelve TM helices. Three molecules of GSH are bound, shown in green sticks. Covalent modification of a cytosolic cysteine residue by electrophilic compounds activates the enzyme by pre-organizing regions of the TM helices, highlighted in pink, as revealed by H/D exchange kinetic analysis.

H/D Exchange MS of CcO

The redox-driven proton pump cytochrome *c* oxidase (CcO) is the terminal electron acceptor in the respiratory chains of aerobic organisms that catalyzes the

reduction of O_2 to H_2O .²⁵⁹ The enzyme consists of four subunits donating a total of twenty-two TM helices. H/D exchange MS of CcO solubilized in DDM demonstrates that distinct redox-linked conformational changes in the catalytic cycle of CcO involve the opening and closing of specific proton pathways (Figure 31) and provide protons alternative access to opposite sides of the membrane.²⁶⁰ In addition, this method coupled to mutagenesis reveals the structural location of a gate that controls directional proton flow to either the active site or the exiting pathway of the enzyme.²⁶¹

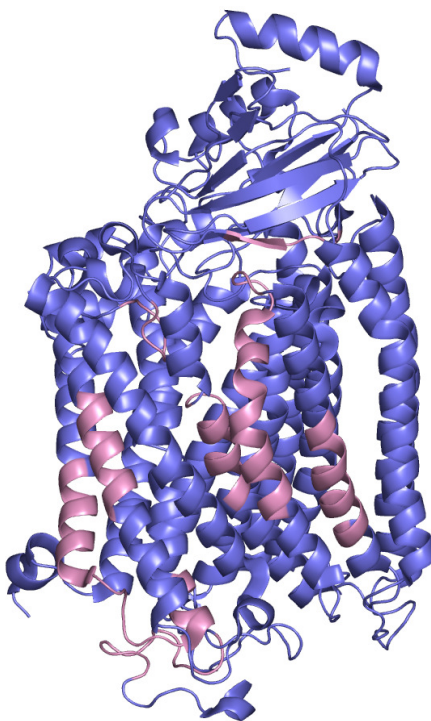


Figure 31. H/D exchange MS of CcO. CcO is an integral membrane protein with a total of twenty-two TM helices. The proton pump is the terminal electron acceptor in the respiratory chains of a variety of organisms. Several redox-dependent conformational changes that occur during the catalytic cycle are revealed by H/D exchange, highlighted in pink.

H/D Exchange MS of Bacteriorhodopsin

The light-driven proton pump bacteriorhodopsin is an integral membrane protein with seven membrane-spanning helices that undergoes a conformational change upon absorbing a photon, resulting in an electrochemical gradient.²⁶² The protein, solubilized in a mixture of 1,2-dimyristoyl-*sn*-glycero-3-phosphocholine (DMPC) and 2[(3-cholamidopropyl)dimethylammonio]-2-hydroxy-1-propanesulfonate (CHAPSO), was denatured by the addition of sodium dodecyl sulfate (SDS), and the structure of the unfolded state was monitored by H/D exchange MS to probe the hydrogen-bonded side-chain interactions within the plane of the membrane (Figure 32).²⁶³ The results confirm a double-mutant cycle analysis, which indicates that most hydrogen-bond interactions within the bilayer or micelle are only modestly stabilizing.²⁶³

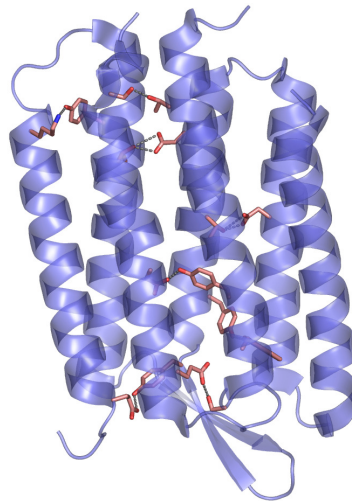


Figure 32. H/D exchange MS of bacteriorhodopsin. Bacteriorhodopsin is a light-driven proton pump with a total of seven TM helices. The hydrogen-bonding interactions of several membrane-embedded residues, highlighted in pink, were analyzed by H/D exchange and confirmed to be only modestly stabilizing.

H/D Exchange MS of β_2 AR

The β_2 -adrenergic G protein-coupled receptor (β_2 AR) plays a critical role in the signaling of many biological processes including glycogenolysis, gluconeogenesis, potassium uptake, and smooth muscle relaxation.²⁶⁴ The seven-TM helix protein is a therapeutic target for diseases including asthma.²⁶⁵ H/D exchange MS of the DDM-solubilized protein reveals the dynamic flexibility of regions within the bilayer (Figure 33).²⁶⁶ In addition, the structural perturbations induced by the binding of an inverse agonist indicates that several small secondary elements are functionally important regions.²⁶⁶

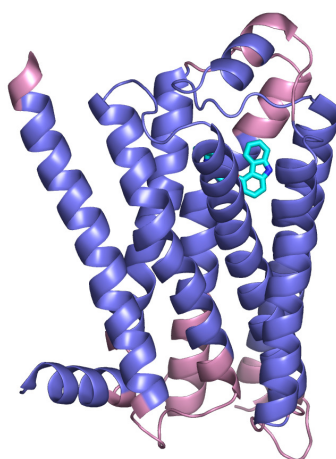


Figure 33. H/D exchange MS of β_2 AR. β_2 AR is a GPCR involved in a multitude of biological processes and has a total of seven TM helices. H/D exchange kinetic analysis reveals several small secondary regions, highlighted in pink, that are involved in the binding of an inverse agonist, shown in cyan sticks.

H/D Exchange MS of GGCX

A key regulator of blood coagulation that is essential for hemostasis, γ -glutamyl carboxylase (GGCX) is an integral membrane protein predicted to have five TM helices.²⁶⁷ GGCX was analyzed by H/D exchange MS solubilized in phospholipid bilayer

nanodiscs,²⁶⁸ which offer a controllable, stable, and monodisperse bilayer similar to that of the native phospholipid membrane.²⁶⁹ The uniformly-sized bilayer was used to perform global topography analysis of GGcX, but the significance of the H/D exchange kinetic analysis is yet to be interpreted. Still, the nanodisc technique represents a unique method for addressing the challenges of performing structural studies of membrane proteins in physiologically relevant conditions.²⁶⁸

Taken together, these studies reveal the diverse utility of H/D exchange MS analyses. With respect to membrane proteins, the technique offers a solution to making the conformational determinations of proteins that were once nearly impossible. From global topography determinations to identifying ligand-binding sites to revealing the dynamic functions of proteins, H/D exchange has proven to be crucial to observing structural dynamics within the bilayer.

Challenges of Membrane Protein H/D Exchange MS

Because spectral analyses are performed on peptides of varying length, one of the difficulties in H/D exchange MS studies has been in the ability to identify individual amide sites of deuterium incorporation. One method by which spatial resolution has been improved upon involves multiple analyses, altering digestion conditions to obtain peptides that overlap in amino acid sequence. These adjustments include changing digestion time, varying protease concentration, adding denaturants, or utilizing multiple acidic proteases with differing specificities.²⁷⁰

Another method by which resolution may be improved is by utilizing MS/MS fragmentation. This has been a much less fruitful method due to the phenomenon of

proton migration, or “scrambling,” of the ionized peptides caused by collision-induced dissociation (CID), resulting in randomization of deuterium incorporation on the parent ion. Alternative fragmentation methods such as electron capture dissociation (ECD) and electron transfer dissociation (ETD) occur more rapidly than CID, impart relatively low internal energy to the parent ion, and have in some cases minimized the scrambling phenomenon.²⁷¹⁻²⁷³

A challenge of membrane protein MS in general, and indeed membrane protein H/D exchange MS in particular, involves detergents. The use of detergents is crucial to various membrane protein protocols with respect to solubilization and stabilization. The presence of detergents in MS analyses, however, can cause suppression of ionization from the ESI source, adduct formation, and interference with peptide ion signals.^{254,274,275} Still, these difficulties can be surmounted by utilizing detergents that are compatible with the electrospray source. Detergents that are anionic like SDS and cationic like laurel dimethylamine oxide, as well as non-ionic polyoxyethylenes including Tween 20 and Triton X-100, tend to suppress peptide ionization.²⁵⁴ However, zwitterionic detergents like CHAPS and nonionic saccharides including *n*-dodecyl- β -D-glucoside and DDM display limited ionization suppression and adduct formation and have proven useful in membrane protein H/D exchange analyses.^{260,266}

An alternative to using an ESI-compatible detergent is to remove the detergent from the sample prior to MS analysis. With respect to H/D exchange MS, this can be performed either before or after the proteolysis step. Common protocols for the removal of detergents prior to proteolysis include dialysis, desalting chromatography,²⁷⁶ or removal by polystyrene or cyclodextrin.^{277,278} Such methods, however, commonly result

in protein precipitation. Less common protocols utilize organic solvent extraction,²⁷⁹ detergent precipitation by acetone or trichloroacetic acid,²⁸⁰ or protein isolation by polyacrylamide gel electrophoresis.²⁸¹ These methods, however, inherently involve the denaturation of proteins and poor recovery of hydrophobic peptides.

Detergent removal may also be performed after the proteolysis step of the H/D exchange MS protocol utilizing chromatography or organic solvent extraction.²⁸²⁻²⁸⁴ While the proteolysis of hydrophobic regions of a membrane protein typically results in shorter, more soluble peptides, these detergent removal techniques tend to suffer the same problems as whole-protein detergent removal in the form of peptide precipitation and poor hydrophobic peptide yields.

One alternative to these methods includes the use of cleavable detergents like acid-labile surfactants (ALS). After hydrolysis by acidification, the hydrophobic portion of the ALS is easily removed by centrifugation, eliminating ionization suppression from the ESI source.^{285,286} While this method has advantages over those previously mentioned, precipitation of hydrophobic peptides can still occur, resulting in potentially valuable data loss. Yet another alternative, nonionic detergent extraction with chlorinated solvents, has recently shown promise as a method of detergent removal that has displayed minimal effect on ESI-MS analysis.²⁸⁷ While persisting as one of the main challenges of membrane protein H/D exchange MS, effective detergent use or removal continues to be an active area of research.

Prospects for H/D Exchange MS

One of the promising prospects for H/D exchange MS is its potential for automation. In this regard, initial studies involve completely automated protein *de novo* sequencing of proteolytic peptides by MS/MS, which has been aided greatly with the advent of powerful computational tools.²⁸⁸ The deuterium labeling protocol itself has been automated with the use of robotics,²⁸⁹ and several software packages have been developed that reduce the labor-intensive task of data processing.²⁹⁰ The high-throughput potential of H/D exchange MS for the screening of conformational changes induced by inhibitor binding presents a potentially significant aid in the understanding of the structure-function relationship.

It is conceivable that H/D exchange kinetic data could be used as constraints in computational modeling and docking studies, aiding in structure prediction. In addition, structural studies of membrane proteins utilizing MS coupled with alternative labeling methods represent an as-yet untapped area of H/D exchange research. These labeling methods include hydroxyl radical foot-printing, oxidative methionine labeling, and electrophysiology-coordinated photo-labeling, which have been successfully used in the analysis of protein-protein interactions,²⁹¹ conformational dynamics in the native lipid environment,²⁹² and structural studies within living cells,²⁹³ respectively. It is feasible that studies in similar conditions could be performed utilizing H/D exchange as an alternative to these techniques.

Kinetic analysis of H/D exchange has been used for decades to probe the structural properties of proteins. The advent of the soft ionization techniques of ESI and MALDI allowed these analyses to be performed using MS on whole proteins. The results

have revealed the utility of H/D exchange MS as a method for observing a wide range of conformational events. Its application to the structural characterization of membrane proteins has proven to be quite successful where traditional methods such as NMR and X-ray crystallography continue to be challenging. In addition, the determination of the conformational dynamics of catalysis in nearly any solution condition represents a unique application of H/D exchange.

While challenges of membrane protein MS remain, particularly with regard to the use of detergents, progress continues to be made. The potential of the technique for automation and its application to high throughput systems represent exciting avenues for structure-function research. The virtually un-tapped field of membrane protein conformation in physiologically relevant systems represents a possible new frontier in H/D exchange MS studies. While already proving its potential, the future prospects of this method for scientific research are particularly exciting.

Purpose of These Studies

The terminal prostanoid synthase MPGES1 plays an important role in the pathology of inflammation. Since its identification as a promising therapeutic target over ten years ago, an extraordinary amount of research has been invested into the enzyme. From its identification to its functional characterization to its structural determination to the discovery of drug leads, studies of MPGES1 continue to aid inflammation research. The purpose of this study is to analyze the structure of MPGES1 and to make observations of its dynamic physical interactions with various ligands in the hope of

furthering the understanding of the function of this enzyme and to ultimately aid in the discovery of new treatments for inflammatory disease.

Structure-based Drug Design

In the past, drug discovery often began with the identification of a lead compound that was typically a natural ligand of a protein or was discovered through the random screening of compounds in *in vitro* or *in vivo* assays.²⁹⁴ Using standard medicinal chemistry, the lead structure is systematically modified through iterative cycles of syntheses of new compounds, which are then assayed for biological activity to derive a structure-activity relationship with respect to some measure of therapeutic efficiency.²⁹⁵ Then emerged high through-put screening (HTS), a method of mechanized testing and rapid assay systems allowing researchers to quickly detect biological activities of extremely large libraries of compounds of diverse structures.²⁹⁶ This method is used extensively today.

Still, another method of drug discovery is structure-based drug design, or rational drug design, a method used in the pharmaceutical industry and academia since the late 1980s.²⁹⁷ This method first involves the identification of a protein target that plays a critical role in an important physiological or pathological pathway, followed by the determination of that target's structure, often by crystallography or NMR. Proteins bind their ligands in specific conformations, and the affinity and specificity of binding is dependent on the chemistry and topographies of their complimentary surfaces. Structural information regarding the conformation of the protein-ligand complex, as well as the molecular interactions between the protein and ligand, are used to rationally modify the

ligand to produce novel analogs that are more potent and/or specific. One famous example of the successful use of this approach is the design of HIV protease inhibitors as AIDS antivirals.²⁹⁸

By analyzing the structure of MPGES1, and by observing the conformational dynamics associated with interactions of MPGES1 with various ligands, it is the aim of this study to better understand the relationship between the structure and the function of the protein, as well as to gain knowledge regarding the mechanism by which the enzyme is inhibited.

Structural Topology of MPGES1

At the initiation of this project, no crystal structure existed for MPGES1. In fact, at that time the only MAPEG superfamily member with a determined crystal structure was MGST1.¹⁶² As a means of predicting the structure of MPGES1, a sequence alignment with MGST1 was performed to locate homologous TM helices, and several computational algorithms for predicting membrane-spanning regions of membrane proteins were utilized. In order to provide physical evidence in support of these prediction methods, backbone amide H/D exchange MS was chosen as a technique to analyze the local and global protein topology of detergent-solubilized MPGES1. Monitoring the selective exchange of hydrogen for deuterium along the protein backbone is a sensitive technique that probes the solvent-accessibility of different regions of a protein, and it also reveals structural motion as a result of various experimental conditions. As summarized in the previous section, H/D exchange kinetic analysis has

become a well-established method for assessing protein structure, and it has been used successfully in the prediction of the overall topology of integral membrane proteins.²⁵⁰

Here, the membrane-spanning regions of MPGES1 are determined utilizing H/D exchange MS kinetic analysis of the enzyme solubilized in two different, structurally distinct detergents. As this effort was nearing completion, the three-dimensional crystal structure of MPGES1 was determined by electron microscopy of two-dimensional crystals in the presence of phospholipids.¹⁶⁶ This allowed for a direct comparison of the determined crystal structure with the H/D exchange topology determinations, as well as with the topologies predicted computationally and by the MGST1 sequence alignment.

The results demonstrate that the overall topology is in agreement amongst these techniques, revealing a protein with four membrane-spanning regions per subunit. In addition, the MPGES1 protein structure is only slightly perturbed as a function of solubilization agent, i.e. phospholipids or the structurally dissimilar detergents CHAPS or DDM, and the structural perturbation is most likely due to interactions between the enzyme and the head groups of the corresponding solubilizing compound.

Location of Inhibitor Binding Sites

In addition to the determination of protein topology, H/D exchange kinetic analysis has been used successfully in observing ligand binding events and assessing protein biopharmaceutical comparability.^{299,300} The second aim of this project addresses inhibitor binding by MPGES1. Although the structure of the protein complexed with GSH has been determined, there is yet to be determined an apo-structure or inhibitor-bound structure of the enzyme.

In light of this, backbone amide H/D exchange MS was utilized to map the binding sites of different types of inhibitors of MPGES1. The results reveal two spatially distinct binding sites, which include the cofactor site as well as a hydrophobic cleft composed of TM helices of neighboring subunits predicted to harbor the substrate-binding site. Analysis of the H/D exchange behavior of the cofactor site confirms the atypical observation that MPGES1 and the closely related MGST1 bind the common cofactor/primary substrate GSH in differing locations and conformations. In addition, H/D exchange kinetics of inhibitors competitive for PGH₂ binding reveal a site within a hydrophobic environment capable of binding a hydrophobic ligand. This knowledge of the locations of the binding sites for these inhibitors could in principal be used as a preliminary guide in structure-based drug design.

Inhibition by 15d-PGJ₂

The cyPG 15d-PGJ₂ is a dehydration product of PGD₂ that binds to PPAR γ with an EC₅₀ value in the low micromolar range,⁷⁹ which may impart the anti-inflammatory signaling properties associated with this mediator, as described in the Eicosanoid section of this introduction. In addition, this lipid mediator has been reported to irreversibly inhibit the pro-inflammatory enzyme MPGES1 with an IC₅₀ value of 0.3 μ M, which may also contribute its anti-inflammatory properties.³⁰¹ The chemical properties of 15d-PGJ₂ are likely dominated by the electrophilic α,β -unsaturated carbonyl group on the cyclopentenone ring that results in the formation of Michael adducts with sulfhydryl-containing nucleophiles including GSH and cellular proteins.^{302,303} As such, this

prostanoid represents a unique inhibitor of MPGES1, unlike those that bind to the cofactor site or those that are synthesized as pharmacologically active inhibitors.

As a naturally occurring inhibitor, 15d-PGJ₂ may form a covalent adduct or involve allosteric binding to MPGES1, and the final aim of this project involves the elucidation of its mechanism of inhibition. A series of biochemical and MS experiments suggest that 15d-PGJ₂ inhibits MPGES1 by covalent adduction of the enzyme at a cytosolic cysteine residue, as well as by binding to the PGH₂ substrate-binding site. Inasmuch as GSH is the most abundant low molecular weight thiol in most cells, it is likely that the most physiologically relevant 15d-PGJ₂ species is that of the GSH adduct.³⁰⁴ However, stable forms of this conjugate display no inhibitory effect on MPGES1 *in vitro*. Still, since the GSH adduct of 15d-PGJ₂ is likely the predominant form of the prostanoid *in vivo*, its chemical structure, as well as its spontaneous kinetics of formation, were determined by MS/MS fragmentation, two-dimensional NMR spectroscopy, and spectrophotometry.

Inflammation research has been, and continues to be, an important field of study. Though relatively new to the field, MPGES1 has garnered much interest due to its promise as a therapeutic target. In the pursuit of furthering the understanding of the function of this enzyme, as well as in aiding in the development of new drug leads, this study focuses on the structure and conformational dynamics of MPGES1. By gaining insight into the global topology of the protein, locating inhibitor binding sites, and analyzing protein interactions with endogenous inhibitors, this study assists in this worthy pursuit.

CHAPTER II

MATERIALS AND METHODS

Materials

Buffer salts and common chemicals were of the highest quality commercially available. Detergents were from Affymetrix Anatrace, Santa Clara, CA. GSO_3^- (**1**) and MK-886 (**4**) were obtained from Sigma, St. Louis, MO. The NovaSAID compound (**2**) was a generous gift from NovaSAID AB, Stockholm, Sweden. MF63 (**3**) was synthesized by the Synthesis Core at the Vanderbilt Institute of Chemical Biology. Prostaglandins including PGD_2 , PGE_2 , $11\beta\text{-PGE}_2$, PGH_2 , and 15-d-PGJ_2 , as well as malondialdehyde were obtained from Cayman Chemical, Ann Arbor, MI. Oasis HLB extractions cartridges were obtained from Waters, Milford, MA.

Methods

Native Protein and C59A Mutant Expression

The human MPGES1 gene with C-terminal hexa-histidine tag was subcloned into a pET-21b vector. For experiments involving the native enzyme, silent mutations were performed for R40, R74, and R123 to correct for codon bias. For experiments involving MPGES1 with Cys-59 mutated the Ala, standard PCR was used with the forward primer GGC CCC CAG TAT GCC AGG AGT GAC CCC and the reverse primer GGG GTC ACT CCT GGC ATA CTG GGG GCC on the native gene with silent R mutations

described above. The resulting mutant enzyme is hereafter referred to as MPGES1 C59A. Both native enzyme and MPGES1 C59A were expressed and prepared by the same protocol, detailed below.

Rosetta 2 (DE3) *E. coli* competent cells were transformed with the expression vector and cultured in a minimal medium (20 mM Na₂HPO₄, 20 mM KH₂PO₄, 90 mM NaCl, 200 mM NH₄Cl, 130 μM CaCl₂, 1 mM MgSO₄, 0.4% glucose, 0.3% casamino acids) at 37 °C and 250 rpm. The cell culture was cooled to 15 °C when an OD₆₀₀ of 0.7 was reached, and expression was induced by the addition of 2 mM IPTG. The cells were cultured further at 15 °C and 200 rpm for 36 to 40 hours. Cells were harvested by centrifugation at 6,500 × g, 4 °C, for 5 minutes and stored at -20 °C. Frozen cell pellets were resuspended in cold lysis buffer (50 mM KH₂PO₄, 300 mM KCl, 1 mM GSH, 1 mM DTT, 1 mM EDTA, 10% glycerol, pH 8.0). Lysozyme was added to 0.2 mg/mL and stirred for 2 hours at 4 °C. Cells were subsequently lysed further, utilizing sonication (60% power, 50% duty cycle, 2 minutes on, 4 minutes off) on ice, until no longer viscous. Cellular debris was cleared by centrifugation at 10,000 × g, 4 °C, for 30 minutes.

Enzyme Preparation

The membrane fraction of the above cleared lysate was isolated using ultracentrifugation at 100,000 × g, 4 °C, for 2 hours. Pellets were washed with 50 mM KH₂PO₄, pH 8.0, and resuspended in cold extraction buffer (50 mM KH₂PO₄, 300 mM KCl, 1 mM GSH, 5 mM imidazole, 10% glycerol, 0.5% DDM, pH 8.0). The enzyme was solubilized by gently stirring at 4 °C, overnight. The solubilized enzyme was added to Ni-NTA agarose (~5 mL per 25 g of wet cells), equilibrated with extraction buffer, and was

incubated by inverting at 4 °C for 1 hour. Resin was applied to a gravity column and was washed with a similar buffer, containing 35 mM imidazole. MPGES1 was then eluted with a similar buffer, containing 250 mM imidazole. The elution was concentrated to ~1.5 column volumes and then dialyzed, MWCO 6-8 kDa, against 1 L cold ion exchange buffer (50 mM KH₂PO₄, 1 mM GSH, 20% glycerol, 1% polyoxyethylene(10)dodecyl ether, pH 7.0) at 4 °C overnight. The dialyzed protein was then applied to sulfopropyl sepharose (~3 mL per 25 g of wet cells), equilibrated with ion exchange buffer, in a gravity column. The resin was washed with a similar buffer, containing 1% CHAPS, and was eluted with a linear KCl gradient, 0-200 mM, in a similar buffer, containing 0.5% CHAPS. The extent of purification of the protein was subsequently estimated by SDS PAGE. Purified MPGES1 was concentrated in an Amicon ultrafiltration system, MWCO 10 kDa, to 1 mg/mL and was then dialyzed, MWCO 10 kDa, against 200 mL cold MS buffer (50 mM KH₂PO₄, 300 mM KCl, 1 mM GSH, 1 mM DTT, 7.5% glycerol, 1% CHAPS, pH 7.0) at 4 °C overnight.

For preparation of the DDM-solubilized enzyme, CHAPS was replaced with equal concentration (w/v) amounts of DDM at the sulfopropyl sepharose chromatography step, as well as in all subsequent steps. For preparation of the glutathione sulfonate (GSO₃⁻)-bound enzyme, GSH was replaced with equimolar amounts of GSO₃⁻ at the sulfopropyl sepharose chromatography step, as well as in all subsequent steps. For analyses involving 15d-PGJ₂, DTT was not included in either the last chromatography step or final dialysis. Instead, these buffers were purged with argon. Inasmuch as MPGES1 is unstable when the GSH cofactor-binding site is unoccupied, apo-MPGES1

experiments were not possible. As such, in all described experiments MPGES1 is complexed with either GSH or GSO_3^- , as noted.

Preparation of 9-(S-Glutathionyl)-15d-PGJ₂

The conjugation of GSH to 15d-PGJ₂ was initiated by the addition of 1.5 mL of 10 mM GSH in 100 mM KH₂PO₄, pH 7.0, to 500 μg of 15d-PGJ₂ at 40 °C for 30 minutes. The reaction was stopped by the addition of 100 μL of 70% H₂SO₄, after which the sample was applied to a 6cc Oasis hydrophilic-lipophilic balance (HLB) solid-phase extraction cartridge that was previously activated with methanol and hydrated with 50 mM ammonium acetate, pH 3. The sample was washed with 50 mM ammonium acetate, pH 3, and eluted with methanol. After evaporation under nitrogen, the sample was reconstituted in 15% CH₃CN and 0.01% formic acid and stored on dry ice. It was subsequently purified by HPLC, monitoring at 308 nm, using a Beckman 5 μ, 80 Å C18 column (4.6 mm x 25 cm), and eluted at 1 mL/min with a gradient of 15% to 95% CH₃CN and 0.01% formic acid over a 30-minute period. After collecting the 9-(S-glutathionyl)-15d-PGJ₂ peak at approximately 20 minutes on dry ice, the sample was dried under vacuum and stored desiccated at -80 °C.

Preparation of 9-(S-Glutathionyl)-11-hydroxy-15d-PGJ₂ and 11-Hydroxy-15d-PGJ₂

The 9-(S-glutathionyl)-11-hydroxy-15d-PGJ₂ adduct of 15d-PGJ₂ was prepared by adding 40 μL of a 25 mM solution of 15d-PGJ₂ in DMSO to 160 μL of 6.3 mM GSH in 100 mM KH₂PO₄, pH 7.0, and incubating at 22 °C for one hour. The adduct was then reduced by the addition of 10 μL of a 1 M suspension of NaBH₃CN in THF and storing

overnight at 4 °C. The reaction was subsequently diluted ten-fold in 20 mM Tris, pH 8.0. The product was purified by diethylaminoethyl weak anion exchange chromatography, washing with 20 mM Tris, pH 8.0, and eluting with 100 mM KH₂PO₄, pH 7.5, containing 1 M KCl, 1% glycerol, and 1% CHAPS. The 11-hydroxy-15d-PGJ₂ was prepared as above without the reaction with GSH.

Structure of 9-(S-Glutathionyl)-15d-PGJ₂ and 9-(S-Glutathionyl)-11-hydroxy-15d-PGJ₂

The structure of the glutathionyl adduct of 15d-PGJ₂ was determined by LC-MS/MS, as well as by 2D NMR spectroscopy. For MS analysis, the borohydride-reduced GSH adduct was prepared as described above. In addition, a cysteine adduct was prepared as described above, replacing GSH with equimolar L-cysteine. Analysis was performed by reversed-phase LC-MS/MS, using a Phenomenex Synergi 2.5 μ, Hydro-RP, 100 Å C18 column (100 x 2.00 mm), and eluting at 0.2 mL/min with a gradient of 15% to 95% CH₃CN and 0.01% formic acid over a 30 min period. Ions of *m/z* 300 to 1300 were detected on a ThermoFinnigan TSQ triple-quadrupole mass spectrometer using positive electrospray ionization. The PG adduct was identified with a mass corresponding to the monoisotopic mass of GSH or cysteine plus the monoisotopic mass of reduced 15d-PGJ₂, and the site of adduction was determined by MS/MS fragmentation.

The diastereoselectivity of the reaction of GSH with 15d-PGJ₂ was determined by 2D NMR spectroscopy at high field. NMR data were acquired either using a 22.1 T Bruker magnet equipped with a Bruker AV-III console or a 14.9 T Bruker magnet equipped with a Bruker AV-III console. All spectra were acquired in 3 mm NMR tubes using a Bruker 5 mm TCI cryogenically cooled NMR probe. Chemical shifts were

referenced internally to CD₃OD (3.30 ppm) or D₂O (4.70 ppm), which also served as the ²H lock solvents. For 1D ¹H NMR, typical experimental conditions included 32K data points, 13 ppm sweep width, a recycle delay of 1.5 seconds and 32 scans. For samples acquired in D₂O, water suppression using pre-saturation was implemented in order to reduce the signal of residual H₂O. For 2D ¹H-¹H COSY and DQF-COSY, experimental conditions included 2048 x 512 data matrix, 13 ppm sweep width, recycle delay of 1.5 seconds and 4 scans per increment. The data were processed using squared sine-bell window function, displayed in either the magnitude mode (COSY) or absolute intensity mode (DQF-COSY). Similar experimental parameters were used to acquire 2D ¹H-¹H nuclear Overhauser effect (NOESY) experiments which were acquired with a mixing time of 400 ms. The data were processed using a $\pi/2$ shifted squared sine window function displayed in absolute intensity mode. Multiplicity-edited HSQC experiments were acquired using a 1024 x 256 data matrix, a J(C-H) value of 145 Hz which resulted in a multiplicity selection delay of 34 ms, a recycle delay of 1.5 seconds and 16 scans per increment along with GARP decoupling on ¹³C during the acquisition time (150 ms). The data were processed using a $\pi/2$ shifted squared sine window function and displayed with CH/CH₃ signals phased positive and CH₂ signals phased negative.

Kinetics of the Spontaneous Reaction of GSH with 15d-PGJ₂

The kinetics of the approach to equilibrium were determined at 25 °C under pseudo-first-order conditions with a fixed concentration of 40 μ M 15d-PGJ₂ and a variable excess concentration of GSH ranging between 0.5 to 5.0 mM in 100 mM KH₂PO₄, pH 7.0. Reactions were initiated by the addition of 10 μ L of a 4.0 mM stock

solution of 15d-PGJ₂ in 20 mM KH₂PO₄, pH 7.0, to 990 μL of GSH in the same buffer. The formation of the glutathionyl adduct was observed spectrophotometrically as an exponential decrease in absorbance at 250 nm. The concentration dependence of k_{obs} was used to determine the rate constants for the forward (k_1) and reverse (k_{-1}) reactions from eq. 1:

$$k_{\text{obs}} = k_1[\text{GSH}] + k_{-1} \quad (\text{Eq. 1})$$

In addition, the equilibrium constant for formation (K_f) of 9-(S-glutathionyl)-15d-PGJ₂ was calculated by determining the final concentrations of reactants and products at equilibrium under four different initial reactant concentrations. Two reactions were initiated by the addition of 25 μL of 2 mM 15d-PGJ₂ stock solution in 100 mM KH₂PO₄, pH 7.0, to 475 μL of 105 μM or 211 μM GSH in the same buffer, giving an initial 15d-PGJ₂ concentration of 100 μM and initial concentrations of GSH of 100 μM or 200 μM, respectively. Two additional reactions were initiated by the addition of 50 μL of the same 15d-PGJ₂ stock solution to 450 μL of 111 or 222 μM GSH, giving a 15d-PGJ₂ concentration of 200 μM and GSH concentrations of 100 or 200 μM, respectively. Each reaction mixture was incubated at 4 °C overnight. After equilibrating to 22 °C for one hour the samples were analyzed by HPLC, monitoring the absorbance at 316 nm, using a Phenomenex Synergi 2.5 μ, Hydro-RP, 100 Å C18 column (100 x 2.00 mm), and eluting at 0.2 mL/min with a gradient of 15% to 95% CH₃CN and 0.05% trichloroacetic acid over a 30 min period.

Glutathione Transferase Enzyme Activity Assays

Glutathione transferase activity of native MPGES1 and MPGES1 C59A utilizing CDNB as a secondary substrate was verified using the method previously described.²⁰⁵ Reactions were initiated at 22 °C by the addition of 10 µL of 200 mM CDNB in acetonitrile to 990 µL of 100 mM KH₂PO₄, pH 6.5, containing 4 mM GSH, 1 µM enzyme, and either 0.1% DDM or 1% CHAPS, and were followed over the course of thirty minutes spectrophotometrically at 340 nm. The background spontaneous reaction was also assayed in the same conditions, lacking enzyme.

Glutathione transferase activity of native MPGES1 and MPGES1 C59A utilizing 15d-PGJ₂ as a secondary substrate was analyzed using a similar spectrophotometric assay. Reactions were initiated at 22 °C by the addition of 5 µL of 2.5 mM 15d-PGJ₂ in 100 mM KH₂PO₄, pH 7.0, to 495 µL of 100 mM KH₂PO₄, pH 7.0, containing 1 mM GSH, 1 µM enzyme, 10% glycerol, and 1% CHAPS. The reaction was followed by iterative scans of 440 – 220 nm, monitoring the decrease in absorbance at 250 nm, over the course of several hours. The background spontaneous reaction was also assayed in the same conditions, lacking enzyme.

Prostaglandin E Synthase Activity and Inhibition Assay by Mass Spectrometry

The isomerization of PGH₂ to PGE₂ and its inhibition were verified with a method adapted from that of reference 48, and the detection of PGE₂ by LC-MS/MS was performed as previously published.³⁰⁵ Reactions were initiated at 0 °C by the addition of 100 µL of a 100 nM enzyme stock solution in reaction buffer (100 mM KH₂PO₄, pH 7.5, containing 2.5 mM GSH, 1% glycerol and 1% CHAPS) to 6.7 µL of 75, 150, or 300 µM

PGH₂ in acetone. After a one-minute incubation on ice, unreacted PGH₂ was decomposed to malondialdehyde (MDA) and 12-(S)-hydroxy-8,10-*trans*-5-*cis*-heptadecatrienoic acid (12-HHT) by the addition of 400 μ L of 25 mM FeCl₂ in 50 mM citric acid, pH 3.0, which included 0.5 μ M 11 β -PGE₂ as an internal standard. After solid-phase extraction, the resulting prostaglandins were reconstituted in 5% CH₃CN and analyzed by reversed-phase LC-MS/MS, with a Phenomenex Synergi 2.5 μ , Hydro-RP, 100 Å C18 column (100 x 2.00 mm), and eluted at a flow rate of 0.2 mL/min with 32% CH₃CN and 0.01% formic acid. Single-reaction monitoring (SRM) of the transition *m/z* 351 to 271 was utilized for PGE₂ detection on a ThermoFinnigan TSQ triple-quadrupole mass spectrometer using negative electrospray ionization. To verify inhibition, the procedure was repeated, pre-incubating on ice with inhibitors of the following concentrations: 1 mM MK-886 (**4**) from a 10 mM stock in DMSO; 100 μ M MF63 (**3**) from a 1 mM stock in DMSO; 100 μ M NovaSAID compound (**2**) from a 1 mM stock in DMSO; 5 mM GSO₃⁻ (**1**) from a 400 mM stock in 100 mM KH₂PO₄, pH 7.0; and 100 μ M 15d-PGJ₂ from a 1 mM stock in DMSO. The IC₅₀ value for **1** was determined utilizing the aforementioned procedure, by adding 100 μ L of 1 μ M enzyme, pre-incubated with **1** ranging in concentrations from 0.004 to 37.5 mM, to 3 μ L of 300 μ M PGH₂.

Prostaglandin E Synthase Activity and Inhibition Assay by Fluorescence

The inhibition kinetics of MPGES1 by 15d-PGJ₂ were determined with a method adapted from a previously described technique.¹⁹⁴ The enzyme, complexed with GSO₃⁻, was combined with the inhibitor by addition of 10 μ L of solutions of the 15d-PGJ₂ ranging in concentrations from 0.1 μ M to 5 mM in reaction buffer lacking GSH to 90 μ L

of a 1.1 μM enzyme solution in reaction buffer lacking GSH, giving a final enzyme concentration of 1 μM and a final inhibitor concentration range of 0.01 to 500 μM . An additional incubation was initiated by the addition of 40 μL of a 5 mM stock solution of 15d-PGJ₂ in reaction buffer lacking GSH to 60 μL of 1.7 μM enzyme, giving final concentrations of 2 mM and 1 μM , respectively. After a one-hour incubation on ice, 2.5 μL of a 100 mM stock solution of GSH in 100 mM KH₂PO₄, pH 7.0, were added to the pre-incubated protein, mixed, and incubated at 0 °C for five minutes. The reaction was subsequently initiated by the addition of 100 μL of each sample to 5 μL of 100 μM PGH₂ in acetone and incubated at 22 °C for one minute. Un-reacted PGH₂ was decomposed to MDA and 12-HHT by the addition of 200 μL of 50 mM FeCl₂ in 500 mM KH₂PO₄, pH 2.0. To form a fluorescent complex of MDA in solution, 500 μL of 15 mM thiobarbituric acid (TBA) in 80 mM KH₂PO₄, pH 2.0, was added to the reaction mixture and heated to 80 °C for thirty minutes. Precipitate was removed by centrifugation, and the resulting fluorescent MDA-TBA complex was detected with a Horiba Fluorolog fluorescence spectrometer, tuned to excitation and emission wavelengths of 530 nm and 550 nm, respectively. The same method was used to examine the inhibition of MPGES1 by 11-hydroxy-15d-PGJ₂ and 9-(S-glutathionyl)-11-hydroxy-15d-PGJ₂.

Covalent Modification of MPGES1 by 15d-PGJ₂

The site of adduction of the enzyme by 15d-PGJ₂ was determined by LC-MS/MS sequencing. The covalent modification was initiated by the addition of 2 μL of 25 mM 15d-PGJ₂ in DMSO to 100 μL of 1 mg/mL (60 μM) purified native enzyme in 50 mM KH₂PO₄, pH 7.0, containing 300 mM KCl, 7.5% glycerol, 1% CHAPS, and either 1 mM

GSH or 1 mM GSO₃⁻. After an overnight incubation at 4 °C, the Michael adduct was reduced with NaBH₃CN, as described above for the glutathionyl adduct. For MS analysis, 10 µL of the pre-incubated protein was diluted five-fold in H₂O at 22 °C, after which 50 µL of ice-cold 100 mM KH₂PO₄, pH 2.3, was added, dropping the pH to 2.5. The protein was then digested on ice for five minutes by the addition of 2 µL of 10 mg/mL (290 µM) pepsin in H₂O. The resulting peptides were separated by HPLC on an ice-cold Phenomenex Jupiter 5 µ, 300 Å C18 column (50 x 1.00 mm), and eluted at 0.3 mL/min with a 30-minute gradient of 2-50% CH₃CN and 0.4% formic acid. Ions of *m/z* 300 to 1500 were detected on a ThermoFinnigan TSQ triple-quadrupole mass spectrometer using positive electrospray ionization. Peptides containing the reduced adduct were identified as those with a mass shift corresponding to the monoisotopic mass of reduced 15d-PGJ₂, and were verified by MS/MS sequencing.

In order to determine the regiochemistry of enzyme adduction on 15d-PGJ₂, the procedure from the previous paragraph was repeated on a ThermoFinnigan LTQ ion trap mass spectrometer using positive electrospray ionization. The peptide identified as containing the PG adduct was subject to MS³ fragmentation, selecting for the *y*-ion containing the adducted Cys-59 residue.

Peptide sequencing by Tandem Mass Spectrometry

Prior to H/D exchange MS analyses, both the native enzyme and MPGES1 C59A were sequenced by LC-MS/MS, essentially by the method previously described.¹⁹⁴ The protein was first brought to a concentration of 0.2 mg/mL (12 µM) in ice-cold H₂O. Digestion was performed on ice for five minutes by the addition of 2 µL of 10 mg/mL

(290 μM) pepsin in H_2O . The resulting peptides were separated by reversed-phase HPLC on an ice-cold Phenomenex Jupiter 5 μm , 300 \AA C18 column (50 x 1.00 mm), and eluted at a flow rate of 0.3 mL/min with a thirty-minute gradient of 2-50% CH_3CN and 0.4% formic acid. Scans of m/z 300 to 1500 were utilized for peptide detection on a ThermoFinnigan TSQ triple-quadrupole mass spectrometer using positive electrospray ionization, and peptides were sequenced by data-dependent tandem MS/MS by CID. The putative identity of each peptide was determined from the parent ion m/z value using the MS analysis software MassXpert.³⁰⁶ Each putative identification was subsequently confirmed by database searching, making individual comparison of the MS/MS spectra to the corresponding theoretical fragmentation patterns, as generated by the ProteinProspector software MS-Product.³⁰⁷

Amide Hydrogen/Deuterium Exchange Mass Spectrometry and Kinetic Analysis.

Several kinetic analyses of backbone amide H/D exchange were performed on MPGES1. To make topology determinations, experiments were performed on native MPGES1 in complex with GSH and solubilized in either CHAPS or DDM micelles. To study inhibitor binding, H/D exchange experiments were conducted on native MPGES1•GSH unbound to any inhibitors and compared to MPGES1•**1**, as well as to MPGES1•GSH bound to each of the inhibitors **2**, **3**, and **4**. Additionally, to monitor the structural interaction of MPGES1 with 15d-PGJ₂, H/D exchange kinetic analyses were performed on the native enzyme, as well as the C59A mutant, in complex with either GSH or GSO_3^- , in the presence of 15d-PGJ₂ and compared to identical solution conditions lacking 15d-PGJ₂.

The H/D exchange MS assays were performed essentially as previously described.¹⁹⁴ For studies involving the binding of inhibitors **2** – **4**, overnight pre-incubation at 4 °C was initiated by the addition of 4 µL of 5 mM inhibitor in DMSO to 200 µL of 1 mg/mL (60 µM) purified MPGES1•GSH in 50 mM KH₂PO₄, pH 7.0, containing 300 mM KCl, 7.5% glycerol, and 1% CHAPS. The binding of inhibitor **1** was analyzed on 200 µL of 1 mg/mL (60 µM) purified MPGES1•GSO₃⁻ in the same buffer. For studies of 15d-PGJ₂ binding, pre-incubation of the enzyme with the PG was initiated by the addition of 4 µL of 25 mM 15d-PGJ₂ in DMSO to 200 µL of 1 mg/mL (60 µM) purified native enzyme or C59A mutant in 50 mM KH₂PO₄, pH 7.0, containing 300 mM KCl, 7.5% glycerol, 1% CHAPS, and either 1 mM GSH or 1 mM GSO₃⁻, and was incubated overnight at 4 °C.

It is important to emphasize that all H/D exchange experiments, except when specifically mentioned, were performed on MPEGS1 solubilized in CHAPS detergent micelles. The detergent CHAPS was ultimately chosen in inhibitor-binding studies due to its minimal suppression of ionization from the electrospray source. Final inhibitor concentrations were as follows: 1 mM **1**, 100 µM each of **2**, **3**, and **4**, and 500 µM 15d-PGJ₂.

Deuterium incorporation was initiated by a five-fold dilution of 10 µL of the pre-incubated protein solution into D₂O at 22 °C. The incorporation was then quenched by a two-fold dilution in ice-cold 100 mM KH₂PO₄, pH 2.3. The protein was then digested on ice for five minutes by the addition of 2 µL of 10 mg/mL (290 µM) pepsin in H₂O. The resulting peptides were separated by reversed-phase HPLC on an ice-cold Phenomenex Jupiter 5 µ, 300 Å C18 column (50 x 1.00 mm), and eluted at a flow rate of 0.3 mL/min

with a fifteen-minute gradient of 2-50% CH₃CN and 0.4% formic acid. Scans of m/z 300 to 1500 were utilized for peptide detection on a ThermoFinnigan TSQ triple-quadrupole mass spectrometer using positive electrospray ionization. Deuterium incorporation was observed as a shift in the centroid of the ion envelope (average mass) for each peptide. In order to correct for deuterium incorporation that occurs after the quenching step, a control for time point zero was performed, in which 10 μ L of the protein solution was added to 50 μ L of ice-cold 100 mM KH₂PO₄, pH 2.3, followed by addition of 40 μ L of ice-cold D₂O and pepsin digestion, as described above. A control sample accounting for the loss of deuterium that occurs during the chromatography step was also performed, in which the peptide was first fully labeled at all exchangeable backbone amide sites by diluting 10 μ L of the protein solution five-fold in D₂O and heating to 40 °C for four hours. This was followed by a two-fold dilution in ice-cold 100 mM KH₂PO₄, pH 2.3, and pepsin digestion, as described above.

The kinetics of backbone amide H/D exchange behavior of each peptide were determined as previously described.¹⁹⁴ The number of deuterons incorporated onto each peptide were calculated, correcting for the loss and gain of deuterium during the analysis, using eq. 2:

$$D = \left[N \left(\frac{m_t - m_{0\%}}{m_{100\%} - m_{0\%}} \right) \right] \quad (\text{Eq. 2})$$

in which D is the number of deuterons incorporated, N is the total number of exchangeable backbone amide sites, m_t is the average mass of the partially deuterated

peptide sample at time t , and $m_{0\%}$ and $m_{100\%}$ are the average masses of the non-deuterated and fully deuterated peptide control samples, respectively.

The number of incorporated deuterons D were plotted as a function of time, on a logarithmic scale, and fit to an equation consisting of a sum of first-order exponential rate terms given by eq. 3:

$$D = N - \sum_{n=1}^N A_n e^{-k_n t} \quad (\text{Eq. 3})$$

in which A_n and k_n are the amplitudes and rate constants of the n th phase of the exchange. The exchange amplitude at time zero (A_{fast}) represents the number of hydrogens that exchange within the first 15 seconds. The value of A_{fast} is the difference between the sum of the fitted amplitudes ($A_1 + A_2 \dots + A_n$) in the intermediate kinetic phases (> 15 s) and the total number of exchangeable sites in the peptide.

Inasmuch as A_{fast} is an extrapolated value and not a fitted parameter, no errors are reported. Given that the errors in the fitted amplitudes A_1 , A_2 , and A_3 are typically $< 10\%$, the errors in A_{fast} are estimated to be $< 20 - 30\%$. The kinetic data were used to identify regions of the enzyme involved in inhibitor binding and were guided by the following criteria. Peptides displaying significant changes in deuterium incorporation rates were those that exhibited an increase or decrease in the number of fast-exchanging (A_{fast}) or slow exchanging sites, comprising 15% of the backbone amide protons in the peptide. For sites exchanging at intermediate rates, a 10-fold change in the rate of exchange for at least one amide site of the peptide was defined as significant.

CHAPTER III

TOPOLOGY OF MICROSOMAL PROSTAGLANDIN E SYNTHASE 1

Results

Prediction of Transmembrane Helices of MPGES1 by Computational Methods

Hydropathy plots calculated from the Kyte-Doolittle algorithm, which progressively evaluates the hydrophilicity and hydrophobicity of a protein as a function of its amino acid sequence,³⁰⁸ were previously utilized to predict that the MAPEG superfamily members share a conserved secondary structure consisting of four TM helices.¹⁶¹ In the study described here, several contemporary computational methods optimized for predicting TM helices of integral membrane proteins from their amino acid sequence were used. These include TMPred, PHDhtm, and SOSUI, and the results of the prediction algorithms are illustrated as a sequence alignment in Figure 34.

TMPred uses an algorithm based on the statistical analysis of a database of naturally-occurring integral membrane proteins to predict membrane-spanning regions.³⁰⁹ The prediction reveals four TM helices, consisting of residues 15 –31, 81 –101, 97 –118, and 127 –146. PHDhtm, a multiple alignment-based neural network system for predicting the location and topology of TM helices,³¹⁰ projects four membrane-embedded helices spanning the residues 16 – 33, 76 – 93, 98 – 117, and 128 – 145. SOSUI predicts secondary structure of membrane proteins utilizing an amphiphilicity index of polar

amino acids of the protein sequence to define membrane-water interfaces.^{311,312} This algorithm displays four TM helices ranging 12 – 34, 73 – 95, 99 – 120, and 129 – 151.

```

          15-AFLLCSTLLVIKMYVVA-31
TM I      16-FLLCSTLLVIKMYVVAI-33
          12-ALPAFLLCSTLLVIKMYVVAIIT-34

          81-PFLFLGFVYSFLGPNPFVAVM-101
TM II     76-METIYPFLFLGFVYSFLG-93
          73-RNDMETIYPFLFLGFVYSFLGPN-95

          97-FVAVMHFLVFLVGRVAHTVAYL-118
TM III    98-VAWMHFLVFLVGRVAHTVAY-117
          99-AWMHFLVFLVGRVAHTVAYLGK-120

          127-SVYTLAQLPCASMALQILW-146
TM IV     128-VYTLAQLPCASMALQIL-145
          129-TYTLAQLPCASMALQILWEAARH-151

```

Figure 34. Prediction of topology of MPGES1 by computational methods. Shown is a qualitative map of the four computationally predicted TM helices of MPGES1 as a function of amino acid sequence. Each color represents an individual computational method with TMPred in black, PHDhtm in blue, and SOSUI in red.

Prediction of Transmembrane Helices of MPGES1 by Sequence Alignment with MGST1

Both MPGES1 and MGST1 belong to the MAPEG superfamily of integral membrane proteins, their activities are GSH-dependent, and the human enzymes share 38% sequence identity. The three-dimensional structure of rat MGST1, to which human MPGES1 shares 36% sequence identity, was determined by electron microscopy of two-dimensional crystals.¹⁶² The structure reveals that the enzyme forms a homotrimer with each subunit contributing four TM helices. ClustalW2, a general purpose computer program that produces biologically meaningful alignments of similar or divergent amino acid sequences,³¹³ was used to predict homologous TM helices of MPGES1, which is shown in Figure 35. The alignment reveals a prediction of TM I spanning residues 12 –

37, TM II ranging 79 – 92, TM III including 96 – 112, and TM IV consisting of 127 – 142.

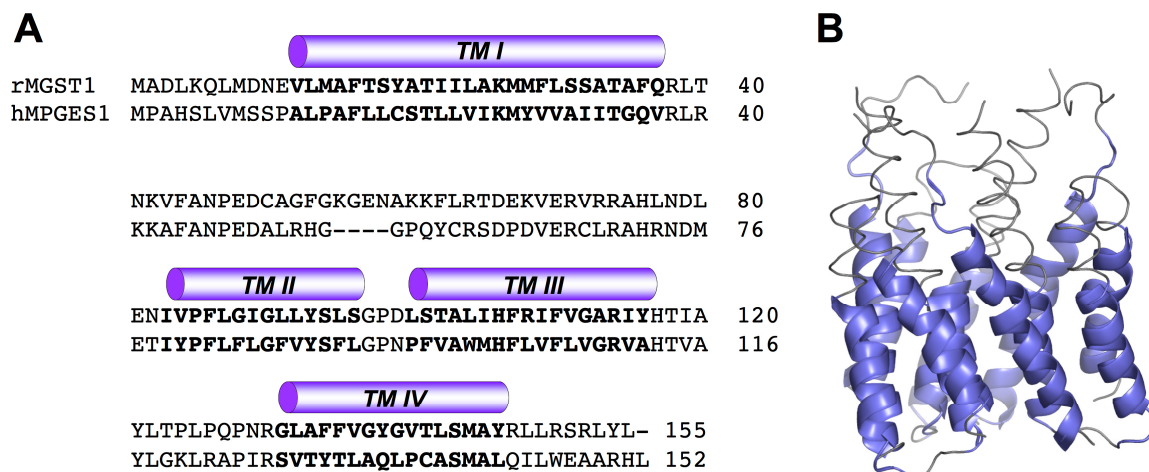


Figure 35. Prediction of topology of MPGES1 by sequence alignment. (A) The sequence alignment of human MPGES1 with rat MGST1, which share 36% sequence identity, reveals four TM helices, as indicated by the purple bars and boldface text. (B) The crystal structure of rat MGST1 was determined to 3.2 Å by electron microscopy of two-dimensional crystals. The regions highlighted in purple correspond to the membrane-embedded regions of the α -helices.

Topology of MPGES1 by Amide H/D Exchange Kinetic Analysis

The analysis of H/D exchange kinetics was performed on 19 peptides, ranging in length from 3 to 16 residues, covering 90% of the entire protein sequence, and assayed over a period of 15 seconds to 8 hours. Two separate analyses were performed: one of MPGES1 solubilized in the detergent CHAPS, and the other of the enzyme solubilized in the detergent DDM, as shown in Figure 36. H/D exchange kinetics can be divided into three general types of rates: fast, intermediate, and slow. In general, fast rates ($k \geq 10 \text{ s}^{-1}$) indicate solvent exposure, while slow rates ($k \leq 10^{-4} \text{ min}^{-1}$) are indicative of amide nitrogens that are either protected from the solvent or are involved in hydrogen

bonding.²⁴⁸ In the case of membrane proteins, peptides that contain a low composition of rapid-exchanging amides and a high composition of slow-exchanging amides indicate regions that are membrane- or micelle-embedded.

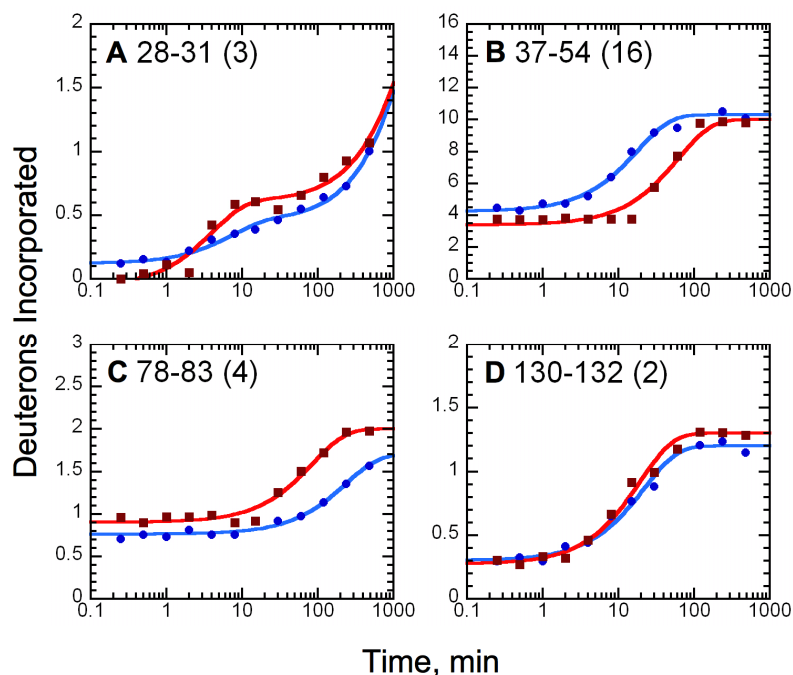


Figure 36. H/D exchange kinetic profiles for MPGES1 as a function of detergent. Shown are the average kinetic profiles for deuterium incorporation as a function of time for MPGES1 solubilized in either CHAPS (blue) or DDM (red), with the number of exchangeable amide protons for each peptide in parentheses. Complete kinetic data for all plots may be found in the Appendix (Figures 60-63).

Membrane-spanning regions of MPGES1 were identified as peptides consisting of at least 80% slow-exchanging amides while having a maximum of 20% fast-exchanging sites (Figure 37). The results reveal that the micelle-embedded regions of MPGES1 are consistent between the two different detergent conditions, with the membrane-spanning regions encompassing residues 14 – 36, 84 – 103, 108 – 123, and 133 – 152.

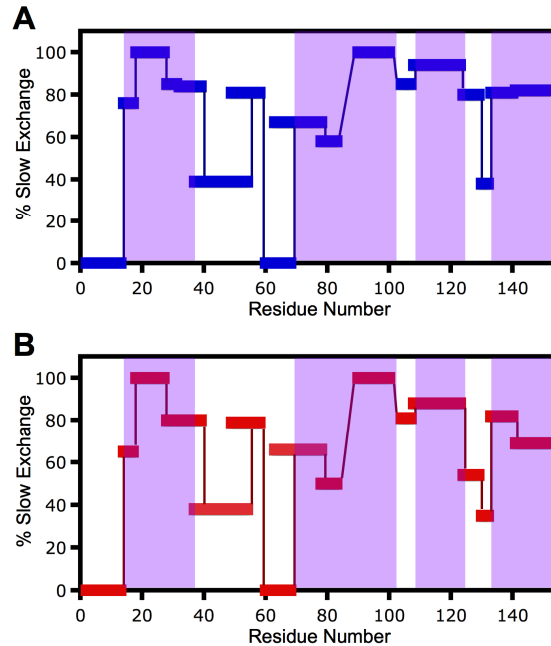


Figure 37. Determination of topology of MPGES1 by H/D exchange MS. The extent of slow-exchanging kinetics is plotted as a function of amino acid sequence for MPGES1 solubilized in either (A) CHAPS or (B) DDM detergent micelles. Highlighted in purple are regions that contain peptides that consist of at least 80% slow-exchanging amides, while having a maximum of 20% fast-exchanging amides, and are predicted to be micelle-embedded regions. Peptide 48-58 is not predicted to be membrane-embedded, as it contains >20% fast-exchanging amides.

Discussion

Comparison of Structural Prediction Methods for MPGES1

The results from the prediction algorithms reveal that MPGES1 contains four TM helices, in agreement with the Kyte-Doolittle prediction.¹⁶¹ The N-terminal region of the first membrane-spanning helix begins within the first twelve-to-sixteen amino acids of the peptide sequence and ends before the thirty-fifth. The prediction for the second TM region is more varied, in that it begins between amino acids R73 and P81 and ends between G93 and M101. The prediction algorithms are most consistent for the third TM, with the N-terminal end within F97 – A99, and the C-terminal end between Y117 and

K120. Finally, the fourth predicted TM is also well conserved amongst the prediction algorithms and begins within S127 – T129 and ends between L145 and H151. A limitation of the computational method, however, is particularly revealed in the case of the algorithm TMPred, which predicts TMs II and III to overlap in amino acid sequence. Clearly, the inclusion of complimentary methods to locate membrane-spanning regions of proteins is beneficial.

Overall, when comparing the computational predictions with the MGST1 sequence alignment and also with the H/D exchange kinetics, it is revealed that there is a high degree of consistency in the determination of the location of TM I (Figure 38). The membrane-spanning region of TM II is relatively uncertain, as the computational methods, sequence alignment, and H/D exchange results reveal a relatively broad range in the terminal ends of the helices. With regard to TM III and TM IV, the predictions made by computation and sequence alignment are highly conserved, while the determinations made from H/D exchange suggest membrane-spanning regions that are shifted to higher-numbered amino acid residues.

12-ALPAFLLCSTLLVIKMYVVAIIT-34
TM I 12-ALPAFLLCSTLLVIKMYVVAIITGQV-37
 14-PAFLLCSTLLVIKMYCCAIITGQ-36

73-RNDMETIYPFLFLGFVYSFLGPNPFVAVM-101
TM II 79-IYPFLFLGFVYSFLGPN-95
 84-FLGFVYSFLGPNPFVAVMHF-103

97-FVAVMHFLVFLVGRVAHTVAYL GK-120
TM III 96-PFVAVMHFLVFLVGRVA-112
 108-VGRVAHTVAYL FKLRA-123

127-SVTYTLAQLPCASMALQILWEAARH-151
TM IV 127-SVTYTLAQLPCASMAL-142
 133-AQLPCASMALQILWEAARHL-152

Figure 38. Comparison of prediction methods. Shown is a qualitative map indicating the locations of the TM helices of MPGES1 as a function of amino acid sequence by computational methods (black), sequence alignment with MGST1 (green), and H/D exchange MS (purple). The intensity of the text for the computational methods reflects the consensus between the three prediction algorithms.

Comparison of Structural Predictions with MPGES1 Crystal Structure

During the course of this study, the crystal structure of human MPGES1 (Figure 39) was determined to 3.5 Å by electron diffraction of two-dimensional crystals in a phospholipid bilayer.¹⁶⁶ It is revealed that MPGES1 is structurally homologous to MGST1, being a homotrimeric protein with four TMs per monomer, as predicted computationally. The crystal structure allows for a comparison of the topology of the protein determined by crystallography from a phospholipid bilayer to that determined by H/D exchange kinetic analysis of detergent-solubilized protein. Also the accuracy of the predictions by computational methods, as well as by the MGST1 sequence alignment can be investigated. By mapping onto the structure the membrane-spanning regions as predicted by computation and sequence alignment, it is revealed that there is a high

degree of accuracy in the predictions. In particular, the large cytosolic loop regions are well predicted and highly conserved between the techniques.

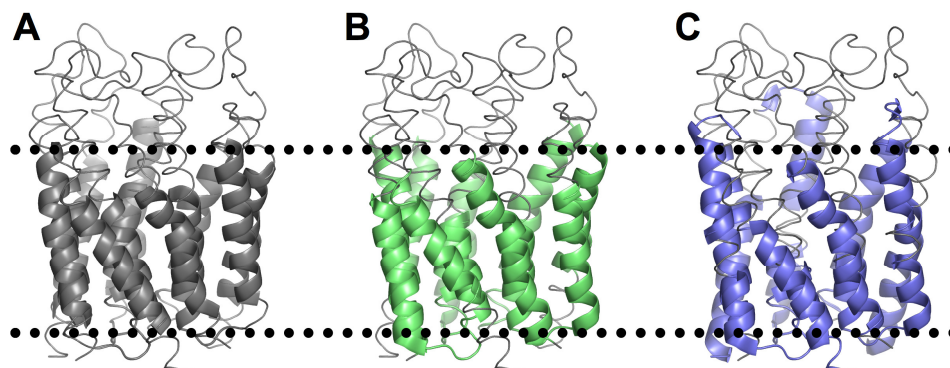


Figure 39. Transmembrane helices of MPGES1. The crystal structure of MPGES1 was determined by electron microscopy of two-dimensional crystals induced in the presence of phospholipids. The membrane embedded regions of MPGES1 as predicted by (A) computation, (B) MGST1 sequence alignment, and (C) H/D exchange kinetics are mapped onto the crystal structure in grey, green, and purple, respectively. The dotted lines represent the lipid bilayer boundaries, as determined from the crystal structure.

The integral membrane regions determined by H/D exchange are largely consistent with the crystal structure, with the exception of TM III, which extends beyond the cytosolic membrane boundary in the crystal structure. This may be due to the difference in solubilization methods, i.e. phospholipid bilayer versus detergent micelle. The structure also gives insight into the relative inconsistency of the prediction for TM II. This helix forms the core of the protein, adopting a polar pocket that opens toward the cytosol, and makes little-to-no contact with the membrane bilayer, affecting the computational prediction as well as the H/D exchange kinetics.

The detergents CHAPS and DDM, depicted in Figure 40, differ with respect to their chemical structures, as well as to their critical micelle concentrations (CMC). While DDM contains a nonionic, polar saccharide head group, CHAPS is a zwitterionic bile

acid derivative. Their CMC values differ by an order of magnitude, with that of DDM being 0.01% (w/v, or 0.2 mM) and CHAPS being 0.5% (w/v, or 8 mM).^{314,315}

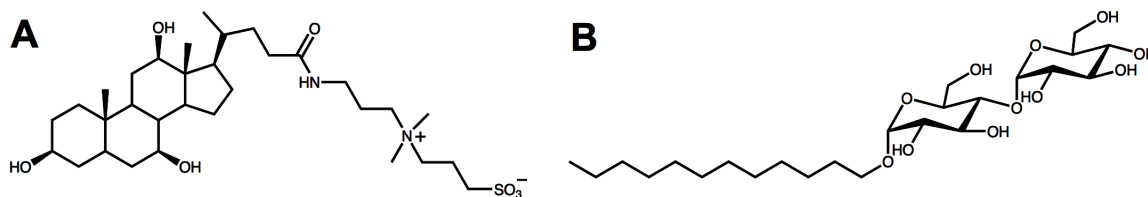


Figure 40. Detergents. The detergents used for the solubilization of MPGES1 for the H/D exchange experiments include (A) CHAPS and (B) DDM and are diverse in both their structures and chemical properties.

Even with this variance in micelle conditions, the observations of fast- and slow-H/D exchange kinetics reveal consistent determinations of the TM helices, suggesting that the protein is in similar conformations in each analysis. However, somewhat subtle differences in H/D exchange behavior do occur within peptides 2-13, 14-17, 60-68, 124-129, and 141-152, as illustrated in Figure 41. When these peptides are mapped onto the crystal structure (Figure 42) it is revealed that they correspond to regions of TM helices at the membrane boundary. As such, the kinetic differences are likely the result of TM-detergent head group interactions.

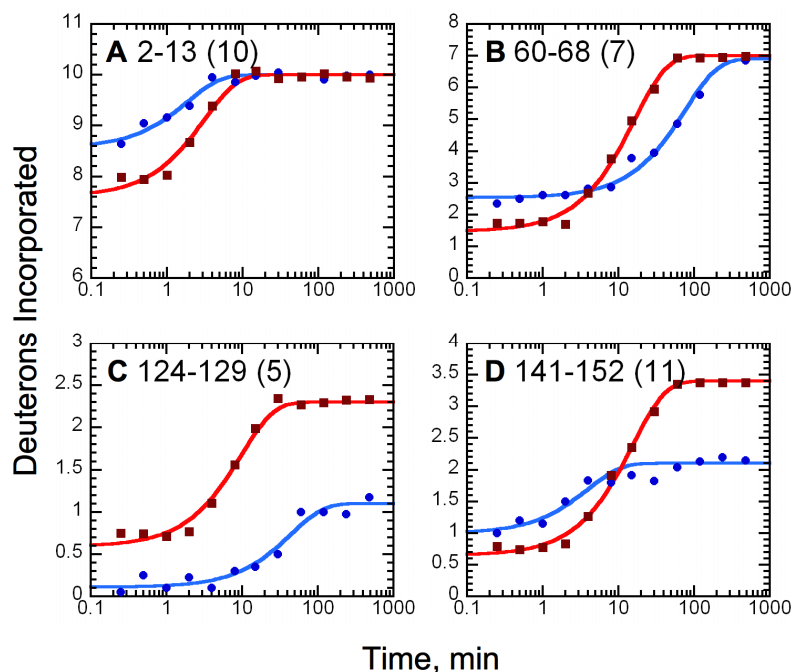


Figure 41. H/D exchange kinetic profiles for MPGES1 at the micelle boundary. Shown are the average kinetic profiles for deuterium incorporation as a function of time for MPGES1 solubilized in either CHAPS (blue) or DDM (red), with the number of exchangeable amide protons for each peptide in parentheses. Complete kinetic data for all plots may be found in the Appendix (Figures 60-63).

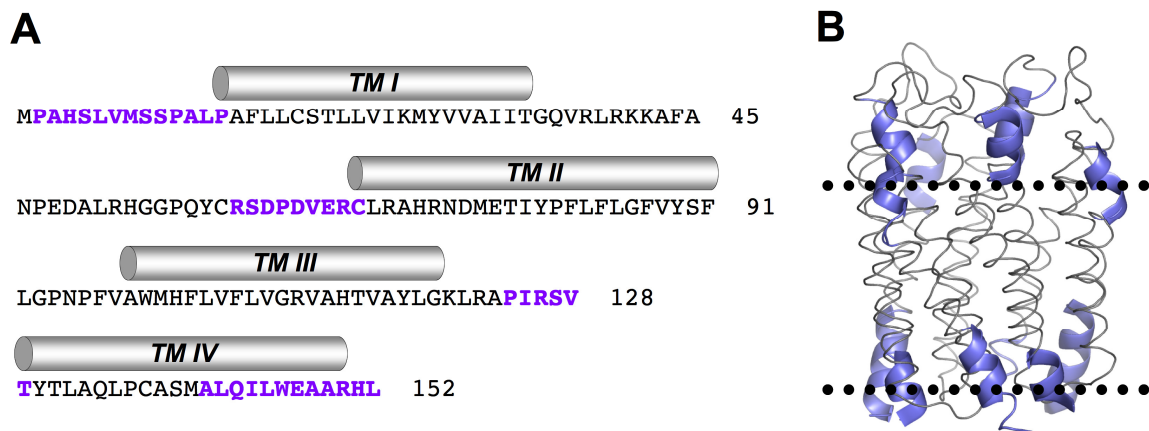


Figure 42. H/D exchange kinetic behavior at the micelle boundary. (A) The amino acid sequence of MPGES1 is shown with grey bars indicating the TM helices, as determined by electron microscopy. Highlighted in purple are regions identified as being kinetically different as a function of detergent micelle. (B) The crystal structure of MPGES1 is shown, with dotted lines representing the membrane boundaries, as determined by electron microscopy. Regions highlighted in purple are the same as those highlighted in (A).

Conclusion

Multiple sequence alignments and hydropathy plots based on amino acid sequence are established methods for protein structure prediction. While these techniques are undoubtedly valuable for making topology predictions of membrane proteins, it is important to validate them with empirical evidence. Here it is shown that H/D exchange can be used as a complimentary tool to improve and verify structure prediction by utilizing experimental data. In particular, the method shows great promise in identifying membrane boundaries of integral membrane proteins by locating regions that interact with detergent and/or phospholipid head groups.

CHAPTER IV

LOCATION OF INHIBITOR BINDING SITES IN THE HUMAN INDUCIBLE PROSTAGLANDIN E SYNTHASE MPGES1

Results

General Considerations

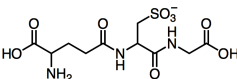
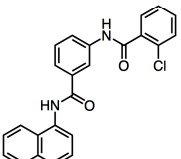
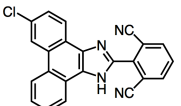
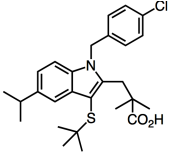
The H/D exchange kinetics of 19 peptides, ranging in size from 3 to 16 residues and covering 90% of the 152 residue protein sequence of MPGES1, were monitored over periods of 15 seconds to 8 hours. A peptic peptide map of the protein used in this study is presented in Figure 58 in the Appendix. As mentioned previously, MPEGS1 is unstable in the absence of GSH or the structurally similar inhibitor glutathione sulfonate (GSO_3^-), so it was not possible to determine the backbone H/D exchange kinetics of the apo-enzyme. The most pertinent H/D exchange kinetic results are illustrated in the figures and tables within this chapter. The remainder of the kinetic data not specifically discussed is documented in the Appendix (Figures 64-67 and 74-78).

Structural Studies of Inhibitor Binding

Known inhibitors of MPGES1 include those molecules that bind within the cofactor GSH site, such as GSO_3^- , **1**, and those molecules that bind elsewhere, presumably the PGH_2 substrate-binding site. The structures of four known inhibitors of human MPGES1 with their corresponding IC_{50} values are illustrated in Table 2. Compounds **2** – **4** are representative of pharmacologically active MPGES1 inhibitors of

varying potency.^{188,230,316} The structural interactions of inhibitors **1** – **4** with MPGES1 were analyzed using the H/D exchange MS technique.

Table 2. Inhibitors of MPGES1 used in H/D exchange kinetic analysis. Shown are the chemical structures and corresponding IC₅₀ values for inhibitors used in this study. These include inhibitor **1**, which binds in the GSH cofactor-binding site of MPGES1, and inhibitors **2** – **4**, which bind within the PGH₂ substrate-binding site.

Inhibitor	Structure	IC ₅₀
1 Glutathione Sulfonate		1.8 mM
2 NovaSAID Compound		60 nM
3 Merck MF63		1.3 nM
4 Merck MK-886		1.6 μM

Binding of Glutathione Sulfonate (1)

Although it is not possible to obtain H/D exchange data from apo-MPGES1, it is possible to probe the cofactor-binding site by comparing the H/D exchange behavior of the MPGES1•GSH complex to that of the MPGES1•**1** complex. The results reveal that replacing GSH with **1** increased deuterium incorporation rates for eight of the nineteen peptides analyzed including peptides 18-23, 28-31, 32-39, 63-78, 78-83, 124-129, 130-132, and 133-140 (Figures 43, 48, and Appendix Figures 64-67). There were no instances

of significant decreases in deuterium incorporation rates. The results indicate that the sulfonate group is sufficient to disrupt the native enzyme structure complexed with GSH.

Several of these aforementioned peptides contain at least one residue that is in close proximity (5 Å) to the sulfur atom of GSH, as indicated by the crystal structure of MPGES1 (Figure 44). These residues include Y28, R110, H113, R126, and Q134. The remaining peptides that display an increase in H/D exchange rates, 18-23, 63-78, and 78-83, are adjacent to the those peptides that do contain a residue close to the GSH sulfur and are located within the GSH binding pocket.¹⁶⁶ Because the sulfhydryl group of GSH is surrounded by protein residues, it is perhaps not unexpected that the introduction of the three additional oxygen atoms of the sulfonate group is sufficient to disrupt the GSH binding site as indicated by the H/D exchange results. Given that the GSH binding pocket is in direct contact with membrane-spanning helices, it is reasonable to assume that adjoining or neighboring TM segments are affected by structural perturbations to the GSH binding site.

It is a bit surprising, however, that there is no significant change to the H/D exchange behavior in peptide 108-123 in TM III as a result of introducing **1** to the GSH-binding site (Figure 43D), which contains two residues (R110 and H113) in close proximity to the sulfhydryl group. This 16-residue peptide in TM III appears to be buried in the core of the protein and is not prone to exchange in the GSH-bound form, with the exception a single amide. This particular site exhibits no significant change in either the amplitude or the rate constant for exchange in the presence of **1** as compared to GSH ($A_1^{\text{GSH}} = 1.07 \pm 0.07$, $k_1^{\text{GSH}} = 0.26 \pm 0.03 \text{ min}^{-1}$ and $A_1^{\mathbf{1}} = 1.04 \pm 0.03$, $k_1^{\mathbf{1}} = 0.17 \pm 0.02 \text{ min}^{-1}$).

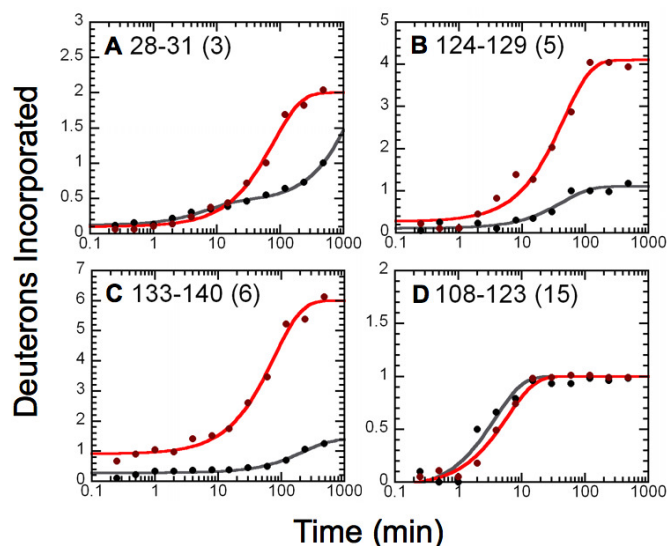


Figure 43. H/D exchange kinetic profiles for MPGES1 at the cofactor site. Shown are the average kinetic profiles for deuterium incorporation as a function of time for MPGES1 complexed with either GSH (black) or **1** (red), with the number of exchangeable amide protons for each peptide in parentheses. The amplitudes and rate constants for each peptide can be found in the Appendix (Figures 64-67).

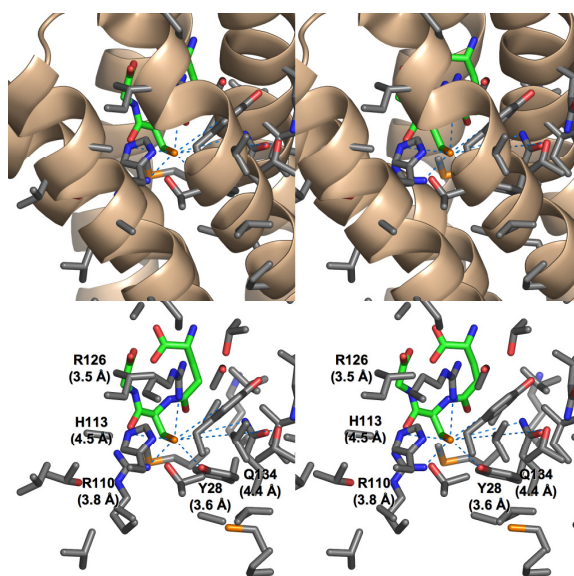


Figure 44. Stereoviews of the residues in close proximity to the sulfhydryl group of GSH. Shown is the three-dimensional structure of the MPEGS1•GSH complex.¹⁶⁶ (Top) α -Helices near the GSH binding site with associated residues shown in stick representation with carbon, oxygen, nitrogen and sulfur shown in grey, red, blue, and yellow respectively. The model of GSH is shown in stick representation with carbon atoms shown in green. (Bottom) Residues near the sulfur of GSH. Those within 5 Å of the sulfur of GSH are labeled with distances.

Binding of inhibitors 2, 3, and 4

The H/D exchange kinetic results of the MPGES1•GSH complex bound to inhibitors **2**, **3**, and **4** were compared with those of the GSH-complexed enzyme in the absence of inhibitors. All three inhibitors increased H/D exchange rates in some peptides and decreased them in others. The most significant observation of these experiments is that the changes in H/D exchange behavior are mainly limited to a set of spatially common peptides, as illustrated in Figures 45 and 46 and Table 3. Most of the affected peptides are relatively short and provide good spatial resolution of the inhibitor-binding site. Inhibitors **2** and **3** display significant effects on seven common peptides, while inhibitor **4** shares four common peptides with inhibitors **2** and **3**. As indicated in Figures 45 and 46, the effects of inhibitor binding on the H/D exchange kinetic behavior of a particular peptide varies. Nevertheless, the results do point to a common binding site for all three inhibitors.

							Inhibitor		
	37-54	78-83	104-107	124-129	130-132	133-140	141-152	2	
	28-31	37-54	78-83	104-107	124-129	130-132	133-140	141-152	3
18-23		78-83	104-107	124-129		133-140		4	

Figure 45. Qualitative map of the effect of inhibitor binding to MPGES1•GSH. Affected peptide segments are numbered for each inhibitor where orange indicates enhanced H/D exchange and blue signifies decreased exchange in the presence of the inhibitor.

In the presence of GSH and **2**, deuterium incorporation rates increase for peptides 37-54, 78-83, 124-129, and 133-140 as compared to GSH alone. Additionally, incorporation rates decreased for peptides 104-107, 130-132, and 141-152. In the presence of GSH and **3**, deuterium incorporation rates increased for peptides 37-54 and 133-140. Deuterium incorporation rates decreased for peptides 28-31, 78-83, 104-107,

124-129, 130-132, and 141-152. In the presence of GSH and **4**, deuterium incorporation rates increased for peptides 18-23, 124-129, and 133-140. Deuterium incorporation rates decreased for peptides 78-83 and 104-107. A few common effects on H/D exchange kinetics and many unique features of H/D exchange behavior associated with individual inhibitors are illustrated in Figure 46 and Table 3.

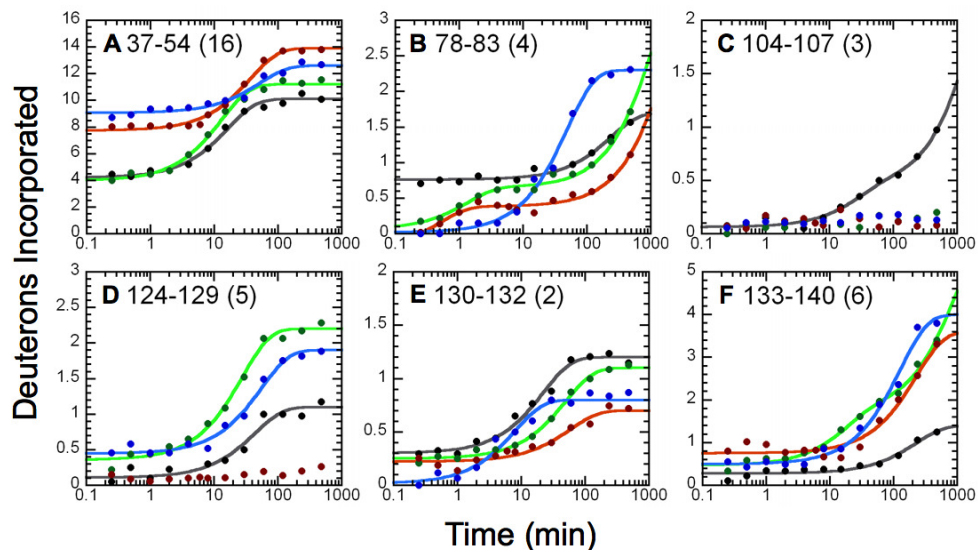


Figure 46. Effects of inhibitor binding on the H/D exchange kinetic profiles of MPGES1. Shown are the average kinetic profiles for deuterium incorporation as a function of time for MPGES1•GSH, with the number of exchangeable amide protons for each peptide in parentheses, in the absence of an inhibitor (black), and in the presence of inhibitor **2** (blue), **3** (red), and **4** (green). The rate constants and amplitudes derived from kinetic analysis are given in Table 3.

Table 3. Amplitudes and rate constants for amide H/D exchange in the analysis of inhibitor binding. Given are the data for selected peptides (from Figure 46) in the presence of GSH and inhibitors **2**, **3** and **4**.

Peptide/ Inhibitor	A_{fast} (D)	A_I (D)	k_I (min^{-1})	A_2 (D)	k_2 (min^{-1})
A 37-54 (16)					
none	3.9	5.90 ± 0.15	0.0601 ± 0.0054	6.18 ± 0.26	$\leq 1 \times 10^{-4}$
2	9.1	3.54 ± 0.12	0.0194 ± 0.0028	3.09 ± 0.69	$\leq 1 \times 10^{-4}$
3	7.9	6.16 ± 0.11	0.0270 ± 0.0020	1.93 ± 0.18	$\leq 1 \times 10^{-4}$
4	3.5	7.34 ± 0.14	0.0792 ± 0.0049	5.19 ± 0.15	$\leq 1 \times 10^{-4}$
B 78-83 (4)					
none	0.8	0.94 ± 0.02	0.00428 ± 0.00038	2.30 ± 0.13	$\leq 1 \times 10^{-4}$
2	0	2.28 ± 0.04	0.0206 ± 0.0014	1.69 ± 0.18	$\leq 1 \times 10^{-4}$
3	0	0.62 ± 0.18	0.609 ± 0.028	3.62 ± 0.02	$\leq 4.80 \times 10^{-4}$
4	0	0.59 ± 0.08	0.749 ± 0.022	3.35 ± 0.03	$\leq 8.29 \times 10^{-4}$
C 104-107 (3)					
none	0	0.37 ± 0.05	0.0365 ± 0.0021	2.56 ± 0.05	$\leq 4.90 \times 10^{-4}$
2	0	3	$\leq 1 \times 10^{-4}$		
3	0	3	$\leq 1 \times 10^{-4}$		
4	0	3	$\leq 1 \times 10^{-4}$		
D 124-129 (5)					
none	0	0.99 ± 0.04	0.0227 ± 0.0022	4.00 ± 0.16	$\leq 1 \times 10^{-4}$
2	0	1.54 ± 0.03	0.0182 ± 0.0017	3.02 ± 0.18	$\leq 1 \times 10^{-4}$
3	0	5	$\leq 1 \times 10^{-4}$		
4	0	1.84 ± 0.04	0.0361 ± 0.0030	2.92 ± 0.10	$\leq 1 \times 10^{-4}$
E 130-132 (2)					
none	0	0.90 ± 0.02	0.0454 ± 0.0046	0.75 ± 0.05	$\leq 1 \times 10^{-4}$
2	0	0.78 ± 0.04	0.125 ± 0.019	1.21 ± 0.04	$\leq 1 \times 10^{-4}$
3	0	0.48 ± 0.02	0.0172 ± 0.0031	1.37 ± 0.10	$\leq 1 \times 10^{-4}$
4	0	0.85 ± 0.01	0.0202 ± 0.0013	0.95 ± 0.05	$\leq 1 \times 10^{-4}$
F 133-140 (6)					
none	0	1.12 ± 0.03	0.00446 ± 0.00055	4.88 ± 0.03	$\leq 1 \times 10^{-4}$
2	0	3.50 ± 0.06	0.00787 ± 0.00061	2.12 ± 0.06	$\leq 1 \times 10^{-4}$
3	0.8	2.85 ± 0.06	0.00440 ± 0.00046	2.40 ± 0.06	$\leq 1 \times 10^{-4}$
4	0	1.25 ± 0.11	0.0567 ± 0.0128	4.28 ± 0.11	$\leq 1.09 \times 10^{-3}$

There are several unique effects that are induced by particular inhibitors. The longest peptide analyzed (37-54), which contains 18 residues and 16 exchangeable sites, extends from the C-terminal end of TM I into the cytosolic loop, partially covers the GSH binding site. The exchange behavior of this particular peptide is profoundly affected by the presence of either of the two tight-binding inhibitors (**2** or **3**), as indicated in Figures 47 and 48. The amplitudes of the rapidly exchanging sites increases from $A_{fast} = 4$ in the MPGES1•GSH complex to $A_{fast} = 8$ to 9 in the inhibitor-bound complexes. As indicated in Figure 47, the two tight-binding inhibitors appear to increase the conformational

dynamics of the cytosolic domain. In contrast, the MPGES1•GSH•**4** complex behaves similarly to MPGES1•GSH in this region.

Another striking difference amongst the inhibitors **2** – **4** is revealed in peptide 124-129 (Figure 46). While inhibitors **2** and **4** provoke an increase in amplitude of exchange by about one deuteron relative to the MPGES1•GSH complex, inhibitor **3** completely inhibits H/D exchange.

In spite of these differences, all three inhibitors share common attributes as clearly observed in peptide 104-107 (Figure 46C) and peptide 133-140 (Figure 46F). All inhibitors prevent the relatively slow exchange in peptide 104-107, whereas, in peptide 133-140 they enhance H/D exchange. The response of peptide 78-83 (Figure 46B) is a more complex situation in which all inhibitors decrease the exchange of one site (A_{fast}) but have mixed effects on the second site. Finally, although the single exchange site in peptide 130-132 (Figure 46E) differs in a subtle manner from one inhibitor to another, the relative changes in amplitudes and rate constants are distinguishable (Table 3).

Figure 47 reveals the common spatial distribution of the effects of the three inhibitors on the H/D exchange behavior of the MPGES1•GSH complex. The effects for all three compounds are primarily located in TM II, TM III, and TM IV toward the luminal side of the GSH binding site. There is also a clear distinction between **4** and the two tight-binding inhibitors, **2** and **3**, which result in much more extensive changes in the H/D exchange behavior in the cytosolic loop and helices encompassing the substrate binding cleft.

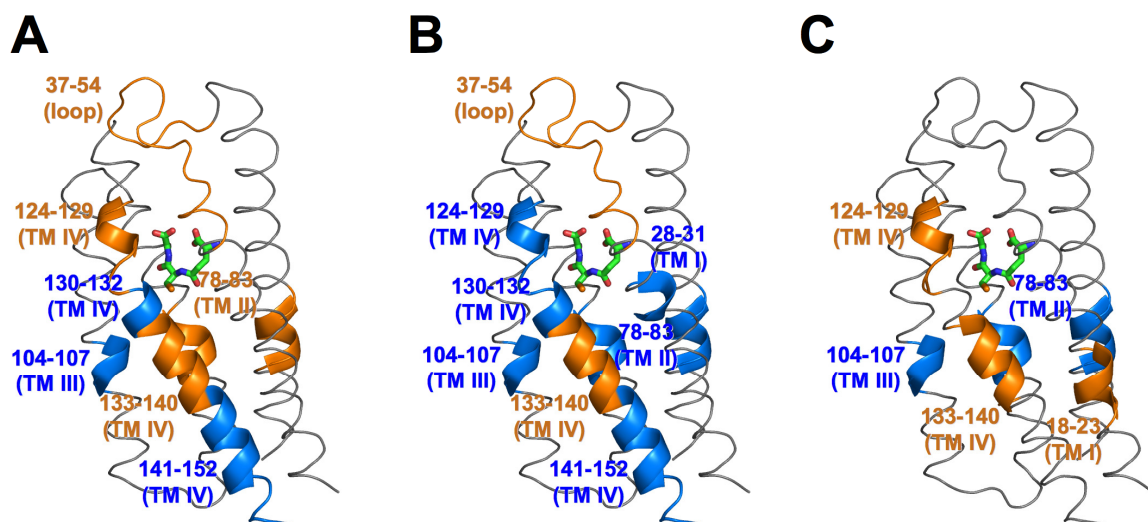


Figure 47. The impact of inhibitor binding on the H/D exchange behavior of the MPGES1•GSH complex. The effects of inhibitors **2**, **3** and **4** are shown in figures A, B, and C, respectively, with GSH shown in stick representation. Regions of enhanced exchange are shown in orange while those with decreased exchange are in blue. Only one potential binding site in the trimer is illustrated for clarity.

Discussion

Binding of 1 Suggests Differences in the Location of GSH in MPGES1 and MGST1

Interestingly, very large differences in H/D exchange behavior were observed between the MPGES1•GSH and MPGES1•**1** complexes. Previous comparisons of the GSH and **1** complexes of a soluble class Mu GST indicated very limited and highly localized differences in H/D exchange kinetics near the $-\text{SH}/-\text{SO}_3^-$ groups,³¹⁷ as opposed to the very broad regions observed for MPGES1. The results of this experiment also contrast with a previous comparison of the H/D exchange kinetics of another MAPEG homologue, MGST1,^{183,194} which shares 38% sequence identity with MPGES1. Like the soluble class Mu enzymes, the differences in H/D exchange behavior between

the MGST1•GSH complex and MGST1•1 are relatively small and localized near the GSH binding site, as determined by electron diffraction and as indicated in Figure 48.

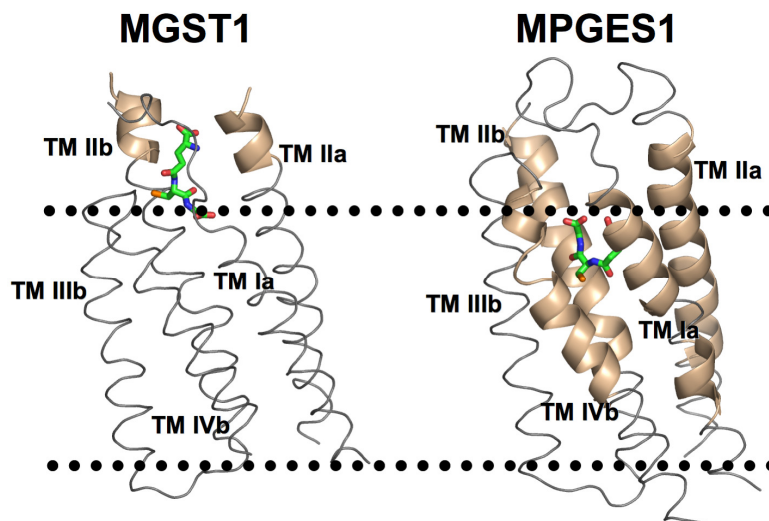


Figure 48. Comparison of the differential impact of GSH/1 binding on MPGES1. Shown are the kinetics of backbone H/D exchange of MGST1•GSH vs. MGST1•1 (left) and MPGES1•GSH vs. MPGES1•1 (right) and the location of the GSH binding site in the proteins as defined by three-dimensional electron diffraction from two-dimensional crystals.^{162,166} The dotted lines indicate the approximate location of the cytosolic (top) and luminal (bottom) boundaries of the microsomal membrane. One binding site is shown for clarity.

When comparing the crystal structure of MGST1 to those of the structurally homologous MAPEG members MPGES1 and LTC4S, the differences in location of the GSH binding sites and shape of the GSH molecules are obvious, as illustrated in Figures 48 and 49. While the molecular density and electron density of GSH in MPGES1 and LTC4S co-localize in the protein within the plane of the bilayer,^{163,164,166} the density for GSH in the MGST1 structure is located in the cytosolic domain of the protein.¹⁶² Moreover, the conformation of the GSH molecule is U-shaped in MPEGS1 and LTC4S but C-shaped in MGST1. This is a novel observation in which homologous proteins (~

40% sequence identical) in the same superfamily appear to bind the common substrate (or cofactor) GSH in a different location and conformation. This difference was initially attributed, in part, to an ambiguity in the location of the GSH binding site in MGST1 due to the anisotropy in the resolution of the diffraction data from the two-dimensional crystals. However, comparison of the H/D exchange kinetic results of the enzymes bound to either GSH or **1** appear to confirm the different locations of the GSH binding sites, at least in the cases of MGST1 and MPEGS1.

Binding of Inhibitors 2, 3, and 4 Define a Consensus Hydrophobic Cleft

Ago *et al.*,¹⁶³ as well as Martinez Molina *et al.*,¹⁶⁴ reported in 2007 the X-ray crystal structures of the GSH-bound LTC4S at resolutions of 3.3 and 2.15 Å, respectively. In each case, LTC4S was crystallized in the presence of the detergent DDM, and in each case, a detergent molecule was observed to be bound in an ordered fashion within a hydrophobic cleft comprised of TM Ia, TM IIb and TM IVb adjacent to the GSH binding site (Figure 49A). The authors of both studies proposed this location to be the LTA₄ substrate-binding site for LTC4S.

A structural comparison of MPGES1 with LTC4S was used to locate the equivalent hydrophobic cleft within MPGES1, as illustrated in Figure 49B. Coincidentally, the majority of the peptides involved in inhibitor binding, as determined by H/D exchange MS, are localized within this hydrophobic cleft. The only exception is that of the large cytosolic loop connecting TM I to TM II. In this case, the loop becomes more flexible when the enzyme is inhibitor-bound, perhaps due to a conformational

change typically induced by substrate binding, and serving the purpose of facilitating product release into the cytosol.

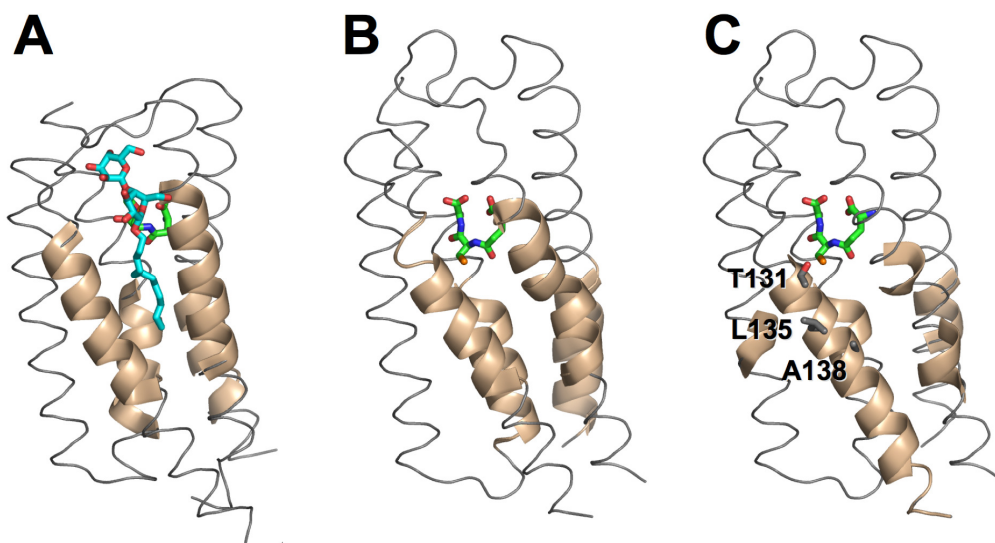


Figure 49. Definition of the hydrophobic cleft. The proposed substrate binding site is defined in (A) LTC4S by co-crystallization with GSH in the presence of the detergent DDM. The DDM (cyan) and GSH (green) molecules are shown in stick representation. DDM is thought to reside in the LTA₄ binding site. The homologous cleft is defined in (B) MPGES1 by structural comparison of LTC4S with MPGES1. The hydrophobic cleft is located in (C) MPEGS1 by H/D exchange kinetics in the presence of inhibitors **2**, **3** and **4**. The side chains of T131, L135 and A138 in TM IV are shown in stick representation. One binding site is shown for clarity.

It has been recently noted that the efficacy of MPGES1 inhibitors is species dependent and defined, in part, by residues located on one face of TM IV.¹⁸⁸ For example, inhibitor **2**, which is very potent toward the human enzyme is ineffective against the rat orthologue. This interspecies difference has been ascribed by mutagenesis to three specific residues, T131, L135, and A138 on TM IV of the human enzyme. These critical residues are located within the hydrophobic cleft at the subunit interface where the backbone exhibits a significant enhancement in H/D exchange kinetics when the enzyme is bound to inhibitors **2**, **3** or **4**, as illustrated in Figures 46F, 47A and 49C. This

behavior suggests that the binding of these three inhibitors increase the conformational dynamics of the protein backbone in this section of TM IV. The H/D exchange results are clearly consistent with the mutagenesis analysis that identifies this region as crucial for inhibitor binding.

It should be noted that it is not possible to conclusively determine from this data if any of the inhibitors **2**, **3** or **4** displace GSH upon binding to the hydrophobic cleft. However, this possibility seems unlikely, particularly with respect to inhibitors **2** and **4**. Compound **2** inhibits MPGES1 by a strictly competitive mechanism vs. the substrate PGH₂, while compound **4** inhibits by a mixed-type mechanism with a predominant competitive component against PGH₂.³¹⁸ Moreover, both **2** and **4**, along with pharmacologically similar inhibitors exhibit a predominantly noncompetitive component when GSH is the varied substrate. This information argues that inhibitors **2**, **3**, and **4** do not displace GSH in the inhibited complexes.

Conclusion

Backbone amide H/D exchange kinetics analysis is an excellent tool to map inhibitor-binding sites in purified integral membrane protein targets. Differences in the location of inhibitor sites and their individual impact on the conformational dynamics of proteins are easily distinguishable. The H/D exchange kinetics of MPGES1•GSH and MPGES1•**1** reveal discrete differences in the exchange behavior of the complexes as compared to previous studies with the related enzyme MGST1. These observations suggest that there are fundamental differences in the mode of binding of GSH to MPGES1, in which it acts as a cofactor, and MGST1, in which it is a substrate. Finally,

since there is no crystal structure or NMR structure of MPGES1 bound to an inhibitor, the H/D exchange kinetic data reported here represent the only physical evidence for the location of an inhibitor binding site.

CHAPTER V

OBSERVATION OF TWO MODES OF INHIBITION OF HUMAN MICROSOMAL PROSTAGLANDIN E SYNTHASE 1 BY THE CYCLOPENTENONE 15-DEOXY- $\Delta^{12,14}$ -PROSTAGLANDIN J₂

Results

Kinetics of the Spontaneous Reaction of 15d-PGJ₂ with GSH

The spontaneous reaction of GSH with 15d-PGJ₂ (Figure 50) was previously reported,³⁰² but not with respect to its kinetics. The kinetics of the approach to equilibrium for the reaction at pH 7.0 and 25 °C, determined under pseudo-first-order conditions with [GSH] \gg [15d-PGJ₂], gives rate-constants of $k_1 = 0.75 \pm 0.02 \text{ M}^{-1} \text{ s}^{-1}$ and $k_{-1} = (2.0 \pm 0.7) \times 10^{-4} \text{ s}^{-1}$ for the forward and reverse reactions, respectively. An equilibrium constant for the formation of the adduct is estimated from $K_f = k_1/k_{-1} \approx 3800 \pm 1000 \text{ M}^{-1}$. Analysis by HPLC of reaction mixtures of GSH and 15d-PGJ₂ at various concentrations reveals a similar value of $K_f = 1700 \pm 200 \text{ M}^{-1}$.

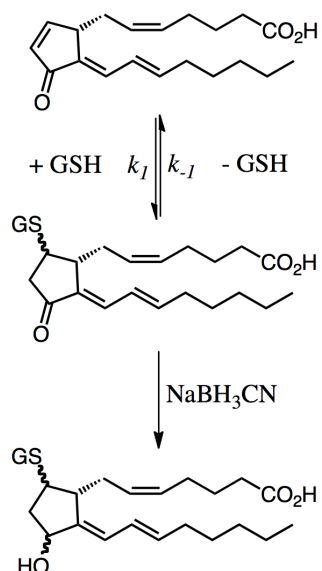


Figure 50. Reaction of 15d-PGJ₂ with GSH. GSH spontaneously adds to an electrophilic carbon on 15d-PGJ₂ via Michael addition at room temperature and neutral pH. Reduction of the keto group on the cyclopentenone ring of the adduct prevents the retro-Michael reaction.

Regiochemistry of the Spontaneous Reaction of 15d-PGJ₂ with GSH and L-Cys

The reaction of 15d-PGJ₂ with GSH or L-Cys results in one major peak on analysis by HPLC. Further analysis by LC-MS/MS fragmentation reveals position C-9 of 15d-PGJ₂ to be the predominant site of Michael addition by both GSH and L-Cys, consistent with what was previously reported for GSH.³⁰² However, both of these adducts are labile under the ESI conditions in the mass spectrometer. Reduction of the keto group of the 15d-PGJ₂ adducts by NaBH₃CN addition (Figure 50) results in stable compounds for more definitive analysis by MS/MS (Appendix Figure 79). This analysis shows positive evidence for adduction at position C-9 and no definitive evidence for adduction at positions C-13 or C-15. The observation of a single major species by HPLC and the absence of any MS/MS evidence for exclusive addition to C-13 or C-15 suggest that the major site of adduction is C-9.

Diastereoselectivity of the Reaction of GSH with 15d-PGJ₂

A previous study suggested that the stereochemistry of addition of GSH to 15d-PGJ₂ occurs on the *si*-face (bottom) of the 9-10 double bond of the cyclopentenone ring giving (*9S*)-S-glutathionyl-15d-PGJ₂ (*9S*-GS-15d-PGJ₂).³⁰² However, examination of the addition utilizing molecular models suggests that the attack of the nucleophile from the *si*-face is significantly more hindered and less likely to occur than addition from the top (*re*-face). Therefore, the structure of the GSH adduct was reinvestigated utilizing high-field NMR spectroscopy.

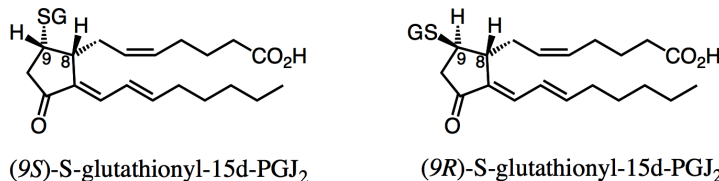


Figure 51. Stereoselectivity of GSH addition. The spontaneous addition of GSH to 15d-PGJ₂ can theoretically result in the formation of two diastereomers. The stereochemistry at position C-8 would indicate, however, that the *9R* species to be that which is predominately formed spontaneously, as a result of steric hindrance.

A detailed NMR analysis of the purified adduct at 600 MHz and 900 MHz in D₂O and CD₃OD were consistent only with the *9R*-GS-15d-PGJ₂ diastereomer, which results from the *re*-face addition of GSH. The NMR assignments for this molecule were established using 2D ¹H-¹H COSY/DQF-COSY and NOESY along with 2D ¹H-¹³C HSQC experiments. The stereochemistry of the GSH adduct was determined by analysis of the protons H7 (2.36, 2.27 ppm), H8 (3.06 ppm), H9 (4.57 ppm), and H10 (2.81, 3.05 ppm). In the one-dimensional ¹H-NMR spectrum in CD₃OD, H9 appears as two doublets,

which strongly suggests coupling between two protons and not three. These doublets were assigned to coupling between H9 to the two protons on C10, and this was confirmed in the 2D COSY. The COSY experiment shows two correlations between H9 and the two H10 protons and no correlation between H9-H8. The NOESY spectrum also reveals correlations between the C10 protons and H9, but gives no evidence of a correlation between H9-H8. The lack of a coupling between H8-H9 can be explained if the bond angle between these two protons approaches 90°, which is unique to the 9*R*-GS-15d-PGJ₂ diastereomer.

Upon switching the solvent from CD₃OD to D₂O, changes were observed in the chemical shifts for the protons H7 (2.41, 2.45 ppm), H8 (3.17 ppm), H9 (4.75 ppm), and H10 (3.03, 3.20 ppm). A triplet was observed for H9 in D₂O, which is again consistent with coupling to two protons (H10). Results from both 2D COSY and DQF-COSY reveal coupling between H9 to H10 but no evidence of coupling between H8-H9. This was further supported by the 2D NOESY experiment, which also fails to show any correlation between H8-H9. The NMR spectra of 9-GS-15d-PGJ₂ are provided in the Appendix (Figures 80-82).

Covalent Modification of MPGES1 by 15d-PGJ₂

The inhibition studies of MPGES1 by 15d-PGJ₂ by Quraishi *et al.* suggested that the inhibition is possibly due to a covalent modification of the enzyme.³⁰¹ Analysis of the three-dimensional structure of MPGES1 determined by Jegerschöld *et al.* indicates that there are three buried cysteine residues and one surface-exposed cysteine (C59) per subunit of the homotrimeric protein.¹⁶⁶ LC-MS/MS sequencing of the native MPGES1

enzyme covalently modified by the 15d-PGJ₂ and digested with pepsin revealed that C59 of the peptide 49-59 was the specific and exclusive site of adduction. Initial estimates utilizing TIC chromatographs of the adducted and un-adducted peptide 49-59 suggested that only about 20% of the C59 residues were modified by 15d-PGJ₂. Since the GSH and L-Cys adducts of 15d-PGJ₂ are labile under the ESI conditions of the mass spectrometer, further analyses were made of the modified enzyme stabilized by reduction with NaBH₃CN. This analysis of MPGES1 complexed with GSH revealed that approximately 80-90% of the enzyme is modified under the experimental conditions of the H/D exchange assay, while the MPGES1•GSO₃⁻ complex appears to be fully adducted.

The regiochemistry of the protein adduct was determined by MS³ experiments on the peptic peptide containing C59 (residues 49-59). This peptide was subjected to MS³ fragmentation selecting for the y-ion of the adducted C59 residue. The results, shown in Figure 84 in the Appendix, provide evidence only for site of adduction, at position C-9 of 15d-PGJ₂, consistent with what is observed for the GSH and L-Cys adducts. However, the absence of evidence for addition to C-13 or C-15 of 15d-PGJ₂ does not exclude its occurrence.

Considerations of the Catalytic Properties of Native MPGES1 and the C59A Mutant

The catalytic and physical properties of native MPGES1 and MPGES1 C59A were analyzed and compared, particularly with respect to their GSH transferase and PGH₂ isomerase activities. The MPGES1 C59A protein exhibits a catalytic activities toward GSH and PGH₂ that are indistinguishable from those of the native enzyme.

Neither the native enzyme nor the C59A mutant catalyze the addition of GSH to 15d-PGJ₂.

Inhibition of MPGES1 by 15d-PGJ₂

The native enzyme is inhibited by 15d-PGJ₂ with an IC₅₀ value of 0.6 μM (Figure 52), consistent with that previously reported,³⁰¹ while the C59A mutant is inhibited with an IC₅₀ value of 12 μM (Figure 52B). Moreover, increasing the substrate concentration fails to rescue the activity of native MPGES1, following pre-incubation with 15d-PGJ₂, suggesting that the inhibition is not competitive (Figure 53A), while the inhibition of MPGES1 C59A is reversible with increasing concentrations of PGH₂ (Figure 53B). The inhibition of the native enzyme utilizing 11-hydroxy-15d-PGJ₂ (11-OH-15d-PGJ₂) as an inhibitor is similar to that of the C59A mutant, having IC₅₀ values of 11 μM and 16 μM, respectively (Figure 52). Neither enzyme is appreciably inhibited by 9-GS-11-OH-15d-PGJ₂.

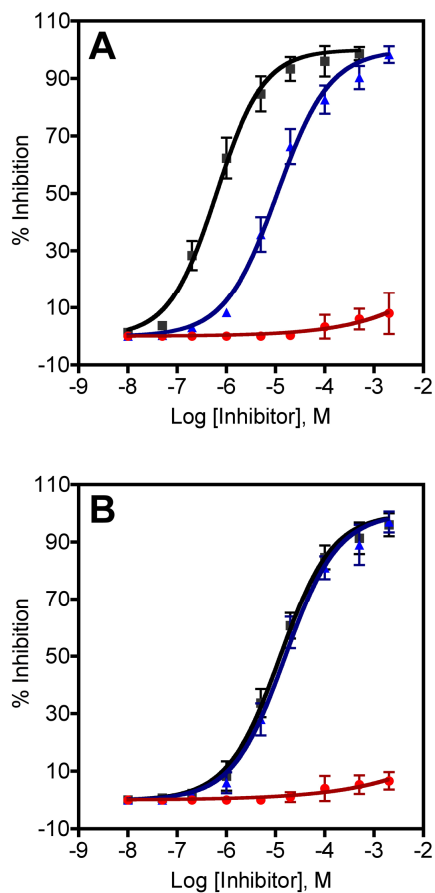


Figure 52. Inhibition of the isomerase activity of MPGES1. The inhibition of the native enzyme (panel A) and the C59A mutant (panel B) by 15d-PGJ₂ (black), 11-OH-15d-PGJ₂ (blue), and 9-GS-11-OH-15d-PGJ₂ (red). The IC₅₀ values, 95% confidence range, and Hill coefficients are given in the parentheses for MPGES1; [15d-PGJ₂ (0.6 μM, 0.5 – 0.8 μM, 0.91)], [11-OH-15d-PGJ₂ (11 μM, 9 – 13 μM, 0.84) and 9-GS-11-OH-15d-PGJ₂ (>>1 mM) and for C59A MPGES1; [15d-PGJ₂ (12 μM, 11 – 14 μM, 0.81)], [11-OH-15d-PGJ₂ (16 μM, 13 – 19 μM, 0.79) and 9-GS-11-OH-15d-PGJ₂ (>>1 mM)].

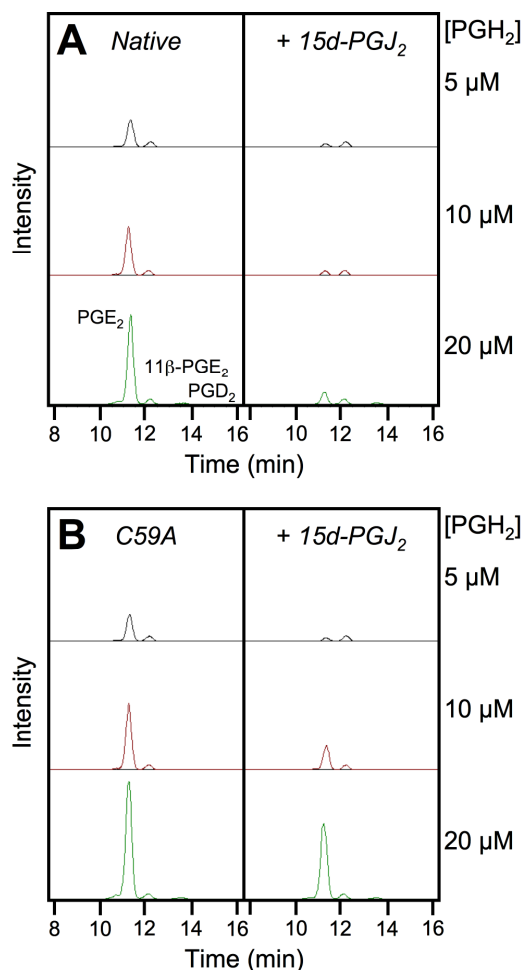


Figure 53. Recovery of the isomerase activity of MPGES1. (A) Assay of native and 15d-PGJ₂-modified MPGES1 and (B) the C59A mutant in the absence and presence of 100 μM 15d-PGJ₂, at three different concentrations of the substrate, PGH₂.

H/D Exchange MS of Native MPGES1 and MPGES1 C59A

The backbone H/D exchange kinetics of the native MPGES1 enzyme, complexed with GSH, and in the presence or absence of 15d-PGJ₂ were compared. Kinetic plots for some selected peptides are shown in Figure 54. A complete set of the kinetic plots for all peptides along with the amplitudes and rate constants for the fits of the data are provided in the Appendix (Figures 84-93). These data reveal that peptides within proximity of, or containing, the residue C59 (peptides 37-54, 49-59, and 60-68) (Figure 55A) display

decreased deuterium incorporation rates when adducted with 15d-PGJ₂. This was not unexpected, since 15d-PGJ₂ is adducted to C59. In addition to these changes, however, peptides within the α -helical core of the protein (peptides, 78-83, 104-107, 124-129, 130-132, 133-140, and 141-152) also display significant differences in H/D exchange behavior (Figures 54C, 54D, 55A). On further inspection, it was observed that these regions were spatially similar to those identified as constituting the hydrophobic substrate binding cleft by H/D exchange experiments of MPGES1•GSH in the presence of inhibitors competitive for PGH₂ binding,³¹⁹ as described in the previous chapter.

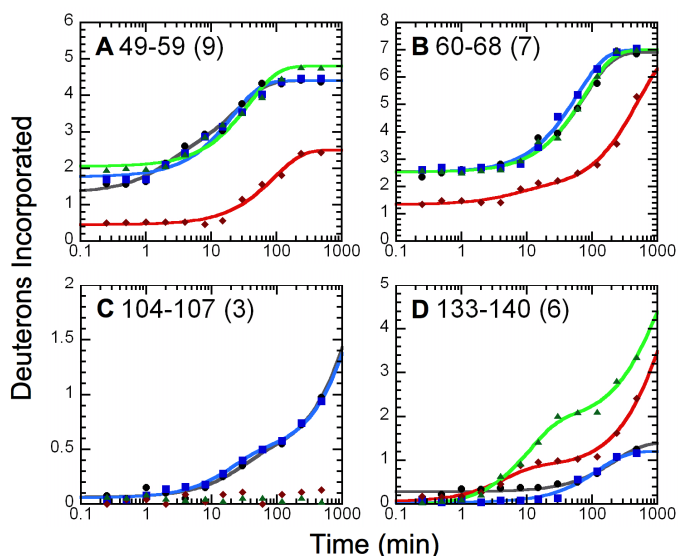


Figure 54. H/D exchange kinetic profiles of MPGES1•GSH as a function of 15d-PGJ₂. Shown are the selected kinetic data of the native enzyme (black) and C59A mutant (blue) of MPGES1 in complex with GSH in the absence of 15d-PGJ₂ and the native (red) and the C59A mutant (green) enzyme in the presence of 15d-PGJ₂. The number of exchangeable sites is given in parentheses. The amplitudes and rate constants for the fits of the data can be found in the Appendix (Figures 84-93).

To further explore the possibility that MPGES1 binds 15d-PGJ₂ in its substrate-binding site, the above experiments were repeated with the MPGES1 C59A mutant. The

H/D exchange kinetics of the C59A mutant in complex with GSH are essentially the same as those of the native enzyme in the absence of 15d-PGJ₂, as shown in Figure 54. However, the H/D exchange behavior of MPGES1 C59A in the presence of GSH and 15d-PGJ₂ are remarkably different than those of the native enzyme. In this case, regions in close proximity of A59 display no significant difference in deuterium incorporation rates. Regions within the CHAPS micelle (18-23, 78-83, 104-107, 124-129, 130-132, 133-140, and 141-152), however, do display changes (Figure 55B), which are associated with the non-covalent binding of 15d-PGJ₂ to the substrate-binding site.

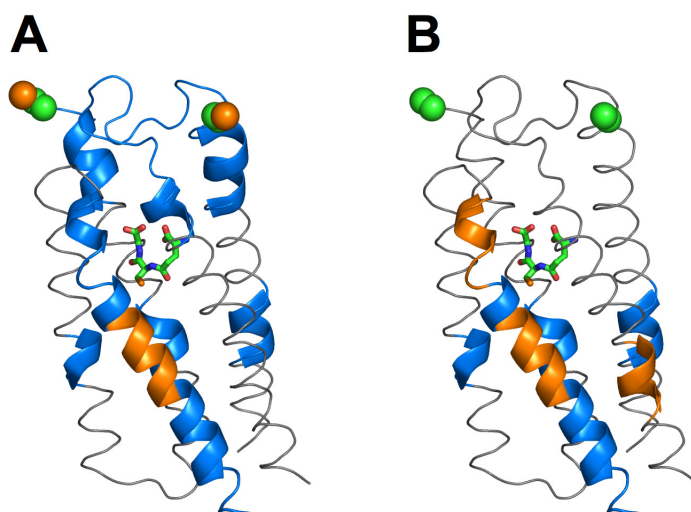


Figure 55. Structural impact of 15d-PGJ₂ binding on MPGES1•GSH. H/D exchange results mapped to the secondary structural elements (A) in the native protein and (B) in the C59A mutant. The representation of the three-dimensional structure of MPGES1 was derived from PDB file 3DWW.¹⁶⁶ GSH is shown in stick representation, and C59 and A59 are depicted with spheres. The blue and orange peptides indicate regions with decreased and increased rates of exchange, respectively, in the presence of 15d-PGJ₂. A single binding site is shown for clarity.

In order to eliminate contributions of the spontaneous adduction of 15d-PGJ₂ to the cofactor GSH, the H/D exchange kinetic analysis of native MPGES1, as well as

MPGES1 C59A, complexed with GSO_3^- were performed in the absence and presence of 15d-PGJ₂ (Figures 56 and 57). Here, peptide 37-54 (Figure 57A) still displays an overall decrease in deuterium incorporation rates for the native enzyme, whereas peptides 49-59 and 60-68 no longer display this large change in kinetics. This may be due to the fact that GSO_3^- binding distorts the structural conformation of MPGES1,³¹⁹ complicating the data interpretation. Regions within the detergent micelle (peptides 78-83, 104-107, 130-132, and 141-152) still exhibit substantial changes in H/D exchange kinetics, suggesting that the enzyme binds 15d-PGJ₂ within in the substrate-binding site, even in the absence of GSH.

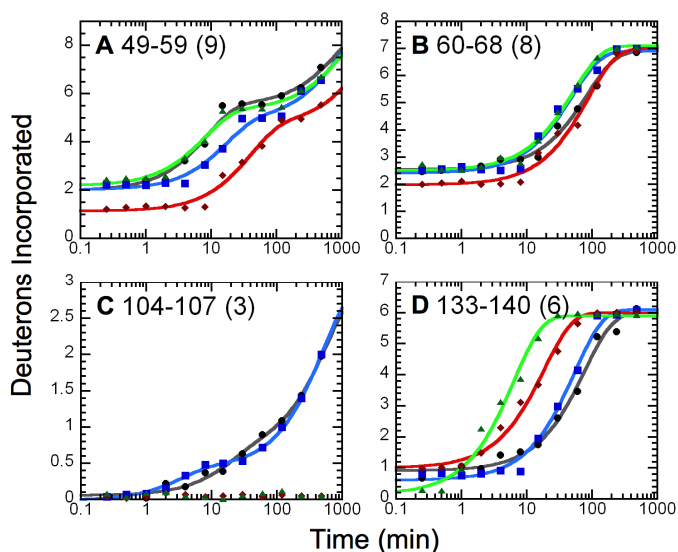


Figure 56. H/D exchange kinetic profiles of $\text{MPGES1}\cdot\text{GSO}_3^-$ as a function of 15d-PGJ₂. Shown are the selected kinetic data of the native enzyme (black) and C59A mutant (blue) of MPGES1 in complex with GSO_3^- in the absence of 15d-PGJ₂ and the native enzyme (red) and the C59A mutant (green) in the presence of 15d-PGJ₂. The number of exchangeable sites is given in parentheses. The amplitudes and rate constants for the fits of the data can be found in the Appendix (Figures 84-93).

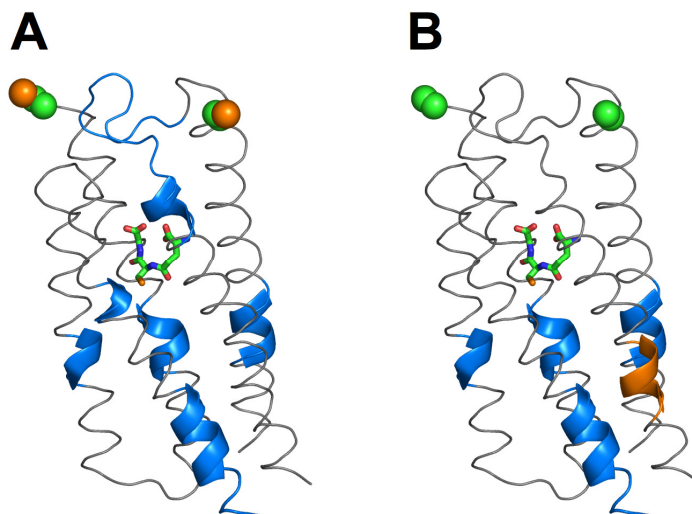


Figure 57. Structural impact of 15d-PGJ₂ binding on MPGES1•GSO₃⁻. H/D exchange results mapped to the secondary structural elements (A) in the native protein and (B) in the C59A mutant. The representation of the three-dimensional structure of MPGES1 was derived from PDB file 3DWW.¹⁶⁶ GSH is shown in stick representation, and C59 and A59 are depicted with spheres. The blue and orange peptides indicate regions with decreased and increased rates of exchange, respectively, in the presence of 15d-PGJ₂. A single binding site is shown for clarity.

Discussion

The Chemistry of 15d-PGJ₂

The formation of 15d-PGJ₂ and its reactions with cellular nucleophiles has been studied by numerous investigators. The regiochemistry of the reaction of GSH, as well as L-Cys, with 15d-PGJ₂ appears to occur predominantly at position C-9, as previously reported by others.^{302,320} This is also shown to be true for the adduction of MPGES1 at residue C59. The NMR results at 600 MHz and 900 MHz in D₂O and CD₃OD suggest that the nucleophile adds to the least hindered face of the 9-10 double-bond of the cyclopentenone ring to give the 9*R*-GS-15d-PGJ₂ diastereomer.

The chemistry and kinetics of the reaction of GSH with 15d-PGJ₂ are key to understanding the cellular concentration of the cyclopentenone and its potential anti-inflammatory properties. The spontaneous reaction with GSH is relatively slow ($\sim 10^{-3} \text{ s}^{-1}$) at pH 7, 25 °C, and physiological concentrations of GSH ($\sim 4 \text{ mM}$). Once formed, the GSH adduct has a half-life of about one hour at room temperature in aqueous solution. It is clear from the chemical equilibrium, though, that virtually all 15d-PGJ₂ is in the form of the 9-GS-adduct. The rates of GSH addition to 15d-PGJ₂, as well as to its precursor PGJ₂, are known to be catalyzed *in vitro* by soluble GSTs.^{320,321} However, the efficiency of the enzyme-catalyzed reactions, at least with respect to PGJ₂, appears to be rather low with $k_{\text{cat}}/K_{\text{M}}$ values of 100 to 300 $\text{M}^{-1} \text{ s}^{-1}$.³²⁰ The exact role of GSTs in the metabolic fate of PGJ₂ and 15d-PGJ₂ is not known.

Inhibition of MPGES1 by 15d-PGJ₂

The anti-inflammatory properties of 15d-PGJ₂ may be associated with its inhibition of MPGES1. The study detailed in the previous chapter showed that the binding of inhibitors competitive for the PGH₂ substrate-binding site induces flexibility in the cytosolic loop connecting TM I to TM II. It was hypothesized that this increased flexibility aids in product release to the cytosol as a result of a normal conformational change induced by substrate binding. As defined in this chapter, the covalent modification of C59, which lies at the interface of the loop with TM II, by 15d-PGJ₂ results in a significant decrease in H/D exchange rates within the cytosolic loop. This suggests that the predominant mechanism of inhibition of MPGES1 by 15d-PGJ₂ may involve the preclusion of product release from the active site (Figure 55). The H/D

exchange kinetic data also reveal that 15d-PGJ₂ binds within the substrate-binding site, competing for PGH₂ binding (Figures 55 and 57). Therefore, inhibition of MPGES1 by 15d-PGJ₂ may involve both the occlusion of substrate from the active site, as well as prevention of product release.

Though it may be compelling to argue that the anti-inflammatory properties of 15d-PGJ₂ are partially due to its inhibition of MPGES1, the *in vitro* evidence refutes this. There are two mechanisms of inhibition: the covalent modification of residue C59 and the competitive inhibition revealed by the inhibition and H/D exchange experiments of the C59A mutant. The most efficient inhibition of the enzyme is via the covalent modification of C59 with an IC₅₀ of 0.6 μM. Since the concentration of 15d-PGJ₂ in the cell is not known, it is not practical to predict if the covalent modification of MPGES1 occurs to any significant extent *in vivo*. Though the physical properties of the molecule suggest that the location of 15d-PGJ₂ is likely to be concentrated in or near the membrane where the enzyme is also located, it is highly unlikely that a non-covalent, competitive inhibition of MPGES1 by 15d-PGJ₂ (IC₅₀ ≈ 12 μM) has any biological relevance *in vivo*, since the concentration of free 15d-PGJ₂ in the cell is likely to be well below the micromolar range.⁷⁸

Biological Consequences of 15d-PGJ₂

Although the potential biological effects of 15d-PGJ₂ are interesting, such as those cited in this dissertation and elsewhere, the significance of the findings remains uncertain.⁷⁹ The biological effects of 15d-PGJ₂ formed *in vivo* are controversial considering that the formation, concentration, location, and metabolic fate of the

molecule are poorly understood.³²² The concentration of 15d-PGJ₂ in human urine has been estimated to be in the low pM range, suggesting that its level is insufficient to support biological activity.⁷⁸ However, the level in urine probably does not reflect local cellular concentrations that could affect bioactivity.

Finally, the transformation of PGD₂ to 15d-PGJ₂ appears to occur by spontaneous chemistry that is unregulated. This fact alone would suggest that 15d-PGJ₂ does not likely play a regulatory role as an anti-inflammatory mediator. However, that does not necessarily preclude it from playing a role under pathological conditions.

Conclusion

The results reported here demonstrate that 15d-PGJ₂ can act as an effective dual-mode inhibitor of MPGES1 *in vitro* and define, from a chemical and physical standpoint, the interaction of the inhibitor with the enzyme. Although the currently available biological data do not rule out an anti-inflammatory role for 15d-PGJ₂ *in vivo*, there is no positive physiological evidence to that effect, particularly with respect to MPGES1 inhibition. The biological data that is currently available do not necessarily preclude an anti-inflammatory signaling role for 15d-PGJ₂ *in vivo*, but the lack of knowledge regarding the *in vivo* concentration of 15d-PGJ₂, its kinetic disposition, and homeostasis leave a significant amount of uncertainty.

CHAPTER VI

CONCLUSION

Discussion

Inflammation, while a protective immune response that is important to the healing process, is implicated in a variety of disease states including atherosclerosis, Alzheimer's disease, RA, and cancer. The critical role that inflammation plays in pathologic events makes its regulation crucial to the prevention and treatment of inflammatory diseases, accounting for the prominence of anti-inflammatory drugs like NSAIDs. The definition of the mechanism of action of NSAIDs as the inhibition of the enzymatic production of PGs shed light on the role of eicosanoids as mediators of pain, inflammation, and fever.

Metabolites of the polyunsaturated fatty acid arachidonic acid not only include the prostanoids, but LTs, LXs, EXs, and CYP-derived metabolites as well. These eicosanoids constitute a widespread family of signaling molecules that have all been shown on some level to be lipid mediators of the inflammatory response. Their synthesis is tightly controlled by a multitude of enzymes in tissues throughout the body. The delicate and complex role that the eicosanoids play in the regulation of normal biological processes, the propagation of pathological events, and the resolution of such events has been studied intensely.

One family of proteins involved in the synthesis of eicosanoids represents a unique set of GSTs known as the MAPEG superfamily. Three members in particular, FLAP, LTC4S, and MPGES1 are directly involved in the synthesis of LTs, Cys-LTs, and

inducible PGE₂, respectively, and therefore represent promising targets for the therapeutic treatment of inflammation.

The focus of this dissertation, MPGES1, is a GSH-dependent isomerase that preferentially utilizes PGH₂ produced by the inducible COX-2, an enzyme highly implicated in a variety of inflammatory diseases and several forms of cancer. As such, MPGES1 has been at the forefront of drug development by groups in the pharmaceutical sector, as well as in academia. Though the three-dimensional crystal structure of MPGES1 was determined by two-dimensional crystallography in 2008, questions have remained regarding its chemical mechanism and physical interaction with inhibitors.

The method of H/D exchange MS has emerged as a useful technique for the structural analysis of integral membrane proteins, such as MPGES1. Given that analyses may be performed in nearly any solution condition or protein concentration, an option not often available with techniques such as X-ray crystallography or NMR, H/D exchange MS was utilized to make structural and conformational dynamic determinations of MPGES1. The initial aim of this project took advantage of the use of structurally divergent detergent micelles to make topography determinations of the enzyme. The technique proved particularly successful in identifying the boundaries of micelles by locating regions of the protein that interact with detergent head groups.

In the absence of a crystal structure of MPGES1 bound to an inhibitor, H/D exchange MS was utilized to map the binding sites of different types of inhibitors of MPGES1 as the second aim of this project. The results reveal two spatially distinct binding sites, which include the cofactor site as well as a hydrophobic cleft, predicted to harbor the substrate-binding site. Analysis of the H/D exchange behavior of the cofactor

site confirms the unusual observation that MPGES1 and the closely related MGST1 bind the common cofactor/primary substrate GSH in differing locations. In addition, H/D exchange kinetics of inhibitors competitive for PGH₂ binding reveal a site within a hydrophobic environment capable of binding a hydrophobic ligand.

The cyPG 15d-PGJ₂ is an endogenous inhibitor of MPGES1 unlike those inhibitors that bind to the cofactor site or those that are synthesized as pharmacologically active inhibitors. Initial biochemical data has suggested that 15d-PGJ₂ may form a covalent adduct or involve allosteric binding to MPGES1, and the final aim of this project involved the elucidation of its mechanism of inhibition. Further investigation of the interaction of 15d-PGJ₂ using biochemical methods along with H/D exchange MS have revealed that covalent adduction of the enzyme at a cytosolic cysteine residue, as well as binding to the PGH₂ substrate-binding site, account for its inhibitory activity. The GSH adduct of 15d-PGJ₂, on the other hand, displayed no inhibitory effect on MPGES1. While 15d-PGJ₂ can act as an effective dual-mode inhibitor of MPGES1 *in vitro*, there is no convincing physiological evidence to suggest that the anti-inflammatory role of this cyPG is due to its role as an inhibitor of MPGES1 *in vivo*.

Future Studies

Though the IC₅₀ values of inhibition for 15d-PGJ₂ and 11-OH-15d-PGJ₂ have been determined for native MPGES1 and MPGES1 C59A, they have only been done so for a single PGH₂ substrate concentration. Varying the substrate concentration will alter the corresponding IC₅₀ value, and these data can be used to kinetically define the mechanism(s) of inhibition. Plotting IC₅₀ values as a function of substrate concentration

is a method that can be used to calculate the inhibition constant (K_i) of each inhibitor for each enzyme, and the slopes of the plots may be used to determine the mechanism of inhibition, whether it be competitive, uncompetitive, non-competitive, or a mixed-type of inhibition.

While there is a chemical mechanism of MPGES1 isomerase activity suggested from its crystal structure, uncertainty remains. To probe whether Arg-126 is the proton donor to oxygen at position C-11 of PGH₂ and the proton acceptor from C-9, additional mutagenesis experiments, coupled with kinetic analysis, may be performed. As Tyr-28 and Tyr-130 are reasonable candidates as proton donors and acceptors in the reaction, mutations of these residues may be made in conjunction with those of Arg-126.

The crystal structure of MPGES1 also suggests that the enzyme binds three molecules of GSH simultaneously, but this may be an artifact of crystallographic conditions. If the enzyme does bind three molecules of GSH, it is unclear if all three sites are simultaneously active. To address these uncertainties, a series of experiments could be designed, such as nano-flow electrospray MS and equilibrium dialysis to determine the number of occupied cofactor sites, and single turnover stopped flow kinetic analysis to monitor the GSH-binding affinity of each site, should they differ.

Additional structural analyses of MPGES1 are in need and are almost certain to come. While the structure of MPGES1 in complex with GSH has been revealing, it would certainly be beneficial to analyze structures of MPGES1 in the absence of GSH and/or bound to inhibitors that are competitive for PGH₂ binding. These observations could reveal aspects of the mechanism of action of the enzyme, as well as aid in structure-based drug design.

The studies described here have alluded to a possible mode of product release from MGPE1. It would be interesting to use alternative methods to define both the mechanism of product release and mechanism of substrate binding. As an alternative to H/D exchange MS, other structural dynamics-dependent labeling techniques coupled to MS could be utilized including hydroxyl radical foot-printing, oxidative methionine labeling, and electrophysiology-coordinated photo-labeling.

Finally, while several H/D exchange MS analyses have been made of MPGES1 and MGST1, the other members of the MAPEG superfamily have not been investigated utilizing this technique. As an example, the method could feasibly be used to monitor the physical interaction of FLAP with 5-LOX, should there be one, at the committed step of LT biosynthesis.

Conclusion

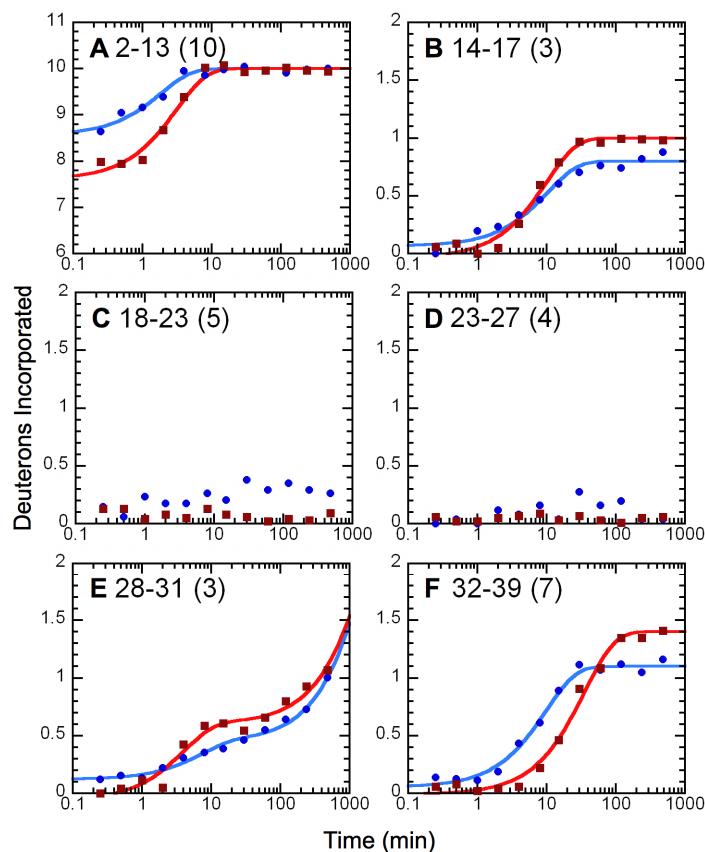
Inflammation research has come a long way since the reverend Edward Stone performed the first clinical trial of willow bark in fever patients in 1763. The discovery of naturally-occurring anti-inflammatory compounds eventually led to the discovery of the mechanism of action of NSAIDs. That discovery gave way to the revelation of eicosanoids as being lipid mediators of not just normal biological functions, but a multitude of pathological processes as well. Along with that came the investigations of the proteins involved in the syntheses of the eicosanoids. We are now at a stage of, not only observing these proteins, but utilizing their structural and functional properties as a means to target them for therapeutic purposes. To this end, it is my hope that the

conformational dynamics studies of MPGES1 described here have played their small role in the increasingly important field of inflammation research.

APPENDIX

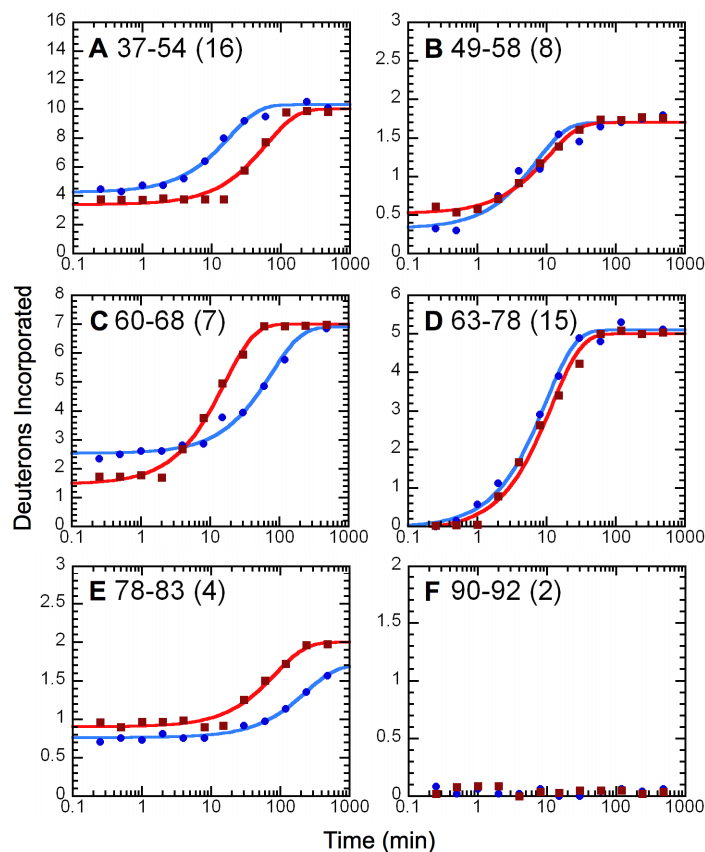


Figure 58. MPGES1 peptic peptide map. White bars, with corresponding residue numbers, represent peptides analyzed for deuterium incorporation. Gray bars indicate the transmembrane helices, as determined by electron microscopy.



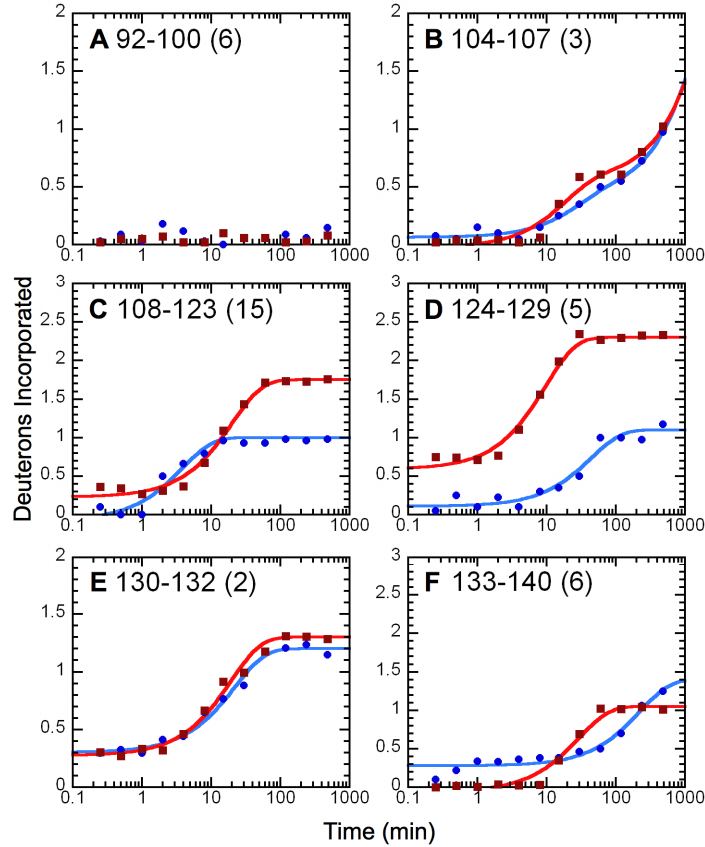
Peptide	A_{fast} (D)	A_I (D)	k_I (min^{-1})	A_2 (D)	k_2 (min^{-1})
A 2-13 (10)					
CHAPS	8.6	1.44 ± 0.10	0.536 ± 0.087		
DDM	7.6	2.40 ± 0.11	0.321 ± 0.040		
B 14-17 (3)					
CHAPS	0	0.74 ± 0.03	0.0971 ± 0.0142	2.29 ± 0.03	$\leq 1 \times 10^{-4}$
DDM	0	1.04 ± 0.04	0.101 ± 0.011	1.96 ± 0.04	$\leq 1 \times 10^{-4}$
C 18-23 (5)					
CHAPS	0	5	$\leq 1 \times 10^{-4}$		
DDM	0	5	$\leq 1 \times 10^{-4}$		
D 23-27 (4)					
CHAPS	0	4	$\leq 1 \times 10^{-4}$		
DDM	0	4	$\leq 1 \times 10^{-4}$		
E 28-31 (3)					
CHAPS	0	0.33 ± 0.03	0.141 ± 0.015	2.55 ± 0.02	$\leq 5.12 \times 10^{-4}$
DDM	0	0.67 ± 0.07	0.252 ± 0.035	2.40 ± 0.05	$\leq 4.94 \times 10^{-4}$
F 32-39 (7)					
CHAPS	0	1.05 ± 0.03	0.102 ± 0.009	5.90 ± 0.04	$\leq 1 \times 10^{-4}$
DDM	0	1.41 ± 0.03	0.0282 ± 0.0023	5.59 ± 0.03	$\leq 1 \times 10^{-4}$

Figure 59. H/D exchange kinetic profiles for MPGES1 as a function of micelle, residues 2 – 39. The total number of exchangeable sites for each peptide is given in parentheses. Deuterium incorporation as a function of time is plotted for the enzyme solubilized in either CHAPS (blue) or DDM (red) detergent micelles and fit to a sum of first-order rate terms, as described in the Materials and Methods chapter.



Peptide	A_{fast} (D)	A_I (D)	k_I (min^{-1})	A_2 (D)	k_2 (min^{-1})
A 37-54 (16)					
CHAPS	3.9	5.90 ± 0.15	0.0601 ± 0.0054	6.18 ± 0.26	$\leq 1 \times 10^{-4}$
DDM	3.4	6.61 ± 0.11	0.0161 ± 0.0022	6.00 ± 0.21	$\leq 1 \times 10^{-4}$
B 49-58 (8)					
CHAPS	0	1.37 ± 0.08	0.141 ± 0.025	6.44 ± 0.07	$\leq 1 \times 10^{-4}$
DDM	0.5	1.18 ± 0.03	0.0943 ± 0.0074	6.30 ± 0.03	$\leq 1 \times 10^{-4}$
C 60-68 (7)					
CHAPS	2.6	4.37 ± 0.08	0.0131 ± 0.0011		
DDM	1.5	5.54 ± 0.09	0.0622 ± 0.0037		
D 63-78 (15)					
CHAPS	0	5.11 ± 0.09	0.103 ± 0.006	10.00 ± 0.12	$\leq 1 \times 10^{-4}$
DDM	0	5.09 ± 0.12	0.0851 ± 0.0067	9.91 ± 0.18	$\leq 1 \times 10^{-4}$
E 78-83 (4)					
CHAPS	0.8	0.94 ± 0.02	0.00428 ± 0.00038	2.30 ± 0.13	$\leq 1 \times 10^{-4}$
DDM	0.9	1.10 ± 0.03	0.0116 ± 0.0014	2.00 ± 0.03	$\leq 1 \times 10^{-4}$
F 90-92 (2)					
CHAPS	0	2	$\leq 1 \times 10^{-4}$		
DDM	0	2	$\leq 1 \times 10^{-4}$		

Figure 60. H/D exchange kinetic profiles for MPGES1 as a function of micelle, residues 37 – 92. The total number of exchangeable sites for each peptide is given in parentheses. Deuterium incorporation as a function of time is plotted for the enzyme solubilized in either CHAPS (blue) or DDM (red) detergent micelles.



Peptide	A_{fast} (D)	A_I (D)	k_I (min^{-1})	A_2 (D)	k_2 (min^{-1})
A 92-100 (6)					
CHAPS	0	6	$\leq 1 \times 10^{-4}$		
DDM	0	6	$\leq 1 \times 10^{-4}$		
B 104-107 (3)					
CHAPS	0	0.37 ± 0.05	0.0365 ± 0.0021	2.56 ± 0.05	$\leq 4.90 \times 10^{-4}$
DDM	0	0.58 ± 0.08	0.0549 ± 0.0020	2.44 ± 0.08	$\leq 4.26 \times 10^{-4}$
C 108-123 (15)					
CHAPS	0	1.07 ± 0.07	0.261 ± 0.029	14.06 ± 0.05	$\leq 1 \times 10^{-4}$
DDM	0	1.52 ± 0.04	0.0497 ± 0.0046	13.25 ± 0.04	$\leq 1 \times 10^{-4}$
D 124-129 (5)					
CHAPS	0	0.99 ± 0.04	0.0227 ± 0.0022	4.00 ± 0.16	$\leq 1 \times 10^{-4}$
DDM	0.6	1.71 ± 0.05	0.103 ± 0.009	2.70 ± 0.15	$\leq 1 \times 10^{-4}$
E 130-132 (2)					
CHAPS	0	0.90 ± 0.02	0.0454 ± 0.0046	0.75 ± 0.05	$\leq 1 \times 10^{-4}$
DDM	0.3	1.03 ± 0.03	0.0517 ± 0.0051	0.70 ± 0.05	$\leq 1 \times 10^{-4}$
F 133-140 (6)					
CHAPS	0	1.12 ± 0.03	0.00446 ± 0.00055	4.88 ± 0.03	$\leq 1 \times 10^{-4}$
DDM	0	1.11 ± 0.04	0.0339 ± 0.0045	4.89 ± 0.06	$\leq 1 \times 10^{-4}$

Figure 61. H/D exchange kinetic profiles for MPGES1 as a function of micelle, residues 92 – 140. The total number of exchangeable sites for each peptide is given in parentheses. Deuterium incorporation as a function of time is plotted for the enzyme solubilized in either CHAPS (blue) or DDM (red) detergent micelles.

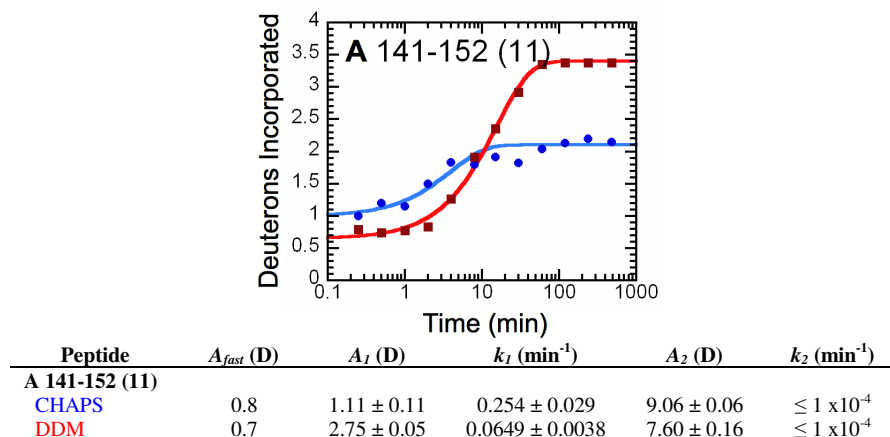


Figure 62. H/D exchange kinetic profiles for MPGES1 as a function of micelle, residues 141 – 152. The total number of exchangeable sites for each peptide is given in parentheses. Deuterium incorporation as a function of time is plotted for the enzyme solubilized in either CHAPS (blue) or DDM (red) detergent micelles.

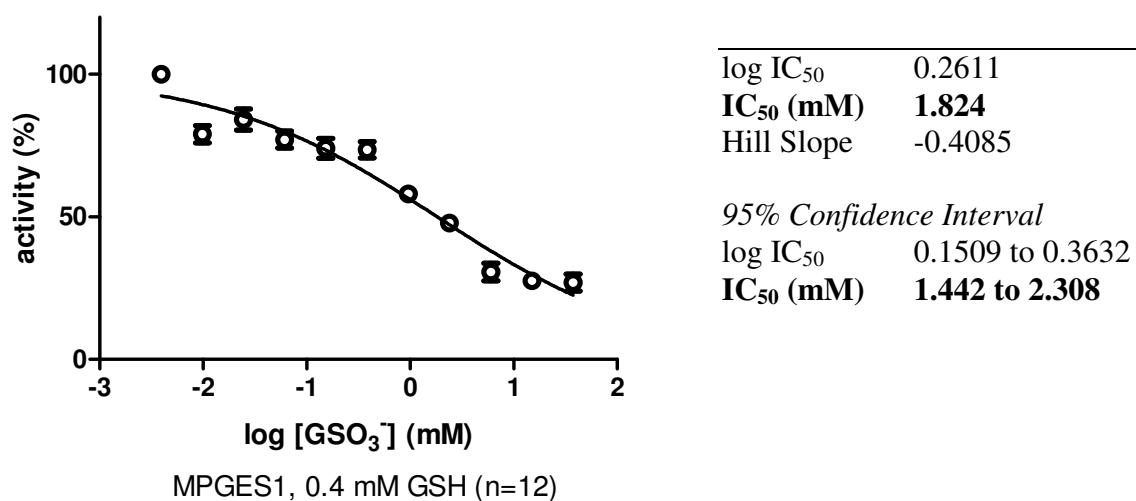
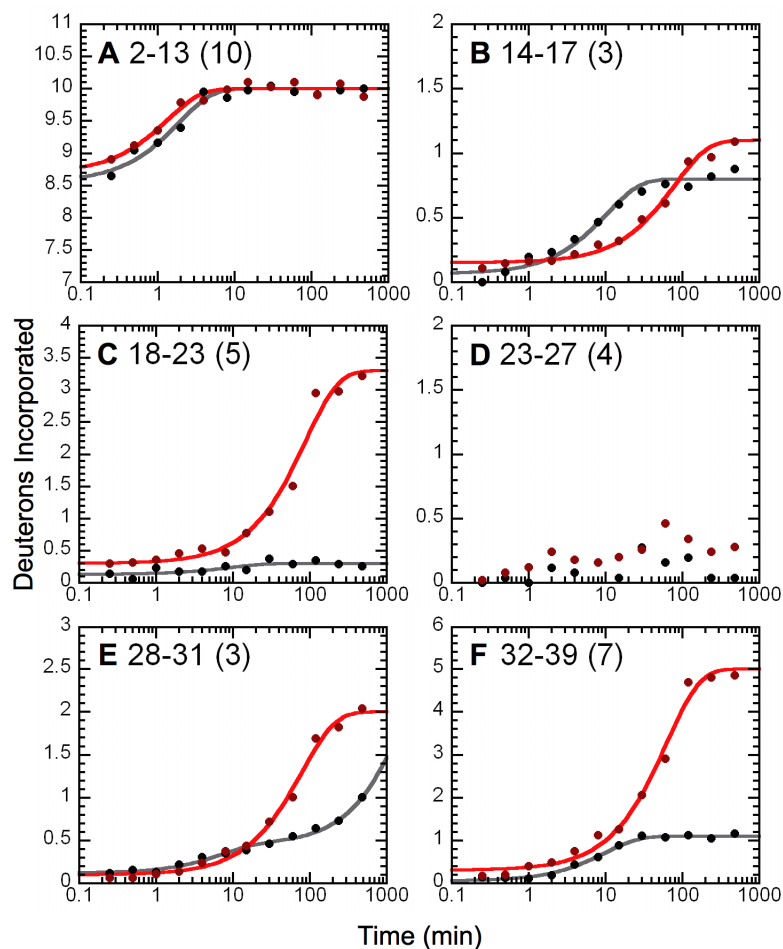
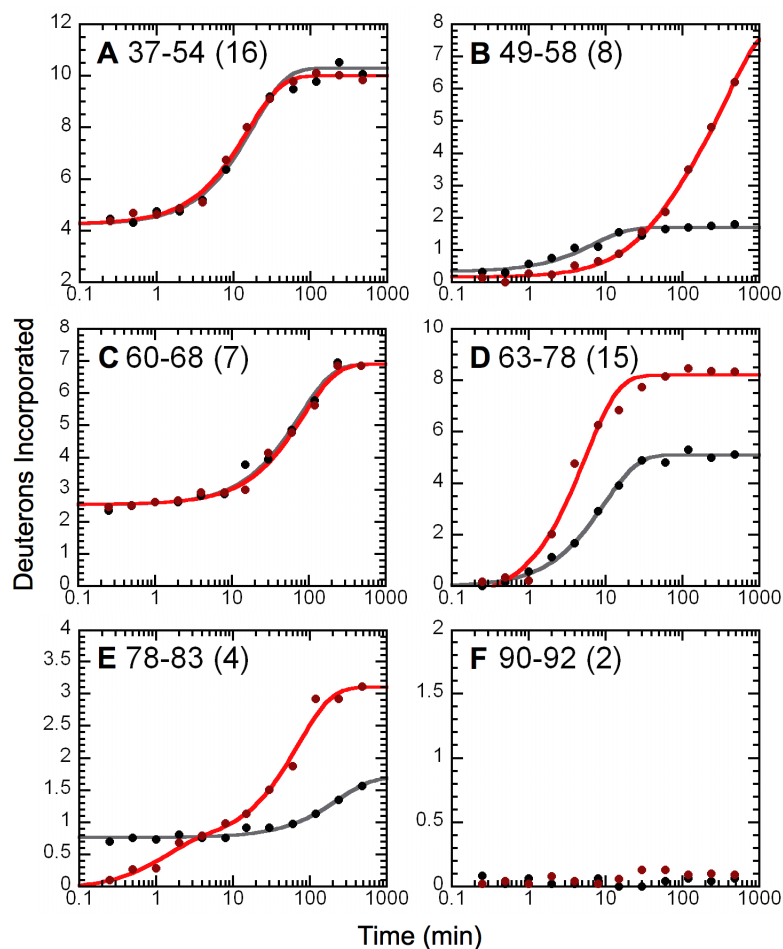


Figure 63. Determination of GSO_3^- IC_{50} . The final concentration of total protein is 15 $\mu\text{g/ml}$, PGH_2 is 10 μM , GSH is 0.4 mM, and GSO_3^- from 0.004 to 37.5 mM. The number of replicate experiments is twelve.



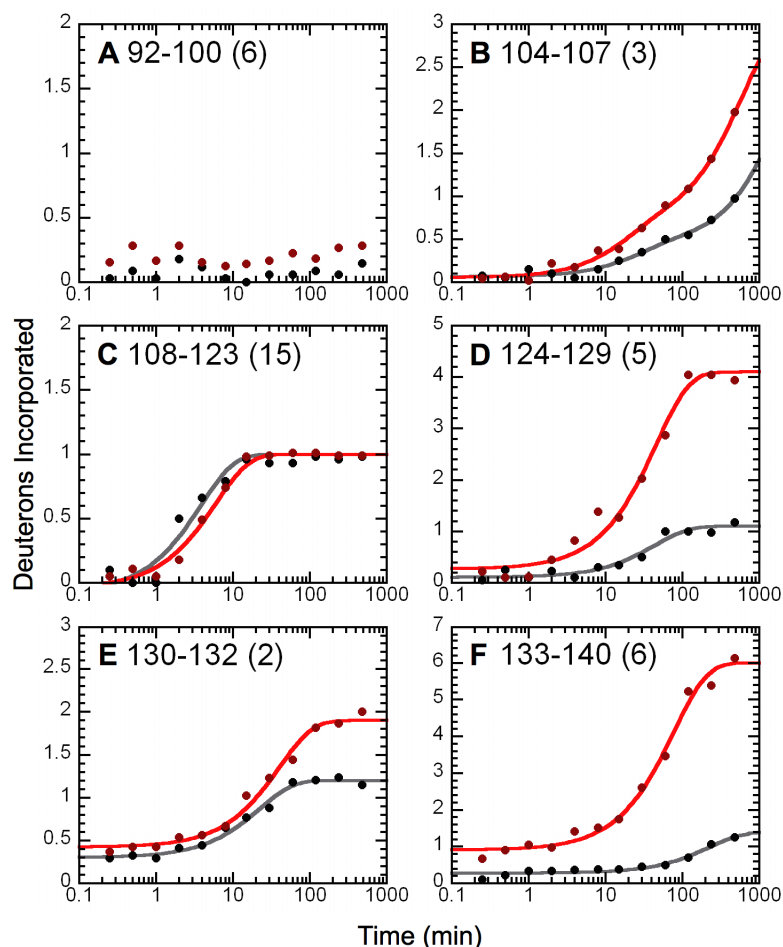
Peptide	A_{fast} (D)	A_I (D)	k_I (min^{-1})	A_2 (D)	k_2 (min^{-1})
A 2-13 (10)					
GSH	8.6	1.44 ± 0.10	0.536 ± 0.087		
1	8.7	1.31 ± 0.11	0.747 ± 0.132		
B 14-17 (3)					
GSH	0	0.74 ± 0.03	0.0971 ± 0.0142	2.29 ± 0.03	$\leq 1 \times 10^{-4}$
1	0	0.95 ± 0.02	0.0127 ± 0.0011	2.06 ± 0.10	$\leq 1 \times 10^{-4}$
C 18-23 (5)					
GSH	0	5	$\leq 1 \times 10^{-4}$		
1	0	3.00 ± 0.07	0.0115 ± 0.0012	1.70 ± 0.07	$\leq 1 \times 10^{-4}$
D 23-27 (4)					
GSH	0	4	$\leq 1 \times 10^{-4}$		
1	0	4	$\leq 1 \times 10^{-4}$		
E 28-31 (3)					
GSH	0	0.33 ± 0.03	0.141 ± 0.015	2.55 ± 0.02	$\leq 5.12 \times 10^{-4}$
1	0	1.90 ± 0.03	0.0127 ± 0.0009	1.16 ± 0.26	$\leq 1 \times 10^{-4}$
F 32-39 (7)					
GSH	0	1.05 ± 0.03	0.102 ± 0.009	5.90 ± 0.04	$\leq 1 \times 10^{-4}$
1	0	4.69 ± 0.09	0.0161 ± 0.0013	2.00 ± 0.09	$\leq 1 \times 10^{-4}$

Figure 64. H/D exchange kinetic profiles for MPGES1 as a function of GSH/1 binding, residues 2 – 39. Shown are the average kinetic profiles for deuterium incorporation as a function of time for MPGES1 in complex with either GSH (black) or inhibitor **1** (red), with the number of exchangeable amide protons for each peptide in parentheses. The data were fit to a sum of first-order rate terms, as described in the Materials and Methods chapter.



Peptide	A_{fast} (D)	A_I (D)	k_I (min^{-1})	A_2 (D)	k_2 (min^{-1})	A_3 (D)	k_3 (min^{-1})
A 37-54 (16)							
GSH	3.9	5.90 ± 0.15	0.0601 ± 0.0054	6.18 ± 0.26	$\leq 1 \times 10^{-4}$		
1	4.3	5.75 ± 0.11	0.0649 ± 0.0045	5.96 ± 0.21	$\leq 1 \times 10^{-4}$		
B 49-58 (8)							
GSH	0	1.37 ± 0.08	0.141 ± 0.025	6.44 ± 0.07	$\leq 1 \times 10^{-4}$		
1	0	1.89 ± 0.46	0.0210 ± 0.0065	5.95 ± 0.47	$\leq 2.54 \times 10^{-3}$		
C 60-68 (7)							
GSH	2.6	4.37 ± 0.08	0.0131 ± 0.0011				
1	2.6	4.36 ± 0.07	0.0119 ± 0.0009				
D 63-78 (15)							
GSH	0	5.11 ± 0.09	0.103 ± 0.006	10.00 ± 0.12	$\leq 1 \times 10^{-4}$		
1	0	8.73 ± 0.33	0.185 ± 0.021	7.05 ± 0.31	$\leq 1 \times 10^{-4}$		
E 78-83 (4)							
GSH	0.8	0.94 ± 0.02	0.00428 ± 0.00038	2.30 ± 0.13	$\leq 1 \times 10^{-4}$		
1	0	0.72 ± 0.19	0.802 ± 0.053	2.42 ± 0.12	0.0141 ± 0.0018	0.86 ± 0.12	$\leq 1 \times 10^{-4}$
F 90-92 (2)							
GSH	0	2	$\leq 1 \times 10^{-4}$				
1	0	2	$\leq 1 \times 10^{-4}$				

Figure 65. H/D exchange kinetic profiles for MPGES1 as a function of GSH/1 binding, residues 37 – 92. Shown are the average kinetic profiles for deuterium incorporation as a function of time for MPGES1 in complex with either GSH (black) or inhibitor **1** (red), with the number of exchangeable amide protons for each peptide in parentheses.



Peptide	A_{fast} (D)	A_1 (D)	k_1 (min^{-1})	A_2 (D)	k_2 (min^{-1})
A 92-100 (6)					
GSH	0	6	$\leq 1 \times 10^{-4}$		
1	0	6	$\leq 1 \times 10^{-4}$		
B 104-107 (3)					
GSH	0	0.37 ± 0.05	0.0365 ± 0.0021	2.56 ± 0.05	$\leq 4.90 \times 10^{-4}$
1	0	0.60 ± 0.07	0.0535 ± 0.0051	2.35 ± 0.07	$\leq 1.72 \times 10^{-3}$
C 108-123 (15)					
GSH	0	1.07 ± 0.07	0.261 ± 0.029	14.06 ± 0.05	$\leq 1 \times 10^{-4}$
1	0	1.04 ± 0.03	0.168 ± 0.016	13.98 ± 0.13	$\leq 1 \times 10^{-4}$
D 124-129 (5)					
GSH	0	0.99 ± 0.04	0.0227 ± 0.0022	4.00 ± 0.16	$\leq 1 \times 10^{-4}$
1	0	3.83 ± 0.11	0.0220 ± 0.0025	0.90 ± 0.11	$\leq 1 \times 10^{-4}$
E 130-132 (2)					
GSH	0	0.90 ± 0.02	0.0454 ± 0.0046	0.75 ± 0.05	$\leq 1 \times 10^{-4}$
1	0.5	1.48 ± 0.03	0.0248 ± 0.0024		
F 133-140 (6)					
GSH	0	1.12 ± 0.03	0.00446 ± 0.00055	4.88 ± 0.03	$\leq 1 \times 10^{-4}$
1	0.9	5.09 ± 0.09	0.0130 ± 0.0010		

Figure 66. H/D exchange kinetic profiles for MPGES1 as a function of GSH/**1** binding, residues 92 – 140. Shown are the average kinetic profiles for deuterium incorporation as a function of time for MPGES1 in complex with either GSH (black) or inhibitor **1** (red), with the number of exchangeable amide protons for each peptide in parentheses.

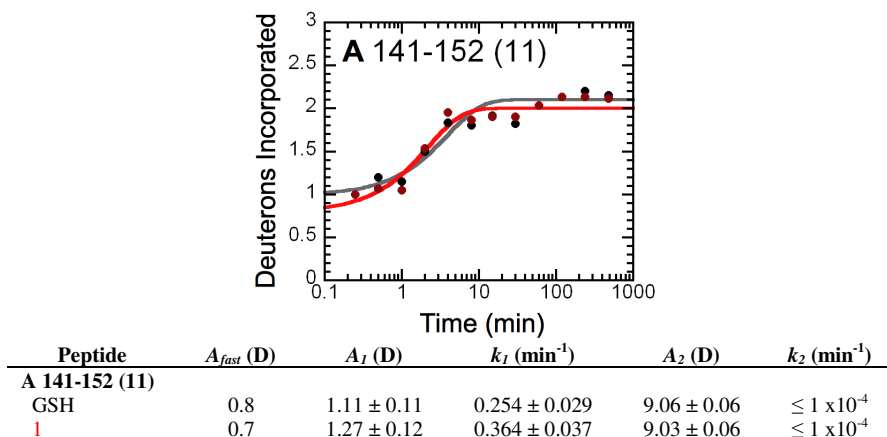


Figure 67. H/D exchange kinetic profiles for MPGES1 as a function of GSH/1 binding, residues 141 – 152. Shown are the average kinetic profiles for deuterium incorporation as a function of time for MPGES1 in complex with either GSH (black) or inhibitor **1** (red), with the number of exchangeable amide protons for each peptide in parentheses.

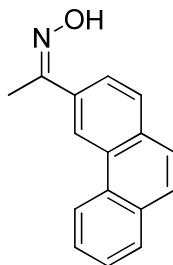


Figure 68. Synthesis of MF63, step 1: 1-(3-phenanthryl)ethanone oxime. To a solution of 1-(3-phenanthryl)ethanone in 25 mL of ethanol was added 4 g of hydroxylamine hydrochloride. The reaction mixture was heated to reflux followed by the addition of 7 mL of pyridine. After 3 h, the reaction was cooled down to room temperature and the solvent was removed *in vacuo*. Ice was added to the residue and the mixture was stirred for 1 h. The resulting off-white solid was filtered and washed with water. 5.02 g of the product (94 %) was obtained by recrystallization from ether.

^1H NMR (CDCl_3 , 400 MHz) δ (ppm) 8.93 (s, 1H), 8.74 (d, $J = 8.2$ Hz, 1H), 7.92 (d, $J = 7.2$ Hz, 1H), 7.90 (dd, $J = 8.4, 14.0$ Hz, 2H), 7.76 (dd, $J = 8.8, 14.8$ Hz, 2H), 7.71-7.60 (m, 2H), 2.49 (s, 3H); LCMS, single peak, 1.51 min, m/e, 236.28 (M+1).

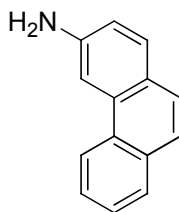


Figure 69. Synthesis of MF63, step 2: 3-phenanthrylamine. To 60 g of polyphosphoric acid was added 5.02 g of 1-(3-phenanthryl)ethanone oxime at room temperature. The reaction mixture was stirred at 100 °C for 2 h, cooled down to room temperature followed by the addition of ice. Stirred 30 minutes, filtered and washed with water. This white solid was then placed in 50 mL of methanol and 4 mL of concentrated HCl. The reaction was refluxed overnight, cooled down to room temperature and concentrated down. A mixture of ethyl acetate/water was added to the residue and the resulting solution was made basic with 10 N KOH. The aqueous layer was extracted with ethyl acetate and combined organic layers were washed with water, brine, dried over MgSO₄ and solvent was removed under reduced pressure to afford 3.74g (90%) of 3-phenanthrylamine as a beige solid. LCMS, single peak, 1.09 min, m/e, 194.24 (M+1).

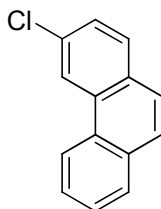


Figure 70. Synthesis of MF63, step 3: 3-chlorophenanthrene. 3.39 g of CuCl₂ and 4.84 mL of *t*-butyl nitrite were dissolved in 10 mL of acetonitrile. The 3-phenanthrylamine (3.74 g) was added over 10 minutes as a solution in 6 mL of acetonitrile. The reaction was stirred for 45 minutes at 65 °C, cooled down to room temperature followed by the addition of 100 mL of 1 N HCl. The aqueous layer was extracted with dichloromethane and combined organic layers were washed with water, brine, dried over MgSO₄ and solvent was removed under reduced pressure. The residue was purified by flash chromatography on silica gel (hexane/ethyl acetate = 7/3) to produce 2.53 g (63%) of 3-chlorophenanthrene as a white solid. ¹H NMR (CDCl₃, 400 MHz) δ (ppm) 8.65 (d, *J* = 1.6 Hz, 1H), 8.60 (d, *J* = 8.0 Hz, 1H), 7.90 (dd, *J* = 1.6, 8.0 Hz, 1H), 7.82 (d, *J* = 8.4 Hz, 1H), 7.75-7.61 (m, 4H), 7.55 (dd, *J* = 2.0, 8.8 Hz, 1H); LCMS, single peak, 1.75 min, m/e, 213.67 (M+1).

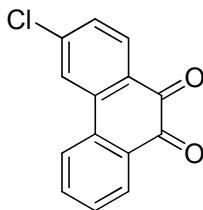


Figure 71. Synthesis of MF63, step 4: 3-chlorophenanthrene-9,10-dione. To a solution of 2.53 g of 3-chlorophenanthrene in 70 mL of acetic acid was added 4.75 g of CrO_3 . The reaction was stirred for 2 h at 100 °C, cooled down to room temperature and poured into 300 mL of water. The suspension was stirred for 1h, filtered and washed with water. The residue was dried under high vacuum to afford 2.5 g (86%) of 3-chlorophenanthrene-9,10-dione. $^1\text{H NMR}$ (CDCl_3 , 400 MHz) δ (ppm) 8.21 (d, $J = 8.0$ Hz, 1H), 8.14 (d, $J = 8.4$ Hz, 1H), 8.00-7.95 (m, 2H), 7.75 (t, $J = 8.0$ Hz, 1H), 7.53 (t, $J = 8.0$ Hz, 1H), 7.44 (dd, $J = 1.6, 8.0$ Hz, 1H); LCMS, single peak, 1.47 min, m/e, 243.66 (M+1).

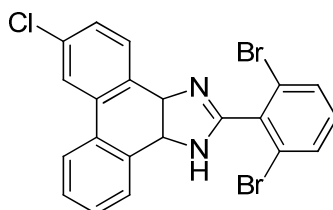
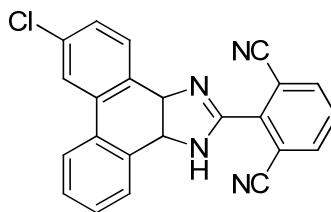
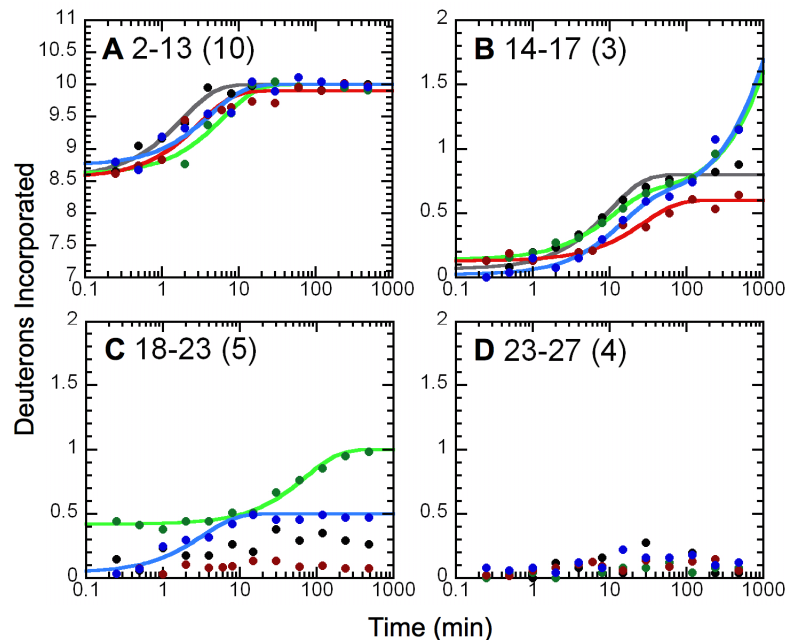


Figure 72. Synthesis of MF63, step 5: 6-chloro-2-(2,6-dibromophenyl)-3a,11b-dihydro-1H-phenanthro[9,10-d]imidazole. To a solution of 0.613 g of 3-chlorophenanthrene-9,10-dione in 25 mL of acetic acid was added 0.8 g of ammonium bicarbonate followed by 1.0 g of 2,6-dibromobenzaldehyde. The reaction was stirred overnight at 130 °C, cooled down to room temperature, and poured into the 40 mL of water. The residue was filtered, washed with water, and purified by flash column chromatography (hexane/ethyl acetate = 6/4) to afford 0.75 g (61%) of white solid product. LCMS, single peak, 1.55 min, m/e, 486.90 (M+1).



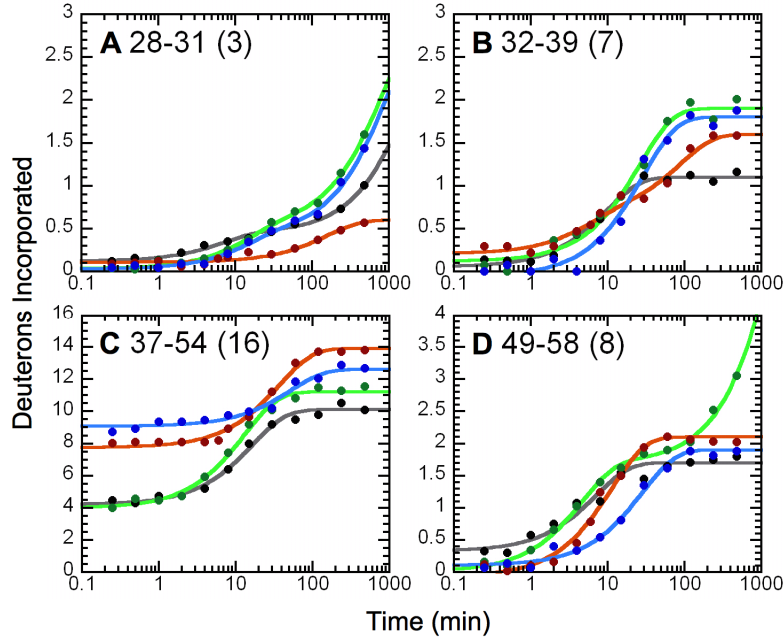
MF63

Figure 73. Synthesis of MF63, final step. To a solution of 0.75 g of 6-chloro-2-(2,6-dibromophenyl)-3a,11b-dihydro-1H-phenanthro[9,10-d]imidazole was added 0.348 g of CuCN. The reaction was stirred overnight at 80 °C, cooled down to room temperature, poured into a mixture of 40 mL of water, 40 mL of ethyl acetate and 5.5 mL of concentrated ammonium hydroxide, and stirred for 1 h at room temperature. The aqueous layer was extracted with ethyl acetate and the combined organic layers were washed with 10% ammonium hydroxide, water, brine, dried over MgSO₄ and solvent was removed under reduced pressure. The residue was purified by flash column chromatography (hexane/ethyl acetate = 5/5) to afford 0.346 g (59%) of 2-(6-chloro-3a,11b-dihydro-1H-phenanthro[9,10-d]imidazol-2-yl)isophthalonitrile. ¹H NMR (DMSO, 400 MHz) δ (ppm) 14.32 (s, 1H), 9.04-8.88 (m, 2H), 8.60-8.36 (m, 4H), 7.98 (t, *J* = 8.0 Hz, 1H), 7.90-7.76 (m, 2H), 7.75-7.67 (m, 1H); LCMS, single peak, 1.54 min, m/e, 381.06 (M+1).



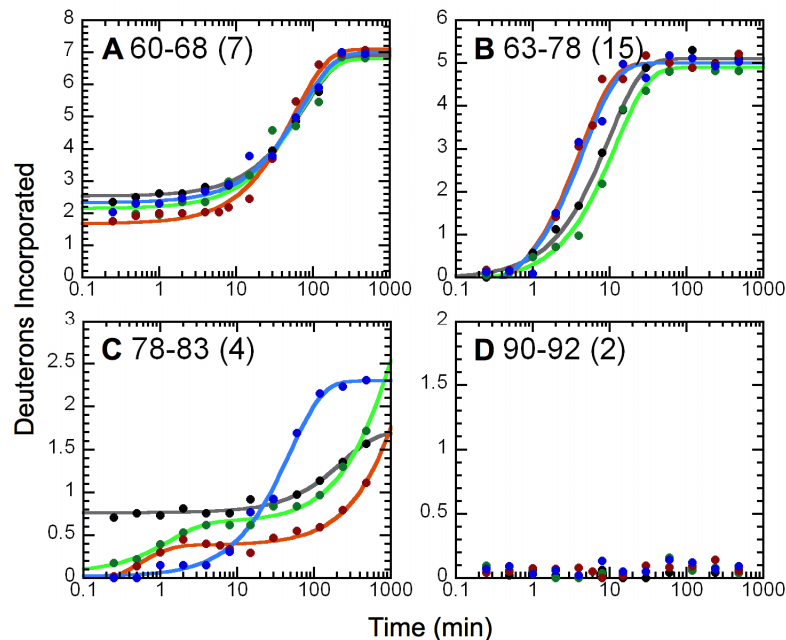
Peptide/ Inhibitor	A_{fast} (D)	A_I (D)	k_I (min^{-1})	A_2 (D)	k_2 (min^{-1})
A 2-13 (10)					
none	8.6	1.44 ± 0.10	0.536 ± 0.087		
2	8.7	1.26 ± 0.11	0.230 ± 0.055		
3	8.7	1.35 ± 0.11	0.321 ± 0.063		
4	8.6	1.39 ± 0.07	0.158 ± 0.025		
B 14-17 (3)					
none	0	0.74 ± 0.03	0.0971 ± 0.0142	2.29 ± 0.03	$\leq 1 \times 10^{-4}$
2	0	0.59 ± 0.07	0.0723 ± 0.0134	2.39 ± 0.07	$\leq 6.05 \times 10^{-4}$
3	0	0.47 ± 0.03	0.0358 ± 0.0077	2.48 ± 0.05	$\leq 1 \times 10^{-4}$
4	0	0.51 ± 0.02	0.0965 ± 0.0113	2.35 ± 0.02	$\leq 5.18 \times 10^{-4}$
C 18-23 (5)					
none	0	5	$\leq 1 \times 10^{-4}$		
2	0	0.46 ± 0.04	0.303 ± 0.070	4.54 ± 0.02	$\leq 1 \times 10^{-4}$
3	0	5	$\leq 1 \times 10^{-4}$		
4	0.31	0.58 ± 0.01	0.0139 ± 0.0014	4.11 ± 0.05	$\leq 1 \times 10^{-4}$
D 23-27 (4)					
none	0	4	$\leq 1 \times 10^{-4}$		
2	0	4	$\leq 1 \times 10^{-4}$		
3	0	4	$\leq 1 \times 10^{-4}$		
4	0	4	$\leq 1 \times 10^{-4}$		

Figure 74. H/D exchange kinetic profiles for MPGES1•GSH as a function of inhibitor binding, residues 2-27. Shown are the average kinetic profiles for deuterium incorporation as a function of time for MPGES1 complexed with GSH in the absence of an inhibitor (black), or in the presence of inhibitor 2 (blue), 3 (red), or 4 (green). The data were fit to a sum of first-order rate terms, as described in the Materials and Methods chapter.



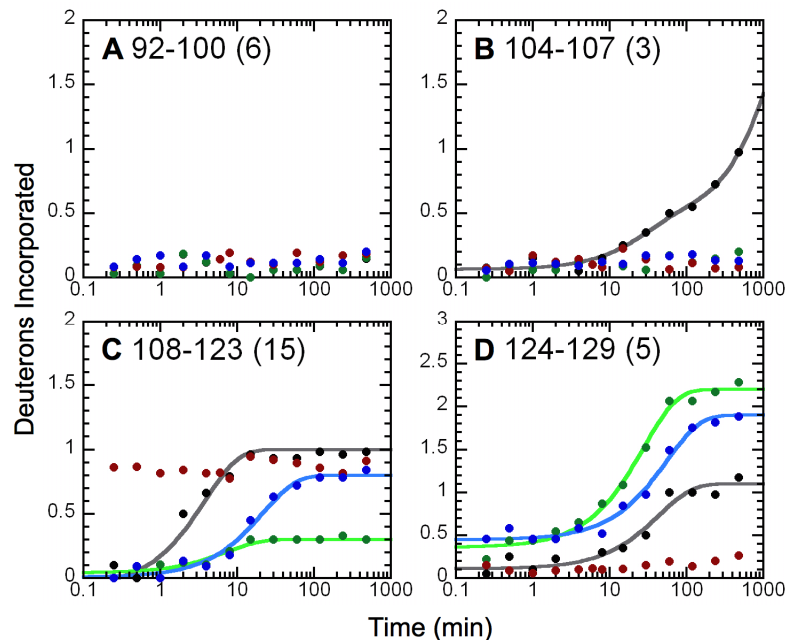
Peptide/ Inhibitor	A_{fast} (D)	A_I (D)	k_I (min^{-1})	A_2 (D)	k_2 (min^{-1})	A_3 (D)	k_3 (min^{-1})
A 28-31 (3)							
none	0	0.33 ± 0.03	0.141 ± 0.015	2.55 ± 0.02	$\leq 5.12 \times 10^{-4}$		
2	0	0.40 ± 0.04	0.0687 ± 0.0170	2.57 ± 0.04	$\leq 1.05 \times 10^{-3}$		
3	0	0.49 ± 0.01	0.00637 ± 0.00078	2.65 ± 0.09	$\leq 1 \times 10^{-4}$		
4	0	0.48 ± 0.04	0.0686 ± 0.0130	2.48 ± 0.03	$\leq 1.19 \times 10^{-3}$		
B 32-39 (7)							
none	0	1.05 ± 0.03	0.102 ± 0.009	5.90 ± 0.04	$\leq 1 \times 10^{-4}$		
2	0	1.85 ± 0.05	0.0345 ± 0.0038	5.22 ± 0.15	$\leq 1 \times 10^{-4}$		
3	0	0.44 ± 0.13	0.186 ± 0.011	0.95 ± 0.14	0.0115 ± 0.0029	5.61 ± 0.14	$\leq 1 \times 10^{-4}$
4	0	1.78 ± 0.05	0.0382 ± 0.0041	5.15 ± 0.13	$\leq 1 \times 10^{-4}$		
C 37-54 (16)							
none	3.9	5.90 ± 0.15	0.0601 ± 0.0054	6.18 ± 0.26	$\leq 1 \times 10^{-4}$		
2	9.1	3.54 ± 0.12	0.0194 ± 0.0028	3.09 ± 0.69	$\leq 1 \times 10^{-4}$		
3	7.9	6.16 ± 0.11	0.0270 ± 0.0020	1.93 ± 0.18	$\leq 1 \times 10^{-4}$		
4	3.5	7.34 ± 0.14	0.0792 ± 0.0049	5.19 ± 0.15	$\leq 1 \times 10^{-4}$		
D 49-58 (8)							
none	0	1.37 ± 0.08	0.141 ± 0.025	6.44 ± 0.07	$\leq 1 \times 10^{-4}$		
2	0	1.80 ± 0.04	0.0354 ± 0.0030	6.16 ± 0.10	$\leq 1 \times 10^{-4}$		
3	0	2.17 ± 0.06	0.0886 ± 0.0075	5.90 ± 0.08	$\leq 1 \times 10^{-4}$		
4	0	1.68 ± 0.06	0.217 ± 0.022	6.31 ± 0.04	$\leq 5.20 \times 10^{-4}$		

Figure 75. H/D exchange kinetic profiles for MPGES1•GSH as a function of inhibitor binding, residues 28-58. Shown are the average kinetic profiles for deuterium incorporation as a function of time for MPGES1 complexed with GSH in the absence of an inhibitor (black), or in the presence of inhibitor 2 (blue), 3 (red), or 4 (green).



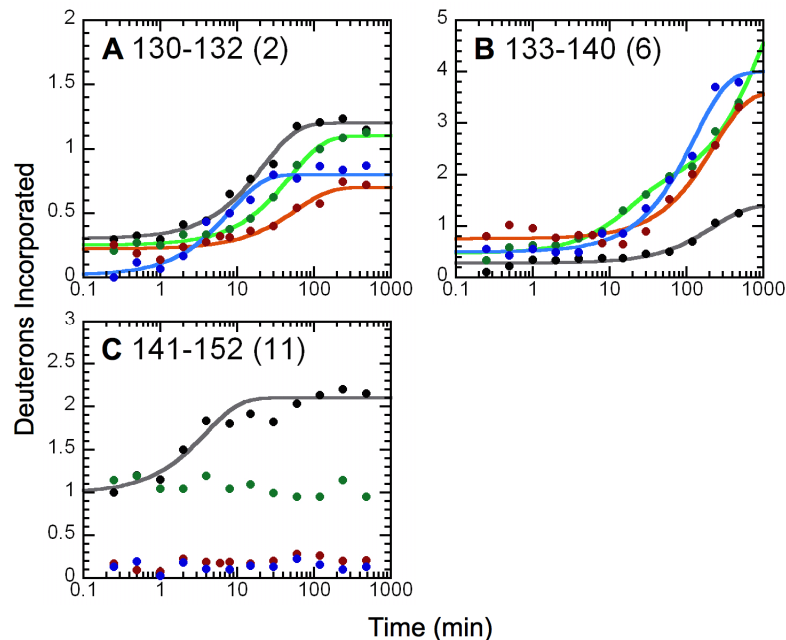
Peptide/ Inhibitor	A_{fast} (D)	A_1 (D)	k_1 (min^{-1})	A_2 (D)	k_2 (min^{-1})
A 60-68 (7)					
none	2.6	4.37 ± 0.08	0.0131 ± 0.0011		
2	2.3	4.68 ± 0.10	0.0141 ± 0.0013		
3	1.6	5.43 ± 0.09	0.0172 ± 0.0013		
4	2.3	4.66 ± 0.15	0.0153 ± 0.0021		
B 63-78 (15)					
none	0	5.11 ± 0.09	0.103 ± 0.006	10.00 ± 0.12	$\leq 1 \times 10^{-4}$
2	0	5.43 ± 0.23	0.215 ± 0.026	10.03 ± 0.21	$\leq 1 \times 10^{-4}$
3	0	5.53 ± 0.21	0.180 ± 0.018	10.00 ± 0.19	$\leq 1 \times 10^{-4}$
4	0	5.00 ± 0.13	0.0844 ± 0.0073	10.02 ± 0.20	$\leq 1 \times 10^{-4}$
C 78-83 (4)					
none	0.8	0.94 ± 0.02	0.00428 ± 0.00038	2.30 ± 0.13	$\leq 1 \times 10^{-4}$
2	0	2.28 ± 0.04	0.0206 ± 0.0014	1.69 ± 0.18	$\leq 1 \times 10^{-4}$
3	0	0.62 ± 0.18	0.609 ± 0.028	3.62 ± 0.02	$\leq 4.80 \times 10^{-4}$
4	0	0.59 ± 0.08	0.749 ± 0.022	3.35 ± 0.03	$\leq 8.29 \times 10^{-4}$
D 90-92 (2)					
none	0	2	$\leq 1 \times 10^{-4}$		
2	0	2	$\leq 1 \times 10^{-4}$		
3	0	2	$\leq 1 \times 10^{-4}$		
4	0	2	$\leq 1 \times 10^{-4}$		

Figure 76. H/D exchange kinetic profiles for MPGES1•GSH as a function of inhibitor binding, residues 60-92. Shown are the average kinetic profiles for deuterium incorporation as a function of time for MPGES1 complexed with GSH in the absence of an inhibitor (black), or in the presence of inhibitor **2** (blue), **3** (red), or **4** (green).



Peptide/ Inhibitor	A_{fast} (D)	A_1 (D)	k_1 (min^{-1})	A_2 (D)	k_2 (min^{-1})
A 92-100 (6)					
none	0	6	$\leq 1 \times 10^{-4}$		
2	0	6	$\leq 1 \times 10^{-4}$		
3	0	6	$\leq 1 \times 10^{-4}$		
4	0	6	$\leq 1 \times 10^{-4}$		
B 104-107 (3)					
none	0	0.37 ± 0.05	0.0365 ± 0.0021	2.56 ± 0.05	$\leq 4.90 \times 10^{-4}$
2	0	3	$\leq 1 \times 10^{-4}$		
3	0	3	$\leq 1 \times 10^{-4}$		
4	0	3	$\leq 1 \times 10^{-4}$		
C 108-123 (15)					
none	0	1.07 ± 0.07	0.261 ± 0.029	14.06 ± 0.05	$\leq 1 \times 10^{-4}$
2	0	0.79 ± 0.03	0.0460 ± 0.0055	14.24 ± 0.05	$\leq 1 \times 10^{-4}$
3	0.9	14.15 ± 0.02	$\leq 1 \times 10^{-4}$		
4	0	0.26 ± 0.02	0.139 ± 0.033	14.69 ± 0.02	$\leq 1 \times 10^{-4}$
D 124-129 (5)					
none	0	0.99 ± 0.04	0.0227 ± 0.0022	4.00 ± 0.16	$\leq 1 \times 10^{-4}$
2	0	1.54 ± 0.03	0.0182 ± 0.0017	3.02 ± 0.18	$\leq 1 \times 10^{-4}$
3	0	5	$\leq 1 \times 10^{-4}$		
4	0	1.84 ± 0.04	0.0361 ± 0.0030	2.92 ± 0.10	$\leq 1 \times 10^{-4}$

Figure 77. H/D exchange kinetic profiles for MPGES1•GSH as a function of inhibitor binding, residues 92-129. Shown are the average kinetic profiles for deuterium incorporation as a function of time for MPGES1 complexed with GSH in the absence of an inhibitor (black), or in the presence of inhibitor **2** (blue), **3** (red), or **4** (green).



Peptide/ Inhibitor	A_{fast} (D)	A_1 (D)	k_1 (min^{-1})	A_2 (D)	k_2 (min^{-1})
A 130-132 (2)					
none	0	0.90 ± 0.02	0.0454 ± 0.0046	0.75 ± 0.05	$\leq 1 \times 10^{-4}$
2	0	0.78 ± 0.04	0.125 ± 0.019	1.21 ± 0.04	$\leq 1 \times 10^{-4}$
3	0	0.48 ± 0.02	0.0172 ± 0.0031	1.37 ± 0.10	$\leq 1 \times 10^{-4}$
4	0	0.85 ± 0.01	0.0202 ± 0.0013	0.95 ± 0.05	$\leq 1 \times 10^{-4}$
B 133-140 (6)					
none	0	1.12 ± 0.03	0.00446 ± 0.00055	4.88 ± 0.03	$\leq 1 \times 10^{-4}$
2	0	3.50 ± 0.06	0.00787 ± 0.00061	2.12 ± 0.06	$\leq 1 \times 10^{-4}$
3	0.8	2.85 ± 0.06	0.00440 ± 0.00046	2.40 ± 0.06	$\leq 1 \times 10^{-4}$
4	0	1.25 ± 0.11	0.0567 ± 0.0128	4.28 ± 0.11	$\leq 1.09 \times 10^{-3}$
C 141-152 (11)					
none	0.8	1.11 ± 0.11	0.254 ± 0.029	9.06 ± 0.06	$\leq 1 \times 10^{-4}$
2	0	11	$\leq 1 \times 10^{-4}$		
3	0	11	$\leq 1 \times 10^{-4}$		
4	1.1	9.92 ± 0.03	$\leq 1 \times 10^{-4}$		

Figure 78. H/D exchange kinetic profiles for MPGES1•GSH as a function of inhibitor binding, residues 130-152. Shown are the average kinetic profiles for deuterium incorporation as a function of time for MPGES1 complexed with GSH in the absence of an inhibitor (black), or in the presence of inhibitor **2** (blue), **3** (red), or **4** (green).

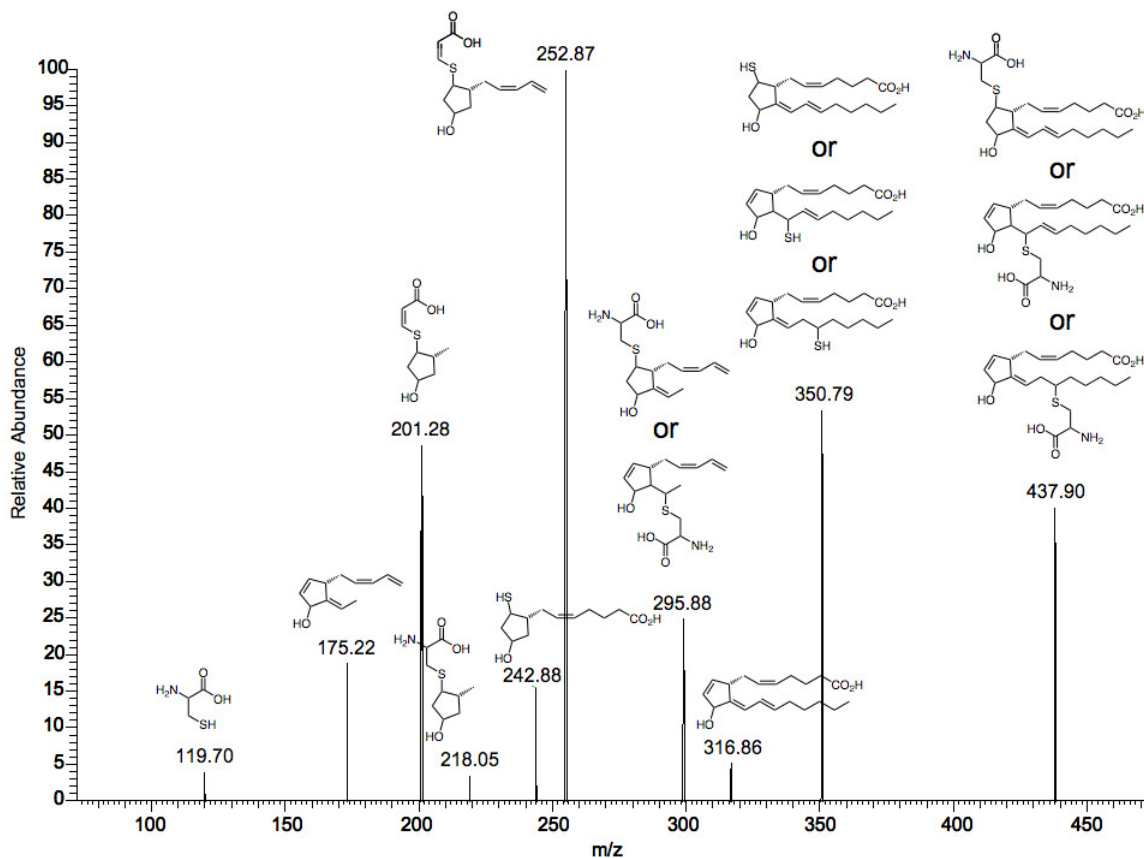


Figure 79. Fragmentation spectrum of Cys-15d-PGJ₂. The reduced form of the cysteine/15d-PGJ₂ adduct was subject to MS/MS fragmentation following reduction by NaBH₃CN. Fragments in the low-mass range indicate that cysteine forms a Michael adduct at position C-9 of 15d-PGJ₂.

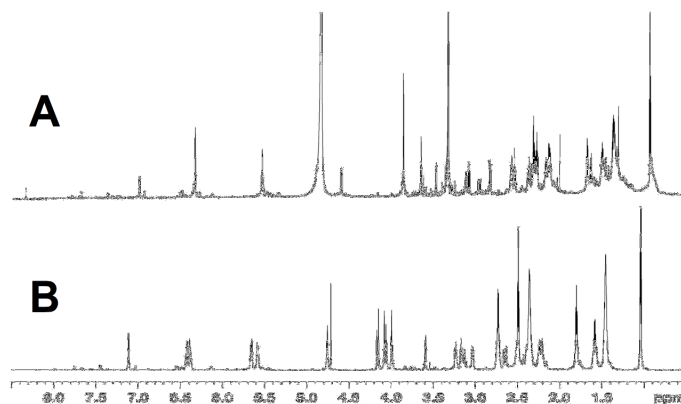


Figure 80. ¹H-NMR Spectra of 9-GS-15d-PGJ₂ at 900 MHz. The sample was solubilized and analyzed in (A) CD₃OD and (B) D₂O. Spectrum A was acquired at 25 °C, while spectrum B was acquired at 45 °C.

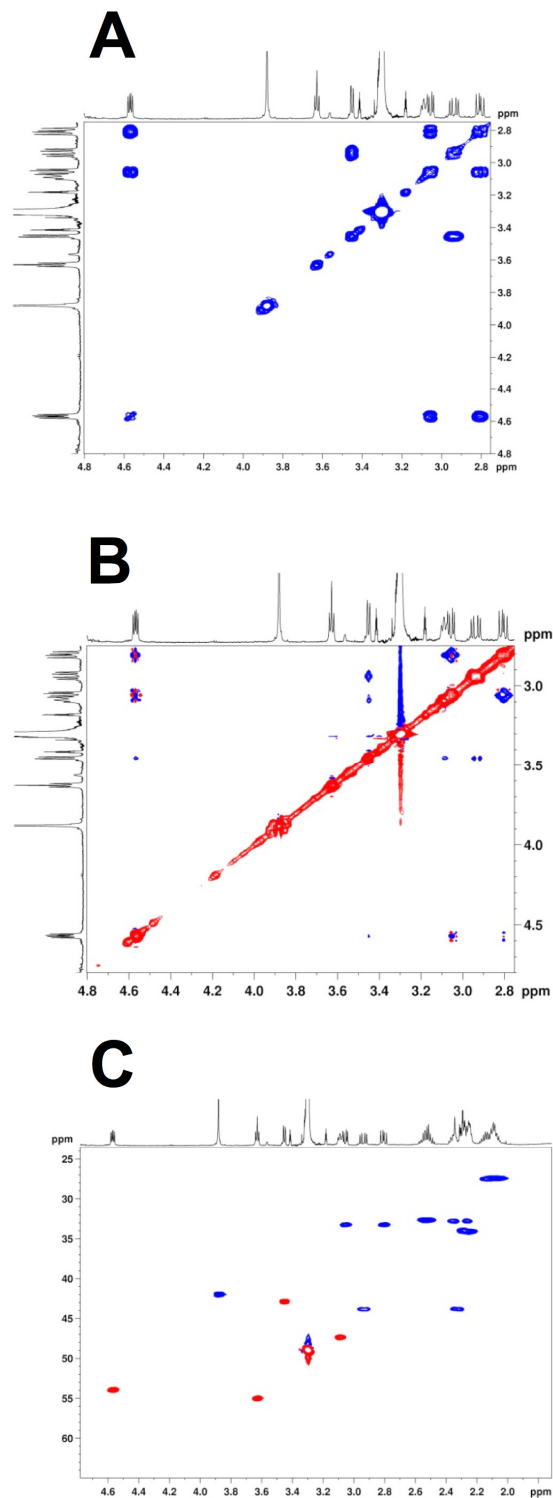


Figure 81. Two-dimensional NMR spectroscopy of 9-GS-15d-PGJ₂ at 600 MHz. The spectra were collected with CD₃OD as the solvent. (A) COSY, (B) NOESY, and (C) HSQC analyses are shown with CH in red and CH₂ in blue. All spectra were acquired at 25 °C.

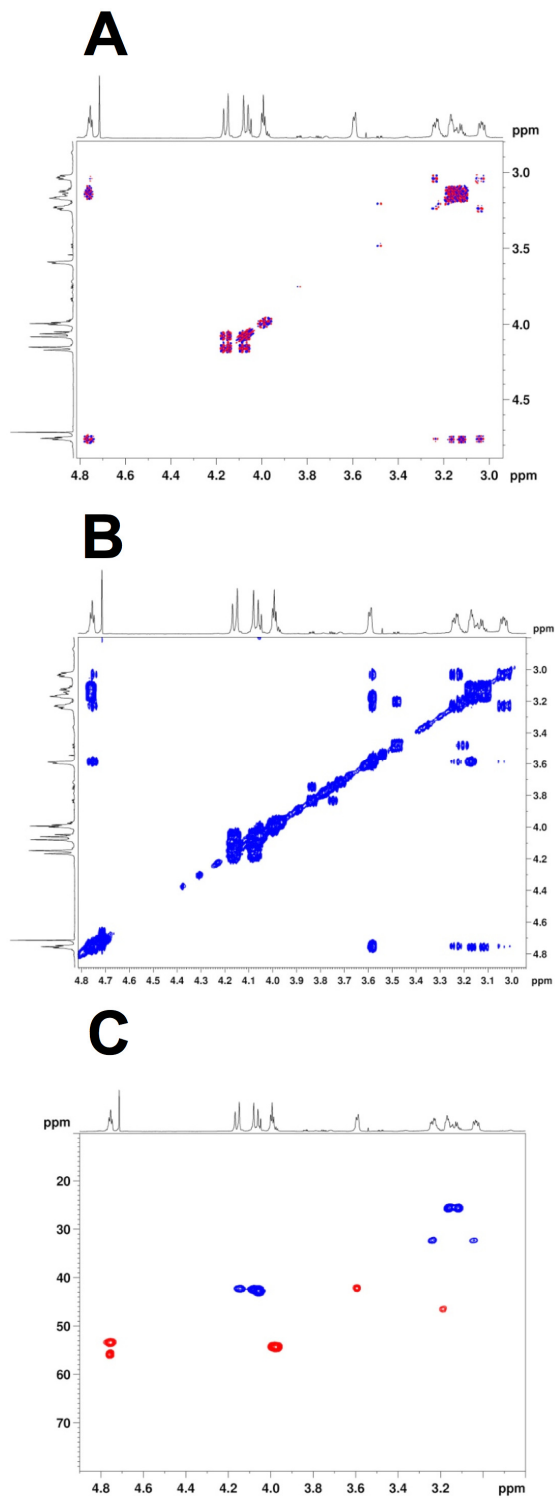


Figure 82. Two-dimensional NMR spectroscopy of 9-GS-15d-PGJ₂ at 900 MHz. spectra were collected with D₂O as the solvent. (A) DFQ-COSY, (B) NOESY, and (C) HSQC analyses are shown with CH in red and CH₂ in blue. All spectra were acquired at 25 °C.

Table 4. NMR Data of the glutathione conjugate of 15d-PGJ₂ in CD₃OD and D₂O.

CD ₃ OD				D ₂ O			
H	n	δ (ppm)	J(Hz)	H	n	δ (ppm)	J(Hz)
<i>Prostaglandin moiety</i>				<i>Prostaglandin moiety</i>			
2	2	2.51 t	6.5	2	2	2.48 t	7.3
3	2	2.15 m	6.7	3	2	1.79 m	7.2
4	2	2.06 m	7.0	4	2	2.22 m	
5	1	5.51 m	3.9,5.8	5	1	5.56 m	7.3,9.8
6	1	5.51 m	3.9,5.8	6	1	5.62 m	7.2,10.1
7a	1	2.27 d	2.1	7a	1	2.41 t	7.5
7b	1	2.36 d	2.4	7b	1	2.51 t	6.8
8	1	3.06 d	5.1	8	1	3.11 d	7.3
9	1	4.57 dd	3.8,4.7	9	1	4.75 t	6.6
10a	1	2.82 dd	4.5,8.7	10a	1	3.02 dd	5.4,8.0
10b	1	3.05 dd	5.1,8.7	10b	1	3.23 dd	6.0,7.7
13	1	6.96 d	8.3	13	1	7.15 d	11.0
14	1	6.30 m	9.0	14	1	6.37 t	6.3
15	1	6.30 m	9.0	15	1	6.37 q	11.3,14.5
16	2	2.25 m	3.2	16	2	2.37 m	5.5,7.8
17	2	1.60 m	7.1,7.4	17	2	1.57 m	6.7,7.2
18	2	1.33 m	3.4,3.6	18	2	1.44 m	
19	2	1.33 m	3.4,3.6	19	2	1.44 m	
20	3	0.91 t	6.8	20	3	1.02 t	6.8
<i>Glutathionyl moiety</i>				<i>Glutathionyl moiety</i>			
glu-α	1	3.63t	6.4	glu-α	1	3.58 d	8.4
glu-βa	1	1.64 dd	7.2,7.5	glu-βa	1	1.78 dd	7.3,8.0
glu-βb	1	2.05 m	6.5	glu-βb	1	2.25 m	
glu-γ	2	2.17 m	7.8	glu-γ	2	2.15 m	
cys-α	1	3.45 d	6.8	cys-α	1	3.15 m	
cys-β	1	2.31 dd	2.1,4.0	cys-β	1	3.11 d	7.38
cys-β	1	2.93 dd	11.8,7.1	cys-β	1	3.17 d	10.2
gly-α	2	3.88 s		gly-α	2	3.52 s	

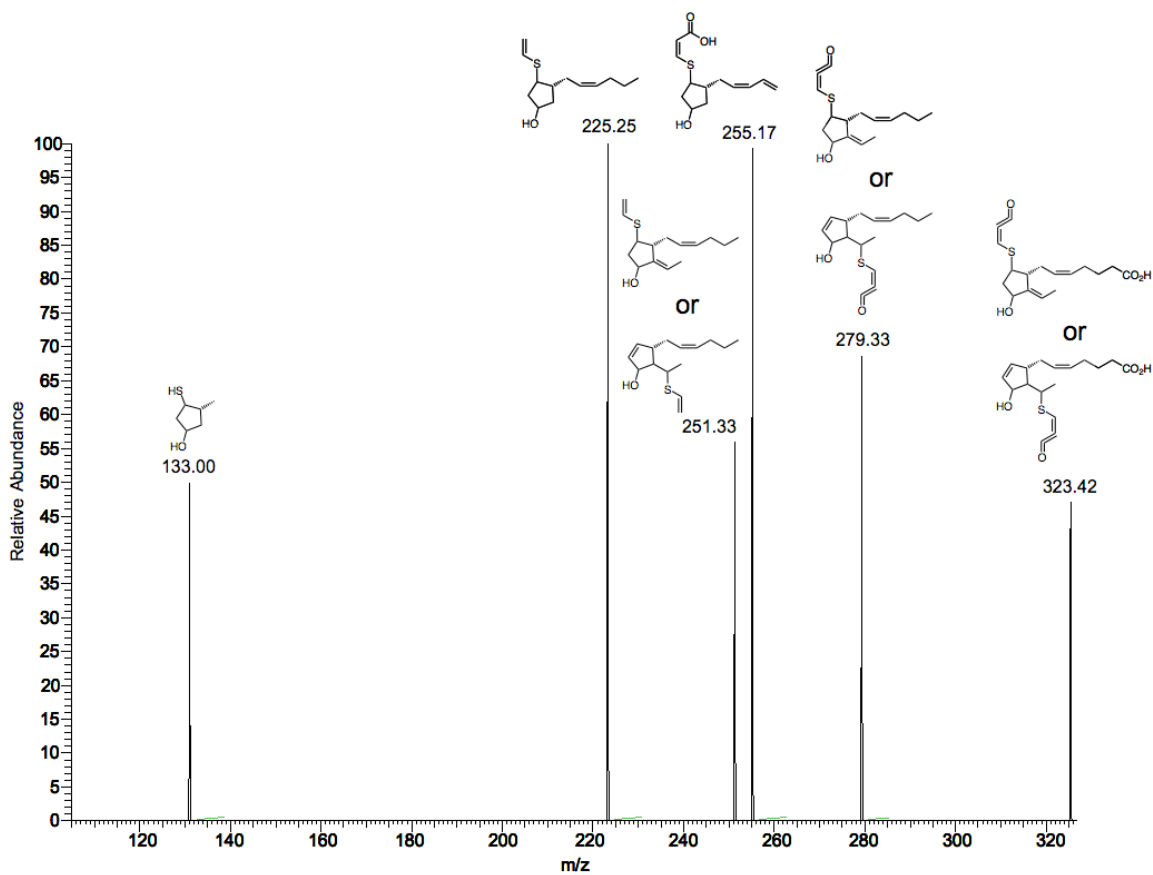
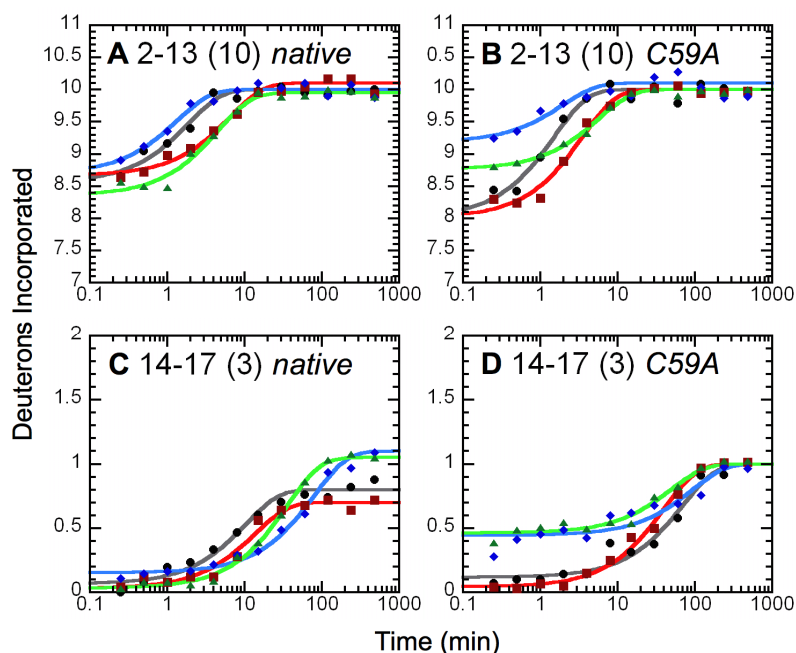
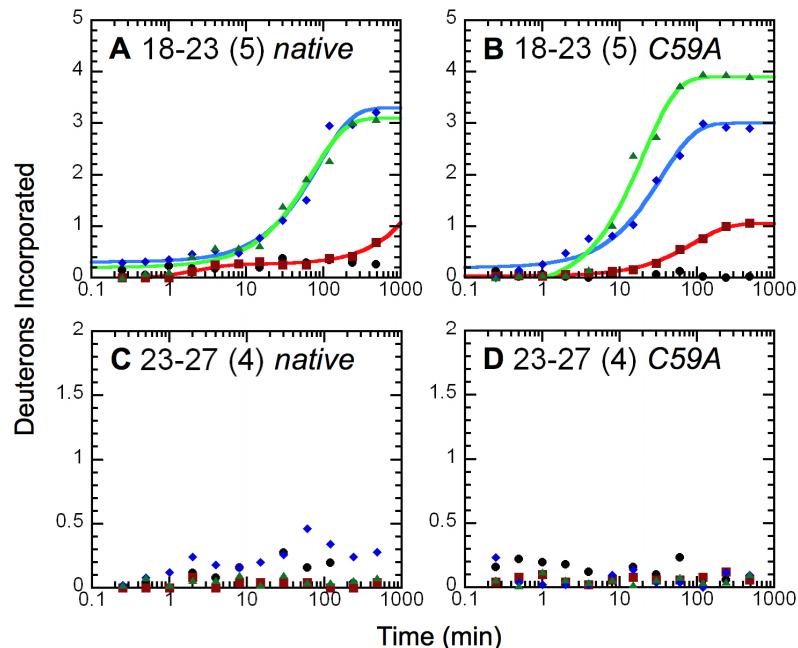


Figure 83. Fragmentation spectrum of MPGES1 C59-15d-PGJ₂. After pepsin digestion, the adduct of peptide 49-59 was subject to fragmentation following reduction by NaBH₃CN, first selecting peptide (49-59)-11-OH-15d-PGJ₂ for MS/MS then C59-11-OH-15d-PGJ₂ for MS³. Fragments in the low-mass range indicate that residue C59 of MPGES1 forms a Michael adduct at position C-9 of 15d-PGJ₂.



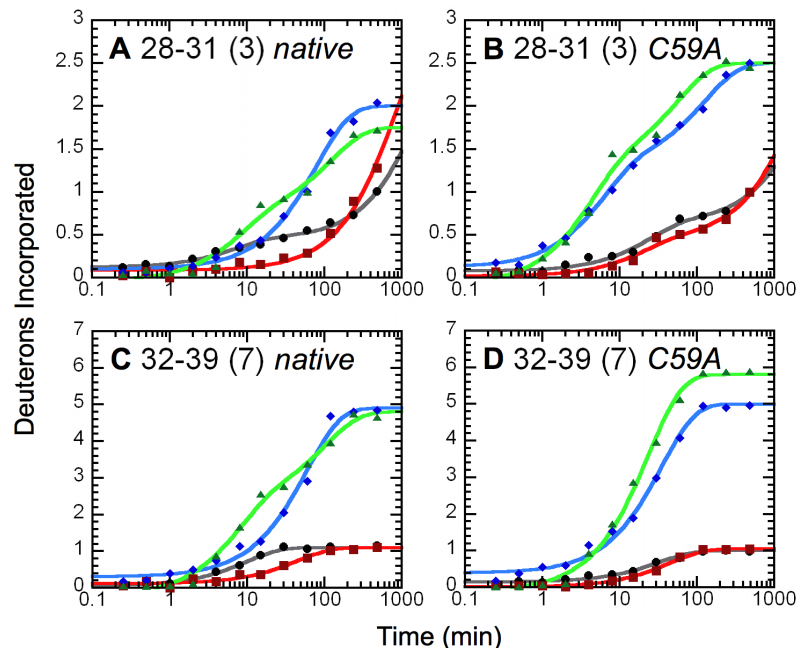
Peptide/Ligand	A_{fast} (D)	A_1 (D)	k_1 (min^{-1})	A_2 (D)	k_2 (min^{-1})
A 2-13 (10) native					
GSH	8.6	1.44 ± 0.10	0.536 ± 0.087		
GSO_3^-	8.7	1.31 ± 0.11	0.747 ± 0.132		
GSH + 15d-PGJ ₂	8.6	1.44 ± 0.10	0.155 ± 0.032		
GSO_3^- + 15d-PGJ ₂	8.4	1.59 ± 0.07	0.221 ± 0.027		
B 2-13 (10) C59A					
GSH	8.0	1.98 ± 0.14	0.661 ± 0.100		
GSO_3^-	9.1	0.92 ± 0.16	0.511 ± 0.204		
GSH + 15d-PGJ ₂	8.0	1.99 ± 0.08	0.285 ± 0.030		
GSO_3^- + 15d-PGJ ₂	8.8	1.24 ± 0.03	0.178 ± 0.014		
C 14-17 (3) native					
GSH	0	0.74 ± 0.03	0.0971 ± 0.0142	2.29 ± 0.03	$\leq 1 \times 10^{-4}$
GSO_3^-	0	0.95 ± 0.02	0.0127 ± 0.0011	2.06 ± 0.10	$\leq 1 \times 10^{-4}$
GSH + 15d-PGJ ₂	0	0.67 ± 0.03	0.0740 ± 0.0108	2.30 ± 0.05	$\leq 1 \times 10^{-4}$
GSO_3^- + 15d-PGJ ₂	0.1	1.02 ± 0.01	0.0282 ± 0.0015	1.91 ± 0.05	$\leq 1 \times 10^{-4}$
D 14-17 (3) C59A					
GSH	0.1	0.88 ± 0.03	0.0145 ± 0.0021	2.06 ± 0.20	$\leq 1 \times 10^{-4}$
GSO_3^-	0.4	0.56 ± 0.03	0.0111 ± 0.0031	2.08 ± 0.05	$\leq 1 \times 10^{-4}$
GSH + 15d-PGJ ₂	0	0.96 ± 0.02	0.0255 ± 0.0019	2.01 ± 0.07	$\leq 1 \times 10^{-4}$
GSO_3^- + 15d-PGJ ₂	0.5	0.54 ± 0.02	0.0203 ± 0.0031	1.95 ± 0.11	$\leq 1 \times 10^{-4}$

Figure 84. H/D exchange kinetic profiles for MPGES1 as a function of 15d-PGJ₂ binding, residues 2-17. The total number of exchangeable sites is given in parentheses. Traces on the left represent those for the native enzyme, while traces on the right represent those for the C59A mutant. The data for enzyme bound to GSH only (black), GSH plus 15d-PGJ₂ (red), GSO_3^- only (blue), and GSO_3^- plus 15d-PGJ₂ (green), were fit to a sum of first-order exponential rate terms, as described in the Materials and Methods chapter.



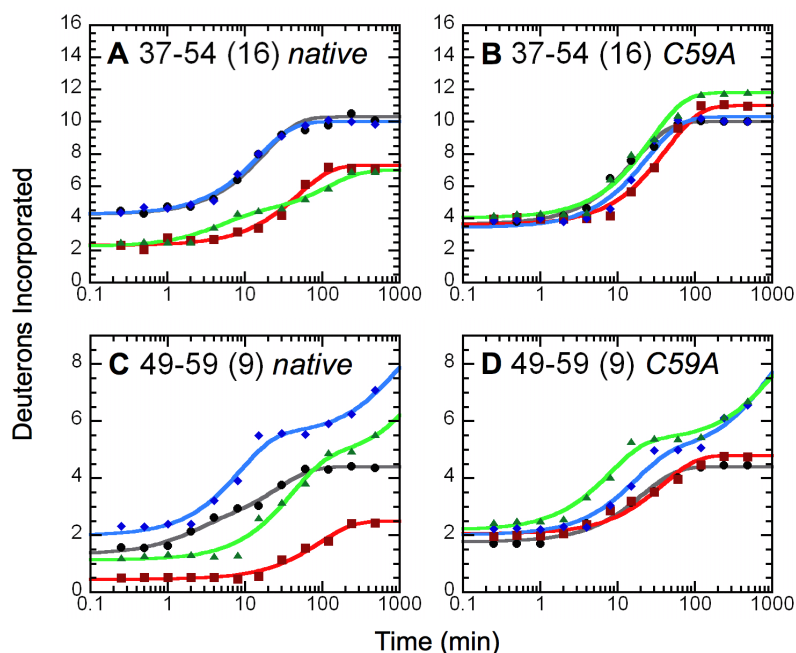
Peptide/Ligand	A_{fast} (D)	A_I (D)	k_I (min^{-1})	A_2 (D)	k_2 (min^{-1})
A 18-23 (5) native					
GSH	0	5	$\leq 1 \times 10^{-4}$		
GSO_3^-	0.3	3.00 ± 0.07	0.0115 ± 0.0012	1.70 ± 0.07	$\leq 1 \times 10^{-4}$
GSH + 15d-PGJ ₂	0	0.32 ± 0.05	0.474 ± 0.184	4.75 ± 0.02	$\leq 1.87 \times 10^{-4}$
GSO_3^- + 15d-PGJ ₂	0	2.90 ± 0.07	0.0140 ± 0.0015	2.08 ± 0.04	$\leq 1 \times 10^{-4}$
B 18-23 (5) C59A					
GSH	0	5	$\leq 1 \times 10^{-4}$		
GSO_3^-	0.2	2.81 ± 0.07	0.0285 ± 0.0028	1.97 ± 0.22	$\leq 1 \times 10^{-4}$
GSH + 15d-PGJ ₂	0.1	1.02 ± 0.01	0.0110 ± 0.0004	3.88 ± 0.12	$\leq 1 \times 10^{-4}$
GSO_3^- + 15d-PGJ ₂	0	4.10 ± 0.11	0.0491 ± 0.0050	1.03 ± 0.25	$\leq 1 \times 10^{-4}$
C 23-27 (4) native					
GSH	0	4	$\leq 1 \times 10^{-4}$		
GSO_3^-	0	4	$\leq 1 \times 10^{-4}$		
GSH + 15d-PGJ ₂	0	4	$\leq 1 \times 10^{-4}$		
GSO_3^- + 15d-PGJ ₂	0	4	$\leq 1 \times 10^{-4}$		
D 23-27 (4) C59A					
GSH	0	4	$\leq 1 \times 10^{-4}$		
GSO_3^-	0	4	$\leq 1 \times 10^{-4}$		
GSH + 15d-PGJ ₂	0	4	$\leq 1 \times 10^{-4}$		
GSO_3^- + 15d-PGJ ₂	0	4	$\leq 1 \times 10^{-4}$		

Figure 85. H/D exchange kinetic profiles for MPGES1 as a function of 15d-PGJ₂ binding, residues 18-27. The total number of exchangeable sites is given in parentheses. Traces on the left represent those for the native enzyme, while traces on the right represent those for the C59A mutant. The data for enzyme bound to GSH only (black), GSH plus 15d-PGJ₂ (red), GSO_3^- only (blue), and GSO_3^- plus 15d-PGJ₂ (green) are shown.



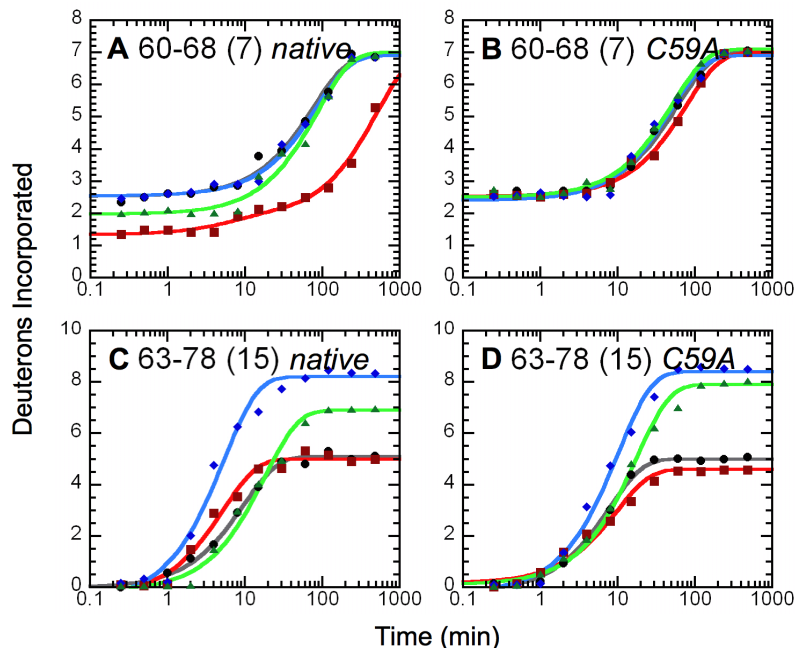
Peptide/Ligand	A_{fast} (D)	A_1 (D)	k_1 (min^{-1})	A_2 (D)	k_2 (min^{-1})	A_3 (D)	k_3 (min^{-1})
A 28-31 (3) native							
GSH	0.1	0.33 ± 0.03	0.141 ± 0.015	2.55 ± 0.02	$\leq 5.12 \times 10^{-4}$		
GSO_3^-	0	1.90 ± 0.03	0.0127 ± 0.0009	1.16 ± 0.26	$\leq 1 \times 10^{-4}$		
GSH + 15d-PGJ ₂	0.1	2.91 ± 0.02	$\leq 1.19 \times 10^{-3}$				
GSO_3^- + 15d-PGJ ₂	0	0.76 ± 0.08	0.122 ± 0.006	1.03 ± 0.02	0.00807 ± 0.00025	1.21 ± 0.08	$\leq 1 \times 10^{-4}$
B 28-31 (3) C59A							
GSH	0.1	0.56 ± 0.05	0.0415 ± 0.0097	2.37 ± 0.05	$\leq 3.29 \times 10^{-4}$		
GSO_3^-	0	1.19 ± 0.08	0.164 ± 0.026	1.19 ± 0.08	0.00783 ± 0.00103	0.62 ± 0.08	$\leq 1 \times 10^{-4}$
GSH + 15d-PGJ ₂	0	0.43 ± 0.06	0.0478 ± 0.0161	2.56 ± 0.06	$\leq 4.83 \times 10^{-4}$		
GSO_3^- + 15d-PGJ ₂	0	1.37 ± 0.19	0.243 ± 0.071	1.21 ± 0.20	0.0178 ± 0.005	0.42 ± 0.02	$\leq 1 \times 10^{-4}$
C 32-39 (7) native							
GSH	0.1	1.05 ± 0.03	0.102 ± 0.009	5.90 ± 0.04	$\leq 1 \times 10^{-4}$		
GSO_3^-	0	4.99 ± 0.09	0.0161 ± 0.0013	2.00 ± 0.09	$\leq 1 \times 10^{-4}$		
GSH + 15d-PGJ ₂	0	0.99 ± 0.03	0.0224 ± 0.0029	5.98 ± 0.11	$\leq 1 \times 10^{-4}$		
GSO_3^- + 15d-PGJ ₂	0	4.95 ± 0.07	0.132 ± 0.017	1.98 ± 0.04	$\leq 1 \times 10^{-4}$		
D 32-39 (7) C59A							
GSH	0.1	0.86 ± 0.02	0.0312 ± 0.0031	6.02 ± 0.07	$\leq 1 \times 10^{-4}$		
GSO_3^-	0.4	4.61 ± 0.07	0.0284 ± 0.0018	2.01 ± 0.24	$\leq 1 \times 10^{-4}$		
GSH + 15d-PGJ ₂	0.1	1.04 ± 0.02	0.0224 ± 0.0015	5.87 ± 0.08	$\leq 1 \times 10^{-4}$		
GSO_3^- + 15d-PGJ ₂	0	5.90 ± 0.08	0.0421 ± 0.0022	1.34 ± 0.21	$\leq 1 \times 10^{-4}$		

Figure 86. H/D exchange kinetic profiles for MPGES1 as a function of 15d-PGJ₂ binding, residues 28-39. The total number of exchangeable sites is given in parentheses. Traces on the left represent those for the native enzyme, while traces on the right represent those for the C59A mutant. The data for enzyme bound to GSH only (black), GSH plus 15d-PGJ₂ (red), GSO_3^- only (blue), and GSO_3^- plus 15d-PGJ₂ (green) are shown.



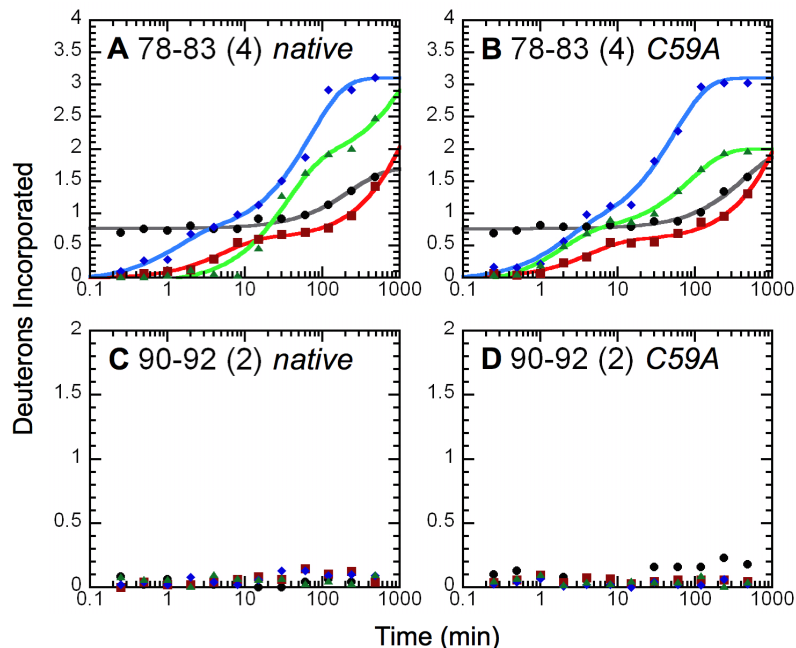
Peptide/Ligand	A_{fast} (D)	A_1 (D)	k_1 (min^{-1})	A_2 (D)	k_2 (min^{-1})	A_3 (D)	k_3 (min^{-1})
A 37-54 (16) native							
GSH	3.9	5.90 ± 0.15	0.0601 ± 0.0054	6.18 ± 0.26	$\leq 1 \times 10^{-4}$		
GSO_3^-	4.3	5.75 ± 0.11	0.0649 ± 0.0045	5.96 ± 0.21	$\leq 1 \times 10^{-4}$		
GSH + 15d-PGJ ₂	1.8	4.99 ± 0.12	0.0205 ± 0.0021	9.17 ± 0.57	$\leq 1 \times 10^{-4}$		
GSO_3^- + 15d-PGJ ₂	2.2	1.95 ± 0.03	0.206 ± 0.027	2.81 ± 0.03	0.00848 ± 0.00020	9.00 ± 0.03	$\leq 1 \times 10^{-4}$
B 37-54 (16) C59A							
GSH	3.5	6.38 ± 0.14	0.0591 ± 0.0045	6.08 ± 0.26	$\leq 1 \times 10^{-4}$		
GSO_3^-	3.8	6.88 ± 0.21	0.0410 ± 0.0049	5.33 ± 0.51	$\leq 1 \times 10^{-4}$		
GSH + 15d-PGJ ₂	3.5	7.40 ± 0.17	0.0235 ± 0.0022	5.13 ± 0.06	$\leq 1 \times 10^{-4}$		
GSO_3^- + 15d-PGJ ₂	3.6	7.78 ± 0.20	0.0364 ± 0.0036	4.67 ± 0.25	$\leq 1 \times 10^{-4}$		
C 49-59 (9) native							
GSH	1.4	1.02 ± 0.16	0.491 ± 0.027	2.05 ± 0.18	0.0380 ± 0.0039	4.56 ± 0.19	$\leq 1 \times 10^{-4}$
GSO_3^-	2.0	3.53 ± 0.26	0.117 ± 0.015	3.49 ± 0.23	$\leq 1.14 \times 10^{-3}$		
GSH + 15d-PGJ ₂	0.5	2.05 ± 0.05	0.0108 ± 0.0011	6.43 ± 0.16	$\leq 1 \times 10^{-4}$		
GSO_3^- + 15d-PGJ ₂	1.1	3.54 ± 0.25	0.0252 ± 0.0024	4.33 ± 0.26	$\leq 4.44 \times 10^{-4}$		
D 49-59 (9) C59A							
GSH	1.8	2.64 ± 0.09	0.0473 ± 0.0049	4.58 ± 0.16	$\leq 1 \times 10^{-4}$		
GSO_3^-	2.0	2.86 ± 0.31	0.0606 ± 0.0063	4.13 ± 0.30	$\leq 1.16 \times 10^{-3}$		
GSH + 15d-PGJ ₂	2.1	2.75 ± 0.08	0.0259 ± 0.0032	4.15 ± 0.19	$\leq 1 \times 10^{-4}$		
GSO_3^- + 15d-PGJ ₂	2.2	3.12 ± 0.21	0.125 ± 0.024	3.70 ± 0.18	$\leq 9.67 \times 10^{-4}$		

Figure 87. H/D exchange kinetic profiles for MPGES1 as a function of 15d-PGJ₂ binding, residues 37-59. The total number of exchangeable sites is given in parentheses. Traces on the left represent those for the native enzyme, while traces on the right represent those for the C59A mutant. The data for enzyme bound to GSH only (black), GSH plus 15d-PGJ₂ (red), GSO_3^- only (blue), and GSO_3^- plus 15d-PGJ₂ (green) are shown.



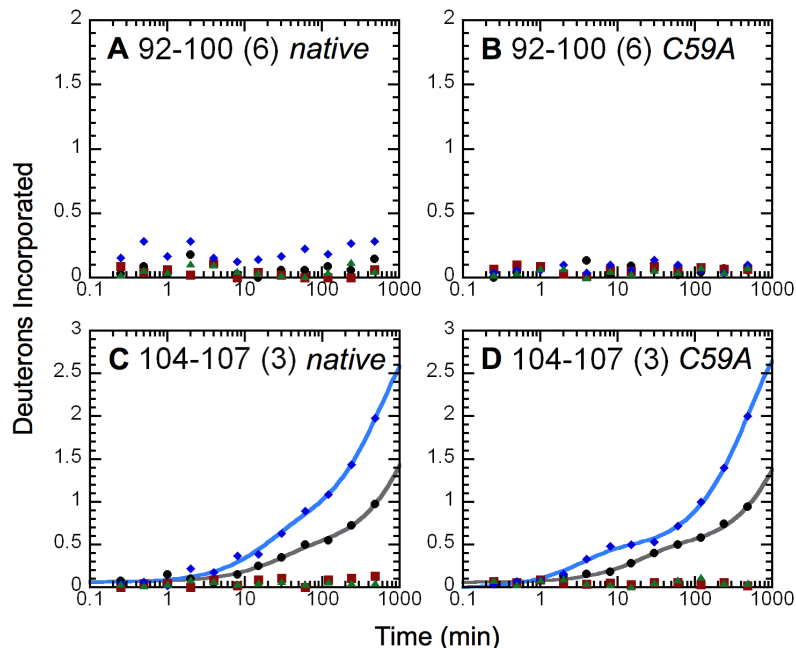
Peptide/Ligand	A_{fast} (D)	A_1 (D)	k_1 (min^{-1})	A_2 (D)	k_2 (min^{-1})
A 60-68 (7) native					
GSH	2.6	4.37 ± 0.08	0.0131 ± 0.0011		
GSO_3^-	2.6	4.36 ± 0.07	0.0119 ± 0.0009		
GSH + 15d-PGJ ₂	1.3	0.54 ± 0.18	0.160 ± 0.015	5.12 ± 0.16	$\leq 1.99 \times 10^{-3}$
GSO_3^- + 15d-PGJ ₂	1.1	5.03 ± 0.11	0.0116 ± 0.0011	0.84 ± 0.11	$\leq 1 \times 10^{-4}$
B 60-68 (7) C59A					
GSH	2.5	4.48 ± 0.06	0.0168 ± 0.0010		
GSO_3^-	2.5	4.50 ± 0.11	0.0202 ± 0.0021		
GSH + 15d-PGJ ₂	2.5	4.48 ± 0.06	0.0129 ± 0.0008		
GSO_3^- + 15d-PGJ ₂	2.4	4.60 ± 0.07	0.0193 ± 0.0012		
C 63-78 (15) native					
GSH	0	5.11 ± 0.09	0.103 ± 0.006	10.00 ± 0.12	$\leq 1 \times 10^{-4}$
GSO_3^-	0	8.73 ± 0.33	0.185 ± 0.021	7.05 ± 0.31	$\leq 1 \times 10^{-4}$
GSH + 15d-PGJ ₂	0	5.36 ± 0.20	0.189 ± 0.021	10.03 ± 0.20	$\leq 1 \times 10^{-4}$
GSO_3^- + 15d-PGJ ₂	0	7.04 ± 0.18	0.0553 ± 0.0053	8.46 ± 0.35	$\leq 1 \times 10^{-4}$
D 63-78 (15) C59A					
GSH	0	5.19 ± 0.07	0.128 ± 0.006	9.97 ± 0.09	$\leq 1 \times 10^{-4}$
GSO_3^-	0	8.61 ± 0.20	0.0982 ± 0.0076	6.76 ± 0.28	$\leq 1 \times 10^{-4}$
GSH + 15d-PGJ ₂	0	4.44 ± 0.15	0.103 ± 0.012	10.66 ± 0.18	$\leq 1 \times 10^{-4}$
GSO_3^- + 15d-PGJ ₂	0	7.80 ± 0.15	0.0573 ± 0.0039	7.31 ± 0.23	$\leq 1 \times 10^{-4}$

Figure 88. H/D exchange kinetic profiles for MPGES1 as a function of 15d-PGJ₂ binding, residues 60-78. The total number of exchangeable sites is given in parentheses. Traces on the left represent those for the native enzyme, while traces on the right represent those for the C59A mutant. The data for enzyme bound to GSH only (black), GSH plus 15d-PGJ₂ (red), GSO_3^- only (blue), and GSO_3^- plus 15d-PGJ₂ (green) are shown.



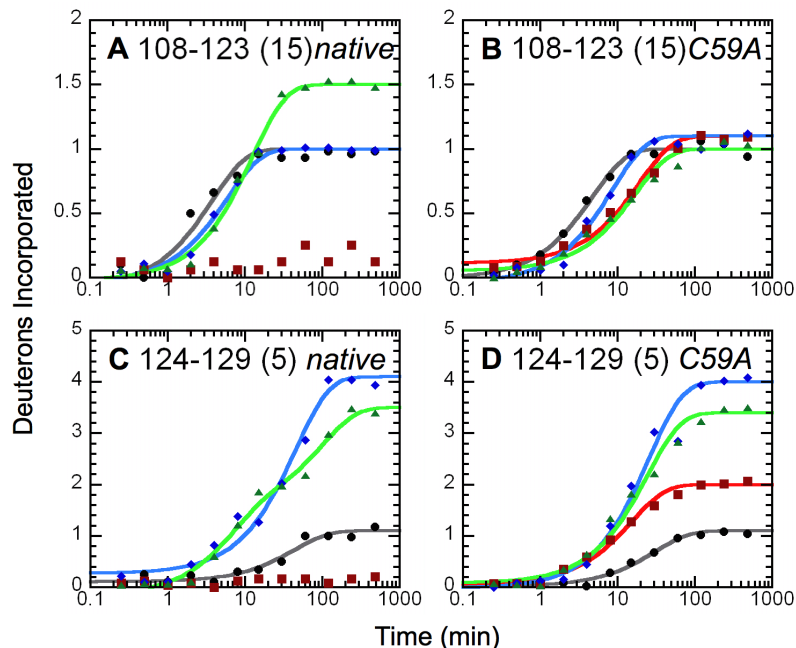
Peptide/Ligand	A_{fast} (D)	A_1 (D)	k_1 (min^{-1})	A_2 (D)	k_2 (min^{-1})	A_3 (D)	k_3 (min^{-1})
A 78-83 (4) native							
GSH	0.8	0.94 ± 0.02	0.00428 ± 0.00038	2.30 ± 0.13	$\leq 1 \times 10^{-4}$		
GSO_3^-	0	0.72 ± 0.19	0.802 ± 0.053	2.42 ± 0.12	0.0141 ± 0.0018	0.86 ± 0.12	$\leq 1 \times 10^{-4}$
GSH + 15d-PGJ ₂	0	0.61 ± 0.04	0.193 ± 0.036	3.40 ± 0.03	$\leq 5.47 \times 10^{-4}$		
GSO_3^- + 15d-PGJ ₂	0	1.88 ± 0.06	0.0296 ± 0.0025	2.20 ± 0.07	$\leq 7.05 \times 10^{-4}$		
B 78-83 (4) C59A							
GSH	0.8	1.24 ± 0.02	0.00227 ± 0.00016	1.99 ± 0.02	$\leq 1 \times 10^{-4}$		
GSO_3^-	0.1	0.78 ± 0.17	0.555 ± 0.031	2.35 ± 0.14	0.0187 ± 0.0025	0.76 ± 0.29	$\leq 1 \times 10^{-4}$
GSH + 15d-PGJ ₂	0	0.58 ± 0.05	0.235 ± 0.058	3.43 ± 0.03	$\leq 5.16 \times 10^{-4}$		
GSO_3^- + 15d-PGJ ₂	0	0.83 ± 0.07	0.551 ± 0.053	1.28 ± 0.05	0.0113 ± 0.0012	1.89 ± 0.06	$\leq 1 \times 10^{-4}$
C 90-92 (2) native							
GSH	0	2	$\leq 1 \times 10^{-4}$				
GSO_3^-	0	2	$\leq 1 \times 10^{-4}$				
GSH + 15d-PGJ ₂	0	2	$\leq 1 \times 10^{-4}$				
GSO_3^- + 15d-PGJ ₂	0	2	$\leq 1 \times 10^{-4}$				
D 90-92 (2) C59A							
GSH	0	2	$\leq 1 \times 10^{-4}$				
GSO_3^-	0	2	$\leq 1 \times 10^{-4}$				
GSH + 15d-PGJ ₂	0	2	$\leq 1 \times 10^{-4}$				
GSO_3^- + 15d-PGJ ₂	0	2	$\leq 1 \times 10^{-4}$				

Figure 89. H/D exchange kinetic profiles for MPGES1 as a function of 15d-PGJ₂ binding, residues 78-92. The total number of exchangeable sites is given in parentheses. Traces on the left represent those for the native enzyme, while traces on the right represent those for the C59A mutant. The data for enzyme bound to GSH only (black), GSH plus 15d-PGJ₂ (red), GSO_3^- only (blue), and GSO_3^- plus 15d-PGJ₂ (green) are shown.



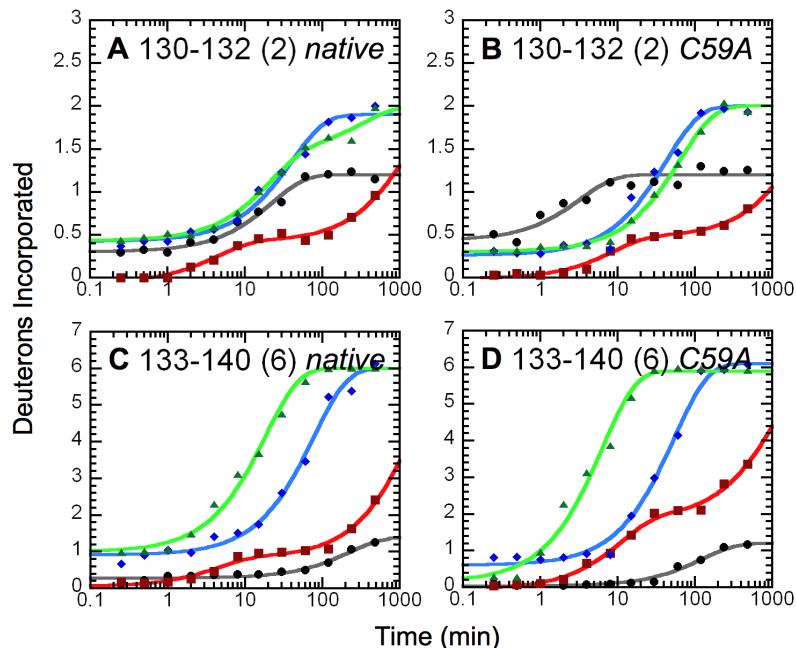
Peptide/Ligand	A_{fast} (D)	A_I (D)	k_I (min^{-1})	A_2 (D)	k_2 (min^{-1})
A 92-100 (6) native					
GSH	0	6	$\leq 1 \times 10^{-4}$		
GSO_3^-	0	6	$\leq 1 \times 10^{-4}$		
GSH + 15d-PGJ ₂	0	6	$\leq 1 \times 10^{-4}$		
GSO_3^- + 15d-PGJ ₂	0	6	$\leq 1 \times 10^{-4}$		
B 92-100 (6) C59A					
GSH	0	6	$\leq 1 \times 10^{-4}$		
GSO_3^-	0	6	$\leq 1 \times 10^{-4}$		
GSH + 15d-PGJ ₂	0	6	$\leq 1 \times 10^{-4}$		
GSO_3^- + 15d-PGJ ₂	0	6	$\leq 1 \times 10^{-4}$		
C 104-107 (3) native					
GSH	0.1	0.37 ± 0.05	0.0365 ± 0.0021	2.56 ± 0.05	$\leq 4.90 \times 10^{-4}$
GSO_3^-	0.1	0.60 ± 0.07	0.0535 ± 0.0051	2.35 ± 0.07	$\leq 1.72 \times 10^{-3}$
GSH + 15d-PGJ ₂	0	3	$\leq 1 \times 10^{-4}$		
GSO_3^- + 15d-PGJ ₂	0	3	$\leq 1 \times 10^{-4}$		
D 104-107 (3) C59A					
GSH	0.1	0.40 ± 0.03	0.0498 ± 0.0088	2.54 ± 0.03	$\leq 4.49 \times 10^{-4}$
GSO_3^-	0	0.44 ± 0.03	0.299 ± 0.061	2.56 ± 0.02	$\leq 1.98 \times 10^{-3}$
GSH + 15d-PGJ ₂	0	3	$\leq 1 \times 10^{-4}$		
GSO_3^- + 15d-PGJ ₂	0	3	$\leq 1 \times 10^{-4}$		

Figure 90. H/D exchange kinetic profiles for MPGES1 as a function of 15d-PGJ₂ binding, residues 92-107. The total number of exchangeable sites is given in parentheses. Traces on the left represent those for the native enzyme, while traces on the right represent those for the C59A mutant. The data for enzyme bound to GSH only (black), GSH plus 15d-PGJ₂ (red), GSO_3^- only (blue), and GSO_3^- plus 15d-PGJ₂ (green) are shown.



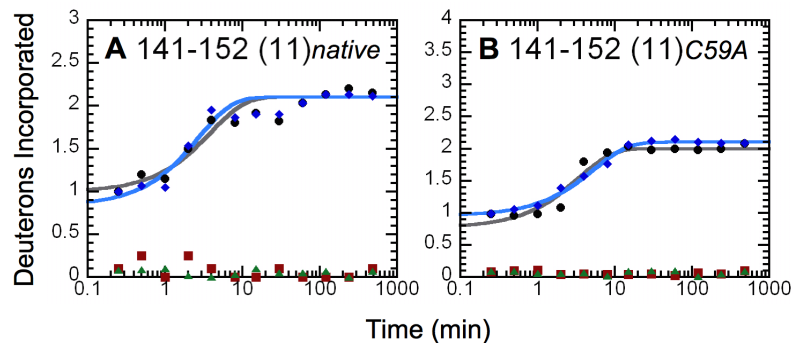
Peptide/Ligand	A_{fast} (D)	A_1 (D)	k_1 (min^{-1})	A_2 (D)	k_2 (min^{-1})	A_3 (D)	k_3 (min^{-1})
A 108-123 (15) native							
GSH	0	1.07 ± 0.07	0.261 ± 0.029	14.06 ± 0.05	$\leq 1 \times 10^{-4}$		
GSO_3^-	0	1.04 ± 0.03	0.168 ± 0.016	13.98 ± 0.13	$\leq 1 \times 10^{-4}$		
GSH + 15d-PGJ ₂	0	15	$\leq 1 \times 10^{-4}$				
GSO_3^- + 15d-PGJ ₂	0	1.52 ± 0.03	0.0798 ± 0.0057	13.46 ± 0.05	$\leq 1 \times 10^{-4}$		
B 108-123 (15) C59A							
GSH	0	1.00 ± 0.03	0.211 ± 0.027	13.98 ± 0.02	$\leq 1 \times 10^{-4}$		
GSO_3^-	0	1.14 ± 0.04	0.118 ± 0.013	13.96 ± 0.04	$\leq 1 \times 10^{-4}$		
GSH + 15d-PGJ ₂	0	0.99 ± 0.03	0.0524 ± 0.0053	13.97 ± 0.05	$\leq 1 \times 10^{-4}$		
GSO_3^- + 15d-PGJ ₂	0	0.95 ± 0.03	0.0592 ± 0.0074	14.09 ± 0.05	$\leq 1 \times 10^{-4}$		
C 124-129 (5) native							
GSH	0	0.99 ± 0.04	0.0227 ± 0.0022	4.00 ± 0.16	$\leq 1 \times 10^{-4}$		
GSO_3^-	0.3	3.83 ± 0.11	0.0220 ± 0.0025	0.90 ± 0.11	$\leq 1 \times 10^{-4}$		
GSH + 15d-PGJ ₂	0	5	$\leq 1 \times 10^{-4}$				
GSO_3^- + 15d-PGJ ₂	0	1.69 ± 0.03	0.147 ± 0.016	1.96 ± 0.03	0.00986 ± 0.00027	1.35 ± 0.03	$\leq 1 \times 10^{-4}$
D 124-129 (5) C59A							
GSH	0	1.08 ± 0.03	0.0323 ± 0.0031	3.92 ± 0.07	$\leq 1 \times 10^{-4}$		
GSO_3^-	0	4.02 ± 0.14	0.0391 ± 0.0052	1.17 ± 0.33	$\leq 1 \times 10^{-4}$		
GSH + 15d-PGJ ₂	0	1.94 ± 0.05	0.0650 ± 0.0058	3.17 ± 0.06	$\leq 1 \times 10^{-4}$		
GSO_3^- + 15d-PGJ ₂	0	3.32 ± 0.10	0.0412 ± 0.0046	1.68 ± 0.18	$\leq 1 \times 10^{-4}$		

Figure 91. H/D exchange kinetic profiles for MPGES1 as a function of 15d-PGJ₂ binding, residues 108-129. The total number of exchangeable sites is given in parentheses. Traces on the left represent those for the native enzyme, while traces on the right represent those for the C59A mutant. The data for enzyme bound to GSH only (black), GSH plus 15d-PGJ₂ (red), GSO₃⁻ only (blue), and GSO₃⁻ plus 15d-PGJ₂ (green) are shown.



Peptide/Ligand	A_{fast} (D)	A_1 (D)	k_1 (min^{-1})	A_2 (D)	k_2 (min^{-1})
A 130-132 (2) <i>native</i>					
GSH	0.4	0.90 ± 0.02	0.0454 ± 0.0046	0.75 ± 0.05	$\leq 1 \times 10^{-4}$
GSO_3^-	0.5	1.48 ± 0.03	0.0248 ± 0.0024		
GSH + 15d-PGJ ₂	0	0.48 ± 0.04	0.225 ± 0.059	1.58 ± 0.03	$\leq 8.24 \times 10^{-4}$
GSO_3^- + 15d-PGJ ₂	0.4	1.01 ± 0.13	0.0485 ± 0.0015	0.56 ± 0.13	$\leq 3.10 \times 10^{-3}$
B 130-132 (2) <i>C59A</i>					
GSH	0.3	0.77 ± 0.08	0.301 ± 0.084	0.89 ± 0.05	$\leq 1 \times 10^{-4}$
GSO_3^-	0.3	1.74 ± 0.05	0.0235 ± 0.0026		
GSH + 15d-PGJ ₂	0	0.48 ± 0.04	0.118 ± 0.026	1.53 ± 0.03	$\leq 4.82 \times 10^{-4}$
GSO_3^- + 15d-PGJ ₂	0.3	1.70 ± 0.02	0.0155 ± 0.0008		
C 133-140 (6) <i>native</i>					
GSH	0	1.12 ± 0.03	0.00446 ± 0.00055	4.88 ± 0.03	$\leq 1 \times 10^{-4}$
GSO_3^-	0.9	5.09 ± 0.09	0.0130 ± 0.0010		
GSH + 15d-PGJ ₂	0	0.87 ± 0.10	0.226 ± 0.028	5.16 ± 0.07	$\leq 7.19 \times 10^{-4}$
GSO_3^- + 15d-PGJ ₂	1.0	5.00 ± 0.11	0.0544 ± 0.0042		
D 133-140 (6) <i>C59A</i>					
GSH	0	1.17 ± 0.03	0.00811 ± 0.00082	4.80 ± 0.04	$\leq 1 \times 10^{-4}$
GSO_3^-	0.5	5.50 ± 0.10	0.0185 ± 0.0014		
GSH + 15d-PGJ ₂	0	1.91 ± 0.11	0.0933 ± 0.0145	4.13 ± 0.10	$\leq 9.43 \times 10^{-4}$
GSO_3^- + 15d-PGJ ₂	0.3	5.75 ± 0.18	0.159 ± 0.015		

Figure 92. H/D exchange kinetic profiles for MPGES1 as a function of 15d-PGJ₂ binding, residues 130-140. The total number of exchangeable sites is given in parentheses. Traces on the left represent those for the native enzyme, while traces on the right represent those for the C59A mutant. The data for enzyme bound to GSH only (black), GSH plus 15d-PGJ₂ (red), GSO₃⁻ only (blue), and GSO₃⁻ plus 15d-PGJ₂ (green) are shown.



Peptide/Ligand	A_{fast} (D)	A_T (D)	k_T (min^{-1})	A_2 (D)	k_2 (min^{-1})
A 141-152 (11) <i>native</i>					
GSH	0.8	1.11 ± 0.11	0.254 ± 0.029	9.06 ± 0.06	$\leq 1 \times 10^{-4}$
GSO_3^-	0.7	1.27 ± 0.12	0.364 ± 0.037	9.03 ± 0.06	$\leq 1 \times 10^{-4}$
GSH + 15d-PGJ ₂	0	11	$\leq 1 \times 10^{-4}$		
GSO_3^- + 15d-PGJ ₂	0	11	$\leq 1 \times 10^{-4}$		
B 141-152 (11) <i>C59A</i>					
GSH	0.8	1.23 ± 0.10	0.290 ± 0.060	8.98 ± 0.07	$\leq 1 \times 10^{-4}$
GSO_3^-	1.0	1.15 ± 0.03	0.186 ± 0.015	8.87 ± 0.03	$\leq 1 \times 10^{-4}$
GSH + 15d-PGJ ₂	0	11	$\leq 1 \times 10^{-4}$		
GSO_3^- + 15d-PGJ ₂	0	11	$\leq 1 \times 10^{-4}$		

Figure 93. H/D exchange kinetic profiles for MPGES1 as a function of 15d-PGJ₂ binding, residues 141-152. The total number of exchangeable sites is given in parentheses. Traces on the left represent those for the native enzyme, while traces on the right represent those for the C59A mutant. The data for enzyme bound to GSH only (black), GSH plus 15d-PGJ₂ (red), GSO_3^- only (blue), and GSO_3^- plus 15d-PGJ₂ (green) are shown.

REFERENCES

1. Weiss, U., Inflammation. *Nature* **2002**, 420, 845.
2. Bernhagen, J., Bacher, M., Calandra, T., Metz, C. N., Doty, S. B., Donnelly, T., Bucala, R., An Essential Role For Macrophage Migration Inhibitory Factor In The Tuberculin Delayed-Type Hypersensitivity Reactions. *J. Exp. Med.* **1996**, 183, 277-282.
3. Snyderman, R., Regulatory mechanisms of a chemoattractant receptor on human polymorphonuclear leukocytes. *Rev Infect Dis* **1985**, 7, (3), 390-4.
4. Khor, B., Gardet, A., Xavier, R. J., Genetics And Pathogenesis Of Inflammatory Bowel Disease. *Nature* **2011**, 474, 307-317.
5. Geha, R. S., Regulation of IgE synthesis: The molecular basis and implications for clinical modulation. *Allergy Asthma Immunol Res* **1999**, 20, 1-8.
6. Papp, K.; Vegh, P.; Tchorbanov, A.; Vassilev, T.; Erdei, A.; Prechl, J., Progression of lupus-like disease drives the appearance of complement-activating IgG antibodies in MRL/lpr mice. *Rheumatology (Oxford)* **2010**, 49, (12), 2273-80.
7. Clynes, R., Maizes, J. S., Modulation of immune complex-induced inflammation in vivo by the coordinate expression of activation and inhibitory Fc receptors. *J Exp Med* **1999**, 189, 179-186.
8. Vane, J. R., The fight against rheumatism: from willow bark to COX-1 sparing drugs. *J Physiol Pharmacol* **2000**, 51, (4 Pt 1), 573-86.
9. Jack, D. B., One hundred years of aspirin. *Lancet* **1997**, 350, (9075), 437-9.
10. Hawkey, C. J., COX-2 chronology. *Gut* **2005**, 54, (11), 1509-14.
11. Craven, L. L., Experiences with aspirin (Acetylsalicylic acid) in the nonspecific prophylaxis of coronary thrombosis. *Miss Valley Med J* **1953**, 75, (1), 38-44.
12. Rainsford, K. D., Anti-inflammatory drugs in the 21st century. *Subcell Biochem* **2007**, 42, 3-27.
13. Rainsford, K. D., Profile and mechanisms of gastrointestinal and other side effects of nonsteroidal anti-inflammatory drugs (NSAIDs). *Am J Med* **1999**, 107, (6A), 27S-35S; discussion 35S-36S.
14. Otterness, I. G.; Daumy, G. O.; Gollaher, M. G., Jr.; Downs, J. T.; Zuzel, T. J.; Bliven, M. L.; Merenda, J. M., Determining selectivity of drugs by quantitative two-dimensional gel analysis. A study of tenidap, piroxicam, and dexamethasone. *Biochem Pharmacol* **1996**, 52, (6), 917-25.

15. Rainsford, K. D.; Skerry, T. M.; Chindemi, P.; Delaney, K., Effects of the NSAIDs meloxicam and indomethacin on cartilage proteoglycan synthesis and joint responses to calcium pyrophosphate crystals in dogs. *Vet Res Commun* **1999**, 23, (2), 101-13.
16. Vane, J. R., Inhibition of prostaglandin synthesis as a mechanism of action for aspirin-like drugs. *Nat New Biol* **1971**, 231, (25), 232-5.
17. Smith, J. B.; Willis, A. L., Aspirin selectively inhibits prostaglandin production in human platelets. *Nat New Biol* **1971**, 231, (25), 235-7.
18. Goldblatt, W. M., A depressor substance in seminal fluid. *J Soc Chem Ind* **1933**, 52, 1056-1057.
19. Smith, W. L., The eicosanoids and their biochemical mechanisms of action. *Biochem J* **1989**, 259, (2), 315-24.
20. Bergstrom, S.; Samuelsson, B., The prostaglandins. *Endeavour* **1968**, 27, (102), 109-13.
21. Ferreira, S. H.; Vane, J. R., Prostaglandins: their disappearance from and release into the circulation. *Nature* **1967**, 216, (5118), 868-73.
22. Irvine, R. F., How is the level of free arachidonic acid controlled in mammalian cells? *Biochem J* **1982**, 204, (1), 3-16.
23. Cockcroft, S., G-protein-regulated phospholipases C, D, and A₂-mediated signaling in neutrophils. *Biochim Biophys Acta* **1992**, 1113, (2), 135-160.
24. Capdevila, J. H.; Falck, J. R.; Dishman, E.; Karara, A., Cytochrome P-450 arachidonate oxygenase. *Methods Enzymol* **1990**, 187, 385-94.
25. Samuelsson, B.; Dahlen, S. E.; Lindgren, J. A.; Rouzer, C. A.; Serhan, C. N., Leukotrienes and lipoxins: structures, biosynthesis, and biological effects. *Science* **1987**, 237, (4819), 1171-6.
26. Pagels, W. R.; Sachs, R. J.; Marnett, L. J.; Dewitt, D. L.; Day, J. S.; Smith, W. L., Immunochemical evidence for the involvement of prostaglandin H synthase in hydroperoxide-dependent oxidations by ram seminal vesicle microsomes. *J Biol Chem* **1983**, 258, (10), 6517-23.
27. Serhan, C. N.; Hamberg, M.; Samuelsson, B., Trihydroxytetraenes: a novel series of compounds formed from arachidonic acid in human leukocytes. *Biochem Biophys Res Commun* **1984**, 118, (3), 943-9.
28. Schievella, A. R.; Regier, M. K.; Smith, W. L.; Lin, L. L., Calcium-mediated translocation of cytosolic phospholipase A₂ to the nuclear envelope and endoplasmic reticulum. *J Biol Chem* **1995**, 270, (51), 30749-54.

29. Xu, G. Y.; McDonagh, T.; Yu, H. A.; Nalefski, E. A.; Clark, J. D.; Cumming, D. A., Solution structure and membrane interactions of the C2 domain of cytosolic phospholipase A2. *J Mol Biol* **1998**, 280, (3), 485-500.
30. Hamberg, M.; Samuelsson, B., Detection and isolation of an endoperoxide intermediate in prostaglandin biosynthesis. *Proc Natl Acad Sci U S A* **1973**, 70, (3), 899-903.
31. Hamberg, M.; Samuelsson, B., On the mechanism of the biosynthesis of prostaglandins E-1 and F-1-alpha. *J Biol Chem* **1967**, 242, (22), 5336-43.
32. Hamberg, M.; Samuelsson, B., Oxygenation of unsaturated fatty acids by the vesicular gland of sheep. *J Biol Chem* **1967**, 242, (22), 5344-54.
33. Marnett, L. J.; Rowlinson, S. W.; Goodwin, D. C.; Kalgutkar, A. S.; Lanzo, C. A., Arachidonic acid oxygenation by COX-1 and COX-2. Mechanisms of catalysis and inhibition. *J Biol Chem* **1999**, 274, (33), 22903-6.
34. Lazarus, M.; Kubata, B. K.; Eguchi, N.; Fujitani, Y.; Urade, Y.; Hayaishi, O., Biochemical characterization of mouse microsomal prostaglandin E synthase-1 and its colocalization with cyclooxygenase-2 in peritoneal macrophages. *Arch Biochem Biophys* **2002**, 397, (2), 336-41.
35. Hla, T.; Bishop-Bailey, D.; Liu, C. H.; Schaeffers, H. J.; Trifan, O. C., Cyclooxygenase-1 and -2 isoenzymes. *Int J Biochem Cell Biol* **1999**, 31, (5), 551-7.
36. Dubois, R. N.; Abramson, S. B.; Crofford, L.; Gupta, R. A.; Simon, L. S.; Van De Putte, L. B.; Lipsky, P. E., Cyclooxygenase in biology and disease. *FASEB J* **1998**, 12, (12), 1063-73.
37. Tanabe, T.; Tohnai, N., Cyclooxygenase isozymes and their gene structures and expression. *Prostaglandins Other Lipid Mediat* **2002**, 68-69, 95-114.
38. Shimizu, T.; Yamamoto, S.; Hayaishi, O., Purification of PGH-PGD isomerase from rat brain. *Methods Enzymol* **1982**, 86, 73-7.
39. Tanaka, Y.; Ward, S. L.; Smith, W. L., Immunochemical and kinetic evidence for two different prostaglandin H-prostaglandin E isomerases in sheep vesicular gland microsomes. *J Biol Chem* **1987**, 262, (3), 1374-81.
40. Hayashi, H.; Fuji, Y.; Watanabe, K.; Urade, Y.; Hayashi, O., Enzymatic conversion of prostaglandin H₂ to prostaglandin F_{2α} by aldehyde reductase from human liver: Comparison to the prostaglandin F synthetases from bovine lung. *J Biol Chem* **1989**, 264, 1036-1040.
41. DeWitt, D. L.; Smith, W. L., Purification of prostacyclin synthase from bovine aorta by immunoaffinity chromatography. Evidence that the enzyme is a hemoprotein. *J Biol Chem* **1983**, 258, (5), 3285-93.

42. Ullrich, V.; Haurand, M., Thromboxane synthase as a cytochrome P450 enzyme. *Adv Prostaglandin Thromboxane Leukot Res* **1983**, 11, 105-10.
43. Urade, Y.; Watanabe, K.; Hayaishi, O., Prostaglandin D, E, and F synthases. *J Lipid Mediat Cell Signal* **1995**, 12, (2-3), 257-73.
44. Toh, H.; Kubodera, H.; Nakajima, N.; Sekiya, T.; Eguchi, N.; Tanaka, T.; Urade, Y.; Hayaishi, O., Glutathione-independent prostaglandin D synthase as a lead molecule for designing new functional proteins. *Protein Eng* **1996**, 9, (12), 1067-82.
45. Kanaoka, Y.; Urade, Y., Hematopoietic prostaglandin D synthase. *Prostaglandins Leukot Essent Fatty Acids* **2003**, 69, (2-3), 163-7.
46. Jakobsson, P. J.; Thoren, S.; Morgenstern, R.; Samuelsson, B., Identification of human prostaglandin E synthase: a microsomal, glutathione-dependent, inducible enzyme, constituting a potential novel drug target. *Proc Natl Acad Sci U S A* **1999**, 96, (13), 7220-5.
47. Watanabe, K.; Kurihara, K.; Suzuki, T., Purification and characterization of membrane-bound prostaglandin E synthase from bovine heart. *Biochim Biophys Acta* **1999**, 1439, (3), 406-14.
48. Tanioka, T.; Nakatani, Y.; Semmyo, N.; Murakami, M.; Kudo, I., Molecular identification of cytosolic prostaglandin E2 synthase that is functionally coupled with cyclooxygenase-1 in immediate prostaglandin E2 biosynthesis. *J Biol Chem* **2000**, 275, (42), 32775-82.
49. Thoren, S.; Jakobsson, P. J., Coordinate up- and down-regulation of glutathione-dependent prostaglandin E synthase and cyclooxygenase-2 in A549 cells. Inhibition by NS-398 and leukotriene C4. *Eur J Biochem* **2000**, 267, (21), 6428-34.
50. Murakami, M.; Naraba, H.; Tanioka, T.; Semmyo, N.; Nakatani, Y.; Kojima, F.; Ikeda, T.; Fueki, M.; Ueno, A.; Oh, S.; Kudo, I., Regulation of prostaglandin E2 biosynthesis by inducible membrane-associated prostaglandin E2 synthase that acts in concert with cyclooxygenase-2. *J Biol Chem* **2000**, 275, (42), 32783-92.
51. Tanikawa, N.; Ohmiya, Y.; Ohkubo, H.; Hashimoto, K.; Kangawa, K.; Kojima, M.; Ito, S.; Watanabe, K., Identification and characterization of a novel type of membrane-associated prostaglandin E synthase. *Biochem Biophys Res Commun* **2002**, 291, (4), 884-9.
52. Ueno, N.; Takegoshi, Y.; Kamei, D.; Kudo, I.; Murakami, M., Coupling between cyclooxygenases and terminal prostanoid synthases. *Biochem Biophys Res Commun* **2005**, 338, (1), 70-6.
53. Watanabe, K., Prostaglandin F synthase. *Prostaglandins Other Lipid Mediat* **2002**, 68-69, 401-7.

54. Tanabe, T.; Ullrich, V., Prostacyclin and thromboxane synthases. *J Lipid Mediat Cell Signal* **1995**, 12, (2-3), 243-55.
55. Yokoyama, C.; Miyata, A.; Ihara, H.; Ullrich, V.; Tanabe, T., Molecular cloning of human platelet thromboxane A synthase. *Biochem Biophys Res Commun* **1991**, 178, (3), 1479-84.
56. Breyer, R. M.; Bagdassarian, C. K.; Myers, S. A.; Breyer, M. D., Prostanoid receptors: subtypes and signaling. *Annu Rev Pharmacol Toxicol* **2001**, 41, 661-90.
57. Monneret, G.; Gravel, S.; Diamond, M.; Rokach, J.; Powell, W. S., Prostaglandin D2 is a potent chemoattractant for human eosinophils that acts via a novel DP receptor. *Blood* **2001**, 98, (6), 1942-8.
58. Williams, T. J.; Jose, P. J., Mediation of increased vascular permeability after complement activation. Histamine-independent action of rabbit C5a. *J Exp Med* **1981**, 153, (1), 136-53.
59. Moncada, S.; Gryglewski, R.; Bunting, S.; Vane, J. R., An enzyme isolated from arteries transforms prostaglandin endoperoxides to an unstable substance that inhibits platelet aggregation. *Nature* **1976**, 263, (5579), 663-5.
60. Main, I. H., The Inhibitory Actions of Prostaglandins on Respiratory Smooth Muscle. *Br J Pharmacol Chemother* **1964**, 22, 511-9.
61. Ferreira, S. H.; Nakamura, M.; de Abreu Castro, M. S., The hyperalgesic effects of prostacyclin and prostaglandin E2. *Prostaglandins* **1978**, 16, (1), 31-7.
62. Feldberg, W.; Saxena, P. N., Fever produced by prostaglandin E1. *J Physiol* **1971**, 217, (3), 547-56.
63. Hayaishi, O.; Urade, Y., Prostaglandin D2 in sleep-wake regulation: recent progress and perspectives. *Neuroscientist* **2002**, 8, (1), 12-5.
64. Haeggstrom, J. Z.; Rinaldo-Matthis, A.; Wheelock, C. E.; Wetterholm, A., Advances in eicosanoid research, novel therapeutic implications. *Biochem Biophys Res Commun* **2010**, 396, (1), 135-9.
65. Bunting, S.; Moncada, S.; Vane, J. R., The prostacyclin--thromboxane A2 balance: pathophysiological and therapeutic implications. *Br Med Bull* **1983**, 39, (3), 271-6.
66. de Nucci, G.; Gryglewski, R. J.; Warner, T. D.; Vane, J. R., Receptor-mediated release of endothelium-derived relaxing factor and prostacyclin from bovine aortic endothelial cells is coupled. *Proc Natl Acad Sci U S A* **1988**, 85, (7), 2334-8.

67. Day, R. O., Francis, H., Vial, J., Geisslinger, G., Williams, K. M., Naproxen concentrations in plasma and synovial fluid and effects on prostanoid concentrations. *J Rheumatol* **1995**, 22, (12), 2295-2303.
68. Hata, A. N.; Breyer, R. M., Pharmacology and signaling of prostaglandin receptors: multiple roles in inflammation and immune modulation. *Pharmacol Ther* **2004**, 103, (2), 147-66.
69. Saxena, P. N.; Beg, M. M.; Singhal, K. C.; Ahmad, M., Prostaglandin-like activity in the cerebrospinal fluid of febrile patients. *Indian J Med Res* **1979**, 70, 495-8.
70. Aronoff, D. M.; Carstens, J. K.; Chen, G. H.; Toews, G. B.; Peters-Golden, M., Short communication: differences between macrophages and dendritic cells in the cyclic AMP-dependent regulation of lipopolysaccharide-induced cytokine and chemokine synthesis. *J Interferon Cytokine Res* **2006**, 26, (11), 827-33.
71. Stier, C. T., Jr.; Roberts, L. J., 2nd; Wong, P. Y., Renal response to 9 alpha, 11 beta-prostaglandin F2 in the rat. *J Pharmacol Exp Ther* **1987**, 243, (2), 487-91.
72. Starczewski, M.; Voigtmann, R.; Peskar, B. A.; Peskar, B. M., Plasma levels of 15-keto-13,14-dihydro-prostaglandin E2 in patients with bronchogenic carcinoma. *Prostaglandins Leukot Med* **1984**, 13, (3), 249-58.
73. Straus, D. S.; Glass, C. K., Cyclopentenone prostaglandins: new insights on biological activities and cellular targets. *Med Res Rev* **2001**, 21, (3), 185-210.
74. Renedo, M.; Gayarre, J.; Garcia-Dominguez, C. A.; Perez-Rodriguez, A.; Prieto, A.; Canada, F. J.; Rojas, J. M.; Perez-Sala, D., Modification and activation of Ras proteins by electrophilic prostanoids with different structure are site-selective. *Biochemistry* **2007**, 46, (22), 6607-16.
75. Forman, B. M.; Tontonoz, P.; Chen, J.; Brun, R. P.; Spiegelman, B. M.; Evans, R. M., 15-Deoxy-delta 12, 14-prostaglandin J2 is a ligand for the adipocyte determination factor PPAR gamma. *Cell* **1995**, 83, (5), 803-12.
76. Cernuda-Morollon, E.; Pineda-Molina, E.; Canada, F. J.; Perez-Sala, D., 15-Deoxy-Delta 12,14-prostaglandin J2 inhibition of NF-kappaB-DNA binding through covalent modification of the p50 subunit. *J Biol Chem* **2001**, 276, (38), 35530-6.
77. Rossi, A.; Kapahi, P.; Natoli, G.; Takahashi, T.; Chen, Y.; Karin, M.; Santoro, M. G., Anti-inflammatory cyclopentenone prostaglandins are direct inhibitors of IkappaB kinase. *Nature* **2000**, 403, (6765), 103-8.
78. Bell-Parikh, L. C.; Ide, T.; Lawson, J. A.; McNamara, P.; Reilly, M.; FitzGerald, G. A., Biosynthesis of 15-deoxy-delta12,14-PGJ2 and the ligation of PPARgamma. *J Clin Invest* **2003**, 112, (6), 945-55.

79. Powell, W. S., 15-Deoxy-delta12,14-PGJ2: endogenous PPARgamma ligand or minor eicosanoid degradation product? *J Clin Invest* **2003**, 112, (6), 828-30.
80. Penning, T. D.; Talley, J. J.; Bertenshaw, S. R.; Carter, J. S.; Collins, P. W.; Docter, S.; Graneto, M. J.; Lee, L. F.; Malecha, J. W.; Miyashiro, J. M.; Rogers, R. S.; Rogier, D. J.; Yu, S. S.; Anderson Gd; Burton, E. G.; Cogburn, J. N.; Gregory, S. A.; Koboldt, C. M.; Perkins, W. E.; Seibert, K.; Veenhuizen, A. W.; Zhang, Y. Y.; Isakson, P. C., Synthesis and biological evaluation of the 1,5-diarylpyrazole class of cyclooxygenase-2 inhibitors: identification of 4-[5-(4-methylphenyl)-3-(trifluoromethyl)-1H-pyrazol-1-yl]benzene nesulfonamide (SC-58635, celecoxib). *J Med Chem* **1997**, 40, (9), 1347-65.
81. Chan, C. C.; Boyce, S.; Brideau, C.; Charleson, S.; Cromlish, W.; Ethier, D.; Evans, J.; Ford-Hutchinson, A. W.; Forrest, M. J.; Gauthier, J. Y.; Gordon, R.; Gresser, M.; Guay, J.; Kargman, S.; Kennedy, B.; Leblanc, Y.; Leger, S.; Mancini, J.; O'Neill G, P.; Ouellet, M.; Patrick, D.; Percival, M. D.; Perrier, H.; Prasit, P.; Rodger, I.; Tagari, P.; Therien, M.; Vickers, P.; Visco, D.; Wang, Z.; Webb, J.; Wong, E.; Xu, L. J.; Young, R. N.; Zamboni, R.; Riendeau, D., Rofecoxib [Vioxx, MK-0966; 4-(4'-methylsulfonylphenyl)-3-phenyl-2-(5H)-furanone]: a potent and orally active cyclooxygenase-2 inhibitor. Pharmacological and biochemical profiles. *J Pharmacol Exp Ther* **1999**, 290, (2), 551-560.
82. Bjarnason, I.; Macpherson, A. J., Intestinal toxicity of non-steroidal anti-inflammatory drugs. *Pharmacol Ther* **1994**, 62, (1-2), 145-57.
83. Bresalier, R. S.; Sandler, R. S.; Quan, H.; Bolognese, J. A.; Oxenius, B.; Horgan, K.; Lines, C.; Riddell, R.; Morton, D.; Lanas, A.; Konstam, M. A.; Baron, J. A., Cardiovascular events associated with rofecoxib in a colorectal adenoma chemoprevention trial. *N Engl J Med* **2005**, 352, (11), 1092-102.
84. Samuelsson, B., Leukotrienes: mediators of immediate hypersensitivity reactions and inflammation. *Science* **1983**, 220, (4597), 568-75.
85. Peters-Golden, M.; Henderson, W. R., Jr., Leukotrienes. *N Engl J Med* **2007**, 357, (18), 1841-54.
86. Lewis, R. A.; Austen, K. F.; Soberman, R. J., Leukotrienes and other products of the 5-lipoxygenase pathway. Biochemistry and relation to pathobiology in human diseases. *N Engl J Med* **1990**, 323, (10), 645-55.
87. Funk, C. D.; Furci, L.; FitzGerald, G. A., Molecular cloning, primary structure, and expression of the human platelet/erythroleukemia cell 12-lipoxygenase. *Proc Natl Acad Sci U S A* **1990**, 87, (15), 5638-42.
88. Conrad, D. J.; Kuhn, H.; Mulkins, M.; Highland, E.; Sigal, E., Specific inflammatory cytokines regulate the expression of human monocyte 15-lipoxygenase. *Proc Natl Acad Sci U S A* **1992**, 89, (1), 217-21.

89. Mandal, A. K.; Jones, P. B.; Bair, A. M.; Christmas, P.; Miller, D.; Yamin, T. T.; Wisniewski, D.; Menke, J.; Evans, J. F.; Hyman, B. T.; Bacskai, B.; Chen, M.; Lee, D. M.; Nikolic, B.; Soberman, R. J., The nuclear membrane organization of leukotriene synthesis. *Proc Natl Acad Sci U S A* **2008**, 105, (51), 20434-9.
90. Hammarberg, T.; Provost, P.; Persson, B.; Radmark, O., The N-terminal domain of 5-lipoxygenase binds calcium and mediates calcium stimulation of enzyme activity. *J Biol Chem* **2000**, 275, (49), 38787-93.
91. Plante, H.; Picard, S.; Mancini, J.; Borgeat, P., 5-Lipoxygenase-activating protein homodimer in human neutrophils: evidence for a role in leukotriene biosynthesis. *Biochem J* **2006**, 393, (Pt 1), 211-8.
92. Shimizu, T.; Radmark, O.; Samuelsson, B., Enzyme with dual lipoxygenase activities catalyzes leukotriene A4 synthesis from arachidonic acid. *Proc Natl Acad Sci U S A* **1984**, 81, (3), 689-93.
93. Haeggstrom, J. Z., Leukotriene A4 hydrolase/aminopeptidase, the gatekeeper of chemotactic leukotriene B4 biosynthesis. *J Biol Chem* **2004**, 279, (49), 50639-42.
94. Snelgrove, R. J.; Jackson, P. L.; Hardinson, M. T.; Noerager, B. D.; Kinloch, A.; Gaggar, A.; Shastry, S.; Rowe, S. M.; Shim, Y. M.; Hussell, T.; Blalock, J. E., A critical role for the LTA₄H in limiting chronic pulmonary neutrophilic inflammation. *Science* **2010**, 330, 90-94.
95. Nicholson, D. W.; Ali, A.; Vaillancourt, J. P.; Calaycay, J. R.; Mumford, R. A.; Zamboni, R. J.; Ford-Hutchinson, A. W., Purification to homogeneity and the N-terminal sequence of human leukotriene C4 synthase: a homodimeric glutathione S-transferase composed of 18-kDa subunits. *Proc Natl Acad Sci U S A* **1993**, 90, (5), 2015-9.
96. Drazen, J. M.; Israel, E.; O'Byrne, P. M., Treatment of asthma with drugs modifying the leukotriene pathway. *N Engl J Med* **1999**, 340, (3), 197-206.
97. Anderson, M. E.; Allison, R. D.; Meister, A., Interconversion of leukotrienes catalyzed by purified gamma-glutamyl transpeptidase: concomitant formation of leukotriene D4 and gamma-glutamyl amino acids. *Proc Natl Acad Sci U S A* **1982**, 79, (4), 1088-91.
98. Kozak, E. M.; Tate, S. S., Glutathione-degrading enzymes of microvillus membranes. *J Biol Chem* **1982**, 257, (11), 6322-7.
99. Nagaoka, I.; Yamashita, T., Studies on the leukotriene D4-metabolizing enzyme of rat leukocytes, which catalyzes the conversion of leukotriene D4 to leukotriene E4. *Biochim Biophys Acta* **1987**, 922, (1), 8-17.
100. Adachi, H.; Kubota, I.; Okamura, N.; Iwata, H.; Tsujimoto, M.; Nakazato, H.; Nishihara, T.; Noguchi, T., Purification and characterization of human microsomal dipeptidase. *J Biochem* **1989**, 105, (6), 957-61.

101. Campbell, B. J.; Baker, S. F.; Shukla, S. D.; Forrester, L. J.; Zahler, W. L., Bioconversion of leukotriene D4 by lung dipeptidase. *Biochim Biophys Acta* **1990**, 1042, (1), 107-12.
102. An, S.; Schmidt, F. J.; Campbell, B. J., Molecular cloning of sheep lung dipeptidase: a glycosyl phosphatidylinositol-anchored ectoenzyme that converts leukotriene D4 to leukotriene E4. *Biochim Biophys Acta* **1994**, 1226, (3), 337-40.
103. Leier, I.; Jedlitschky, G.; Buchholz, U.; Keppler, D., Characterization of the ATP-dependent leukotriene C4 export carrier in mastocytoma cells. *Eur J Biochem* **1994**, 220, (2), 599-606.
104. Lam, B. K.; Gagnon, L.; Austen, K. F.; Soberman, R. J., The mechanism of leukotriene B4 export from human polymorphonuclear leukocytes. *J Biol Chem* **1990**, 265, (23), 13438-41.
105. Tager, A. M.; Luster, A. D., BLT1 and BLT2: the leukotriene B(4) receptors. *Prostaglandins Leukot Essent Fatty Acids* **2003**, 69, (2-3), 123-34.
106. Kanaoka, Y.; Boyce, J. A., Cysteinyl leukotrienes and their receptors: cellular distribution and function in immune and inflammatory responses. *J Immunol* **2004**, 173, (3), 1503-10.
107. Borgeat, P.; Naccache, P. H., Biosynthesis and biological activity of leukotriene B4. *Clin Biochem* **1990**, 23, (5), 459-68.
108. Ott, V. L.; Cambier, J. C.; Kappler, J.; Marrack, P.; Swanson, B. J., Mast cell-dependent migration of effector CD8+ T cells through production of leukotriene B4. *Nat Immunol* **2003**, 4, (10), 974-81.
109. Hedqvist, P.; Dahlen, S. E., Pulmonary and vascular effects of leukotrienes imply involvement in asthma and inflammation. *Adv Prostaglandin Thromboxane Leukot Res* **1983**, 11, 27-32.
110. Peters-Golden, M.; Canetti, C.; Mancuso, P.; Coffey, M. J., Leukotrienes: underappreciated mediators of innate immune responses. *J Immunol* **2005**, 174, (2), 589-94.
111. Narala, V. R.; Adapala, R. K.; Suresh, M. V.; Brock, T. G.; Peters-Golden, M.; Reddy, R. C., Leukotriene B4 is a physiologically relevant endogenous peroxisome proliferator-activated receptor-alpha agonist. *J Biol Chem* **2010**, 285, (29), 22067-74.
112. Bain, G.; King, C. D.; Rewolinski, M.; Schaab, K.; Santini, A. M.; Shapiro, D.; Moran, M.; van de Wetering de Rooij, S.; Roffel, A. F.; Schuilenga-Hut, P.; Milne, G. L.; Lorrain, D. S.; Li, Y.; Arruda, J. M.; Hutchinson, J. H.; Prasit, P.; Evans, J. F., Pharmacodynamics and pharmacokinetics of AM103, a novel inhibitor of 5-lipoxygenase-activating protein (FLAP). *Clin Pharmacol Ther* **2010**, 87, (4), 437-44.

113. Romano, M.; Serhan, C. N., Lipoxin generation by permeabilized human platelets. *Biochemistry* **1992**, 31, (35), 8269-77.
114. Serhan, C. N., On the relationship between leukotriene and lipoxin production by human neutrophils: evidence for differential metabolism of 15-HETE and 5-HETE. *Biochim Biophys Acta* **1989**, 1004, (2), 158-68.
115. Serhan, C. N., Leukocyte transmigration, chemotaxis, and oxygenated derivatives of arachidonic acid: when is chirality important? *Am J Respir Cell Mol Biol* **1995**, 12, (3), 251-3.
116. Lecomte, M.; Laneuville, O.; Ji, C.; DeWitt, D. L.; Smith, W. L., Acetylation of human prostaglandin endoperoxide synthase-2 (cyclooxygenase-2) by aspirin. *J Biol Chem* **1994**, 269, (18), 13207-15.
117. Claria, J.; Serhan, C. N., Aspirin triggers previously undescribed bioactive eicosanoids by human endothelial cell-leukocyte interactions. *Proc Natl Acad Sci U S A* **1995**, 92, (21), 9475-9.
118. Fiore, S.; Maddox, J. F.; Perez, H. D.; Serhan, C. N., Identification of a human cDNA encoding a functional high affinity lipoxin A4 receptor. *J Exp Med* **1994**, 180, (1), 253-60.
119. Badr, K. F.; DeBoer, D. K.; Schwartzberg, M.; Serhan, C. N., Lipoxin A4 antagonizes cellular and in vivo actions of leukotriene D4 in rat glomerular mesangial cells: evidence for competition at a common receptor. *Proc Natl Acad Sci U S A* **1989**, 86, (9), 3438-42.
120. Godson, C.; Mitchell, S.; Harvey, K.; Petasis, N. A.; Hogg, N.; Brady, H. R., Cutting edge: lipoxins rapidly stimulate nonphlogistic phagocytosis of apoptotic neutrophils by monocyte-derived macrophages. *J Immunol* **2000**, 164, (4), 1663-7.
121. Freire-de-Lima, C. G.; Xiao, Y. Q.; Gardai, S. J.; Bratton, D. L.; Schiemann, W. P.; Henson, P. M., Apoptotic cells, through transforming growth factor-beta, coordinately induce anti-inflammatory and suppress pro-inflammatory eicosanoid and NO synthesis in murine macrophages. *J Biol Chem* **2006**, 281, (50), 38376-84.
122. Pouliot, M.; Clish, C. B.; Petasis, N. A.; Van Dyke, T. E.; Serhan, C. N., Lipoxin A(4) analogues inhibit leukocyte recruitment to *Porphyromonas gingivalis*: a role for cyclooxygenase-2 and lipoxins in periodontal disease. *Biochemistry* **2000**, 39, (16), 4761-8.
123. Leonard, M. O.; Hannan, K.; Burne, M. J.; Lappin, D. W.; Doran, P.; Coleman, P.; Stenson, C.; Taylor, C. T.; Daniels, F.; Godson, C.; Petasis, N. A.; Rabb, H.; Brady, H. R., 15-Epi-16-(para-fluorophenoxy)-lipoxin A(4)-methyl ester, a synthetic analogue of 15-epi-lipoxin A(4), is protective in experimental ischemic acute renal failure. *J Am Soc Nephrol* **2002**, 13, (6), 1657-62.

124. Schottelius, A. J.; Giesen, C.; Asadullah, K.; Fierro, I. M.; Colgan, S. P.; Bauman, J.; Guilford, W.; Perez, H. D.; Parkinson, J. F., An aspirin-triggered lipoxin A4 stable analog displays a unique topical anti-inflammatory profile. *J Immunol* **2002**, 169, (12), 7063-70.
125. Paul-Clark, M. J.; Van Cao, T.; Moradi-Bidhendi, N.; Cooper, D.; Gilroy, D. W., 15-epi-lipoxin A4-mediated induction of nitric oxide explains how aspirin inhibits acute inflammation. *J Exp Med* **2004**, 200, (1), 69-78.
126. Gronert, K.; Maheshwari, N.; Khan, N.; Hassan, I. R.; Dunn, M.; Laniado Schwartzman, M., A role for the mouse 12/15-lipoxygenase pathway in promoting epithelial wound healing and host defense. *J Biol Chem* **2005**, 280, (15), 15267-78.
127. Karp, C. L.; Flick, L. M.; Yang, R.; Uddin, J.; Petasis, N. A., Cystic fibrosis and lipoxins. *Prostaglandins Leukot Essent Fatty Acids* **2005**, 73, (3-4), 263-70.
128. Levy, B. D.; Bonnans, C.; Silverman, E. S.; Palmer, L. J.; Marigowda, G.; Israel, E., Diminished lipoxin biosynthesis in severe asthma. *Am J Respir Crit Care Med* **2005**, 172, (7), 824-30.
129. Bryant, R. W.; Schewe, T.; Rapoport, S. M.; Bailey, J. M., Leukotriene formation by a purified reticulocyte lipoxygenase enzyme. Conversion of arachidonic acid and 15-hydroperoxyeicosatetraenoic acid to 14, 15-leukotriene A4. *J Biol Chem* **1985**, 260, (6), 3548-55.
130. Maas, R. L.; Brash, A. R., Evidence for a lipoxygenase mechanism in the biosynthesis of epoxide and dihydroxy leukotrienes from 15(S)-hydroperoxyicosatetraenoic acid by human platelets and porcine leukocytes. *Proc Natl Acad Sci U S A* **1983**, 80, (10), 2884-8.
131. Feltenmark, S.; Gautam, N.; Brunnstrom, A.; Griffiths, W.; Backman, L.; Edenius, C.; Lindbom, L.; Bjorkholm, M.; Claesson, H. E., Eoxins are proinflammatory arachidonic acid metabolites produced via the 15-lipoxygenase-1 pathway in human eosinophils and mast cells. *Proc Natl Acad Sci U S A* **2008**, 105, (2), 680-5.
132. Nelson, D. R.; Koymans, L.; Kamataki, T.; Stegeman, J. J.; Feyereisen, R.; Waxman, D. J.; Waterman, M. R.; Gotoh, O.; Coon, M. J.; Estabrook, R. W.; Gunsalus, I. C.; Nebert, D. W., P450 superfamily: update on new sequences, gene mapping, accession numbers and nomenclature. *Pharmacogenetics* **1996**, 6, (1), 1-42.
133. Node, K.; Huo, Y.; Ruan, X.; Yang, B.; Spiecker, M.; Ley, K.; Zeldin, D. C.; Liao, J. K., Anti-inflammatory properties of cytochrome P450 epoxygenase-derived eicosanoids. *Science* **1999**, 285, (5431), 1276-9.
134. Roman, R. J., P-450 metabolites of arachidonic acid in the control of cardiovascular function. *Physiol Rev* **2002**, 82, (1), 131-85.

135. Inceoglu, B.; Jinks, S. L.; Ulu, A.; Hegedus, C. M.; Georgi, K.; Schmelzer, K. R.; Wagner, K.; Jones, P. D.; Morisseau, C.; Hammock, B. D., Soluble epoxide hydrolase and epoxyeicosatrienoic acids modulate two distinct analgesic pathways. *Proc Natl Acad Sci U S A* **2008**, 105, (48), 18901-6.
136. Liu, Y.; Zhang, Y.; Schmelzer, K.; Lee, T. S.; Fang, X.; Zhu, Y.; Spector, A. A.; Gill, S.; Morisseau, C.; Hammock, B. D.; Shyy, J. Y., The antiinflammatory effect of laminar flow: the role of PPARgamma, epoxyeicosatrienoic acids, and soluble epoxide hydrolase. *Proc Natl Acad Sci U S A* **2005**, 102, (46), 16747-52.
137. Heizer, M. L.; McKinney, J. S.; Ellis, E. F., 14,15-Epoxyeicosatrienoic acid inhibits platelet aggregation in mouse cerebral arterioles. *Stroke* **1991**, 22, (11), 1389-93.
138. Hill, E.; Fitzpatrick, F.; Murphy, R. C., Biological activity and metabolism of 20-hydroxyeicosatetraenoic acid in the human platelet. *Br J Pharmacol* **1992**, 106, (2), 267-74.
139. Bednar, M. M.; Gross, C. E.; Balazy, M. K.; Belosludtsev, Y.; Colella, D. T.; Falck, J. R.; Balazy, M., 16(R)-hydroxy-5,8,11,14-eicosatetraenoic acid, a new arachidonate metabolite in human polymorphonuclear leukocytes. *Biochem Pharmacol* **2000**, 60, (3), 447-55.
140. Serhan, C. N.; Chiang, N.; Van Dyke, T. E., Resolving inflammation: dual anti-inflammatory and pro-resolution lipid mediators. *Nat Rev Immunol* **2008**, 8, (5), 349-61.
141. Serhan, C. N., Novel lipid mediators and resolution mechanisms in acute inflammation: to resolve or not? *Am J Pathol* **2010**, 177, (4), 1576-91.
142. Coleman, J. O. D.; Blake-Kalff, M. M. A.; Davies, T. G. E., Detoxification of xenobiotics by plants: Chemical modification and vacuolar compartmentation. *Trends Plant Sci* **1997**, 2, 144-151.
143. Keen, J. H.; Jakoby, W. B., Glutathione transferases. Catalysis of nucleophilic reactions of glutathione. *J Biol Chem* **1978**, 253, (16), 5654-7.
144. Armstrong, R. N., Structure, catalytic mechanism, and evolution of the glutathione transferases. *Chem Res Toxicol* **1997**, 10, (1), 2-18.
145. Hayes, J. D.; Flanagan, J. U.; Jowsey, I. R., Glutathione transferases. *Annu Rev Pharmacol Toxicol* **2005**, 45, 51-88.
146. Oakley, A. J., Glutathione transferases: new functions. *Curr Opin Struct Biol* **2005**, 15, (6), 716-23.
147. Frova, C., Glutathione transferases in the genomics era: new insights and perspectives. *Biomol Eng* **2006**, 23, (4), 149-69.

148. Sheehan, D.; Meade, G.; Foley, V. M.; Dowd, C. A., Structure, function and evolution of glutathione transferases: implications for classification of non-mammalian members of an ancient enzyme superfamily. *Biochem J* **2001**, 360, (Pt 1), 1-16.
149. Pearson, W. R., Phylogenies of glutathione transferase families. *Methods Enzymol* **2005**, 401, 186-204.
150. Stourman, N. V.; Branch, M. C.; Schaab, M. R.; Harp, J. M.; Ladner, J. E.; Armstrong, R. N., Structure and function of YghU, a nu-class glutathione transferase related to YfcG from Escherichia coli. *Biochemistry* **2011**, 50, (7), 1274-81.
151. Dixon, D. P.; Davies, B. G.; Edwards, E., Functional divergence in the glutathione transferase superfamily in plants. *J Biol Chem* **2002**, 227, 30859-30869.
152. Allocati, N.; Casalone, E.; Masulli, M.; Ceccarelli, I.; Carletti, E.; Parker, M. W.; Di Ilio, C., Functional analysis of the evolutionarily conserved proline 53 residue in Proteus mirabilis glutathione transferase B1-1. *FEBS Lett* **1999**, 445, (2-3), 347-50.
153. Robinson, A.; Huttley, G. A.; Booth, H. S.; Board, P. G., Modelling and bioinformatics studies of the human Kappa-class glutathione transferase predict a novel third glutathione transferase family with similarity to prokaryotic 2-hydroxychromene-2-carboxylate isomerases. *Biochem J* **2004**, 379, (Pt 3), 541-52.
154. Ladner, J. E.; Parsons, J. F.; Rife, C. L.; Gilliland, G. L.; Armstrong, R. N., Parallel evolutionary pathways for glutathione transferases: structure and mechanism of the mitochondrial class kappa enzyme rGSTK1-1. *Biochemistry* **2004**, 43, (2), 352-61.
155. Li, J.; Xia, Z.; Ding, J., Thioredoxin-like domain of human kappa class glutathione transferase reveals sequence homology and structure similarity to the theta class enzyme. *Protein Sci* **2005**, 14, (9), 2361-9.
156. Bernat, B. A.; Laughlin, L. T.; Armstrong, R. N., Fosfomycin resistance protein (FosA) is a manganese metalloglutathione transferase related to glyoxalase I and the extradiol dioxygenases. *Biochemistry* **1997**, 36, (11), 3050-5.
157. Cao, M.; Bernat, B. A.; Wang, Z.; Armstrong, R. N.; Helmann, J. D., FosB, a cysteine-dependent fosfomycin resistance protein under the control of sigma(W), an extracytoplasmic-function sigma factor in Bacillus subtilis. *J Bacteriol* **2001**, 183, (7), 2380-3.
158. Fillgrove, K. L.; Pakhomova, S.; Newcomer, M. E.; Armstrong, R. N., Mechanistic diversity of fosfomycin resistance in pathogenic microorganisms. *J Am Chem Soc* **2003**, 125, (51), 15730-1.
159. Jakobsson, P. J.; Morgenstern, R.; Mancini, J.; Ford-Hutchinson, A.; Persson, B., Common structural features of MAPEG -- a widespread superfamily of membrane associated proteins with highly divergent functions in eicosanoid and glutathione metabolism. *Protein Sci* **1999**, 8, (3), 689-92.

160. Jakobsson, P. J.; Morgenstern, R.; Mancini, J.; Ford-Hutchinson, A.; Persson, B., Membrane-associated proteins in eicosanoid and glutathione metabolism (MAPEG). A widespread protein superfamily. *Am J Respir Crit Care Med* **2000**, 161, (2 Pt 2), S20-4.
161. Bresell, A.; Weinander, R.; Lundqvist, G.; Raza, H.; Shimoji, M.; Sun, T. H.; Balk, L.; Wiklund, R.; Eriksson, J.; Jansson, C.; Persson, B.; Jakobsson, P. J.; Morgenstern, R., Bioinformatic and enzymatic characterization of the MAPEG superfamily. *FEBS J* **2005**, 272, (7), 1688-703.
162. Holm, P. J.; Bhakat, P.; Jegerschold, C.; Gyobu, N.; Mitsuoka, K.; Fujiyoshi, Y.; Morgenstern, R.; Hebert, H., Structural basis for detoxification and oxidative stress protection in membranes. *J Mol Biol* **2006**, 360, (5), 934-45.
163. Ago, H.; Kanaoka, Y.; Irikura, D.; Lam, B. K.; Shimamura, T.; Austen, K. F.; Miyano, M., Crystal structure of a human membrane protein involved in cysteinyl leukotriene biosynthesis. *Nature* **2007**, 448, (7153), 609-12.
164. Martinez Molina, D.; Wetterholm, A.; Kohl, A.; McCarthy, A. A.; Niegowski, D.; Ohlson, E.; Hammarberg, T.; Eshaghi, S.; Haeggstrom, J. Z.; Nordlund, P., Structural basis for synthesis of inflammatory mediators by human leukotriene C4 synthase. *Nature* **2007**, 448, (7153), 613-6.
165. Ferguson, A. D.; McKeever, B. M.; Xu, S.; Wisniewski, D.; Miller, D. K.; Yamin, T. T.; Spencer, R. H.; Chu, L.; Ujjainwalla, F.; Cunningham, B. R.; Evans, J. F.; Becker, J. W., Crystal structure of inhibitor-bound human 5-lipoxygenase-activating protein. *Science* **2007**, 317, (5837), 510-2.
166. Jegerschold, C.; Pawelzik, S. C.; Purhonen, P.; Bhakat, P.; Gheorghe, K. R.; Gyobu, N.; Mitsuoka, K.; Morgenstern, R.; Jakobsson, P. J.; Hebert, H., Structural basis for induced formation of the inflammatory mediator prostaglandin E2. *Proc Natl Acad Sci U S A* **2008**, 105, (32), 11110-5.
167. Morgenstern, R.; Guthenberg, C.; Depierre, J. W., Microsomal glutathione S-transferase. Purification, initial characterization and demonstration that it is not identical to the cytosolic glutathione S-transferases A, B and C. *Eur J Biochem* **1982**, 128, (1), 243-8.
168. Yoshimoto, T.; Soberman, R. J.; Lewis, R. A.; Austen, K. F., Isolation and characterization of leukotriene C4 synthetase of rat basophilic leukemia cells. *Proc Natl Acad Sci U S A* **1985**, 82, (24), 8399-403.
169. Miller, D. K.; Gillard, J. W.; Vickers, P. J.; Sadowski, S.; Leveille, C.; Mancini, J. A.; Charleson, P.; Dixon, R. A. F.; Ford-Hutchinson, A. W.; Fortin, R.; Gauthier, J. Y.; Rodkey, J.; Rosen, R.; Rouzer, C. A.; Sigal, I. S.; Strader, C. D.; Evans, J. F., Identification and isolation of a membrane protein necessary for leukotriene production. *Nature* **1990**, 343, 278-281.

170. Jakobsson, P. J.; Mancini, J. A.; Ford-Hutchinson, A. W., Identification and characterization of a novel human microsomal glutathione S-transferase with leukotriene C4 synthase activity and significant sequence identity to 5-lipoxygenase-activating protein and leukotriene C4 synthase. *J Biol Chem* **1996**, 271, (36), 22203-10.
171. Jakobsson, P. J.; Mancini, J. A.; Riendeau, D.; Ford-Hutchinson, A. W., Identification and characterization of a novel microsomal enzyme with glutathione-dependent transferase and peroxidase activities. *J Biol Chem* **1997**, 272, (36), 22934-9.
172. Shimizu, T.; Izumi, T.; Seyama, Y.; Tadokoro, K.; Radmark, O.; Samuelsson, B., Characterization of leukotriene A4 synthase from murine mast cells: evidence for its identity to arachidonate 5-lipoxygenase. *Proc Natl Acad Sci U S A* **1986**, 83, (12), 4175-9.
173. Rouzer, C. A.; Matsumoto, T.; Samuelsson, B., Single protein from human leukocytes possesses 5-lipoxygenase and leukotriene A4 synthase activities. *Proc Natl Acad Sci U S A* **1986**, 83, (4), 857-61.
174. Gillard, J.; Ford-Hutchinson, A. W.; Chan, C.; Charleson, S.; Denis, D.; Foster, A.; Fortin, R.; Leger, S.; McFarlane, C. S.; Morton, H.; et al., L-663,536 (MK-886) (3-[1-(4-chlorobenzyl)-3-t-butyl-thio-5-isopropylindol-2-yl]-2,2 - dimethylpropanoic acid), a novel, orally active leukotriene biosynthesis inhibitor. *Can J Physiol Pharmacol* **1989**, 67, (5), 456-64.
175. Polyak, K.; Xia, Y.; Zweier, J. L.; Kinzler, K. W.; Vogelstein, B., A model for p53-induced apoptosis. *Nature* **1997**, 389, (6648), 300-5.
176. Mitchell, J. A.; Belvisi, M. G.; Akarasereenont, P.; Robbins, R. A.; Kwon, O. J.; Croxtall, J.; Barnes, P. J.; Vane, J. R., Induction of cyclo-oxygenase-2 by cytokines in human pulmonary epithelial cells: regulation by dexamethasone. *Br J Pharmacol* **1994**, 113, (3), 1008-14.
177. Huang, M.; Stolina, M.; Sharma, S.; Mao, J. T.; Zhu, L.; Miller, P. W.; Wollman, J.; Herschman, H.; Dubinett, S. M., Non-small cell lung cancer cyclooxygenase-2-dependent regulation of cytokine balance in lymphocytes and macrophages: up-regulation of interleukin 10 and down-regulation of interleukin 12 production. *Cancer Res* **1998**, 58, (6), 1208-16.
178. Smith, W. L., Prostanoid biosynthesis and mechanisms of action. *Am J Physiol* **1992**, 263, (2 Pt 2), F181-91.
179. Persson, B.; Argos, P., Prediction of transmembrane segments in proteins utilising multiple sequence alignments. *J Mol Biol* **1994**, 237, (2), 182-92.
180. Cserzo, M.; Wallin, E.; Simon, I.; von Heijne, G.; Elofsson, A., Prediction of transmembrane alpha-helices in prokaryotic membrane proteins: the dense alignment surface method. *Protein Eng* **1997**, 10, (6), 673-6.

181. Schmidt-Krey, I.; Mitsuoka, K.; Hirai, T.; Murata, K.; Cheng, Y.; Fujiyoshi, Y.; Morgenstern, R.; Hebert, H., The three-dimensional map of microsomal glutathione transferase 1 at 6 Å resolution. *EMBO J* **2000**, 19, (23), 6311-6.
182. Hebert, H.; Jegerschild, C., The structure of membrane associated proteins in eicosanoid and glutathione metabolism as determined by electron crystallography. *Curr Opin Struct Biol* **2007**, 17, (4), 396-404.
183. Busenlehner, L. S.; Alander, J.; Jegerschild, C.; Holm, P. J.; Bhakat, P.; Hebert, H.; Morgenstern, R.; Armstrong, R. N., Location of substrate binding sites within the integral membrane protein microsomal glutathione transferase-1. *Biochemistry* **2007**, 46, (10), 2812-22.
184. Sun, T. H.; Morgenstern, R., Binding of glutathione and an inhibitor to microsomal glutathione transferase. *Biochem J* **1997**, 326 (Pt 1), 193-6.
185. Morgenstern, R.; Svensson, R.; Bernat, B. A.; Armstrong, R. N., Kinetic analysis of the slow ionization of glutathione by microsomal glutathione transferase MGST1. *Biochemistry* **2001**, 40, (11), 3378-84.
186. Svensson, R.; Alander, J.; Armstrong, R. N.; Morgenstern, R., Kinetic characterization of thiolate anion formation and chemical catalysis of activated microsomal glutathione transferase 1. *Biochemistry* **2004**, 43, (27), 8869-77.
187. Alander, J.; Lengqvist, J.; Holm, P. J.; Svensson, R.; Gerbaux, P.; Heuvel, R. H.; Hebert, H.; Griffiths, W. J.; Armstrong, R. N.; Morgenstern, R., Microsomal glutathione transferase 1 exhibits one-third-of-the-sites-reactivity towards glutathione. *Arch Biochem Biophys* **2009**, 487, (1), 42-8.
188. Pawelzik, S. C.; Uda, N. R.; Spahiu, L.; Jegerschild, C.; Stenberg, P.; Hebert, H.; Morgenstern, R.; Jakobsson, P. J., Identification of key residues determining species differences in inhibitor binding of microsomal prostaglandin E synthase-1. *J Biol Chem* **2010**, 285, (38), 29254-61.
189. Andersson, C.; Mosialou, E.; Adang, A. E.; Mulder, G. J.; van der Gen, A.; Morgenstern, R., Studies on the activity and activation of rat liver microsomal glutathione transferase with a series of glutathione analogues. *J Biol Chem* **1991**, 266, (4), 2076-9.
190. Soderstrom, M.; Hammarstrom, S.; Mannervik, B., Leukotriene C synthase in mouse mastocytoma cells. An enzyme distinct from cytosolic and microsomal glutathione transferases. *Biochem J* **1988**, 250, (3), 713-8.
191. Andersson, C.; Mosialou, E.; Weinander, R.; Morgenstern, R., Enzymology of microsomal glutathione S-transferase. *Adv Pharmacol* **1994**, 27, 19-35.

192. Morgenstern, R.; DePierre, J. W.; Ernster, L., Activation of microsomal glutathione S-transferase activity by sulfhydryl reagents. *Biochem Biophys Res Commun* **1979**, 87, (3), 657-63.
193. Morgenstern, R.; DePierre, J. W., Microsomal glutathione transferase. Purification in unactivated form and further characterization of the activation process, substrate specificity and amino acid composition. *Eur J Biochem* **1983**, 134, (3), 591-7.
194. Busenlehner, L. S.; Codreanu, S. G.; Holm, P. J.; Bhakat, P.; Hebert, H.; Morgenstern, R.; Armstrong, R. N., Stress sensor triggers conformational response of the integral membrane protein microsomal glutathione transferase 1. *Biochemistry* **2004**, 43, (35), 11145-52.
195. Mosialou, E.; Ekstrom, G.; Adang, A. E.; Morgenstern, R., Evidence that rat liver microsomal glutathione transferase is responsible for glutathione-dependent protection against lipid peroxidation. *Biochem Pharmacol* **1993**, 45, (8), 1645-51.
196. Mosialou, E.; Piemonte, F.; Andersson, C.; Vos, R. M.; van Bladeren, P. J.; Morgenstern, R., Microsomal glutathione transferase: lipid-derived substrates and lipid dependence. *Arch Biochem Biophys* **1995**, 320, (2), 210-6.
197. Siritantikorn, A.; Johansson, K.; Ahlen, K.; Rinaldi, R.; Suthiphongchai, T.; Wilairat, P.; Morgenstern, R., Protection of cells from oxidative stress by microsomal glutathione transferase 1. *Biochem Biophys Res Commun* **2007**, 355, (2), 592-6.
198. Aniya, Y.; Teruya, M., Activation of hepatic microsomal glutathione S-transferase of rats by a glutathione depletor, diethylmaleate. *J Pharmacobiodyn* **1992**, 15, (9), 473-9.
199. Evans, J. F.; Ferguson, A. D.; Mosley, R. T.; Hutchinson, J. H., What's all the FLAP about?: 5-lipoxygenase-activating protein inhibitors for inflammatory diseases. *Trends Pharmacol Sci* **2008**, 29, (2), 72-8.
200. Newcomer, M. E.; Gilbert, N. C., Location, location, location: compartmentalization of early events in leukotriene biosynthesis. *J Biol Chem* **2010**, 285, (33), 25109-14.
201. Rinaldo-Matthis, A.; Haeggstrom, J. Z., Structures and mechanisms of enzymes in the leukotriene cascade. *Biochimie* **2010**, 92, (6), 676-81.
202. Penrose, J. F.; Gagnon, L.; Goppelt-Struebe, M.; Myers, P.; Lam, B. K.; Jack, R. M.; Austen, K. F.; Soberman, R. J., Purification of human leukotriene C4 synthase. *Proc Natl Acad Sci U S A* **1992**, 89, (23), 11603-6.
203. Metters, K. M.; Sawyer, N.; Nicholson, D. W., Microsomal glutathione S-transferase is the predominant leukotriene C4 binding site in cellular membranes. *J Biol Chem* **1994**, 269, (17), 12816-23.

204. Nugteren, D. H.; Christ-Hazelhof, E., Chemical and enzymic conversions of the prostaglandin endoperoxide PGH₂. *Adv Prostaglandin Thromboxane Res* **1980**, 6, 129-37.
205. Thoren, S.; Weinander, R.; Saha, S.; Jegerschold, C.; Pettersson, P. L.; Samuelsson, B.; Hebert, H.; Hamberg, M.; Morgenstern, R.; Jakobsson, P. J., Human microsomal prostaglandin E synthase-1: purification, functional characterization, and projection structure determination. *J Biol Chem* **2003**, 278, (25), 22199-209.
206. Arthur, J. R., The glutathione peroxidases. *Cell Mol Life Sci* **2000**, 57, (13-14), 1825-35.
207. Rinaldo-Matthis, A.; Wetterholm, A.; Martinez Molina, D.; Holm, J.; Niegowski, D.; Ohlson, E.; Nordlund, P.; Morgenstern, R.; Haeggstrom, J. Z., Arginine 104 is a key catalytic residue in leukotriene C₄ synthase. *J Biol Chem* **2010**, 285, (52), 40771-6.
208. Hammarberg, T.; Hamberg, M.; Wetterholm, A.; Hansson, H.; Samuelsson, B.; Haeggstrom, J. Z., Mutation of a critical arginine in microsomal prostaglandin E synthase-1 shifts the isomerase activity to a reductase activity that converts prostaglandin H₂ into prostaglandin F₂α. *J Biol Chem* **2009**, 284, (1), 301-5.
209. Krogh, A.; Larsson, B.; von Heijne, G.; Sonnhammer, E. L., Predicting transmembrane protein topology with a hidden Markov model: application to complete genomes. *J Mol Biol* **2001**, 305, (3), 567-80.
210. Overington, J. P.; Al-Lazikani, B.; Hopkins, A. L., How many drug targets are there? *Nat Rev Drug Discov* **2006**, 5, (12), 993-6.
211. Carpenter, E. P.; Beis, K.; Cameron, A. D.; Iwata, S., Overcoming the challenges of membrane protein crystallography. *Curr Opin Struct Biol* **2008**, 18, (5), 581-6.
212. Kendrew, J. C.; Bodo, G.; Dintzis, H. M.; Parrish, R. G.; Wyckoff, H.; Phillips, D. C., A three-dimensional model of the myoglobin molecule obtained by x-ray analysis. *Nature* **1958**, 181, (4610), 662-6.
213. Deisenhofer, J.; Epp, O.; Miki, K.; Huber, R.; Michel, H., Structure of the protein subunits in the photosynthetic reaction centre of *Rhodospseudomonas viridis* at 3 Å resolution. *Nature* **1985**, 318, 618-624.
214. Huang, X.; Yan, W.; Gao, D.; Tong, M. L.; Tai, H. H.; Zhan, C. G., Structural and functional characterization of human microsomal prostaglandin E synthase-1 by computational modeling and site-directed mutagenesis. *Bioorg Med Chem* **2006**, 14, (10), 3553-3562.
215. Gudis, K.; Sakamoto, C., The role of cyclooxygenase in gastric mucosal protection. *Dig Dis Sci* **2005**, 50 Suppl 1, S16-23.

216. Chan, C. C.; Boyce, S.; Brideau, C.; Charleson, S.; Cromlish, W.; Ethier, D.; Evans, J.; Ford-Hutchinson, A. W.; Forrest, M. J.; Gauthier, J. Y.; Gordon, R.; Gresser, M.; Guay, J.; Kargman, S.; Kennedy, B.; Leblanc, Y.; Leger, S.; Mancini, J.; O'Neill, G. P.; Ouellet, M.; Patrick, D.; Percival, M. D.; Perrier, H.; Prasit, P.; Rodger, I.; et al., Rofecoxib [Vioxx, MK-0966; 4-(4'-methylsulfonylphenyl)-3-phenyl-2-(5H)-furanone]: a potent and orally active cyclooxygenase-2 inhibitor. Pharmacological and biochemical profiles. *J Pharmacol Exp Ther* **1999**, 290, (2), 551-60.
217. McAdam, B. F.; Catella-Lawson, F.; Mardini, I. A.; Kapoor, S.; Lawson, J. A.; FitzGerald, G. A., Systemic biosynthesis of prostacyclin by cyclooxygenase (COX)-2: the human pharmacology of a selective inhibitor of COX-2. *Proc Natl Acad Sci U S A* **1999**, 96, (1), 272-7.
218. Kearney, P. M.; Baigent, C.; Godwin, J.; Halls, H.; Emberson, J. R.; Patrono, C., Do selective cyclo-oxygenase-2 inhibitors and traditional non-steroidal anti-inflammatory drugs increase the risk of atherothrombosis? Meta-analysis of randomised trials. *BMJ* **2006**, 332, (7553), 1302-8.
219. Trebino, C. E.; Stock, J. L.; Gibbons, C. P.; Naiman, B. M.; Wachtmann, T. S.; Umland, J. P.; Pandher, K.; Lapointe, J. M.; Saha, S.; Roach, M. L.; Carter, D.; Thomas, N. A.; Durtschi, B. A.; McNeish, J. D.; Hambor, J. E.; Jakobsson, P. J.; Carty, T. J.; Perez, J. R.; Audoly, L. P., Impaired inflammatory and pain responses in mice lacking an inducible prostaglandin E synthase. *Proc Natl Acad Sci U S A* **2003**, 100, (15), 9044-9.
220. Uematsu, S.; Matsumoto, M.; Takeda, K.; Akira, S., Lipopolysaccharide-dependent prostaglandin E(2) production is regulated by the glutathione-dependent prostaglandin E(2) synthase gene induced by the Toll-like receptor 4/MyD88/NF-IL6 pathway. *J Immunol* **2002**, 168, (11), 5811-6.
221. Kamei, D.; Yamakawa, K.; Takegoshi, Y.; Mikami-Nakanishi, M.; Nakatani, Y.; Oh-Ishi, S.; Yasui, H.; Azuma, Y.; Hirasawa, N.; Ohuchi, K.; Kawaguchi, H.; Ishikawa, Y.; Ishii, T.; Uematsu, S.; Akira, S.; Murakami, M.; Kudo, I., Reduced pain hypersensitivity and inflammation in mice lacking microsomal prostaglandin e synthase-1. *J Biol Chem* **2004**, 279, (32), 33684-95.
222. Mabuchi, T.; Kojima, H.; Abe, T.; Takagi, K.; Sakurai, M.; Ohmiya, Y.; Uematsu, S.; Akira, S.; Watanabe, K.; Ito, S., Membrane-associated prostaglandin E synthase-1 is required for neuropathic pain. *Neuroreport* **2004**, 15, (9), 1395-8.
223. Cheng, Y.; Wang, M.; Yu, Y.; Lawson, J.; Funk, C. D.; Fitzgerald, G. A., Cyclooxygenases, microsomal prostaglandin E synthase-1, and cardiovascular function. *J Clin Invest* **2006**, 116, (5), 1391-9.
224. Jia, Z.; Aoyagi, T.; Yang, T., mPGES-1 protects against DOCA-salt hypertension via inhibition of oxidative stress or stimulation of NO/cGMP. *Hypertension* **2010**, 55, (2), 539-46.

225. Gomez, P. F.; Pillinger, M. H.; Attur, M.; Marjanovic, N.; Dave, M.; Park, J.; Bingham, C. O., 3rd; Al-Mussawir, H.; Abramson, S. B., Resolution of inflammation: prostaglandin E2 dissociates nuclear trafficking of individual NF-kappaB subunits (p65, p50) in stimulated rheumatoid synovial fibroblasts. *J Immunol* **2005**, 175, (10), 6924-30.
226. Brenneis, C.; Coste, O.; Altenrath, K.; Angioni, C.; Schmidt, H.; Schuh, C. D.; Zhang, D. D.; Henke, M.; Weigert, A.; Brune, B.; Rubin, B.; Nusing, R.; Scholich, K.; Geisslinger, G., Anti-inflammatory role of microsomal prostaglandin E synthase-1 in a model of neuroinflammation. *J Biol Chem* **2011**, 286, (3), 2331-42.
227. Chan, M. M.; Moore, A. R., Resolution of inflammation in murine autoimmune arthritis is disrupted by cyclooxygenase-2 inhibition and restored by prostaglandin E2-mediated lipoxin A4 production. *J Immunol* **2010**, 184, (11), 6418-26.
228. Mbalaviele, G.; Pauley, A. M.; Shaffer, A. F.; Zweifel, B. S.; Mathialagan, S.; Mnich, S. J.; Nemirovskiy, O. V.; Carter, J.; Gierse, J. K.; Wang, J. L.; Vazquez, M. L.; Moore, W. M.; Masferrer, J. L., Distinction of microsomal prostaglandin E synthase-1 (mPGES-1) inhibition from cyclooxygenase-2 inhibition in cells using a novel, selective mPGES-1 inhibitor. *Biochem Pharmacol* **2010**, 79, (10), 1445-54.
229. Bruno, A.; Di Francesco, L.; Coletta, I.; Mangano, G.; Alisi, M. A.; Polenzani, L.; Milanese, C.; Anzellotti, P.; Ricciotti, E.; Dovizio, M.; Di Francesco, A.; Tacconelli, S.; Capone, M. L.; Patrignani, P., Effects of AF3442 [N-(9-ethyl-9H-carbazol-3-yl)-2-(trifluoromethyl)benzamide], a novel inhibitor of human microsomal prostaglandin E synthase-1, on prostanoid biosynthesis in human monocytes in vitro. *Biochem Pharmacol* **2010**, 79, (7), 974-81.
230. Xu, D.; Rowland, S. E.; Clark, P.; Giroux, A.; Cote, B.; Guiral, S.; Salem, M.; Ducharme, Y.; Friesen, R. W.; Methot, N.; Mancini, J.; Audoly, L.; Riendeau, D., MF63 [2-(6-chloro-1H-phenanthro[9,10-d]imidazol-2-yl)-isophthalonitrile], a selective microsomal prostaglandin E synthase-1 inhibitor, relieves pyresis and pain in preclinical models of inflammation. *J Pharmacol Exp Ther* **2008**, 326, (3), 754-63.
231. Giroux, A.; Boulet, L.; Brideau, C.; Chau, A.; Claveau, D.; Cote, B.; Ethier, D.; Frenette, R.; Gagnon, M.; Guay, J.; Guiral, S.; Mancini, J.; Martins, E.; Masse, F.; Methot, N.; Riendeau, D.; Rubin, J.; Xu, D.; Yu, H.; Ducharme, Y.; Friesen, R. W., Discovery of disubstituted phenanthrene imidazoles as potent, selective and orally active mPGES-1 inhibitors. *Bioorg Med Chem Lett* **2009**, 19, (20), 5837-41.
232. Chiasson, J. F.; Boulet, L.; Brideau, C.; Chau, A.; Claveau, D.; Cote, B.; Ethier, D.; Giroux, A.; Guay, J.; Guiral, S.; Mancini, J.; Masse, F.; Methot, N.; Riendeau, D.; Roy, P.; Rubin, J.; Xu, D.; Yu, H.; Ducharme, Y.; Friesen, R. W., Trisubstituted ureas as potent and selective mPGES-1 inhibitors. *Bioorg Med Chem Lett* **2011**, 21, (5), 1488-92.
233. Wang, M. T.; Honn, K. V.; Nie, D., Cyclooxygenases, prostanoids, and tumor progression. *Cancer Metastasis Rev* **2007**, 26, (3-4), 525-34.

234. Samuelsson, B.; Morgenstern, R.; Jakobsson, P. J., Membrane prostaglandin E synthase-1: a novel therapeutic target. *Pharmacol Rev* **2007**, 59, (3), 207-24.
235. Elander, N.; Ungerback, J.; Olsson, H.; Uematsu, S.; Akira, S.; Soderkvist, P., Genetic deletion of mPGES-1 accelerates intestinal tumorigenesis in APC(Min/+) mice. *Biochem Biophys Res Commun* **2008**, 372, (1), 249-53.
236. Nakanishi, M.; Montrose, D. C.; Clark, P.; Nambiar, P. R.; Belinsky, G. S.; Claffey, K. P.; Xu, D.; Rosenberg, D. W., Genetic deletion of mPGES-1 suppresses intestinal tumorigenesis. *Cancer Res* **2008**, 68, (9), 3251-9.
237. Hanaka, H.; Pawelzik, S. C.; Johnsen, J. I.; Rakonjac, M.; Terawaki, K.; Rasmuson, A.; Sveinbjornsson, B.; Schumacher, M. C.; Hamberg, M.; Samuelsson, B.; Jakobsson, P. J.; Kogner, P.; Radmark, O., Microsomal prostaglandin E synthase 1 determines tumor growth in vivo of prostate and lung cancer cells. *Proc Natl Acad Sci U S A* **2009**, 106, (44), 18757-62.
238. Kamei, D.; Murakami, M.; Sasaki, Y.; Nakatani, Y.; Majima, K.; Ishii, T.; Uematsu, S.; Akira, S.; Hara, S.; Kudo, I., Microsomal prostaglandin E synthase-1 in both cancer cells and hosts contributes to tumour growth, invasion and metastasis. *Biochem J* **2010**, 425, (2), 361-371.
239. Wishart, D. S.; Sykes, B. D.; Richards, F. M., The chemical shift index: a fast and simple method for the assignment of protein secondary structure through NMR spectroscopy. *Biochemistry* **1992**, 31, (6), 1647-51.
240. Ostermeier, C.; Michel, H., Crystallization of membrane proteins. *Curr Opin Struct Biol* **1997**, 7, (5), 697-701.
241. Wagner, G., Prospects for NMR of large proteins. *J Biomol NMR* **1993**, 3, (4), 375-85.
242. Hvidt, A.; Linderstrom-Lang, K., Exchange of hydrogen atoms in insulin with deuterium atoms in aqueous solutions. *Biochim Biophys Acta* **1954**, 14, (4), 574-5.
243. Zhang, Z.; Smith, D. L., Determination of amide hydrogen exchange by mass spectrometry: a new tool for protein structure elucidation. *Protein Sci* **1993**, 2, (4), 522-31.
244. Fenn, J. B., Electrospray wings for molecular elephants (Nobel lecture). *Angew Chem Int Ed Engl* **2003**, 42, (33), 3871-94.
245. Karas, M.; Hillenkamp, F., Laser desorption ionization of proteins with molecular masses exceeding 10,000 daltons. *Anal Chem* **1988**, 60, (20), 2299-301.
246. Johnson, R. S.; Walsh, K. A., Mass spectrometric measurement of protein amide hydrogen exchange rates of apo- and holo-myoglobin. *Protein Sci* **1994**, 3, (12), 2411-8.

247. Englander, S. W.; Downer, N. W.; Teitelbaum, H., Hydrogen exchange. *Annu Rev Biochem* **1972**, 41, 903-24.
248. Molday, R. S.; Englander, S. W.; Kallen, R. G., Primary structure effects on peptide group hydrogen exchange. *Biochemistry* **1972**, 11, (2), 150-8.
249. Connelly, G. P.; Bai, Y.; Jeng, M. F.; Englander, S. W., Isotope effects in peptide group hydrogen exchange. *Proteins* **1993**, 17, (1), 87-92.
250. Busenlehner, L. S.; Armstrong, R. N., Insights into enzyme structure and dynamics elucidated by amide H/D exchange mass spectrometry. *Arch Biochem Biophys* **2005**, 433, (1), 34-46.
251. Wuthrich, K.; Wagner, G., Nuclear magnetic resonance of labile protons in the basic pancreatic trypsin inhibitor. *J Mol Biol* **1979**, 130, (1), 1-18.
252. Wagner, S.; Bader, M. L.; Drew, D.; de Gier, J. W., Rationalizing membrane protein overexpression. *Trends Biotechnol* **2006**, 24, (8), 364-71.
253. Garavito, R. M.; Ferguson-Miller, S., Detergents as tools in membrane biochemistry. *J Biol Chem* **2001**, 276, (35), 32403-6.
254. Loo, R. R.; Dales, N.; Andrews, P. C., Surfactant effects on protein structure examined by electrospray ionization mass spectrometry. *Protein Sci* **1994**, 3, (11), 1975-83.
255. Demmers, J. A.; Haverkamp, J.; Heck, A. J.; Koeppe, R. E., 2nd; Killian, J. A., Electrospray ionization mass spectrometry as a tool to analyze hydrogen/deuterium exchange kinetics of transmembrane peptides in lipid bilayers. *Proc Natl Acad Sci U S A* **2000**, 97, (7), 3189-94.
256. Stelzer, W.; Poschner, B. C.; Stalz, H.; Heck, A. J.; Langosch, D., Sequence-specific conformational flexibility of SNARE transmembrane helices probed by hydrogen/deuterium exchange. *Biophys J* **2008**, 95, (3), 1326-35.
257. Asuru, A. P.; Busenlehner, L. S., Analysis of human ferrochelatase iron binding via amide hydrogen/deuterium exchange mass spectrometry. *Int J Mass Spectrom* **2010**, 302, 76-84.
258. Man, P.; Montagner, C.; Vernier, G.; Dublet, B.; Chenal, A.; Forest, E.; Forge, V., Defining the interacting regions between apomyoglobin and lipid membrane by hydrogen/deuterium exchange coupled to mass spectrometry. *J Mol Biol* **2007**, 368, (2), 464-72.
259. Svensson-Ek, M.; Abramson, J.; Larsson, G.; Tornroth, S.; Brzezinski, P.; Iwata, S., The X-ray crystal structures of wild-type and EQ(I-286) mutant cytochrome c oxidases from *Rhodobacter sphaeroides*. *J Mol Biol* **2002**, 321, (2), 329-39.

260. Busenlehner, L. S.; Salomonsson, L.; Brzezinski, P.; Armstrong, R. N., Mapping protein dynamics in catalytic intermediates of the redox-driven proton pump cytochrome c oxidase. *Proc Natl Acad Sci U S A* **2006**, 103, (42), 15398-403.
261. Busenlehner, L. S.; Branden, G.; Namslauer, I.; Brzezinski, P.; Armstrong, R. N., Structural elements involved in proton translocation by cytochrome c oxidase as revealed by backbone amide hydrogen-deuterium exchange of the E286H mutant. *Biochemistry* **2008**, 47, (1), 73-83.
262. Henderson, R.; Baldwin, J. M.; Ceska, T. A.; Zemlin, F.; Beckmann, E.; Downing, K. H., Model for the structure of bacteriorhodopsin based on high-resolution electron cryo-microscopy. *J Mol Biol* **1990**, 213, (4), 899-929.
263. Joh, N. H.; Min, A.; Faham, S.; Whitelegge, J. P.; Yang, D.; Woods, V. L.; Bowie, J. U., Modest stabilization by most hydrogen-bonded side-chain interactions in membrane proteins. *Nature* **2008**, 453, (7199), 1266-70.
264. Green, S. A.; Turki, J.; Bejarano, P.; Hall, I. P.; Liggett, S. B., Influence of beta 2-adrenergic receptor genotypes on signal transduction in human airway smooth muscle cells. *Am J Respir Cell Mol Biol* **1995**, 13, (1), 25-33.
265. Conn, P. J.; Christopoulos, A.; Lindsley, C. W., Allosteric modulators of GPCRs: a novel approach for the treatment of CNS disorders. *Nat Rev Drug Discov* **2009**, 8, (1), 41-54.
266. Zhang, X.; Chien, E. Y.; Chalmers, M. J.; Pascal, B. D.; Gatchalian, J.; Stevens, R. C.; Griffin, P. R., Dynamics of the beta2-adrenergic G-protein coupled receptor revealed by hydrogen-deuterium exchange. *Anal Chem* **2010**, 82, (3), 1100-8.
267. Stafford, D. W., The vitamin K cycle. *J Thromb Haemost* **2005**, 3, (8), 1873-8.
268. Hebling, C. M.; Morgan, C. R.; Stafford, D. W.; Jorgenson, J. W.; Rand, K. D.; Engen, J. R., Conformational analysis of membrane proteins in phospholipid bilayer nanodiscs by hydrogen exchange mass spectrometry. *Anal Chem* **2010**, 82, (13), 5415-9.
269. Denisov, I. G.; Grinkova, Y. V.; Lazarides, A. A.; Sligar, S. G., Directed self-assembly of monodisperse phospholipid bilayer Nanodiscs with controlled size. *J Am Chem Soc* **2004**, 126, (11), 3477-87.
270. Cravello, L.; Lascoux, D.; Forest, E., Use of different proteases working in acidic conditions to improve sequence coverage and resolution in hydrogen/deuterium exchange of large proteins. *Rapid Commun Mass Spectrom* **2003**, 17, (21), 2387-93.
271. Pan, J.; Han, J.; Borchers, C. H.; Konermann, L., Hydrogen/deuterium exchange mass spectrometry with top-down electron capture dissociation for characterizing structural transitions of a 17 kDa protein. *J Am Chem Soc* **2009**, 131, (35), 12801-8.

272. Zehl, M.; Rand, K. D.; Jensen, O. N.; Jorgensen, T. J., Electron transfer dissociation facilitates the measurement of deuterium incorporation into selectively labeled peptides with single residue resolution. *J Am Chem Soc* **2008**, 130, (51), 17453-9.
273. Rand, K. D.; Zehl, M.; Jensen, O. N.; Jorgensen, T. J., Protein hydrogen exchange measured at single-residue resolution by electron transfer dissociation mass spectrometry. *Anal Chem* **2009**, 81, (14), 5577-84.
274. Funk, J.; Li, X.; Franz, T., Threshold values for detergents in protein and peptide samples for mass spectrometry. *Rapid Commun Mass Spectrom* **2005**, 19, (20), 2986-8.
275. Rundlett, K. L.; Armstrong, D. W., Mechanism of signal suppression by anionic surfactants in capillary electrophoresis-electrospray ionization mass spectrometry. *Anal Chem* **1996**, 68, (19), 3493-7.
276. Hjelmeland, L. M., Solubilization of native membrane proteins. *Methods Enzymol* **1990**, 182, 253-64.
277. Rigaud, J. L.; Levy, D.; Mosser, G.; Lambert, O., Detergent removal by non-polar polystyrene beads: Applications to membrane protein reconstitution and two-dimensional crystallization. *Eur Biophys J* **1998**, 27, 305-319.
278. Degrip, W. J.; Vanoostrum, J.; Bovee-Geurts, P. H., Selective detergent-extraction from mixed detergent/lipid/protein micelles, using cyclodextrin inclusion compounds: a novel generic approach for the preparation of proteoliposomes. *Biochem J* **1998**, 330 (Pt 2), 667-74.
279. England, S.; Seifter, S., Precipitation techniques. *Methods Enzymol* **1990**, 182, 285-300.
280. Wessel, D.; Flugge, U. I., A method for the quantitative recovery of protein in dilute solution in the presence of detergents and lipids. *Anal Biochem* **1984**, 138, (1), 141-3.
281. Lu, X.; Zhu, H., Tube-gel digestion. *Mol Cell Proteomics* **2005**, 4, (1948-1958).
282. Vissers, J. P.; Hulst, W. P.; Chervet, J. P.; Snijders, H. M.; Cramers, C. A., Automated on-line ionic detergent removal from minute protein/peptide samples prior to liquid chromatography-electrospray mass spectrometry. *J Chromatogr B Biomed Appl* **1996**, 686, (2), 119-28.
283. Yeung, Y. G.; Nieves, E.; Angeletti, R. H.; Stanley, E. R., Removal of detergents from protein digests for mass spectrometry analysis. *Anal Biochem* **2008**, 382, (2), 135-7.
284. Masuda, T.; Tomita, M.; Ishihama, Y., Phase transfer surfactant-aided trypsin digestion for membrane proteome analysis. *J Proteome Res* **2008**, 7, (2), 731-40.

285. Yu, Y. Q.; Gilar, M.; Lee, P. J.; Bouvier, E. S.; Gebler, J. C., Enzyme-friendly, mass spectrometry-compatible surfactant for in-solution enzymatic digestion of proteins. *Anal Chem* **2003**, 75, (21), 6023-8.
286. Chen, E. I.; Cociorva, D.; Norris, J. L.; Yates, J. R., 3rd, Optimization of mass spectrometry-compatible surfactants for shotgun proteomics. *J Proteome Res* **2007**, 6, (7), 2529-38.
287. Rey, M.; Mrazek, H.; Pompach, P.; Novak, P.; Pelosi, L.; Brandolin, G.; Forest, E.; Havlicek, V.; Man, P., Effective removal of nonionic detergents in protein mass spectrometry, hydrogen/deuterium exchange, and proteomics. *Anal Chem* **2010**, 82, (12), 5107-16.
288. Ma, B.; Zhang, K.; Hendrie, C.; Liang, C.; Li, M.; Doherty-Kirby, A.; Lajoie, G., PEAKS: powerful software for peptide de novo sequencing by tandem mass spectrometry. *Rapid Commun Mass Spectrom* **2003**, 17, (20), 2337-42.
289. Hamuro, Y.; Coales, S. J.; Southern, M. R.; Nemeth-Cawley, J. F.; Stranz, D. D.; Griffin, P. R., Rapid analysis of protein structure and dynamics by hydrogen/deuterium exchange mass spectrometry. *J Biomol Tech* **2003**, 14, (3), 171-82.
290. Pascal, B. D.; Chalmers, M. J.; Busby, S. A.; Griffin, P. R., HD desktop: an integrated platform for the analysis and visualization of H/D exchange data. *J Am Soc Mass Spectrom* **2009**, 20, (4), 601-10.
291. Zhu, Y.; Guo, T.; Park, J. E.; Li, X.; Meng, W.; Datta, A.; Bern, M.; Lim, S. K.; Sze, S. K., Elucidating in vivo structural dynamics in integral membrane protein by hydroxyl radical footprinting. *Mol Cell Proteomics* **2009**, 8, (8), 1999-2010.
292. Pan, Y.; Stocks, B. B.; Brown, L.; Konermann, L., Structural characterization of an integral membrane protein in its natural lipid environment by oxidative methionine labeling and mass spectrometry. *Anal Chem* **2009**, 81, (1), 28-35.
293. Leite, J. F.; Blanton, M. P.; Shahgholi, M.; Dougherty, D. A.; Lester, H. A., Conformation-dependent hydrophobic photolabeling of the nicotinic receptor: electrophysiology-coordinated photochemistry and mass spectrometry. *Proc Natl Acad Sci U S A* **2003**, 100, (22), 13054-9.
294. Black, J., Drugs from emasculated hormones: the principle of syntopic antagonism. *Science* **1989**, 245, (4917), 486-93.
295. Mobley, D. L.; Dill, K. A., Binding of small-molecule ligands to proteins: "what you see" is not always "what you get". *Structure* **2009**, 17, (4), 489-98.
296. Zhang, J. H.; Chung, T. D.; Oldenburg, K. R., A Simple Statistical Parameter for Use in Evaluation and Validation of High Throughput Screening Assays. *J Biomol Screen* **1999**, 4, (2), 67-73.

297. Martin, Y. C., Overview of concepts and methods in computer-assisted rational drug design. *Methods Enzymol* **1991**, 203, 587-613.
298. Erickson, J. W., Design and structure of symmetry-based inhibitors of HIV-1 protease. *Drug Dis Design* **1993**, 1, 109-128.
299. Hoofnagle, A. N.; Resing, K. A.; Ahn, N. G., Protein analysis by hydrogen exchange mass spectrometry. *Annu Rev Biophys Biomol Struct* **2003**, 32, 1-25.
300. Houde, D.; Arndt, J.; Domeier, W.; Berkowitz, S.; Engen, J. R., Characterization of IgG1 Conformation and Conformational Dynamics by Hydrogen/Deuterium Exchange Mass Spectrometry. *Anal Chem* **2009**, 81, (14), 5966.
301. Quraishi, O.; Mancini, J. A.; Riendeau, D., Inhibition of inducible prostaglandin E(2) synthase by 15-deoxy-Delta(12,14)-prostaglandin J(2) and polyunsaturated fatty acids. *Biochem Pharmacol* **2002**, 63, (6), 1183-9.
302. Paumi, C. M.; Wright, M.; Townsend, A. J.; Morrow, C. S., Multidrug resistance protein (MRP) 1 and MRP3 attenuate cytotoxic and transactivating effects of the cyclopentenone prostaglandin, 15-deoxy-Delta(12,14)prostaglandin J2 in MCF7 breast cancer cells. *Biochemistry* **2003**, 42, (18), 5429-37.
303. Kim, E. H.; Surh, Y. J., 15-deoxy-Delta12,14-prostaglandin J2 as a potential endogenous regulator of redox-sensitive transcription factors. *Biochem Pharmacol* **2006**, 72, (11), 1516-28.
304. Wu, G.; Fang, Y. Z.; Yang, S.; Lupton, J. R.; Turner, N. D., Glutathione metabolism and its implications for health. *J Nutr* **2004**, 134, (3), 489-92.
305. Murphey, L. J.; Williams, M. K.; Sanchez, S. C.; Byrne, L. M.; Csiki, I.; Oates, J. A.; Johnson, D. H.; Morrow, J. D., Quantification of the major urinary metabolite of PGE2 by a liquid chromatographic/mass spectrometric assay: determination of cyclooxygenase-specific PGE2 synthesis in healthy humans and those with lung cancer. *Anal Biochem* **2004**, 334, (2), 266-75.
306. Rusconi, F., massXpert 2: a cross-platform software environment for polymer chemistry modelling and simulation/analysis of mass spectrometric data. *Bioinformatics* **2009**, 25, (20), 2741-2.
307. Clauser, K. R.; Baker, P.; Burlingame, A. L., Role of accurate mass measurement (+/- 10 ppm) in protein identification strategies employing MS or MS/MS and database searching. *Anal Chem* **1999**, 71, (14), 2871-82.
308. Kyte, J.; Doolittle, R. F., A simple method for displaying the hydrophobic character of a protein. *J Mol Biol* **1982**, 157, (1), 105-32.
309. Hofmann, K.; Stoffel, W., TMbase: A database of membrane spanning proteins segments. *Biol Chem Hoppe Seyler* **1993**, 374, 166.

310. Rost, B., PHD: predicting one-dimensional protein structure by profile-based neural networks. *Methods Enzymol* **1996**, 266, 525-39.
311. Hirokawa, T.; Boon-Chieng, S.; Mitaku, S., SOSUI: classification and secondary structure prediction system for membrane proteins. *Bioinformatics* **1998**, 14, (4), 378-9.
312. Mitaku, S.; Hirokawa, T.; Tsuji, T., Amphiphilicity index of polar amino acids as an aid in the characterization of amino acid preference at membrane-water interfaces. *Bioinformatics* **2002**, 18, 608-616.
313. Larkin, M. A.; Blackshields, G.; Brown, N. P.; Chenna, R.; McGettigan, P. A.; McWilliam, H.; Valentin, F.; Wallace, I. M.; Wilm, A.; Lopez, R.; Thompson, J. D.; Gibson, T. J.; Higgins, D. G., Clustal W and Clustal X version 2.0. *Bioinformatics* **2007**, 23, (21), 2947-8.
314. VanAken, T.; Foxall-VanAken, S.; Castleman, S.; Ferguson-Miller, S., Alkyl glycoside detergents: synthesis and applications to the study of membrane proteins. *Methods Enzymol* **1986**, 125, 27-35.
315. Hjelmeland, L. M.; Nebert, D. W.; Osborne, J. C., Jr., Sulfobetaine derivatives of bile acids: nondenaturing surfactants for membrane biochemistry. *Anal Biochem* **1983**, 130, (1), 72-82.
316. Riendeau, D.; Aspiotis, R.; Ethier, D.; Gareau, Y.; Grimm, E. L.; Guay, J.; Guiral, S.; Juteau, H.; Mancini, J. A.; Methot, N.; Rubin, J.; Friesen, R. W., Inhibitors of the inducible microsomal prostaglandin E2 synthase (mPGES-1) derived from MK-886. *Bioorg Med Chem Lett* **2005**, 15, (14), 3352-5.
317. Codreanu, S. G.; Thompson, L. C.; Hachey, D. L.; Dirr, H. W.; Armstrong, R. N., Influence of the dimer interface on glutathione transferase structure and dynamics revealed by amide H/D exchange mass spectrometry. *Biochemistry* **2005**, 44, (31), 10605-12.
318. Spahiu, L.; Stenberg, P.; Larsson, C.; Wannberg, J.; Alterman, M.; Kull, B.; Nekhotiaeva, N.; Morgenstern, R., A Facilitated Approach to Evaluate the Inhibitor Mode and Potency of Compounds Targeting Microsomal Prostaglandin E Synthase-1. *Assay Drug Dev Technol* **2011**.
319. Prage, E. B.; Pawelzik, S. C.; Busenlehner, L. S.; Kim, K.; Morgenstern, R.; Jakobsson, P. J.; Armstrong, R. N., Location of Inhibitor Binding Sites in the Human Inducible Prostaglandin E Synthase, MPGES1. *Biochemistry* **2011**, 50, (35), 7684-93.
320. Bogaards, J. J.; Venekamp, J. C.; van Bladeren, P. J., Stereoselective conjugation of prostaglandin A2 and prostaglandin J2 with glutathione, catalyzed by the human glutathione S-transferases A1-1, A2-2, M1a-1a, and P1-1. *Chem Res Toxicol* **1997**, 10, (3), 310-7.

321. Brunoldi, E. M.; Zanoni, G.; Vidari, G.; Sasi, S.; Freeman, M. L.; Milne, G. L.; Morrow, J. D., Cyclopentenone prostaglandin, 15-deoxy-Delta12,14-PGJ2, is metabolized by HepG2 cells via conjugation with glutathione. *Chem Res Toxicol* **2007**, 20, (10), 1528-35.
322. Milne, G. L.; Yin, H.; Hardy, K. D.; Davies, S. S.; Roberts, L. J., 2nd, Isoprostane generation and function. *Chem Rev* **2011**, 111, (10), 5973-96.